

HYDRODYNAMIC AND WATER QUALITY MODELING AND TMDL DEVELOPMENT FOR MARYLAND'S COASTAL BAYS SYSTEM

Prepared for:
Maryland Department of the Environment
Science Service Administration
TMDL Technical Development Program
1800 Washington Boulevard, Suite 540
Baltimore, MD 21230

Prepared by:
Harry Wang, Zhengui Wang, Derek Loftis and Yi-cheng Teng
Department of the Physical Sciences, Virginia Institute of Marine Sciences,
College of William and Mary

November 2013

Table of Contents

List of Tables	i
List of Figures	ii
EXECUTIVE SUMMARY	vi
CHAPTER 1: INTRODUCTION.....	1
1.1 Background.....	1
1.2 Study Approach	4
CHAPTER 2: GENERAL CHARACTERISTICS OF MARYLAND COASTAL BAYS WATERSHED..	6
2.1 Physical Setting.....	6
2.2 The terrestrial and atmospheric loading.....	6
2.2.1 Land use distribution.....	7
2.2.2 Non-point source loading.....	9
2.2.3 Point-source loading	10
2.2.4 Shoreline erosion loading	13
2.2.5 Atmospheric loading.....	16
2.2.6 Discussion of Contributing Loads to the Maryland Coastal Bays.....	18
2.3 Data to Support the Water Quality Modeling.....	24
CHAPTER 3: THE THREE-DIMENSIONAL HYDRODYNAMIC MODEL.....	29
3.1 Model description	29
3.2 Model set-up	30
3.3 Hydrodynamic model forcing functions	30
3.4 Hydrodynamic model calibration	33
3.4.1 Water level calibration.....	33
3.4.2 Velocity calibration.....	42
3.4.3 Salinity calibration	46
CHAPTER 4: THE COUPLED WATER QUALITY AND SEDIMENT BENTHIC FLUX MODEL	52
4.1 The ICM Water Quality Model.....	52
4.2. The Sediment Benthic Flux Model	54
4.3 Water Quality Model Set-up.....	56
4.3.1 External loading	56
4.3.2 Initial and boundary conditions	59
4.3.3 Estimation of parameters	59
4.4 Water Quality Model Calibration and Verification	60
4.4.1 Model calibration.....	60
4.4.2 Model verification.....	70
CHAPTER 5: ADDITIONAL MODEL ANALYSES	94
5.1 Adjustments to incorporate the DO Diel Cycle	94
5.2 Sensitivity Analyses.....	112
5.2.1 Ocean City Wastewater Treatment Plant outfall	112
5.2.2 Effect of phytoplankton and organic nutrient settling rate	114
5.2.3 Effects of groundwater discharge	116
6.1. Developing nutrient load reduction scenario	119
6.1.1 Critical conditions.....	119
6.1.2 Margin of Safety (MOS).....	120
6.1.3 Seasonal variation	120
6.2 Developing the TMDL scenario	121
6.3 Final TMDL scenario for MD Coastal Bays – geographic isolation method.....	134

CHAPTER 7: DISCUSSION AND CONCLUSION.....	145
REFERENCES	148
APPENDIX A: Summary of SELFE hydrodynamic model formulations	155
APPENDIX B: The ICM Water Quality Model Formulation	168
APPENDIX C: Summary of Parameters Used for ICM Water Quality Model	203

List of Tables

Table 1.1: TMDL impaired water listing for the Maryland Coastal Bays (MDE 2010).....	3
Table 1.2: HEM3D model water quality state variables	5
Table 2.1: Drainage and water surface area (in acres) of the Maryland Coastal Bays.....	7
Table 2.2: Land use (in acres) for sub-watersheds in MCBs HSPF watershed model	9
Table 2.3 (a): Major point source facilities in Maryland with permits regulating the discharge of nutrients.	11
Table 2.3 (b): Permitted point source facilities in Virginia	12
Table 2.4: TN and TP loads from shoreline erosion for individual bays and entire MCBs	15
Table 2.5: Total baseline nitrogen and phosphorus loads (lbs/year), MD Coastal Bays 2001-2004.....	23
Table 2.6: Summary of data supporting the hydrodynamic and water quality modeling.....	25
Table 3.1: Description and location of field observation stations for current, water level and salinity in the MCBs.....	34
Table 3.2: Statistical measures for modeled versus observed salinity at five basins in MCBs.	51
Table 4.1: The parameter selected for phytoplankton dynamics.....	60
Table 4.2: Model and data comparison statistics for DNR stations.	92
Table 4.3: Model and data comparison statistics for ASIS stations.....	93
Table 4.4: Relative Error in the MCBs model compared with other modeled systems.	93
Table 5.1: Variables, coefficient values and statistical test results for DO diel cycle linear regression model (Perry et al., 2012).	99
Table 5.2: Exceedance rates for Chlorophyll-a under Ocean City WWTP 20%, 40% and 60% incremental reduction scenarios.	113
Table 5.3: Effect of changing settling velocities of phytoplankton and organic nutrients on chlorophyll-a concentration.....	116
Table 6.1: Maximum Practicable Anthropogenic Reduction (MPAR) Percentages for each non-point source sector based on CBP-Phase 5.3.2 scenario results.	122
Table 6.2: DO exceedance rate under baseline conditions and reduction scenarios of 20%, 40%, 60%, natural conditions and MPAR for all DNR and ASIS stations.	124
Table 6.3 (a): Modeled chlorophyll-a exceedance rates under baseline conditions and reduction scenarios of 20%, 40%, 60%, natural and MPAR conditions for non-SAV growing zone with Chl-a endpoint greater than 50 µg/l.	132
Table 6.3 (b): Modeled chlorophyll-a exceedance rates under baseline conditions and reduction scenarios of 20%, 40%, 60%, natural and MPAR conditions for SAV growing zone with Chl-a endpoint greater than 15µg/l.....	133
Table 6.4: Final TMDL reductions needed to meet WQS incorporating Geographic Isolation Scenarios.	135
Table 6.5: DO exceedance rates for TMDL IR (Incremental Reduction) and final TMDL (TMDL GI, incorporating Geographic Isolation Scenario).	136
Table 6.6(a): Chla greater than 50 ug/l exceedance rates for TMDL IR (Incremental Reduction) and final TMDL (TMDL GI, incorporating Geographic Isolation Scenario).....	140
Table 6.6(b): Chla greater than 15 ug/l exceedance rates for TMDL IR (Incremental Reduction) and final TMDL (TMDL GI, incorporating Geographic Isolation Scenario).....	141
Table C-1: Parameters related to algae in the water column.	203
Table C-2: Parameters related to organic carbon in the water column.	205
Table C-3: Parameters related to nitrogen in the water column.....	206
Table C-4: Parameters related to phosphorus in the water column.	208
Table C-5: Parameters related to silica in the water column.....	209
Table C-6. Parameters related to chemical oxygen demand and dissolved oxygen in the water column.....	209
Table C-7: Parameters used in the sediment flux model.	210

List of Figures

Figure 1.1: Location map of MD Coastal Bays System	2
Figure 2.1: Land use distribution in the Maryland Coastal Bays watershed.	8
Figure 2.2: Locations of sampling sites (in red) and land loss polygons (in blue) in Assawoman and Isle of Wight Bays.	14
Figure 2.3: Wet deposition of inorganic nitrogen in 2002 and 2003 in the United States ...	17
Figure 2.4: Total nitrogen load (percentage of total) from source sectors in individual MCBs	19
Figure 2.5: Total nitrogen loading from source sectors in individual MCBs (lbs/year).	20
Figure 2.6: The total phosphorus load (percentage of total) from source sectors in individual MCBs.....	21
Figure 2.7: Total phosphorus load from source sectors in individual MCBs (lbs/year)	22
Figure 2.8: Station location for DNR and ASIS monitoring program in MCBs	26
Figure 2.9: DNR monthly DO data from stations in Saint Martin River (2000-2004)	27
Figure 2.10: Combined DNR and ASIS monthly DO data from stations in Newport Bay (2000-2004).....	28
Figure 3.1 Hydrodynamic model grid in the Maryland Coastal Bays (MCBs).	31
Figure 3.2: Bathymetry for the Maryland Coastal Bays	32
Figure 3.3: Map of field observation stations for water elevation, currents and salinity in the MCBs.	35
Figure 3.4 (a) Tidal calibrations near Ocean City Inlet in the northern portion of the MCBs.....	36
Figure 3.4 (b) Tidal calibrations near Chincoteague Inlet in the southern portion of the MCBs.....	37
Figure 3.4(c): Tidal calibrations across the middle and southern portions of the MCBs. ...	38
Figure 3.5: M2 Tidal profiles along Chincoteague and Sinepuxent Bays transect.....	39
Figure 3.6: Wind record at Ocean City and Wallops Island, September 23 to October 8, 2004.	40
Figure 3.7: Water level verification at A) Ocean City Inlet;, B) South Point; C) Harbor of Refuge, and D) Turville Creek.	41
Figure 3.8: (a) Spatial distribution of surface velocities during maximum flood tide at Ocean City Inlet, October 2004; and (b) Current speed time series comparison along the major axis of the local channel; ADCP measurement (red), and model results (blue).	43
Figure 3.9: Current calibration results at A) Isle of Wight Channel B) Sinepuxent Bay C) Chincoteague Bay Channel; model (red solid line) and data (blue dash line)	44
Figure 3.10: Statistical measures for current comparison at calibration stations A, B. and C, respectively.....	45
Figure 3.11 (a) Areally-weighted daily discharge from USGS flow gauges (01484719 and 0148471320) in MCBs, and (b) Salinity calibration in the tributaries of the northern MCBs.....	47
Figure 3.11 (c): Salinity calibration in the open waters of the northern MCBs	48
Figure 3.11 (d): Salinity calibration in the southern MCBs.....	49
Figure 3.12: Spatial distribution of averaged salinity contour in MCBs over summers of (a) 2003 and (b) 2004.	50

Figure 4.1 Schematic diagram of coupled HSPF watershed, SELFE hydrodynamic, ICM water quality, and sediment benthic models.....	53
Figure 4.2 (a) Schematic diagrams for (a) ICM model water column processes and (b) sediment diagenesis processes.....	55
Figure 4.3 (a) Example the selected segments of HSPF Coastal Bays model segments in the Assawoman Bay, Isle of Wight Bay, Sinepuxent Bay and Newport Bays.....	57
Figure 4.3 (b) Examples of the selected segments of HSPF Coastal Bays model segments in the Chincoteague Bay	58
Figure 4.4 Intensive monitoring stations in (a) Isle of Wight Bay and (b) Maryland Coastal Bays.	61
Figure 4.5 (a) and (b): Comparisons of model prediction and field measurement for chlorophyll-a and DO in the Isle of Wight Bay.	63
Figure 4.5 (c) and (d): Comparisons of model predictions and field measurement for NH_4 and NO_{23} in the Isle of Wight Bay.....	64
Figure 4.5 (e) and (f): Comparisons of model predictions and field measurement for PO_4 and DON in the Isle of Wight Bay.....	65
Figure 4.6 (a) and (b): Comparisons of model predictions and field measurement for Chlorophyll-a and DO in Bay-wide stations.	67
Figure 4.6 (c) and (d): Comparisons of model predictions and field measurements for NH_4 and NO_{23} in Bay-wide stations.....	68
Figure 4.6 (e) and (f): Comparisons of model predictions and field measurement for PO_4 and DON in the Bay-wide stations.....	69
Figure 4.7: MD DNR and ASIS monitoring stations in the Maryland Coastal Bays.	72
Figure 4.8 (a) The flow discharges and (b) Chlorophyll-a concentration from Birch Branch watersheds.....	73
Figure 4.9 (a): DO verification with DNR data, Stations 1-12, 2001- 2005.....	76
Figure 4.9 (b): DO verification with DNR data, Stations 13-24 2001-2005.....	77
Figure 4.9 (c): DO verification with DNR data, Stations 25-27, 2001-2005.....	78
Figure 4.10: Statistical comparison of observed versus modeled DO; Assawoman, Isle of Wight, Newport, and Chincoteague Bays.....	79
Figure 4.11 (a): Chlorophyll-a verification with DNR data Stations 1-12, 2001-2005.....	80
Figure 4.11(b): Chlorophyll-a verification with DNR data Stations 13-24, 2001-2005.....	81
Figure 4.11 (c): Chlorophyll-a verification with DNR data Stations 25-27, 2001-2005.....	82
Figure 4.12 (a): Statistical comparison of observed versus modeled Chlorophyll-a data for Assawoman and Isle of Wight Bays.	83
Figure 4.12 (b): Statistical comparison of observed versus modeled Chlorophyll-a data for Newport, and Chincoteague Bays.....	84
Figure 4.13 (a): SOD calculation at DNR Stations 1-12, 2001- August 2005.....	85
Figure 4.13 (b): SOD calculation at DNR Stations 13-24, 2001- August 2005.....	86
Figure 4.13 (c): SOD calculation at DNR Stations 25-27, 2001- August 2005.....	87
Figure 4.14 (a): DO verification at ASIS Stations 1-9, 2001- August 2005.....	88
Figure 4.14 (b): DO verification at ASIS Stations 10-18, 2001- August 2005.....	89
Figure 4.15 (a): Chlorophyll verification at ASIS Stations 1-9, 2001- August 2005.....	90
Figure 4-15 (b): Chlorophyll verification at ASIS Stations 10-18, 2001-August 2005.....	91
Figure 5.1: ConMon data measured at Bishop’s Landing, July – August, 2005; before (left) and after (right) Fast Fourier transformation.....	95

Figure 5.2: Low-pass-filtered daily DO, DO saturation, salinity, temperature, and Chlorophyll-a data (left); measured (blue) and fitted sinusoidal curve (red) diel cycle of DO (right).....	98
Figure 5.3: DO diel cycle amplitude adjustments for seasonal temperature cycle proportioned to monthly mean temperature.....	100
Figure 5.4 (a): DO daily average (black) and diel (green) time series, Stations XDN7545 and XDN4851, Assawoman Bay, January 1 – December 31 2004.	101
Figure 5.4 (b): DO daily average (black) and diel (green) time series, Stations XDN4486 and XDN3724, St. Martin River, Isle of Wight Bay, January 1 – December 31, 2004.	102
Figure 5.4 (c): DO daily average (black) and diel (green) time series, Stations XDN3445 and TUV0019, Isle of Wight Bay open waters, January 1 – December 31 2004. .	103
Figure 5.4 (e): DO daily average (black) and diel (green) time series, Stations ASSA 4 and ASSA 3, Newport Bay, January 1 – December 31, 2004.	105
Figure 5.4 (f): Daily average (black) and diel (green) time series, Stations XCM1562 and ASSA 7, Chincoteague Bay January 1 – December 31, 2004.....	106
Figure 5.5 (a): Correlation coefficient (R^2) between diel-cycle-adjusted modeled and observed DO, DNR Stations 1-12, baseline conditions, January 2001- August 2005.....	107
Figure 5.5 (b): Correlation coefficient (R^2) between diel-cycle-adjusted modeled and observed DO, DNR Stations 13-24, baseline conditions, January 2001- August 2005.....	108
Figure 5.5 (c): Correlation coefficient (R^2) between diel-cycle-adjusted modeled and observed DO, DNR Stations 25-27, baseline conditions, January 2001- August 2005.....	109
Figure 5.5 (d): Correlation coefficient (R^2) between diel-cycle-adjusted modeled and observed DO, ASIS Station 1-9, baseline conditions, January 2001- August 2005.....	110
Figure 5.5 (e): Correlation coefficient (R^2) between diel-cycle-adjusted modeled and observed DO, ASIS Stations 10-18, baseline conditions, January 2001- August 2005.....	111
Figure 5.6: Sensitivity test comparing the effect of settling velocities of diatom species on Chlorophyll-a concentration at station AYR0017 in 2004.	115
Figure 5.7 (a): Location of Johnson Bay in the middle of the Chincoteague Bay and the nearby DNR stations XBM5932 and XBM3418.	117
Figure 5.7(b): Comparison of modeled total nitrogen concentrations under groundwater release at edge-of-stream vs. bay-floor release, Johnson Bay area, Chincoteague Bay, 2001-2005.	118
Figure 6.1: Response of six stations having the highest DO exceedance rates to the incremental reductions, MPAR and natural conditions scenarios.....	125
Figure 6.2 (a): DO time series, 2001- August 2005, baseline conditions (blue), 60% reduction scenario (magenta), and observed (symbol) at DNR Stations 1-12.....	127
Figure 6.2 (b): DO time series, 2001- August 2005, for baseline conditions (blue), 60% reduction scenario(magenta), and observed (symbol) at DNR Stations: 13 -24....	128
Figure 6.2 (c): DO time series, 2001-August 2005 for baseline conditions (blue), and 60% reduction scenario (magenta), and observed (symbol) at DNR Stations: 25 - 27..	129

Figure 6.2 (d): DO time series, 2001-August 2005, baseline conditions (blue), 60% reduction scenario (magenta) and observed data (symbol) at ASIS Stations:1-9.	130
Figure 6.2 (e): DO time series, 2001-August 2005, baseline conditions (blue), 60% reduction scenario (magenta), and observed data (symbol) at ASIS Stations 10 -18.	131
Figure 6.3 (a): DO time series, 2001-August 2005, baseline conditions (blue), final TMDL (red) and observed (symbol) at DNR Stations 1 -12.....	137
Figure 6.3 (b): DO time series, 2001-August 2005, baseline conditions (blue), final TMDL (red) and observed (symbol) at DNR Stations 13 -24.....	138
Figure 6.3 (c): DO time series, 2001-August 2005, baseline conditions (blue), final TMDL (red) and observed (symbol) at DNR Stations 25-27.....	139
Figure 6.4 (a): Chlorophyll-a time series, 2001-August 2005, baseline conditions (blue), final TMDL (red) and observed (symbol) at DNR Stations 1 -12.....	142
Figure 6.4 (b): Chlorophyll-a time series, 2001-August 2005, baseline conditions (blue), final TMDL (red) and observed (symbol) at DNR Stations 13 -24.....	143
Figure 6.4 (c): Chlorophyll-a time series, 2001-August 2005, baseline conditions (blue), final TMDL (red) and observed (symbol) at DNR Stations 25 -27.....	144

EXECUTIVE SUMMARY

Shallow coastal bays and lagoons are important buffer zones between terrestrial and deeper coastal ecosystems. They are inherently vulnerable to eutrophication, particularly from anthropogenic influences. The Maryland Coastal Bays (MCBs) is a collection of shallow coastal basins including Assawoman Bay, Isle of Wight Bay, Sinepuxent Bay, Newport Bay and Chincoteague Bay adjacent to the Delmarva Peninsula of the US East Coast. The MCBs have shown signs of water quality degradation in recent years. Extensive monitoring has been conducted, demonstrating low dissolved oxygen (DO) and high levels of chlorophyll *a*. It was determined that the MCBs water quality conditions exceed the State's water quality standards, and the MCBs were placed on the State's 303(d) List of impaired water bodies in 1996.

In the current effort, a Hydrodynamic Eutrophication Model 3-D (HEM3D) was developed and used as a tool to simulate the dynamics of physical-biological-chemical processes in the receiving MCBs waters, using the nutrient loads generated by the MCBs Hydrologic Simulation Program-FORTRAN (HSPF) watershed model.

The HEM3D modeling system was calibrated and compared exceedingly well with the intensive field data including water level, current velocity, salinity, chlorophyll *a*, dissolved oxygen (DO), ammonia nitrogen, nitrate nitrogen, phosphate and dissolved organic nitrogen collected during 2001- 2004 by the Maryland Department of Natural Resources (MD-DNR) and the US National Park Service/Assateague Island National Seashore (ASIS). The calibrated and verified hydrodynamic model was used to determine the physical transport time scales for the entire system to be on the order of 2-3 months. Most of the system is nitrogen limited except in the headwaters of the tributaries where the phosphorus and nitrogen can be co-limiting depending on the flow and/or season. The predicted daily mean DO from the HEM3D was further adjusted for the diel cycle using Elgin Perry's statistical analysis results (2012). The empirical corrections for diel cycle were made to the daily mean DO by monthly temperature, daily temperature, daily Photosynthetically Active Radiation (PAR), and daily chlorophyll. In doing so, the DO variability includes the diel cycle, which provides a better representation of full spectrum of DO levels in the MCBs. Following calibration and verification of the HEM3D hydrodynamic and water quality model, sensitivity analyses were conducted to test the effects of (a) Ocean City wastewater treatment plant outfall, (2) phytoplankton and organic nutrient settling rate and (c) ground water discharge. The model was used to evaluate point and nonpoint source loading allocations and reduction scenarios.

The TMDL endpoint for DO requires that daily mean DO concentrations simulated at the model cells corresponding to the water quality stations shall not be below 5 mg/l more than 10 percent of the time, both annually and in the growing season (May 1 – October 31). The TN and TP sources were assessed for the five impaired basins in the MCBs.

It was found that for Assawoman, Isle of Wight, and Newport Bays, the terrestrial sources are the dominant source of loading, whereas in the Sinepuxent and Chincoteague Bays the terrestrial source loading are about equal to that of atmospheric

loading. In determining a final TMDL scenario for management action in MCBs, incremental reductions were conducted. Based on the incremental reduction scenarios including 20%, 40%, 60%, Maximum Practicable Anthropogenic Reduction (MPAR) and the natural condition, the northern Bays (north of Ocean City), particularly in the Saint Martin River, area appear to require the most reductions. The southern portion of the Bay only requires minor reduction. Given this spatial disparity, it is obvious that the load reduction scenario for TMDLs requires including the geographic influences. The “geographic isolation method” was further conducted and the final TMDL reductions needed to meet water quality standards are: 20% for Assawoman Bay, 40% for Isle of Wight Bay (Open Waters), 55-58% for Bishopville Prong/Shingle Landing, 0% for Sinepuxent Bay, 20% for Newport Bay and for the Maryland portion of the Chincoteague Bay.

CHAPTER 1: INTRODUCTION

1.1 Background

The Maryland Coastal Bays system (MCBs) is located along the US Atlantic coast of the Delmarva Peninsula on the eastern edge of the Atlantic coastal plain (Figure 1.1). It consists of a series of coastal bays including the Assateague Island National Seashore. These bays span across three states: Delaware, Maryland and Virginia, and are composed of five major separate basins: (1) Assawoman Bay (2) Isle of Wight Bay (3) Sinepuxent Bay (4) Newport Bay and (5) Chincoteague Bay, from the north to the south as shown in Figure 1.1. In 1991 the United States Environmental Protection Agency's (EPA) Office of Water Assessment and Protection Division published Guidance for Water Quality Based Decisions: the TMDL Process. In 1992, EPA published the final Water Quality Planning and Management Regulation (40 CFR Part 130). Together these documents describe the roles and responsibilities of EPA and the States in meeting the requirements of Section 303(d) of the Clean Water Act (CWA). Section 303(d) requires States to: (1) Identify waters that are and will remain polluted after the application of technology standards; (2) Prioritize these waters, taking into account the severity of their pollution; and (3) Establish TMDLs for these waters at levels necessary to meet applicable water quality standards, taking into account seasonal variations and a protective margin of safety (MOS) to account for uncertainty.

The Maryland Department of the Environment is required to identify waters that are impaired by pollutants. The MCBs were identified in MD's 2010 Section 303(d) Impaired Waters list as impaired and the listings are shown in Table 1.1. The list highlights nitrogen and phosphorus as the major pollutants in the watershed, stating water quality standards are not being met because of excess loads of these substances (Maryland Department of the Environment, 2001). The water quality of this system is considered degraded, as evidenced by substantial increase of nutrients, seasonal hypoxia, macroalgae biomass in areas, annual blooms of brown tide (Wazniak and Gilbert, 2004), and are projected to experience environmental stress due to increased population and intense development (Boynton et al., 1996; Wazniak et al., 2004; Maryland Department of the Environment, 1993). Maryland Department of Natural Resources (2004) documents the most up-to-date (up to 2004) status of the water quality and living resources in the Coastal Bays. Wazniak et al. (2005) further investigated the overall ecosystem health including using high frequency DO measurements to identify diel cycle of DO and the impact of sediment influence from the shoreline erosion. Maryland Department of the Environment (2004) identified the priority areas for wetland restoration. Wazniak et al. (2007) linked the water quality condition to the living resources and Dennison et al. (2009) characterized the physical, chemical, and biological resources of the Coastal Bays and serves as an additional step in providing sound management for the future.

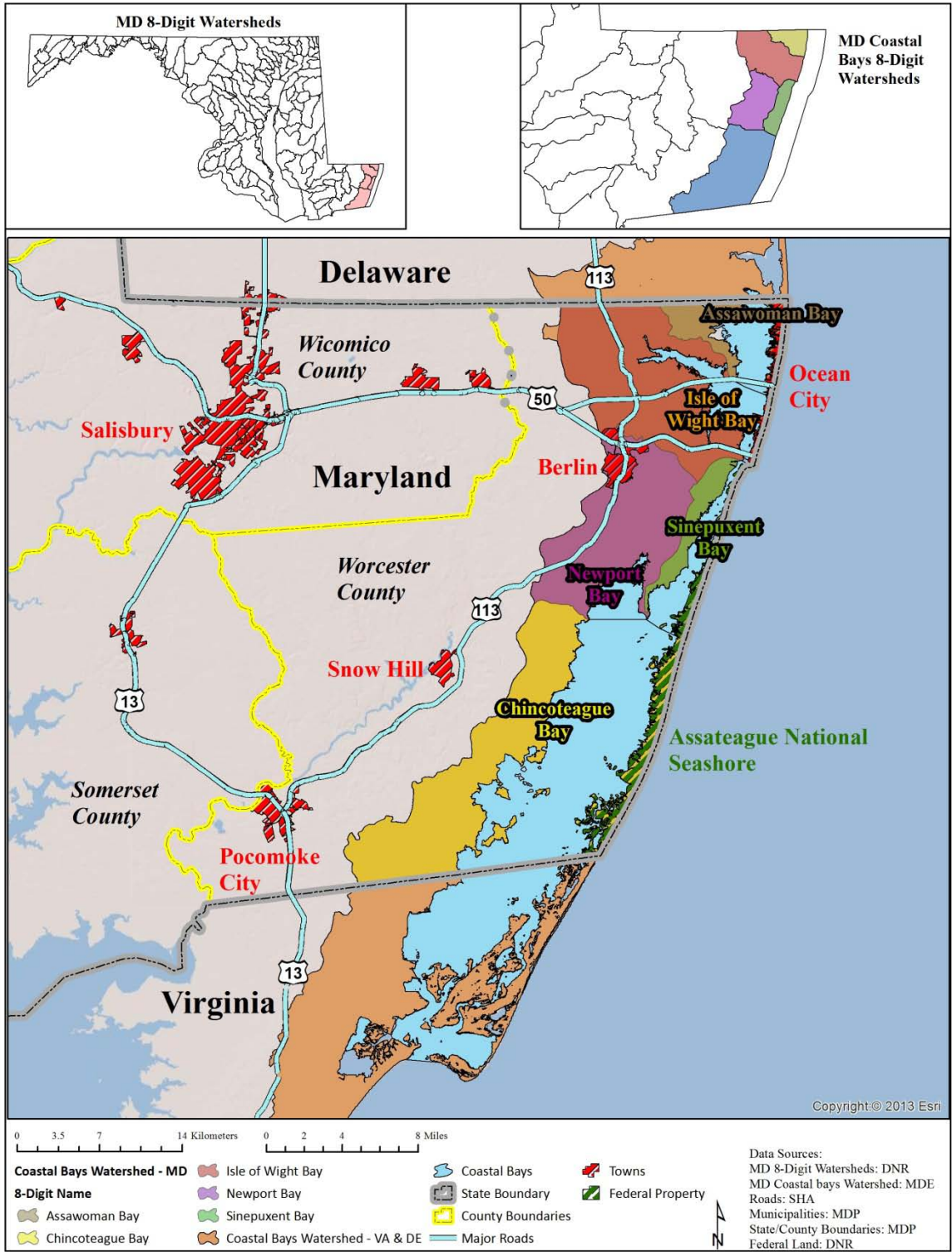


Figure 1.1: Location map of MD Coastal Bays System

Table 1.1: TMDL impaired water listing for the Maryland Coastal Bays (MDE 2010)

Year listed	Watershed	Basin Code	2010 IR Assessment Unit ID	Specific Area	Identified Pollutant	*Listing Category
1996	Assawoman Bay	02130102	MD-02130102-T-Assawoman_Bay	Open water	Nitrogen	5
					Phosphorus	5
			MD-02130102-T-Greys_Creek	Grey's Creek	Nitrogen	5
					Phosphorus	5
1996	Isle Of Wight Bay	02130103	MD-02130103-T-Turville_Creek	Turville Creek	Nitrogen	4a
					Phosphorus	4a
			MD-02130103-T-Manklin_Creek	Manklin Creek	Nitrogen	5
					Phosphorus	5
			MD-02130103-T-Herring_Creek	Herring Creek	Nitrogen	4a
					Phosphorus	4a
			MD-02130103-T-Bishopville_Prong	Bishopville Prong	Nitrogen	4a
					Phosphorus	4a
			MD-02130103-T-StMartin_River	St. Martin River	Nitrogen	4a
					Phosphorus	4a
			MD-02130103-T-Shingle_Landing_Prong	Shingle Landing Prong	Nitrogen	4a
					Phosphorus	4a
MD-02130103-T-Isle_Of_Wight_Bay	Open Water	Nitrogen	5			
		Phosphorus	5			
1996	Newport Bay	02130105	MD-02130105-T-Newport_Creek	Newport Creek	Nitrogen	4a
					MD-02130105-T-Marshall_Creek	Marshall Creek
			Phosphorus	5		
			MD-02130105-T-Kitts_Branch	Kitts Branch	Biochemical Oxygen Demand	4a
			MD-02130105-T-Ayer_Creek	Ayer Creek	Nitrogen	4a
MD-02130105-T-Newport_Bay	Newport Bay	Nitrogen	4a			
1996	Sinepuxent Bay	02130104	MD-02130104-T	Sinepuxent Bay	Nitrogen	5
					Phosphorus	5
1996	Chincoteague Bay	02130106	MD-02130106-T	Chincoteague Bay	Nitrogen	5
					Phosphorus	5

*Definition of listing category: 4a – TMDL developed; 5 – TMDL required.

The main goal of TMDLs is to obtain a projected distribution of pollutant loading in each basin to meet water quality standards. In the MCBs, the determination of loadings and their allocations rely on the water body's complex interactions among physical, chemical and biological processes. Statistical models, expressed in simple mathematical relationships derived from fitting equation to observed data, are usually easy to use and require minimal effort. One weakness of statistical models is that they tend to have large standard errors of prediction, especially when the water quality data have relatively large range of variations spatially. They are most reliable when applied within the range of observation and in a relatively homogeneous and well-mixed system such as lakes. When the interactions of flow, loading, internal chemical and biological

processes are too complicated to be solved through the use of statistical and data analysis techniques, mechanistic computer simulation models are often employed. Mechanistic models are based on physical, chemical and biological mechanisms that govern the water systems. It is formulated upon equations that contain directly definable observable parameters. When properly calibrated and verified, mechanistic models are usually better at representing the physical chemical and biological processes, and carries higher prediction skill for the relationships between loading and water quality condition in the water body systems.

1.2 Study Approach

In order to develop TMDLs in the MCBs that consider complex physical and aquatic biochemical dynamics, a three-dimensional (3-D) hydrodynamic and eutrophication model is needed to simulate algal dynamics and dissolved oxygen levels and to determine acceptable pollutant load allocations for nutrients that can result in attaining water quality standards. A HEM3D (Hydrodynamic and Eutrophication Modeling 3D) developed by Virginia Institute of Marine Science (VIMS) was selected as the modeling framework consisting of the hydrodynamic model SELFE, the water quality model Integral Compartment Water Quality Model (CE-QUAL-ICM or ICM) and the benthic sediment flux model all of which was used to simulate the receiving waters of Maryland Coastal Bays (MCBs).

The hydrodynamic model, an unstructured grid, finite element model SELFE (Semi-implicit, Eulerian, Lagrangian Finite Element model), was selected and used to simulate tidal inlet and estuarine dynamics in the MCBs. The salient feature of the model is that it uses an unstructured grid to better simulate the coastline and the tidal inlets. In addition, the model is capable of simulating the wetting-and-drying process, which is a common feature occurring in the shallow coastal system. Although the model uses a high-resolution grid (on the order of 200-m resolution), it still maintains a relatively large time step without becoming restricted by the CFL (Courant-Friedrichs-Lewy) condition. It does this by using a special advection scheme known as the Eulerian-Lagrangian scheme. In this way, the high-resolution model grids can be used to represent a large model domain without reducing computational efficiency. The model is a general three-dimensional model capable of simulating both 2-dimensional (vertically averaged) and 3-dimensional hydrodynamics and transport processes. In the horizontal, the model uses an unstructured, triangular grid and in the vertical, a terrain following s-coordinate, a variation of the sigma coordinate with higher resolution on the surface and at the bottom. The convective terms are treated by the Eulerian-Lagrangian transport scheme and a semi-implicit method for implementing 3-D equations.

The eutrophication model is a three-dimensional time-variable eutrophication model package CE-QUAL-ICM (Integral Compartment Model). The model includes both the water column eutrophication process and the benthic sediment process, which are dynamically coupled with hydrodynamic and watershed models. The US Army Corps of Engineers originally developed the model for the EPA Chesapeake Bay Program for studying the Chesapeake Bay. In the MCBs, the eutrophication model used has twenty-one model state variables, which consist of five interacting systems: i.e., phytoplankton

dynamics, nitrogen, phosphorus, and silicate cycles, and oxygen dynamics, as shown in Table 1.2. The water column eutrophication model solves the mass-balance equation for each state variable and for each model cell. A detailed description of the water column eutrophication model framework can be found in Cerco and Cole (1994).

A benthic sediment flux model (DiToro and Fitzpatrick, 1993) was coupled with CE-QUAL-ICM. There are two layers; the upper aerobic layer (Layer 1) and the lower anoxic layer (Layer 2) representing the sediment in this model. The sediment process is coupled with the water column eutrophication model through depositional and sediment fluxes. The sediment model is driven by net settling of particulate organic matter from the overlying water column to the sediments (depositional flux). The mineralization of particulate organic matter in the lower anoxic sediment layer produces soluble intermediates, which are quantified as diagenesis fluxes. The intermediates react in the upper oxic and lower anoxic layers, and portions are returned to the overlying water column as sediment fluxes. Computation of sediment fluxes requires mass-balance equations for ammonium, nitrate, phosphate, sulfide/methane, and available silica. Mass-balance equations are solved for these variables for both the upper and lower layers.

Table 1.2: HEM3D model water quality state variables

(1) Cyanobacteria	(12) Labile particulate organic nitrogen
(2) Diatom algae	(13) Dissolved organic nitrogen
(3) Green algae	(14) Ammonia nitrogen
(4) Refractory particulate organic carbon	(15) Nitrate nitrogen
(5) Labile particulate organic carbon	(16) Particulate biogenic silica
(6) Dissolved organic carbon	(17) Dissolved available silica
(7) Refractory particulate organic phosphorus	(18) Chemical oxygen demand
(8) Labile particulate organic phosphorus	(19) Dissolved oxygen
(9) Dissolved organic phosphorus	(20) Salinity
(10) Total phosphate	(21) Temperature
(11) Refractory particulate organic nitrogen	

CHAPTER 2: GENERAL CHARACTERISTICS OF MARYLAND COASTAL BAYS WATERSHED

2.1 Physical Setting

The Maryland Coastal Bays (MCBs) system is characterized as a coastal lagoon system linked to the Atlantic Ocean through two inlets: Ocean City inlet in the north, and Chincoteague inlet in the south. Tidal height is about 1 – 1.3 m at the Ocean City Inlet, 0.5-0.9 m in the Isle of Wight Bay, 0.3-0.5 m in the Assawoman Bay and only 0.1-0.3 m in the middle of Chincoteague Bay. Pritchard (1960) postulated that water entering the two inlets meets in the middle and runs back out the inlets, which explained the low tidal range in the northern Chincoteague Bay. The bays have depths ranging between 0.5 m – 3 m, with deepest portions reaching 10 m in the Inlets. The flushing rate has been estimated to be on the order of 10-30 days in the Northern Coastal Bays and 30-100 days in the Chincoteague Bay (Wang, Taiping, 2009). The MCBs are, in general, poorly flushed with non-stratified condition; thus nutrients and contaminants entering the bays tend to stay for a long period of time, especially in the Chincoteague Bay.

Water temperatures in the MCBs generally range from 5 to 29° C, with an annual average of 14° C. In the Northern Bays there is only a small horizontal gradient in temperature, while in the Chincoteague Bay the temperatures increase toward the confluence of Newport and Sinepuxent Bays until reaching Ocean City inlet. In the individual creeks, however, the temperature can exceed 32° C in the summer. Salinities in the Northern Bays generally decrease with distance from the Ocean City Inlet. The lower portion of the St. Martin River has high salinities whereas the upper, headwater regions and the tributaries can be fresh during the spring season, particularly in wet years. The Chincoteague Bay exhibits fairly high salinity throughout the year in the main stem of the Bay. There is a longitudinal gradient with salinities decreasing toward the confluence of Newport and Sinepuxent Bays. The sediments are mostly sandy on eastern side, silt within the channel, and sand/silt mix along the western shore. The region receives approximately 40 inches of precipitation annually and the watershed has traditionally been dominated by farming and forestry.

2.2 The terrestrial and atmospheric loading

The watershed approach adopted below is the logical basis for managing water resources environmentally. The important relationship between surface areas of water body and point source, non-point source, atmospheric, shoreline erosion loads on its watershed cannot be overemphasized. While point sources can have significant effects, nonpoint source pollutant inputs have increased in recent decades and have degraded water quality in many aquatic systems.

One of the uncommon characteristics of the Maryland Coastal Bays' watershed is that its watershed area is small relative to the water surface area of the receiving bays. Based on MDE report (1993), the overall average drainage area is only 1.7 times of the water surface area. For example, the individual basins' drainage areas and water surface areas are: 1.2, 7.7, 1.1, 8.6, and 0.7 for Assawoman Bay, Isle of Wight Bay,

Sinepuxent Bay, Newport Bay, and Chincoteague Bay respectively, as shown in Table 2.1. These ratios are much smaller than those in many estuarine systems. For example, the drainage area to water surface area ratio for the Chesapeake Bay is 14:1 (EPA Chesapeake Bay Program, 2009). This is especially true for Sinepuxent and Chincoteague Bays which have the smaller watershed to surface area ratios, and thus receive smaller runoff from their basins than do the other Coastal Bays. The rest of the section provides a summary of the sources of nutrient loading into MCBs, which includes (1) non-point source (2) point source (3) shoreline erosion, and (4) atmospheric deposition. For the detail of HSPF watershed modeling, see the companion report VIMS (2013).

Table 2.1: Drainage and water surface area (in acres) of the Maryland Coastal Bays

Coastal Bays	Drainage Area (DA)	Percent of Total DA	Water Surface Area (WSA)	Percent of WSA	Ratio of DA / WSA
Assawoman	6,094	5	5,174	8	1.2
Isle of Wight	36,184	32	4,697	7	7.7
Sinepuxent	6,602	6	5,958	9	1.1
Newport	27,945	25	3,262	5	8.6
Chincoteague	34,718	31	46,592	71	0.7
Total	111,543	100	65,681	100	1.7

2.2.1 Land use distribution

Pollutant loading from the watersheds to the MCBs is primarily a function of land use and land cover within the Bay's watershed. The land use in the Coastal Bays watershed is diverse. Land use information was derived from the Delaware Office of Planning Land Use Database (2002), Worcester County (Maryland) 2004 Land Use database (2009), and for Virginia, 1999 National Land Cover Data [United States Geological Survey (USGS) 1999]. The geographic distribution of the land uses are shown in Figure 2.1. The aggregated land use categories for the MCBs is shown in Table 2.2, which shows that forest and other herbaceous growth occupies 30%, mixed agriculture 29%, water: 26%, urban 12%, and barren or beaches 3%.

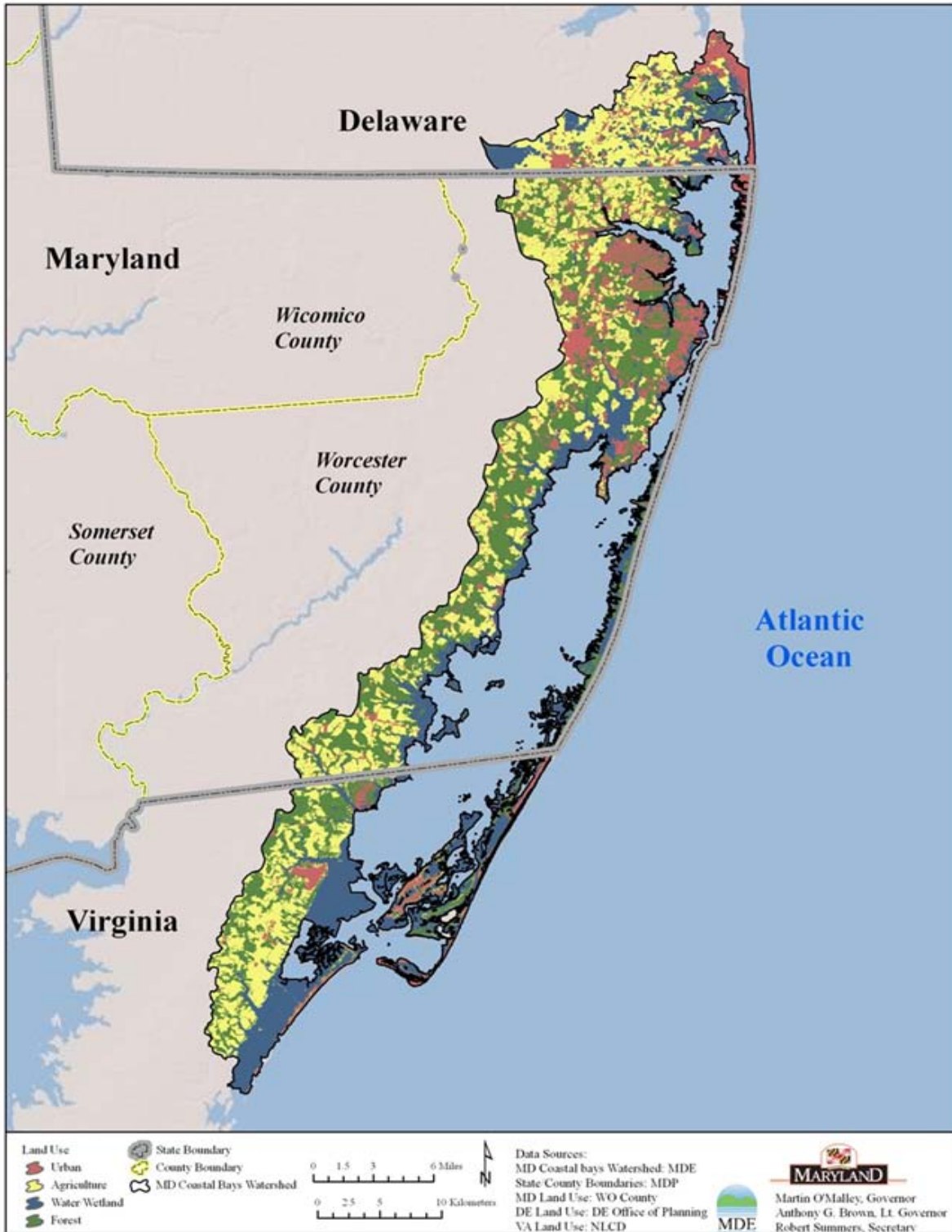


Figure 2.1: Land use distribution in the Maryland Coastal Bays watershed.

Table 2.2: Land use (in acres) for sub-watersheds in MCBs HSPF watershed model

Land use	Assawoman Bay	Isle of Wight Bay	Sinepuxent Bay	Newport Bay	Chincoteague Bay
FOREST	4350.53	12921.6	2340.34	11641.21	31565.53
NHI	2055.03	2368.97	91.78	1398.81	4090.4
NHO	346.23	399.12	15.46	235.67	689.14
NHY	223.37	257.5	9.98	152.04	444.61
NLO	7974.4	9192.64	356.16	5427.99	15872.51
HYO	569.6	656.62	25.44	387.71	1133.75
PAS	306.63	194.31	0	32.26	4850.05
BAR	596.51	823.7	883.99	328.58	3891.35
PERVIOUS	5369.82	6073.28	1335.42	2873.86	3281.46
AFO	594.31	134.57	0	0	28.61
IMPERVIOUS	1468.38	3164.36	502.32	1034.48	757.4
WATER	7766.41	4874.85	1881.66	4869.3	34963.44

2.2.2 Non-point source loading

Non-point source loads come from numerous wide-spread locations or sources that have no well-defined points of origin. These sources are widespread and more difficult to identify and quantify than point sources and, cumulatively, threaten water quality and natural systems. The effects caused by non-point sources differ significantly from those caused by the point sources in their distribution in time and space and often involve complex transport through soil, water, and air. Examples of non-point sources include runoff from urban (lawn care, parking lot, golf course, construction), agriculture (grassland, agriculture operations), pasture, natural forest, animal feeding operation, and septic tank through ground water. Most non-point sources are directly or indirectly driven by precipitation; thus, their loadings are inherently dynamic in nature. The carrier of the pollutants is water as the water runs through the watershed. Therefore, watershed processes involve detail hydrological description of the discharge of the water. From modeling point of view, obtaining the discharge from each of the watersheds is the first task to be carried out; their results required to be calibrated with known, measured gauge.

In the Maryland Coastal Bays, there are two USGS stream gauges used for the calibration: one in Birch Branch watershed and the other in Bassett Creek watershed. They were used for extensive calibration on flows, nitrogen, phosphorus and sediment loads. Because the Maryland Coastal Bays watershed has extensive animal feeding operations, the manure was an important source of non-point load and was estimated from agricultural census. To estimate the nutrient load from the septic tank, the database from 2000 US census for Virginia, Maryland and Delaware was used. The

final nonpoint source loading to the HEM3D water quality model is received from the HSPF watershed model developed by VIMS (Virginia Institute of Marine Science, 2013). For full details about the non-point source loading, please see Chapter 5 of the report entitled, “Maryland Coastal Bays Watershed Modeling Report” by VIMS dated February 2013.

2.2.3 Point-source loading

Point sources are discharges that can be traced back to a specific location at the end of a pipe. Examples include sewage treatment plants, industrial plants, livestock facilities etc. Point sources are regulated by state agency and EPA National Pollutant Discharge Elimination System (NPDES) for pollutants such as BOD, NH₄, TKN, suspended solids and coliform bacteria. In MCBs, point sources were not part of the calibration for the HSPF watershed model whose focus was mainly on the non-point source loads. To account for point sources loads, the point source facilities were incorporated as additional loads into the HEM3D water quality model. The major point sources in MCBs have four categories: (1) industrial facilities, (2) municipal facilities, (3) injection wells and (4) facilities using spray irrigation. The major industrial facilities in Maryland include: Perdue Farm Inc. - Showell Complex; Kelly Foods Corporation, Berlin Properties North, LLC, and Hudson/Tyson Foods. The major municipal facilities in Maryland are: Ocean Pines, Assateague Island National Park, Berlin WWTP, Newark WWTP and Ocean City WWTP, as shown in Table 2.3 (a). The major municipal facilities in Virginia are: US NASA Wallops flight facility, Sunset Bay utilities – South, US Coast Guard Group, Eastern Shore, Comfort Suite Hotel – Chincoteague, Hampton Inn and Suites, Sunset Bay Utilities –North, Chincoteague Landmark WWTP, Taylor landing, and Rays Shanty, as shown in Table 2.3 (b). As part of NPDES program, permit is issued by EPA and MDE that sets specific limits on the type and amount of pollutants these facilities can discharge into receiving waters. The detail of the permitted TN and TP concentration, design flow, and the permit TN and TP loads are presented in Tables 2.5 (a) and (b). A complete list of point source including all minor industrial and municipal facilities can be found in Chapter 6, Tables 16-21 of VIMS (2013).

Table 2.3 (a): Major point source facilities in Maryland with permits regulating the discharge of nutrients.

WS-model segment	MDE Permit #	NPDES #	Facility Name	Period	Flow	TN	TP	TKN	NH3	TN Load (lbs/yr)	TP Load (lb/yr)
					mgd	mg/l	mg/l	mg/l	mg/l		
Industrial Facilities											
187	95DP0051 A	MD00009 65	Perdue Farm, Inc. - Showell Complex	May-Oct	0.8	5	0.5		2	12176.4	1217.64
				Nov-Apr	0.8	5	0.5		5		
76	01DP0266	MD00013 09	Kelly Foods Corporation	May-Sep	0.02	18	0.6	10		1095.88	36.5292
				Oct-Apr	0.02	18	0.6				
76	96DP0375	MD00020 71	Berlin Properties North, LLC (Hudson/Tyson Foods)	May-Oct	0.8	4	0.5	4	2	9741.12	1217.64
				Nov-Apr	0.8	4	0.5		5		
Municipal Facilities											
36	05DP0708	MD00234 77	Ocean Pines WWTP	May-Oct	2.5	3	1.2			72,162	9,132
				Nov-Apr	2.5	16	1.2				
174	05DP2530	MD00210 91	Assateague Island WWTP	Jan-Dec	0.012	3	0.3			110	11
76	98DP0669	MD00226 32	Berlin WWTP	Apr-Oct	0	0	0			3,378	375
				Nov-Mar	0.6	4.5	0.5		0.5		
82	05DP0141	MD00206 30	Newark WWTP	Apr-Oct	0.07	18	3	8	2.3	3,836	639
				Nov-Mar	0.07	18	3	8	7.1		
outside	05DP0596	MD00200 44	Ocean City WWTP	Jan-Dec	14	18	3			767,113	127,852

Table 2.3 (b): Permitted point source facilities in Virginia

Facility Name ¹	Major/	Type	SIC Code	SIC Name	Outfall	Design Flow (mgd)	Estimated Avg. TN Conc. (mg/l)	Estimated Avg. TP Conc. (mg/l)	TN Limit (mg/l)	TP Limit (mg/l)	TN Load (lbs/yr)	TP Load (lbs/yr)
	Minor											
US NASA - Wallops Flight Facility ²	MINOR	Municipal	3769	Guided Missile and Space Vehicle	1	0.3	18.7	2.5	18.7	2.5	17154.3	2293.4
Sunset Bay Utilities - South ³	MINOR	Municipal	5812	Eating Places	1	0.0395	20	15	20	15	2415.7	1811.8
US Coast Guard Group - Eastern Shore ²	MINOR	Municipal	9621	Regulation & Administration of Transportation Programs	1	0.006	18.7	2.5	18.7	2.5	343.1	45.9
Comfort Suite Hotel - Chincoteague ³	MINOR	Municipal	7011	Hotels and Motels	1	0.009	20	15	20	15	550.4	412.8
Hampton Inn and Suites ³	MINOR	Municipal	7011	Hotels and Motels	1	0.01	20	15	20	15	611.6	458.7
Sunset Bay Utilities - North ³	MINOR	Municipal	8811	Private Households	1	0.025	20	15	20	15	1528.9	1146.7
Chincoteague Landmark WWTP ⁴	MINOR	Municipal	4952	Sewerage Systems	1	0.035	18.7	2.5	18.7	2.5	2001.3	267.6
Taylor Landing ³	MINOR	Municipal	7011	Hotels and Motels	1	0.012	20	15	20	15	733.9	550.4
Rays Shanty ^{3,5}	MINOR	Municipal	5812	Eating Places	1	0.0191	20	15	20	15	1168.1	876.1

¹Chincoteague Town WTP was eliminated from the analysis since it is a water supply, surface water discharge permit. Therefore, TN/TP concentrations are expected to be *de minimis*. Only TSS concentrations from the discharge would be of any significance.

²US NASA Wallops Flight Facility and US Coast Guard Group - Eastern are both federal facilities. TN/TP concentrations were estimated based on descriptions of the type of wastewater treatment at the facilities found in a spreadsheet of southeast Virginia treatment plants on VADEQ's website. Outfall 002 at US NASA Wallops Island did not need to be included in the analysis, since the discharge has been inactive since 1993, well before the model calibration time period.

³Estimated TN/TP concentrations associated with the wastewater treatment at these hotels/motels and eateries are based on monitored concentrations at similar facilities in Maryland.

⁴Estimated TN/TP concentrations associated with the municipal WWTP is based on Virginia's default Bay Phase I WIP value used for minor municipal facilities in order to characterize the loadings from these facilities, if they were missing data.

⁵The Design Flow for Ray's Shanty was missing from the Accomack County 2008 Comprehensive Plan Update, which was used to gather the design flows for all of the other facilities. Therefore, to estimate a flow for the facility, the average flow of the other hotel/motel and eatery facilities was applied.

⁶Average TKN weekly and monthly limits are identified within the actual permits for the facilities; however, no TN or TP limits are specified.

2.2.4 Shoreline erosion loading

An important component of the aquatic ecosystem is the sediments, which have a significant influence on both the biology and chemistry of the ecosystem. Sediment can either be suspended in a water column or settle and accumulate at the bottom of a water body. Total suspended sediments can influence water quality and eutrophication process through effects on density, light penetration, and nutrient availability. Through the adsorption-desorption process, it can also regulate the particulate and dissolved component of the chemical species. The sediments from bank loads serve as sources for pollutants. Bank loads are the solids, carbon, and nutrient loads contributed to the water column through shoreline erosion. The bank loads from shoreline erosion can act as a non-point source of nutrients (for TSS, nitrogen and phosphorus), which affect the water quality in the MCBs. In particular, many pollutants and nutrients introduced into the bays can accumulate and remain in the sediment beds which functions as a sink.

On the other hand, the sediments can act as a source of pollutants, either through remobilization of these pollutants by way of natural processes (i.e., diagenetic reactions), or by physical disturbance or mixing from the sediment bed. Maryland Geological Survey (MGS) have conducted a multi-year study to determine the flux of sediments and nutrients eroding from unprotected shorelines bordering Maryland's Coastal Bays. The volume of bank eroded material is quantified from comparison of topographic maps aided by aerial photos separated by time scales of many years. The erosion estimates are, consequently, averaged over periods of the years separated. Wells et al. (1998, 2002, and 2003) conducted surveys for northern Coastal Bays, middle Coastal Bays, and Chincoteague Bays respectively, in which a GIS template of irregular polygons was constructed section by section to determine total sediment, TN and TP loads. An example estimate of the shoreline erosion in the Northern Bays is shown in Figure 2.2, in which the historical shorelines dating from 1942 to 1989 was digitized, classified and inputs into GIS to compared the bank height and quantify losses due to erosion. Different stretches of shoreline erode at different rates. To account for this variability, MGS divided the study area shoreline into 18 segments and land loss polygon was assigned as a number, P#, in the template. Similar procedures for erosion rates were applied to the entire unprotected shoreline of the MCBs, which become part of source of the nutrient loads to the HEM3D water quality model. Table 2.4 shows the TN and TP erosion rate per unit length of shoreline for individual Bays, the total shoreline length for each of Bays, and thus the sum of the total TN and TP loads for the entire MCBs.

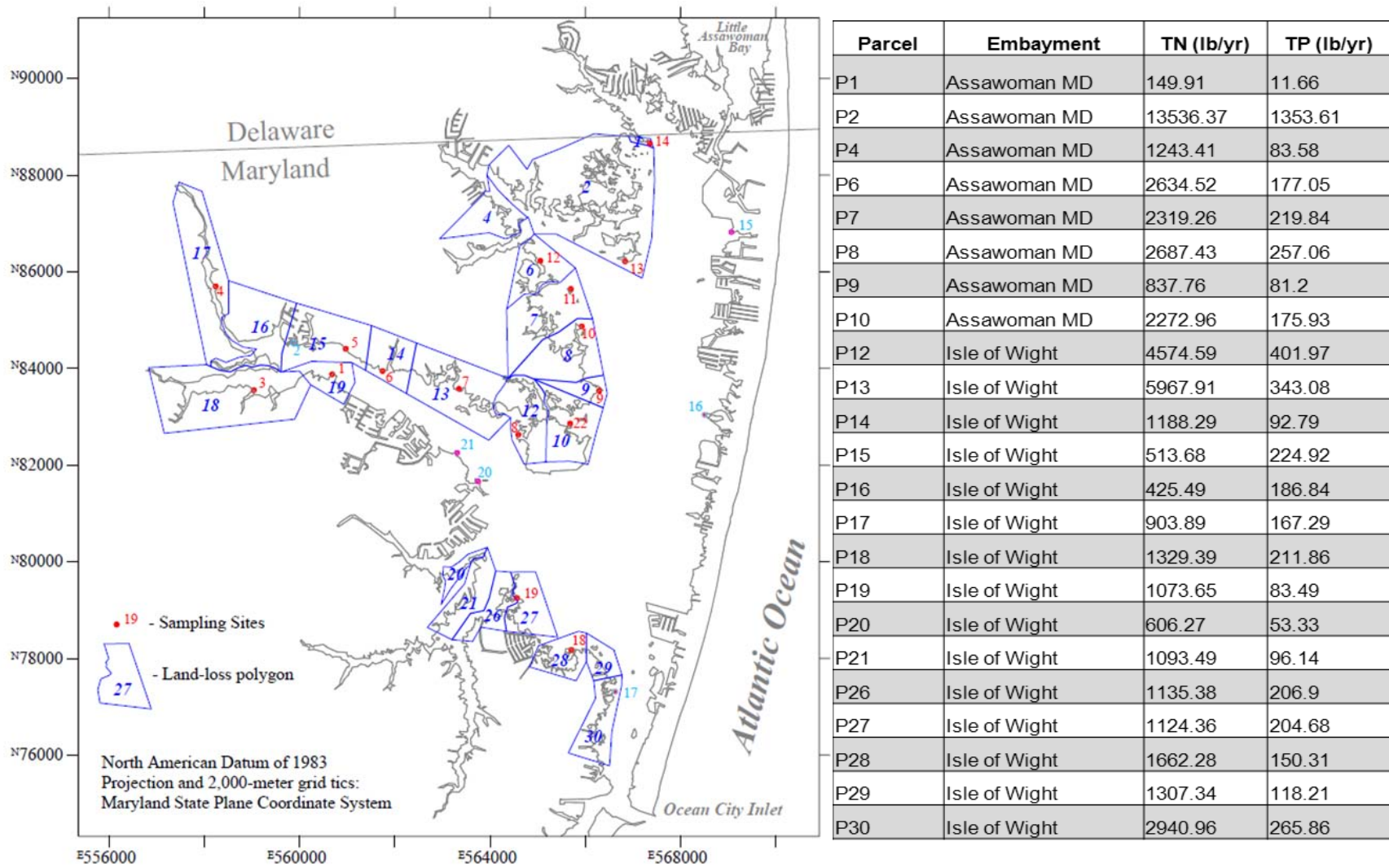


Figure 2.2: Locations of sampling sites (in red) and land loss polygons (in blue) in Assawoman and Isle of Wight Bays.

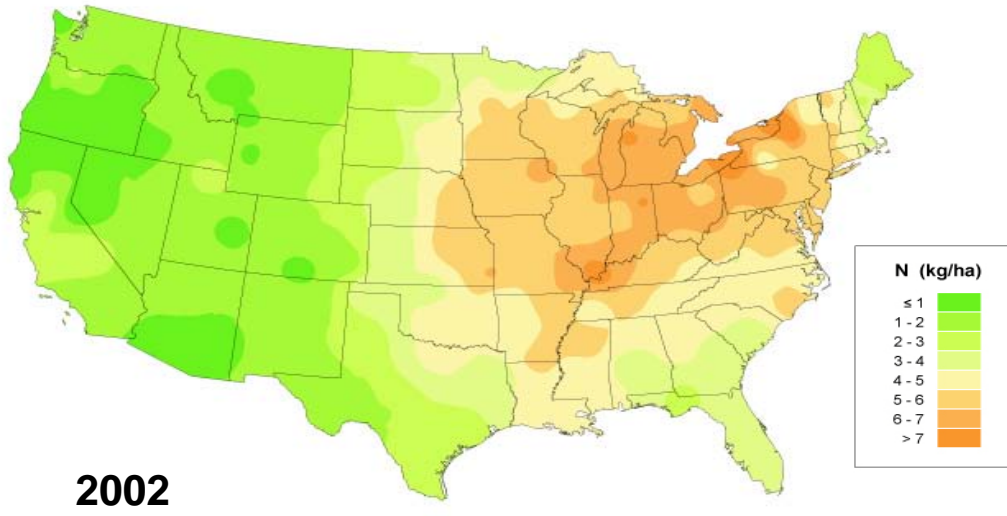
Table 2.4: TN and TP loads from shoreline erosion for individual bays and entire MCBs

Total Nitrogen	Erosion Rate	Shoreline Length (Model)	TN Erosion Load
from Individual Basin	lb/ft/yr	ft	lb/yr
Assawoman Bay in MD	0.0964	113270.01	10924.19
Isle of Wight Bay	0.2009	214437.16	19961.4
Sinepuxent Bay	0.0839	107994.33	9062.32
Newport Bay	0.1023	60790.22	6221.57
Chincoteague Bay	0.1829	796386.3	145659.05
Total Coastal Bays		1292878.03	191828.54
Total Phosphorus	Erosion Rate	Shoreline Length (Model)	TP Erosion Load
from Individual Basin	lb/ft/yr	ft	lb/yr
Assawoman Bay in MD	0.0089	113270.01	1003.42
Isle of Wight Bay	0.022	214437.16	2169.23
Sinepuxent Bay	0.0136	107994.33	1473.32
Newport Bay	0.0137	60790.22	830.55
Chincoteague Bay	0.0252	796386.3	20068.93
Total Coastal Bays		1292878.03	25545.47

2.2.5 Atmospheric loading

Atmospheric deposition is increasingly recognized as a significant external source of pollutants to surface waters. A pollutant from the air may be deposited into water bodies and affect water quality in these systems when pollutants are transferred from the air to the earth's surface (either land or water) by dry- and wet-weather periods as referred to as dry or wet deposition. Nutrients forms in precipitation are generally soluble and those in dry deposition are generally insoluble. Observations of wet depositions are frequently available through National Atmospheric Deposition Program (<http://nadp.sws.uiuc.edu/nadpdata/>). Atmospheric deposition of excess nitrogen can be a major contributor to eutrophication: increased primary production, algal blooms, and changes in algal community composition. Nitrogen deposited from the atmosphere can be a large percentage of the total nitrogen load. In the Chesapeake Bay, 21% of the nitrogen delivered to the Bay is from the atmosphere including both direct deposition to the Bay's water surface and deposition to the watershed that is later transported to the Bay as runoff. In the MCBs HEM3D water quality model, the atmospheric loads are part of the non-point source loads and the deposition on the land becomes part of the allocated load because the air deposition on the land becomes mixed with the nitrogen loadings from the land based sources and, therefore, becomes indistinguishable from land based sources. By contrast, the nitrogen deposition directly onto the MCBs' surface waters is a direct loading onto the surface water, and therefore needs to be linked directly to the HEM3D water quality model. This is especially important for MCBs, for their surface water areas relative to drainage areas are large. The time series of the dry and wet atmospheric deposition was obtained from U.S. EPA Chesapeake Bay Program Office (EPA-CBP) as a product of NOAA's airshed modeling (Grimm and Lynch, 2005). The atmospheric loading calculated by the airshed model was initially as an input for the HEM3D water quality model. It includes both wet and dry deposition for nitrogen and phosphorus. The annual averaged TN and TP loads from the airshed model are estimated as: 13 lb/acre and 0.57 lb/acre, respectively. However, the TN measurement at the Assateague Island NADP station was only reported only 4 - 6 lb/acre of annual atmospheric deposition (see Figure 2.3), which is a factor of 2 to 3 less, for the mid-Atlantic Bight region. It was recognized, however, that the observational measurements recorded only wet deposition. Given the uncertainty about the magnitude of the dry deposition and there being is no atmospheric TP measurement, it was determined that a median value of TN (7.42 lb/acre) and TP (0.37 lb/acre) would be more appropriate to be used as the atmospheric loading for the TMDL after consultation with the scientists and stakeholders in the Maryland Coastal Bays region. Although much less than EPA-CBP airshed modeling results, these loading rates were considered more consistent with the local measurement at Assateague NADP station. The time series for the atmospherically-derived TN and TP loading was thus adjusted down by a factor of 0.57 and 0.65 for TN and TP, respectively.

Inorganic Nitrogen Wet Deposition



Inorganic Nitrogen Wet Deposition

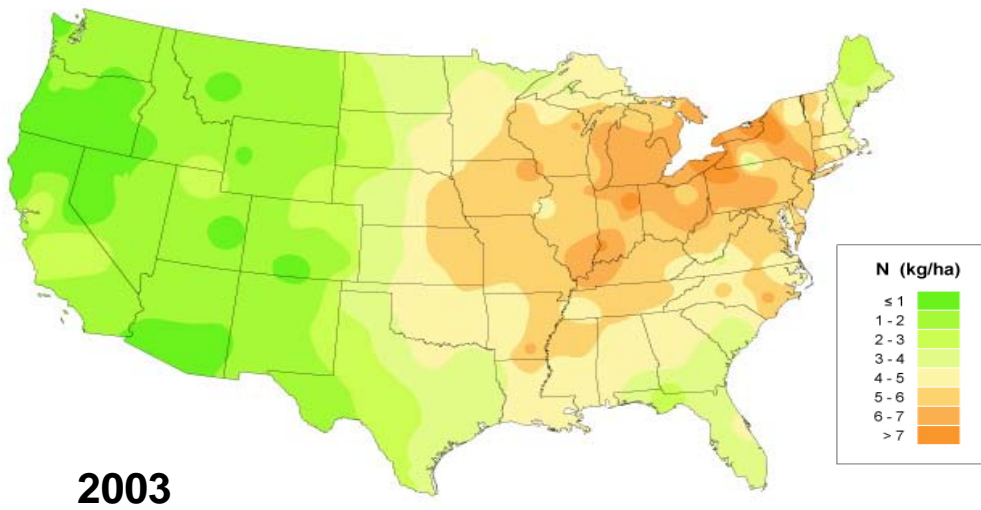


Figure 2.3: Wet deposition of inorganic nitrogen in 2002 and 2003 in the United States
(from National Atmospheric Deposition Program: <http://nadp.sws.uiuc.edu/>)

2.2.6 Discussion of Contributing Loads to the Maryland Coastal Bays

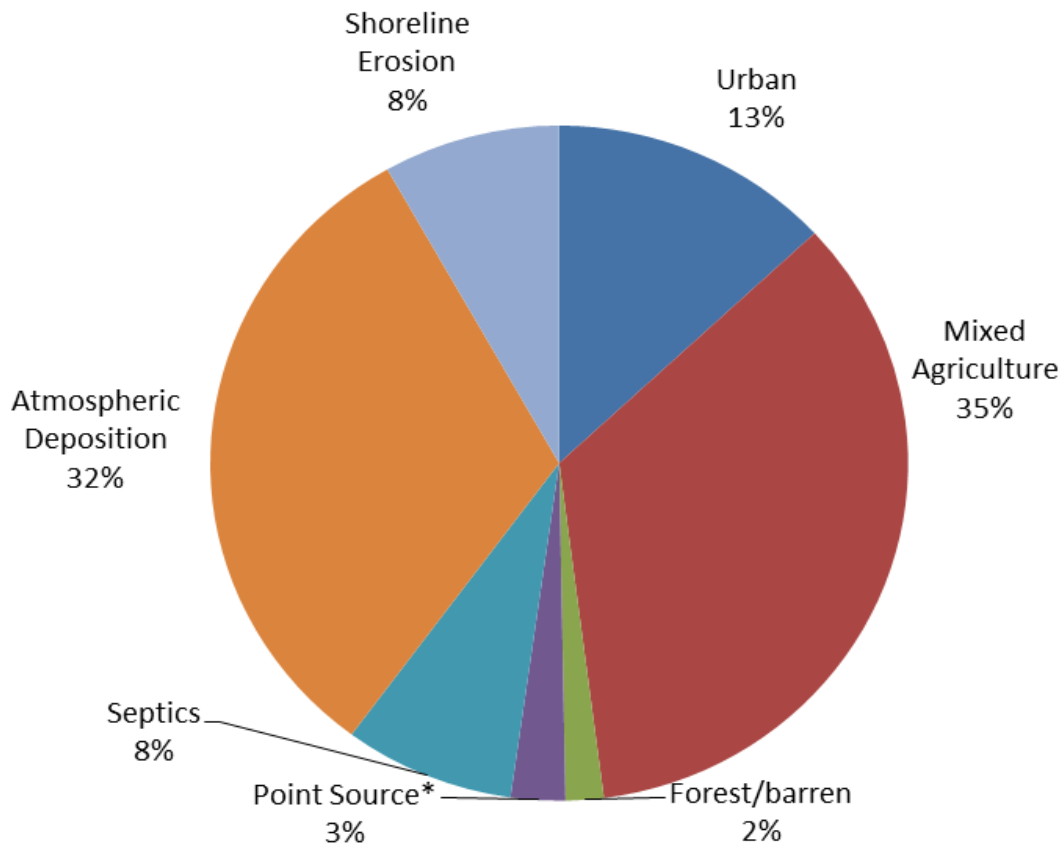
In the MCBs, the non-point source and atmospheric deposition loads are the two largest sources of total nitrogen and total phosphorus to the surface water of the MCBs. Figure 2.4 shows the nitrogen load distribution for the entire MCBs. The non-point source loads from various land uses (13% from urban, 35% from mixed agriculture, and 2% from forest and barren) of the watershed constitute 50% of the total; the atmospherically deposited loads 32%, shoreline erosion 8%, and septic tank 8%, and point source 3%. For the individual basins, the nitrogen load percentage varies significantly, which is shown in Figure 2.5. For example, Isle of Wight Bay has the largest non-point source contribution at 70% versus 12% from atmospheric deposition. In contrast, Chincoteague Bay, which has the largest water surface area to drainage area ratio, non-point source loads comprise 35% of the total, versus atmospheric deposition at 44%

Figure 2.6 depicts the phosphorus load distribution for the entire MCBs. The non-point source loads from various land uses (18% from urban, 34% from mixed agriculture, and 2% from forest and barren) of the watershed constitute 54% of the total; atmospherically deposited loads 23%, shoreline erosion 16%, septic loads 0%, and point source loads 7%. For the individual basins, again, the phosphorus load percentage varies significantly, which is shown in Figure 2.7. For example, Isle of Wight Bay has the largest non-point source contribution at 77% versus 9% from atmospheric deposition. In contrast, Chincoteague Bay, which has the largest water surface area to drainage area ratio, non-point source loads comprise 35% of the total, versus atmospheric deposition at 32%

Overall, the relative contribution of atmospheric and septic loads to the total phosphorus loads is less than that in the case of nitrogen, but the relative contributions of shoreline erosion and point source loads are greater. Table 2.5 further provides a synthesized temporal variation of TN and TP loads from 2001-2004 in which 2002 is the driest year and 2004 is the wettest year during the 4 year period. It can be seen that 2004 has the largest loading and 2002 the lowest, which is consistent with the characterization of wet hydrological year for the former and dry for the latter.

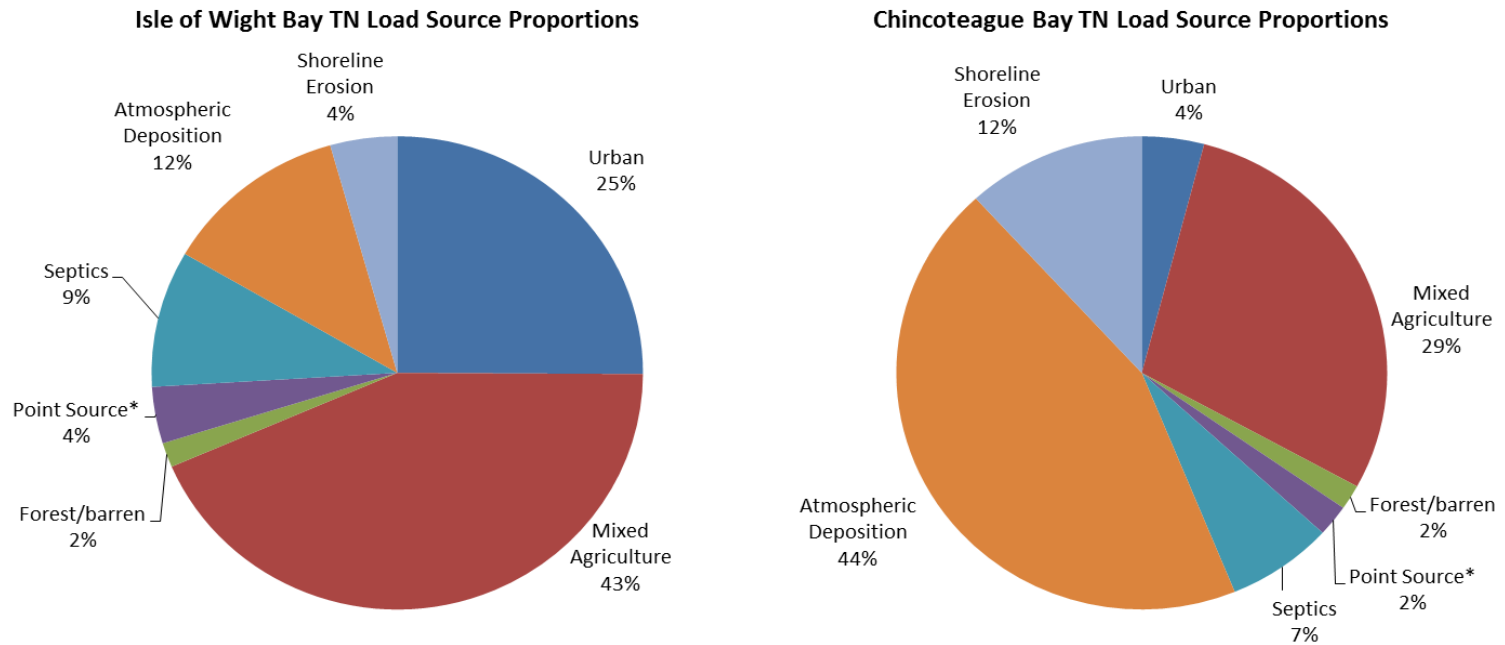
For both nitrogen and phosphorus loads, the point source sector represents a small portion of loads in contrast to the dominance of non-point source loads. Furthermore, based on the areal loading rate defined as the total loading divided by the total water surface area, it is clear that Isle of Wight sub-watershed has the largest TN and TP unit loads (per water surface water area), followed by Newport Bay and Assawoman Bay. The Sinepuxent and Chincoteague Bays have the lowest. This theme is in the same vein as that of drainage to surface water area ratio: the larger drainage area leads to larger non-point source loads. By contrast, a small drainage area to surface water area ratio leads to smaller non-point source load (relative to the water surface area), which is the case for Sinepuxent and Chincoteague Bays.

Entire MD Coastal Bays TN Load Source Proportions



Watershed	Urban	Mixed Agri.	Forest/barren	Point source	Septic tank	Atmos-Phere	Shoreline Erosion
Assawoman Bay	22%	48%	1%	0%	8%	18%	3%
Isle of Wight Bay	25%	43%	2%	4%	9%	12%	4%
Newport Bay	21%	43%	3%	7%	10%	14%	3%
Sinepuxent Bay	24%	7%	2%	1%	8%	48%	10%
Chincoteague Bay	4%	29%	2%	2%	7%	44%	12%
Entire MCBs	13%	35%	2%	3%	8%	32%	8%

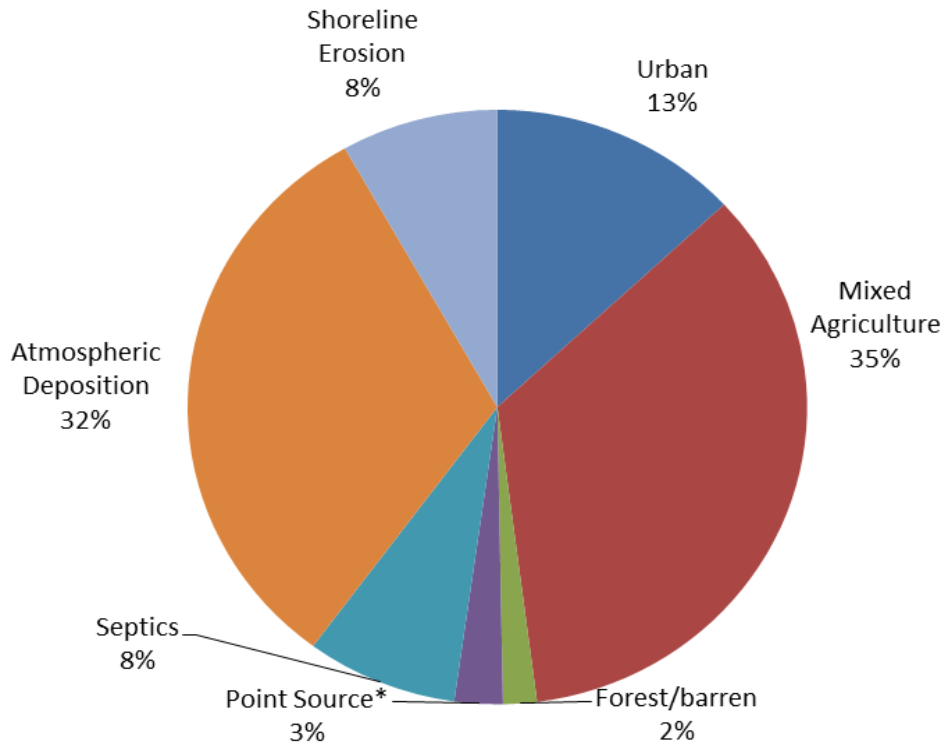
Figure 2.4: Total nitrogen load (percentage of total) from source sectors in individual MCBs



				TN-lb/y				
Watershed	Urban	Mixed	Forest/	Point Source*	Septic	Atmospheric	Shoreline	total
		Agriculture	Barren		Tanks	Deposition	Erosion	
Assawoman Bay	79,111	172,120	5,071	183	29,883	63,362	10,923	360,653
Isle of Wight Bay	106,633	184,675	7,123	16,459	39,672	51,901	18,729	425,192
Newport Bay	46,188	92,167	6,203	14,207	21,183	30,214	6,221	216,382
Sinepuxent Bay	21,662	6,054	1,671	1,220	6,971	43,396	9,064	90,037
Chincoteague Bay	50,562	356,197	20,934	26,507	86,358	547,573	145,725	1,233,856
Entire MCBs	304,155	811,212	41,001	58,576	184,066	736,446	190,664	2,326,120

Figure 2.5: Total nitrogen loading from source sectors in individual MCBs (lbs/year).

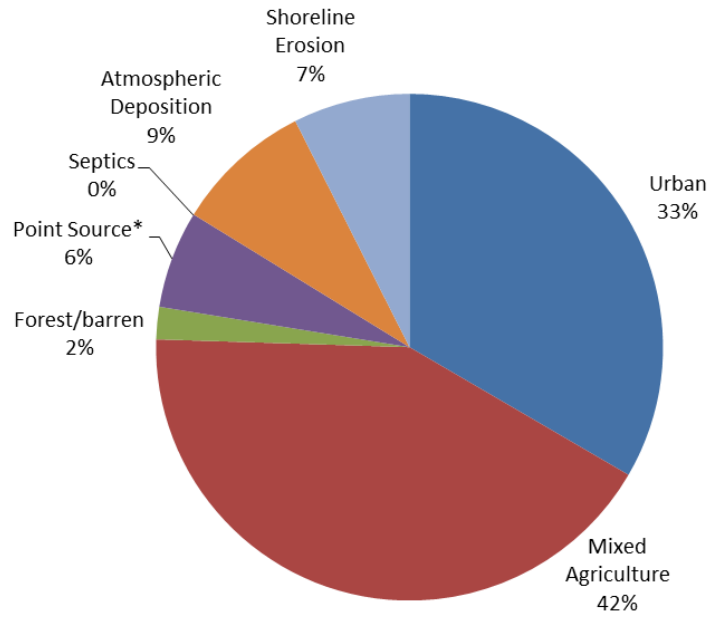
Entire MD Coastal Bays TN Load Source Proportions



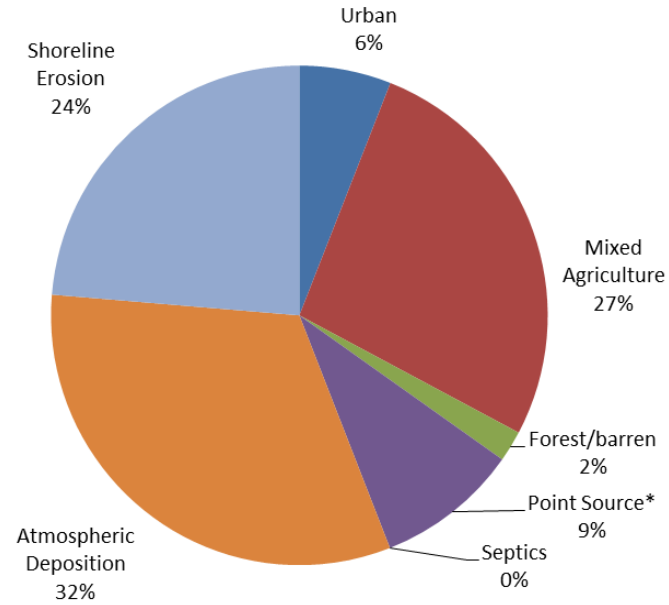
Watershed	Urban	Mixed Agri.	Forest/ barren	Point source	Septic tank	Atmos- phere	Shoreline erosion
Assawoman Bay	31%	50%	2%	0%	0%	13%	4%
Isle of Wight Bay	33%	42%	2%	6%	0%	9%	7%
Newport Bay	31%	41%	4%	8%	0%	11%	6%
Sinepuxent Bay	33%	6%	2%	0%	0%	35%	24%
Chincoteague Bay	6%	27%	2%	9%	0%	32%	24%
Entire MCBs	18%	34%	2%	7%	0%	23%	16%

Figure 2.6: The total phosphorus load (percentage of total) from source sectors in individual MCBs.

Isle of Wight Bay TP Load Source Proportions



Chincoteague Bay TP Load Source Proportions



	TP-lb/y								
Watershed	Urban	Mixed Agriculture	Forest/ barren	Point Source*	Septic Tanks	Atmospheric Deposition	Shoreline Erosion		total
Assawoman Bay	7,376	11,939	433	0	0	3,167	1,008		23,924
Isle of Wight Bay	9,861	12,427	607	1,837	0	2,594	2,196		29,523
Newport Bay	4,407	5,927	529	1,081	0	1,510	833		14,287
Sinepuxent Bay	2,060	388	143	0	0	2,169	1,469		6,229
Chincoteague Bay	5,069	22,727	1,704	7,863	0	27,367	20,078		84,809
Entire MCBs	28,773	53,409	3,415	10,781	0	36,807	25,585		158,771

Figure 2.7: Total phosphorus load from source sectors in individual MCBs (lbs/year)

Table 2.5: Total baseline nitrogen and phosphorus loads (lbs/year), MD Coastal Bays 2001-2004.

2001 Region	Base load (lbs)	
	TN	TP
Assawoman Bay in MD	165000	10244
Isle of Wight Bay	192341	11457
Newport Bay	19879	1153
Sinepuxent Bay	93128	5361
Chincoteague Bay	374389	23296
MD Coastal Bays	844737	51511

2002 Region	Base load (lbs)	
	TN	TP
Assawoman Bay in MD	123513	7567
Isle of Wight Bay	149140	8961
Newport Bay	19291	1103
Sinepuxent Bay	60761	3365
Chincoteague Bay	167866	8622
MD Coastal Bays	520571	29618

2003 Region	Base load (lbs)	
	TN	TP
Assawoman Bay in MD	356218	29179
Isle of Wight Bay	408905	33439
Newport Bay	37903	3714
Sinepuxent Bay	199635	16155
Chincoteague Bay	547000	39133
MD Coastal Bays	1549661	121620

2004 Region	Base load (lbs)	
	TN	TP
Assawoman Bay in MD	382076	36386
Isle of Wight Bay	436454	40446
Newport Bay	41285	4933
Sinepuxent Bay	221706	19972
Chincoteague Bay	598565	46262
MD Coastal Bays	1680086	147999

2.3 Data to Support the Water Quality Modeling

The calibration and verification of a coupled 3-D hydrodynamic and water quality modeling system requires sufficient field observation data to quantify an acceptable level of verification such that confidence is established for use of the modeling system for evaluating various load and waste load allocation scenarios. The tidal data obtained from the tidal gauge station, used for water level calibration in the hydrodynamic model is maintained by USGS at the Ocean City Inlet. The USGS gauge stations in the Birch Branch and Bassett Creek were used for generating non-point source flow as the hydrological inputs. The weather data including wind, cloud cover and precipitation, were obtained from Ocean City Municipal Airport. The topographic data and the shoreline erosion data were provided by Maryland Geological Survey. Table 2.6 summarizes all the monitoring program and observation data which support the hydrodynamic and water quality modeling.

The Coastal Bays Eutrophication Monitoring Program, led by Maryland Department of Natural Resources (DNR), is a cooperative program between State and federal agencies as well as Universities, which started to measure a variety of ecosystem variables and indices in 2001. The monitoring data collected in the Coastal Bays are used to assess the conditions of natural resources and to track the trend changes over time. The information is vital for evaluating the progress of management actions aimed at restoring the Coastal Bays and their tributaries, for determining attainment of water quality criteria and for providing guidance on future actions. Monitoring data are also used for research and for the calibration and verification of the model in the MCBs ecosystem. There is a network of twenty-seven (27) fixed stations routinely monitored by DNR, of which twenty (20) stations are in the Northern Bays and seven (7) in the Southern Bays of the MCBs as shown as DNR stations in Figure 2.8. The major water quality parameters collected once a month include: salinity, temperature, dissolved oxygen, chlorophyll-a, total nitrogen, total phosphorus, dissolved organic carbon, TSS, Secchi depth, ammonia, nitrate, phosphate, and silica, which are used for water quality model calibration and verification. In addition, the National Park Service, Assateague Island (ASIS) has maintained eighteen (18) stations in the Sinepuxent, Newport and Chincoteague Bays, shown as ASIS stations in Figure 2.8. The frequency that ASIS collected is similar to DNR stations, but the parameters, analytical methods and the vertical profile are slightly different. Each of these data sources was useful in the model development and verification processes. In a bay-wide comparison of surface and bottom water quality parameters with model results, both DNR and ASIS data were used. On the other hand, for the southern Bay investigation, beside only ASIS has data coverage in Sinepuxent Bay, DNR data was strictly located in the middle channel, while ASIS data has the coverage on both eastern and western side of the Bay. On an investigation in the Northern Bays, such as Saint Martin River, DNR data provided the monthly DO data from 2000-2004 continuously, as shown in Figure 2.9, which showed severe hypoxia in several of the stations in the Saint Martin Rivers particularly for 2003, 2004 and 2005. In the Southern Bays, the combined ASIS and DNR stations showed a minor hypoxia problem in XCM4878, as shown in Figure 2.10, which was quite different from those seen in the Isle of Wight Bay. The monitoring data was further integrated in a broad basis for assessing nutrient impacts in the Maryland Coastal Bays. The DNR and

ASIS monitoring program are a great asset to the Maryland Coastal Bays; combined they provided the scientific basis for safeguarding the health of the Bay.

Table 2.6: Summary of data supporting the hydrodynamic and water quality modeling.

Data type	Source	Modeling Support
1. Water quality fixed station monitoring data	MDDNR	Water quality model
2. Water quality data at Chincoteague Bay	ASIS	Water quality model
3. DATAflow high frequency data	MDDNR	Diel cycle adjustment
4. Topographic data	MGS (Maryland Geological Survey)	Hydrodynamic model
5. Wind field data	Ocean City municipal airport	Hydrodynamic model
6. PAR (Photosynthetic Active Radiation) data	University of Maryland	Phytoplankton dynamics
7. Stream gauge data	USGS	Hydrodynamic/water shed model
8. Precipitation and cloud cover	Ocean City Municipal airport	Watershed model
9. ADCP current meter data	University of Maryland	Hydrodynamic model
10. Water quality open boundary condition	EPA region III	Water quality model
11. Airshed atmospheric deposition	EPA Chesapeake Bay Program	Water quality model
12. Point source data	MDE (MD Dept. of the Environment)	Watershed model
13. Non-point source data	MDE	Watershed model
14. shoreline erosion data	MGS	Water shed model



Figure 2.8: Station location for DNR and ASIS monitoring program in MCBs

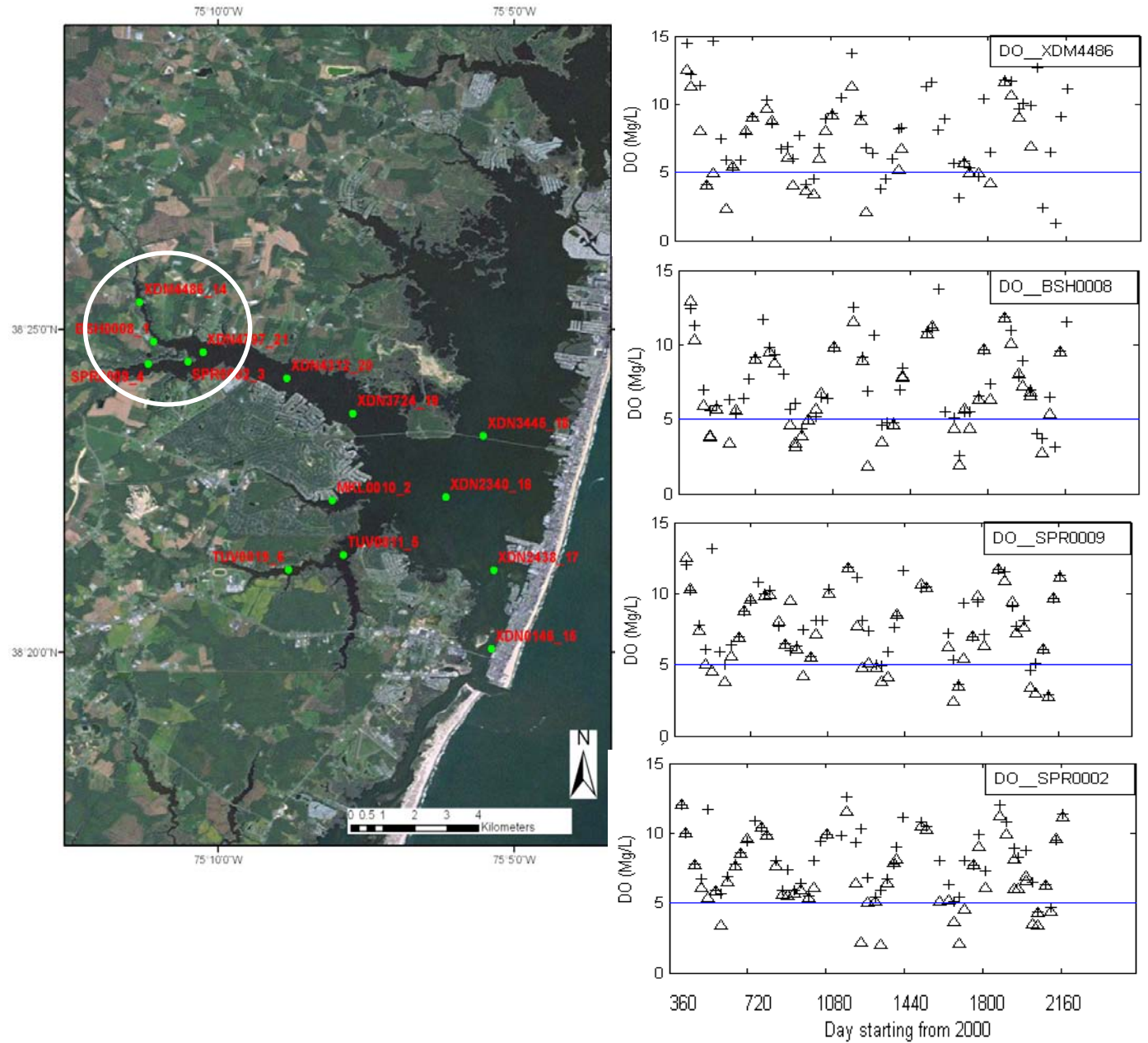


Figure 2.9: DNR monthly DO data from stations in Saint Martin River (2000-2004)

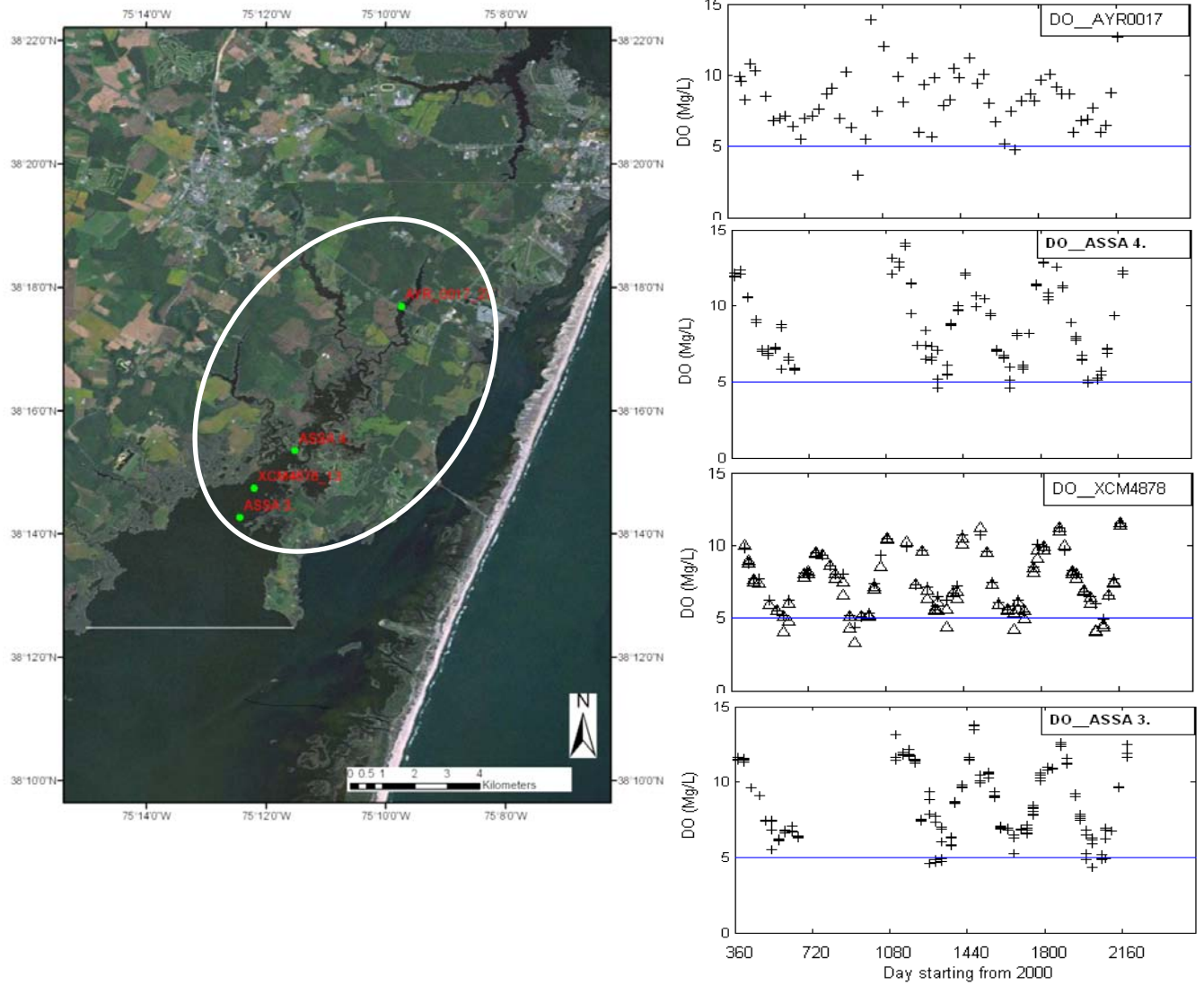


Figure 2.10: Combined DNR and ASIS monthly DO data from stations in Newport Bay (2000-2004)

CHAPTER 3: THE THREE-DIMENSIONAL HYDRODYNAMIC MODEL

Hydrodynamics is the study of fluid in motion; specifically, the motion and the force acting on water. In this project, the hydrodynamic model of Maryland Coastal Bay provides the water velocities, tidal elevation, circulation patterns as well as temperature, salinity, density stratification, and dispersion to drive the eutrophication model. Hydrodynamic processes are an integrated component of the complex ecosystem of the MCBs, which is essential to provide the transport and mixing mechanism for ecological variables.

3.1 Model description

The MCBs are characterized as a system of coastal lagoons connected to the Atlantic Ocean by two inlets: Ocean City Inlet in the north and the Chincoteague Inlet in the south. In order to simulate the MCBs hydrodynamics properly, the model must be able to resolve the two narrow inlets accurately. Among different models, the finite element model uses unstructured, triangular grids and has the advantage that its grid resolution can be flexibly refined in a local region while preserving coarse resolution elsewhere, thus is most suitable model for inlets in systems such as the MCBs. Due to this reason, the Semi-implicit, Eulerian, Lagrangian, Finite Element Model (SELFE) was selected to model hydrodynamics in the MCBs. SELFE is a multifunctional surface water hydrodynamic model which can be coupled with surface wave, sediment transport, and eutrophication models, and is currently maintained at Virginia Institute of Marine Science as a COASTAL OCEAN community model:

http://ccrm.vims.edu/w/index.php/About_SELFE

The SELFE model, depending on its application, can be set up for use in 1-, 2-, and 3-dimension applications. The model utilizes an unstructured triangular grid in the horizontal and hybrid terrain-following S-Z coordinates in the vertical. It uses an efficient semi-implicit time stepping in conjunction with an Eulerian-Lagrangian method (ELM) to treat the advection. As a result, numerical stability is greatly enhanced and errors from the “mode splitting” method are avoided; in fact, the only stability constraints are related to the explicit treatment of the horizontal viscosity and baroclinic pressure gradient, which is much milder than the stringent CFL (Courant, Friedrichs, and Lewy) condition. The default numerical scheme is 2nd-order accurate in space and time, but optional high-order schemes have been developed as well [e.g., the dual Kriging ELM proposed by LeRoux et al., (1997)]. The model also incorporates wetting and drying naturally as part of the semi-implicit scheme, and has been rigorously benchmarked for inundation problems such as tsunami and storm surge simulation (Zhang et al. 2011; NTHMP 2011). As an open-source community-supported model, SELFE has been well demonstrated to be accurate, efficient, robust and flexible, with a wide range of applications from general circulation (Brovchenko et al. 2011), tsunami inundation (Zhang et al. 2011), storm surge (Bertin et al., 2012), ecology (Rodrigues et al. 2009), oil spill (Azevedo et al. 2009), and water quality studies. Details of the SELFE model’s hydrodynamic capabilities are provided in Appendix A.

3.2 Model set-up

The general procedure for the application of the SELFE model in the MCB follows a sequence of steps beginning with model set-up. Model set-up involves (1) the construction of a horizontal triangulated grid of the water body; (2) interpolation of bathymetric data to the grid; (3) generation of the initial and boundary conditions (4) construction of SELFE input files, (5) selection of model parameters and (5) compilation of the paralleled source code with the appropriate computer platform to execute the application. The SELFE input files include the master input file (param.in), files specifying the grid and bathymetry (hgrid.gr3 and vgrid.in), atmospheric forcing files (wind.th and sflux), inflow-outflow file (flux.th), salinity and temperature boundary condition, inflow concentration files (salt.ic and temp.ic), and a hotstart input file (hotstart.in).

The horizontal grid for the MCBs used unstructured, horizontal triangular grid cells and was constructed using a utility tool: xmgredit. Figure 3.1 shows the grid of the entire MCBs model region from Assawoman Bay to Chincoteague Bay including the Ocean City and Chincoteague Inlets, and the surrounding inner continental shelf. The horizontal grid has 12,428 active cells, of which 8,348 are inside the MCBs and 4,080 are in the coastal ocean. The horizontal coordinate system used by the model is a localized UTM system. The water depth data collected by the Maryland Geological Survey (MGS) was interpolated to the horizontal model grid using an arithmetic average of all data points falling within a specific cell. The bathymetry of MCBs presented in Figure 3.2 (using mean sea level as datum) shows most of the bay is shallower than 3 m except near the inlet where it can reach 10 m. The model vertical grid utilizes 5 sigma layers and has varying thicknesses throughout the horizontal model domain.

3.3 Hydrodynamic model forcing functions

Hydrodynamics in the MCBs model are forced by a tidal open boundary at the inner continental shelf (about 10 km offshore), the point and non-point source inflows inland, and the local wind surface wind stress. The hourly tidal elevation open boundary condition was obtained from the interpolation of NOAA's observed water level at Ocean City Inlet and Wachapreague, VA. The monthly salinity and temperature was applied at the Open boundary condition. Inflows include the upstream river inflow calculated from the HSPF model at the following Creeks: Greys Creek, Bishopville Prong, Shingle Landing Prong, St. Martin River, Herring Creek, Turville Creek, Manklin Creek, Ayer Creek, Newport Creek and Marshall Creek. The Ocean City WWTP has two outfalls and was designed for a total of 32 MGD capacity with one for 20 MGD and the other 12 MGD. These outfalls are at 10 m depth in a distance about 1.4 km from shore and within the model's boundary. The discharge rate provided by the Ocean City Public Works was used as an inflow discharge.

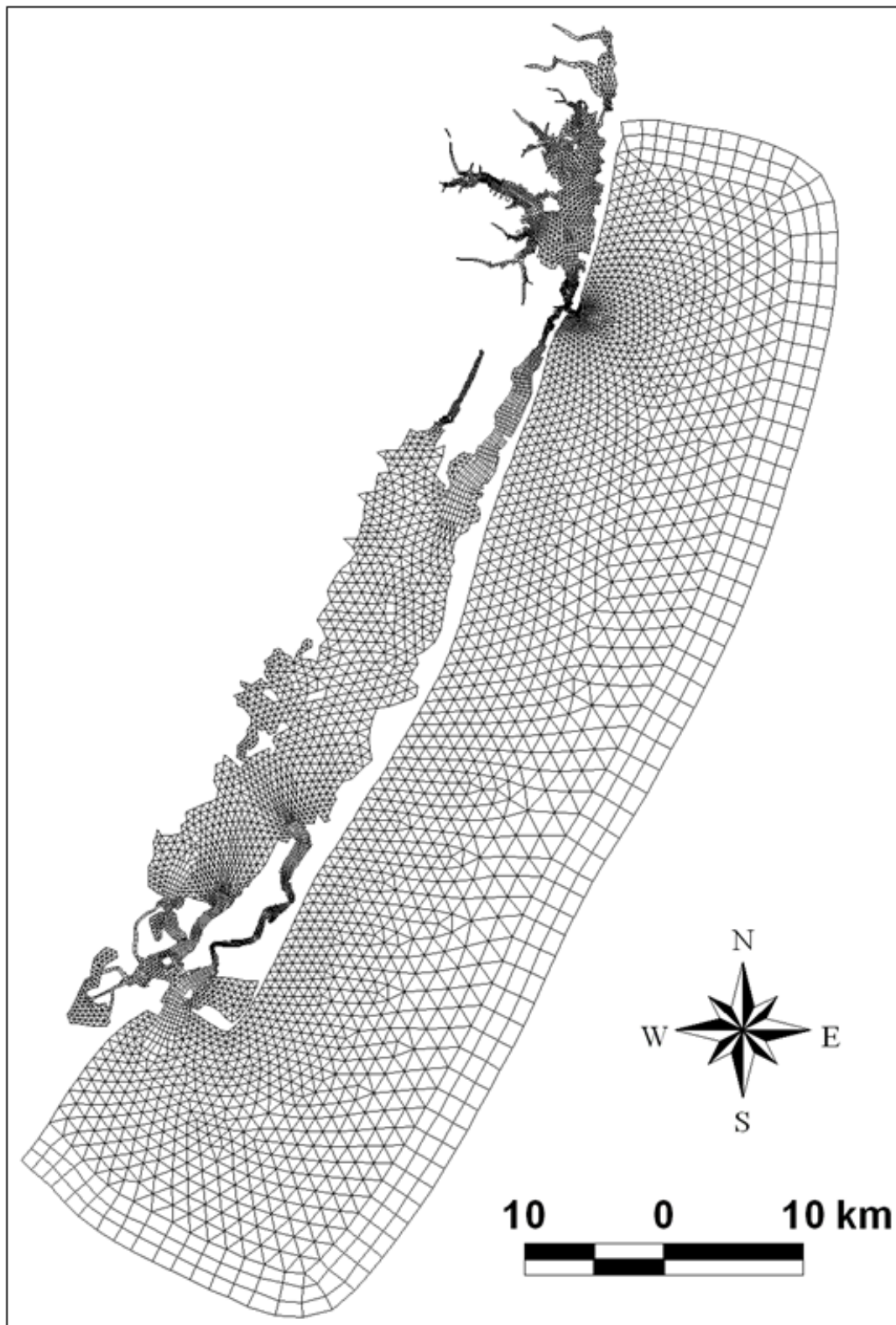


Figure 3.1 Hydrodynamic model grid in the Maryland Coastal Bays (MCBs).

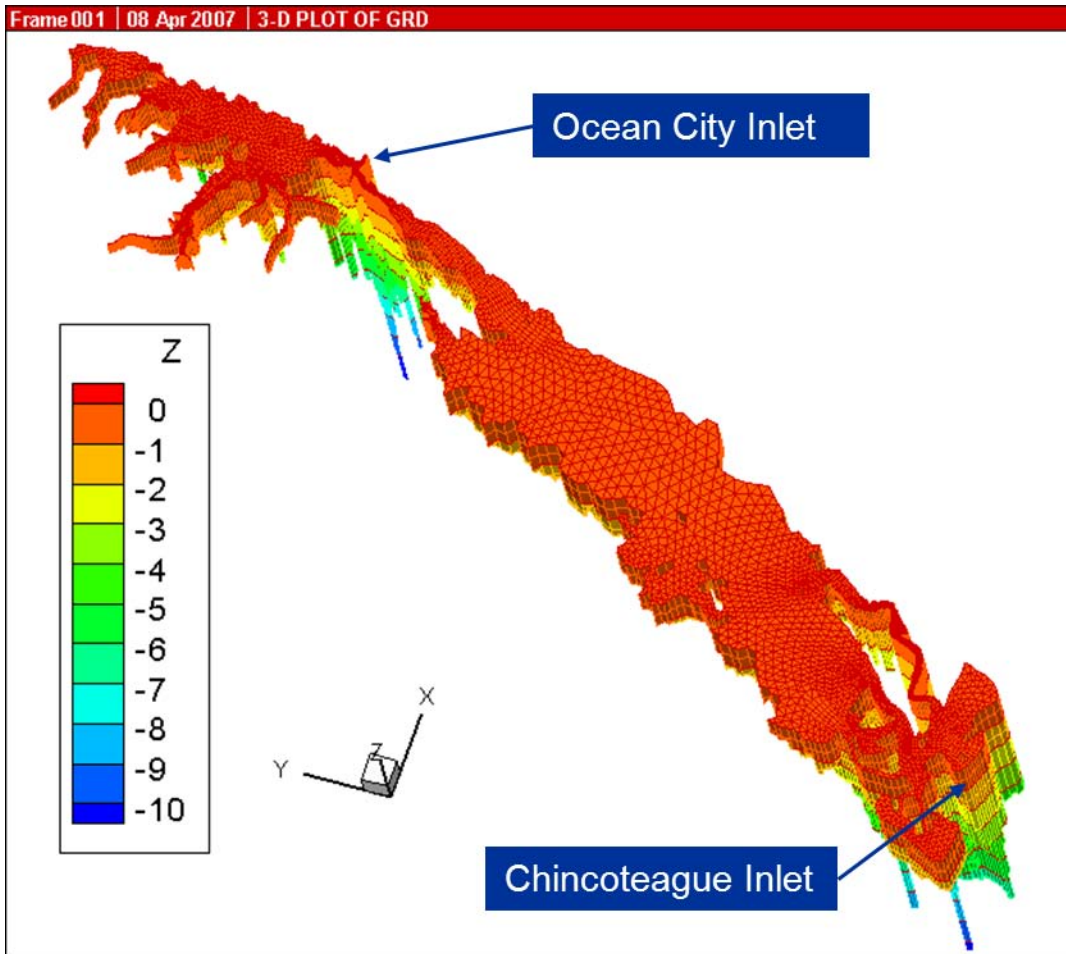


Figure 3.2: Bathymetry for the Maryland Coastal Bays

Atmospheric forcing functions for the model were developed from National Climatic Data Center (NCDC) records from Ocean City Municipal Airport and included wind speed and direction, atmospheric pressure, air temperature, relative humidity, rainfall, and cloud cover at approximately hourly intervals. Wind speed and direction are used internally in the model to provide surface wind stress forcing, while wind speed is used in the prediction of water surface latent and sensible heat exchange. Wind speed at 10 meter height is also used in determination of surface reaeration rates in the eutrophication component of the model. Wind speeds were internally adjusted in the model using input directional sheltering coefficients determined during the calibration.

All model forcing data were assembled for a 4 year period spanning 2001 through 2004. Initial conditions for the hydrodynamic model included a constant water surface elevation corresponding to mean water level, the water temperature and salinity representative of early January 1999. The model was initialized for the entire year of 2000, and the results saved and used as the initial condition of the year 2001.

3.4 Hydrodynamic model calibration

The MCBs hydrodynamic model was calibrated for water level, current velocity, and salinity by comparing model simulation results with field measurements. The calibration was an iterative process, and parameters for bottom friction and stability function (inside the turbulence closure model) were adjusted to produce reasonable tidal elevation and stratification results. Once calibrated, the parameters were not changed and the model was validated with results from runs in different years. The field observation stations and the locations for current, wave level and salinity were shown in Table 3.1, and the map of the field observation stations for water elevation, currents, and salinity in the MCBs is shown in Figure 3.3.

3.4.1 Water level calibration

There is only one permanent active water level monitoring station maintained by National Oceanic and Atmospheric Administration (NOAA) at Ocean City Inlet, MD, (NOAA Station #08570283) inside the MCBs. In order to have enough coverage of different tidal conditions in the MCBs, the astronomical tidal prediction result produced by XTIDE (<http://tbone.biol.sc.edu/tide/index.html>) was used to characterize the spatial variability of the tidal range (shown at station W1-W11 in Table 3.1). The tide generated by XTIDE is solely the astronomical tide, which does not include effects of meteorology condition such as pressure and wind stress on water level. To calibrate surface elevation changes induced by astronomical tides, the SELFE model was run in a two-dimensional vertically integrated mode. The model calculations results of tidal elevation were compared with XTIDE predictions at nine stations, as shown in Figure 3.4 (a) - (c), throughout the MCBs. The model results match XTIDE predictions very well except for the station at Assateague Beach at Tom's Cove (see Figure 3.4 (b)) where the model under-predicted the tidal range. Considering from shoreline data collected which showed around this area is continuously changing, the under-prediction is probably due to the inaccuracy of the local geometry at this station as represented in the model. Similar to many inlet systems, the tidal signal dampens quickly as it propagates from the coastal ocean into the inlets. In the MCBs, the tidal range decreases significantly from the regions outside the inlets in the Atlantic Ocean (~1.6 m) to less than 0.2 m at the Public Landing Station, located in the Northern Chincoteague Bay as shown in Figure 3.4 (c). In contrast, Figure 3.4 (a) shows the M2 tidal range from the coastal ocean into the Ocean City inlet. Tidal range also show similar decrease trend from coastal ocean into the inlet, but the magnitude of the decrease is less than that in the southern portion of the MCBs. Along the transect from Chincoteague in the south and Sinepuxent Bays in the north, the semi-diurnal tidal amplitude show a bi-model features with lowest amplitude about 0.1 m at the public landing and highest amplitude at Chincoteague and Sinepuxent at about 0.5 m. The M2 tidal phase, on the other hand, shows a uni-model distribution with the highest phase at about 150 degree in the public landing.

Table 3.1: Description and location of field observation stations for current, water level and salinity in the MCBs.

Station ID	Name	Type	Source	Latitude	Longitude
C1	Isle of Wight Bay Channel	Current	MDNR	38.3311	-75.0920
C2	Sinepuxent Bay Channel	Current	MDNR	38.3237	-75.1001
C3	Chincoteague Bay Inlet	Current	MDNR	37.8826	-75.4142
W1	Ocean City (Fishing Pier)	Water Level	XTIDE	38.3267	-75.0833
W2	Ocean City Inlet	Water Level	XTIDE, NOAA	38.3283	-75.0917
W3	Ocean City (Isle of Wight Bay)	Water Level	XTIDE	38.3317	-75.0900
W4	North Beach Coast Guard Station	Water Level	XTIDE	38.2000	-75.1500
W5	Assateague Beach, Toms Cove	Water Level	XTIDE	37.8667	-75.3667
W6	Wishart Point, Bogues Bay	Water Level	XTIDE	37.8817	-75.4917
W7	Wallops Island	Water Level	XTIDE	37.8417	-75.4783
W8	Harbor of Refuge	Water Level	MGS	37.9033	-75.4067
W9	Public Landing	Water Level	XTIDE,	38.1483	-75.2850
W10	South Point, Sinepuxent Neck	Water Level	MGS	38.2150	-75.1917
W11	Turville Creek	Water Level	MDNR	38.3554	-75.1499
S1	XDN2438	Salinity	MDNR	38.3546	-75.0891
S2	XDN6454	Salinity	MDNR	38.4417	-75.0775
S3	XDN7261	Salinity	MDNR	38.4528	-75.0639
S4	XDN5737	Salinity	MDNR	38.4283	-75.1050
S5	XDN4312	Salinity	MDNR	38.4041	-75.1473
S6	TUV0011	Salinity	MDNR	38.3585	-75.1314
S7	XCM4878	Salinity	MDNR	38.2457	-75.2033
S8	XCM0159	Salinity	MDNR	38.1682	-75.2369
S9	XBM1301	Salinity	MDNR	38.0215	-75.3332

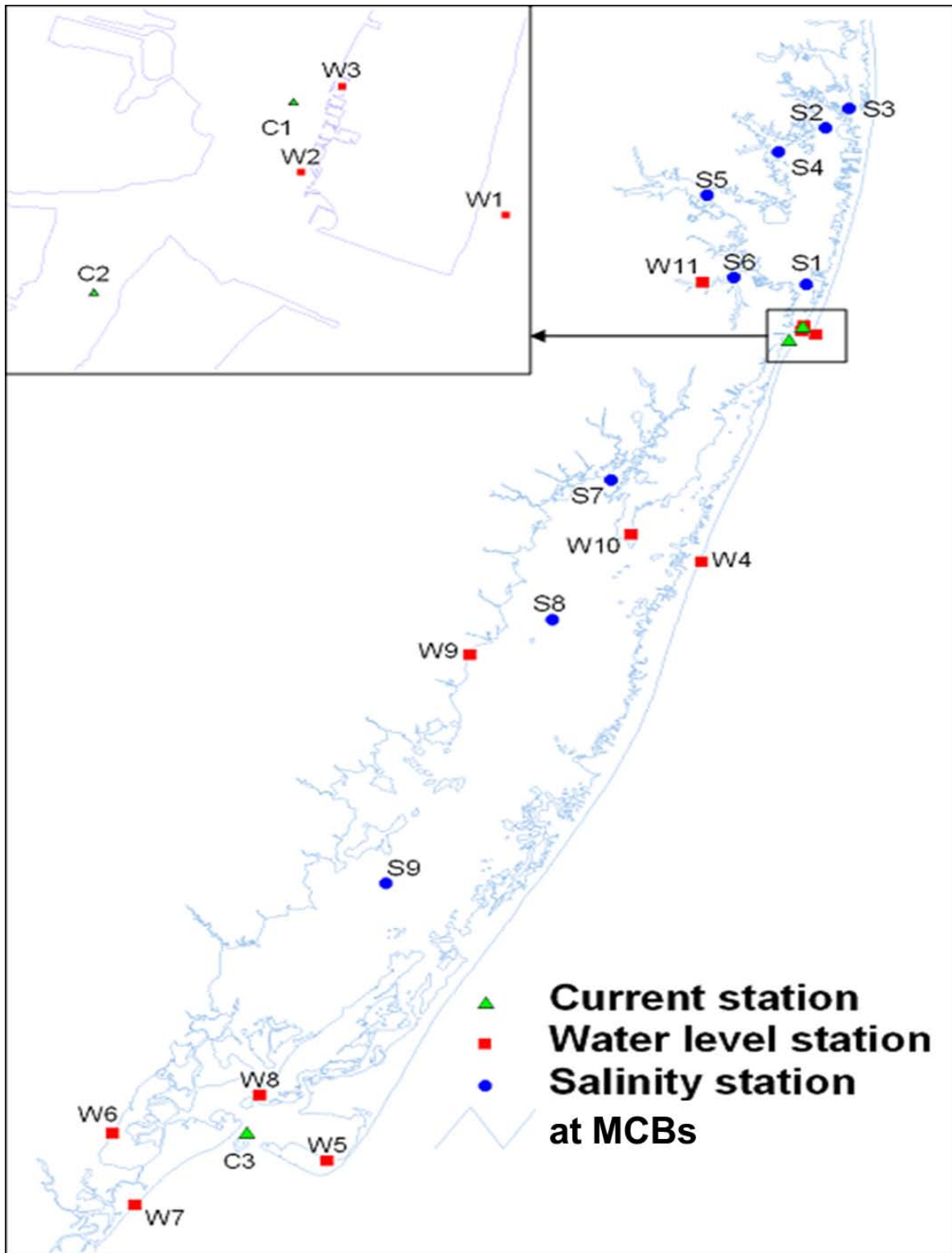


Figure 3.3: Map of field observation stations for water elevation, currents and salinity in the MCBs.

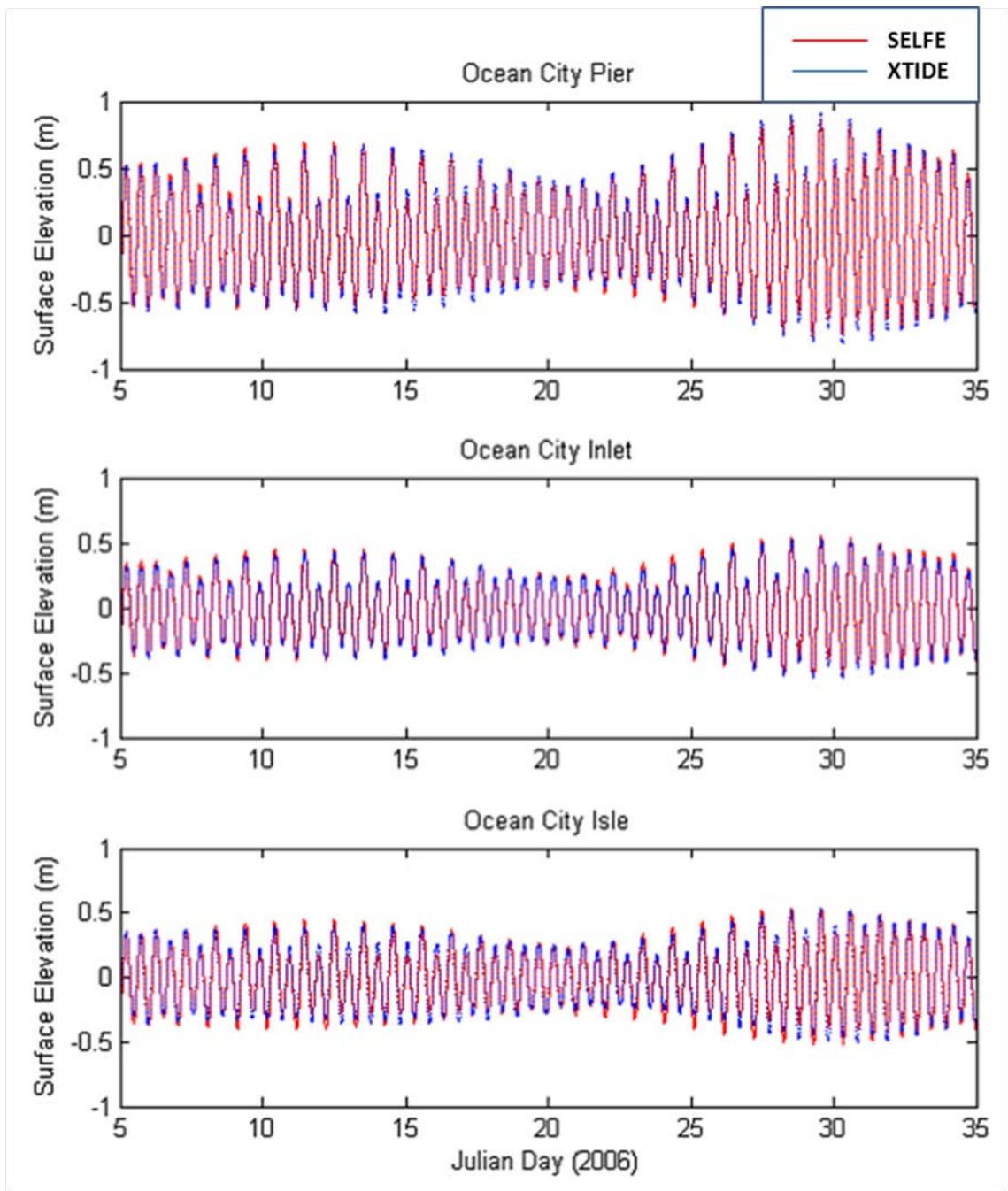


Figure 3.4 (a) Tidal calibrations near Ocean City Inlet in the northern portion of the MCBs.

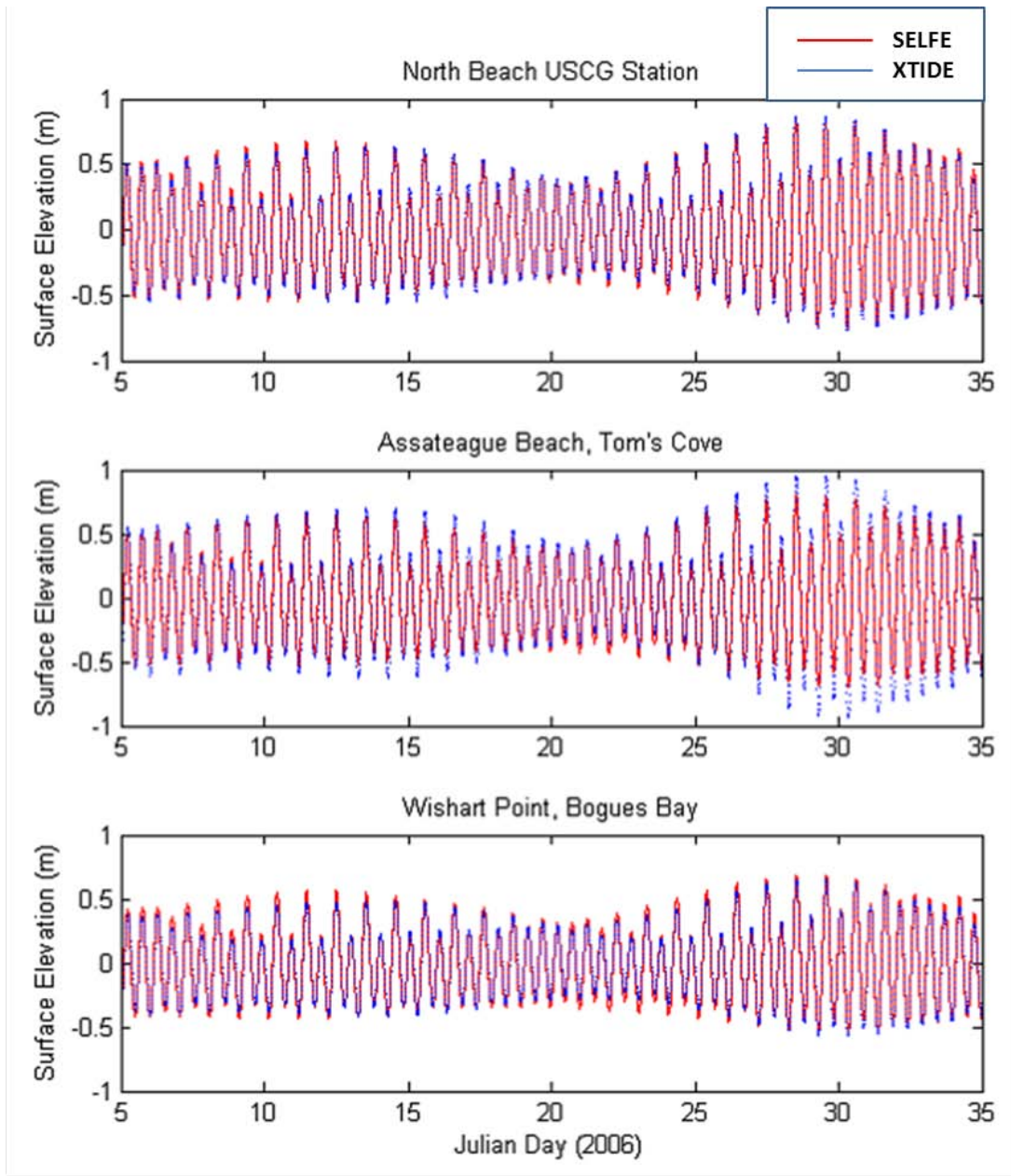


Figure 3.4 (b) Tidal calibrations near Chincoteague Inlet in the southern portion of the MCBs.

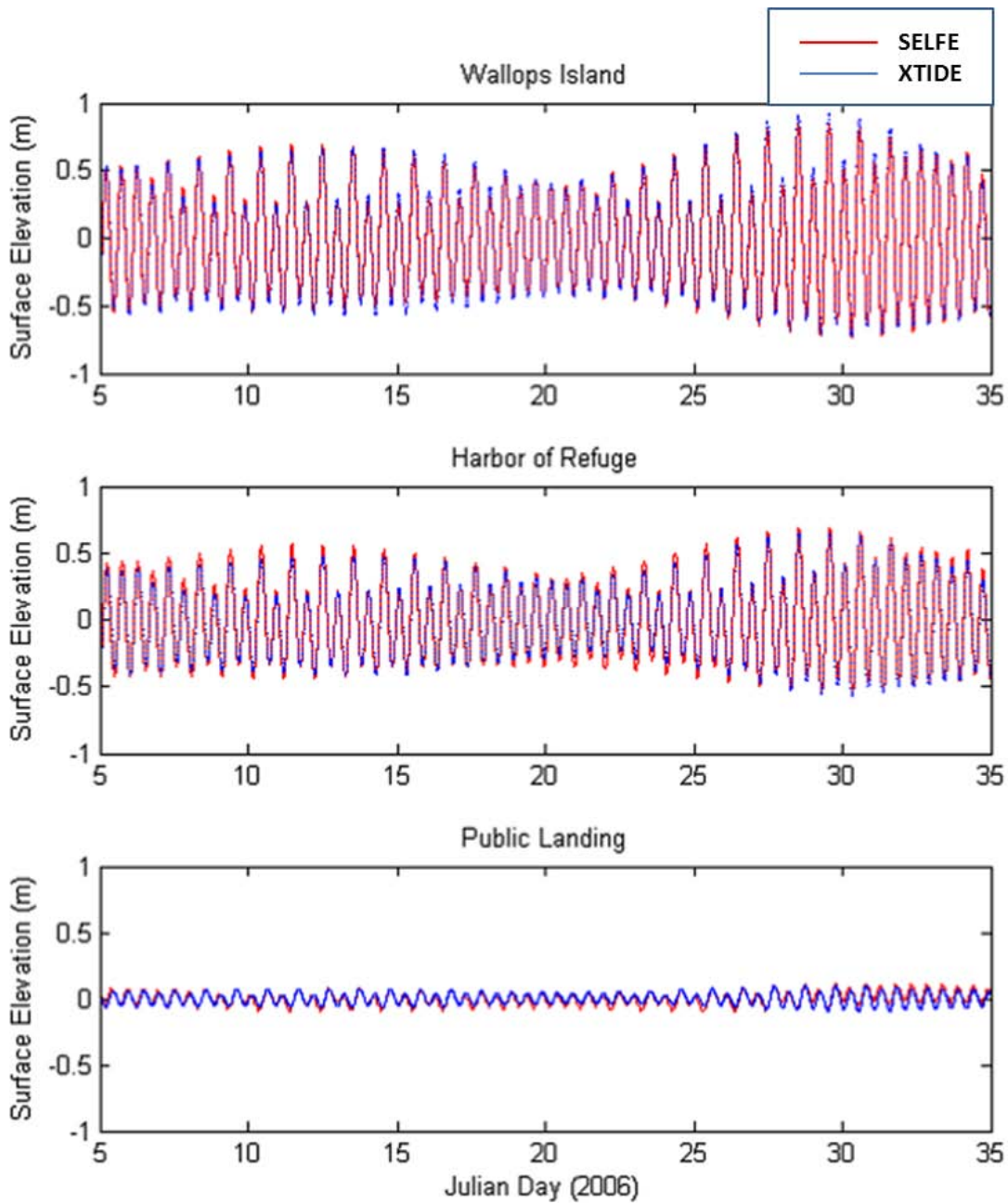


Figure 3.4(c): Tidal calibrations across the middle and southern portions of the MCBs.

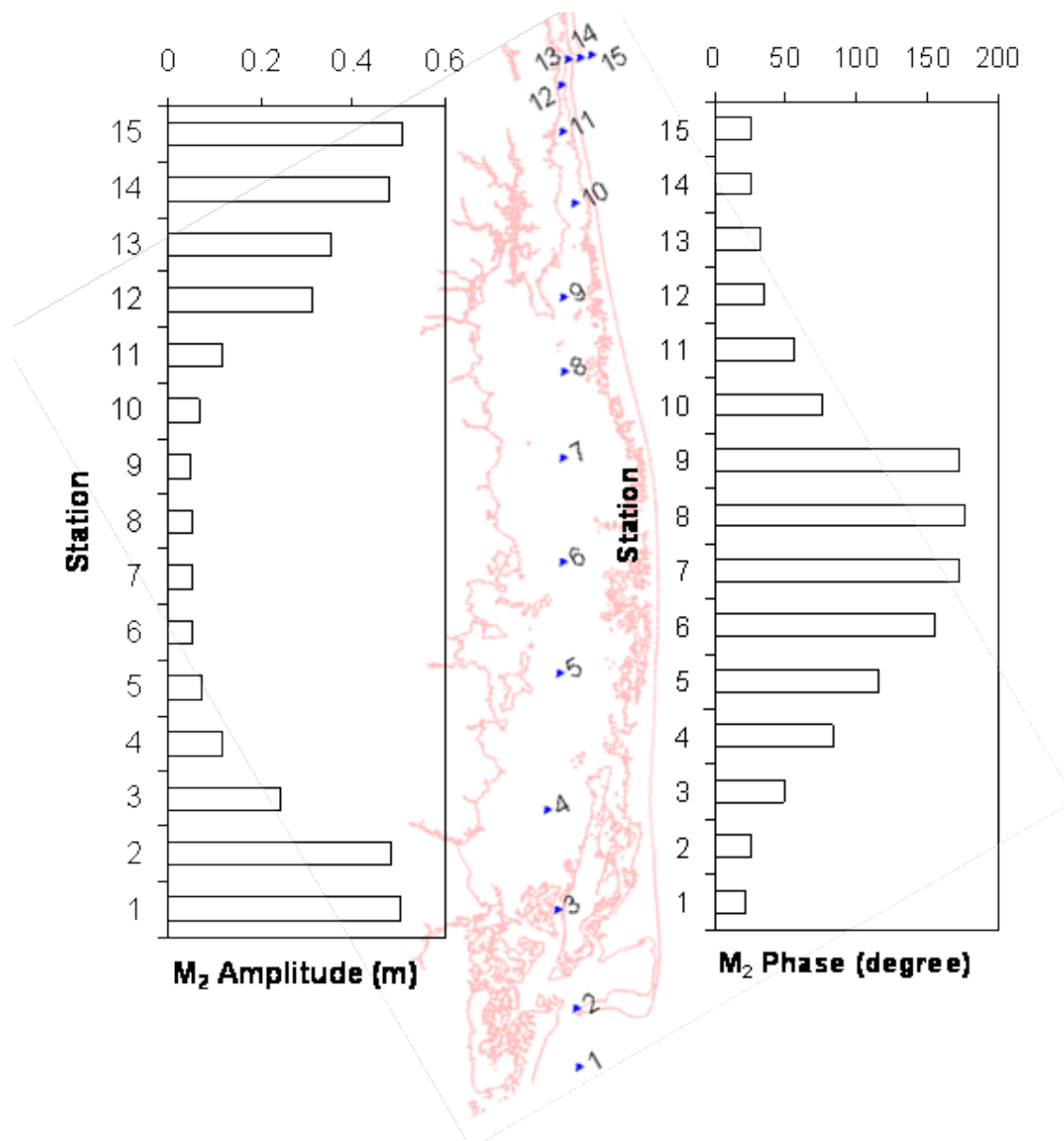


Figure 3.5: M₂ Tidal profiles along Chincoteague and Sinepuxent Bays transect.

The next calibration is aimed at the comparison of model results with the real water level observation, which is influenced both by astronomical and meteorological-induced variation. The real time water level data is collected both by the tidal gauge and the pressure sensor by the National Oceanic and Atmospheric Administration (NOAA), MD DNR, and Maryland Geological Survey (MGS). NOAA has a permanent tidal gauge station inside the Ocean City Inlet. MD DNR deployed a YSI telemetry water quality data logger at its continuous monitoring station at Turville Creek in April 2005. MGS conducted field water level measurements at South Point in Newport Bay and Harbor of Refuge in the Chincoteague Bay in August 2004. The data collected from these 4 stations covered the entire MCBs and were used for model verification bay-wide. In order to model the real water level variation, SELFE require to input the wind speed, direction, and pressure data measured at the 10 meter standard height. The wind

stress is then calculated by applying the wind drag coefficient to the wind speed. The hourly wind data at the two stations are available: one in the north at Ocean City Municipal Airport, MD and the other in the south at Wallops Island, VA were used. Figure 3.6 shows the examples of the wind record in August 2004. The modeled results and observed time series of water level variation is shown in Figure 3.7; the top panel shows the station and lower panel the comparison. The water level variation now consisted of not only the component induced by the tide but also that by the wind displayed as low frequency variations. It can be seen that the amplitude and phase matched the observation quite well. The wind-induced set down, shown as examples at day 269-270 for stations A and C that moves the mean sea level below the mean averaged 0, was captured. A similar phenomenon occurring at day 96 – 98 at Station D was also correctly simulated by the model. Spatially, the model also captured the larger ranges near the two inlet stations and smaller range in the interior of Chincoteague Bay. Proper portrayal of both time series and spatial variation of water level ranges demonstrates the predict capability of the model for both astronomical and wind-induced water level variation.

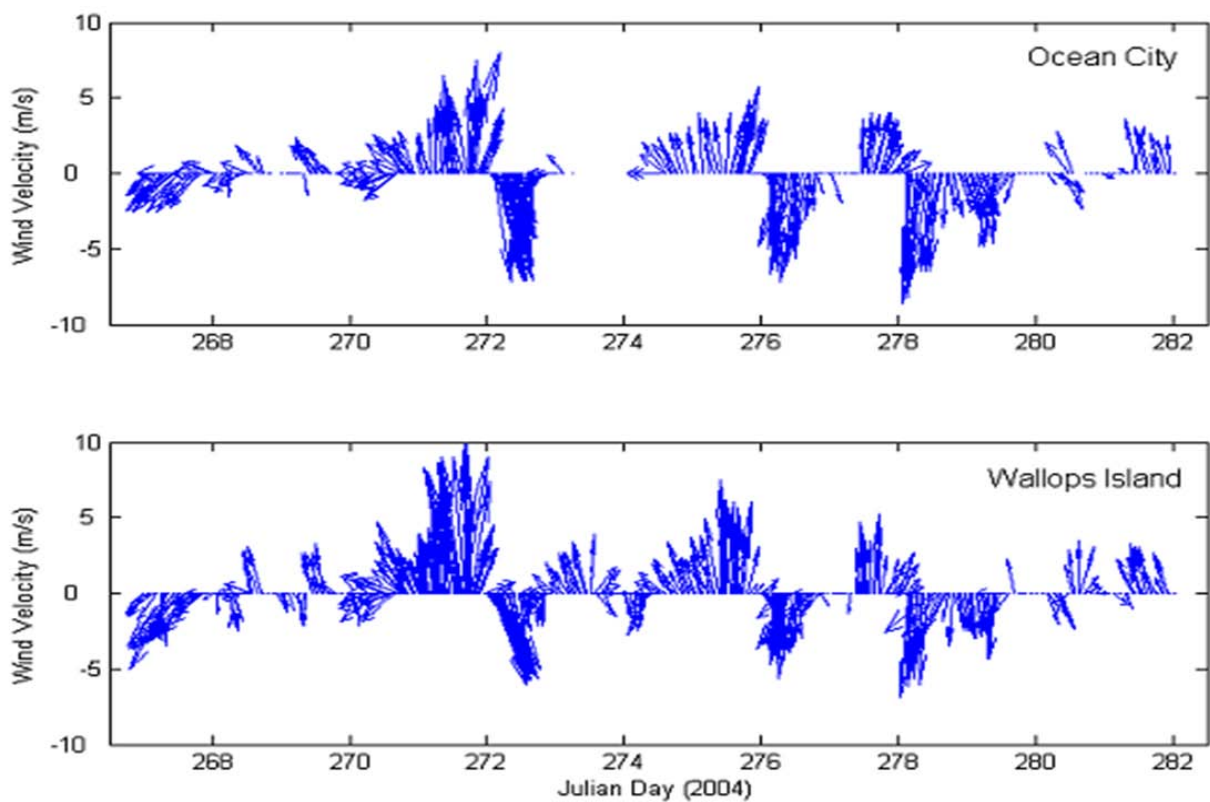


Figure 3.6: Wind record at Ocean City and Wallops Island, September 23 to October 8, 2004.

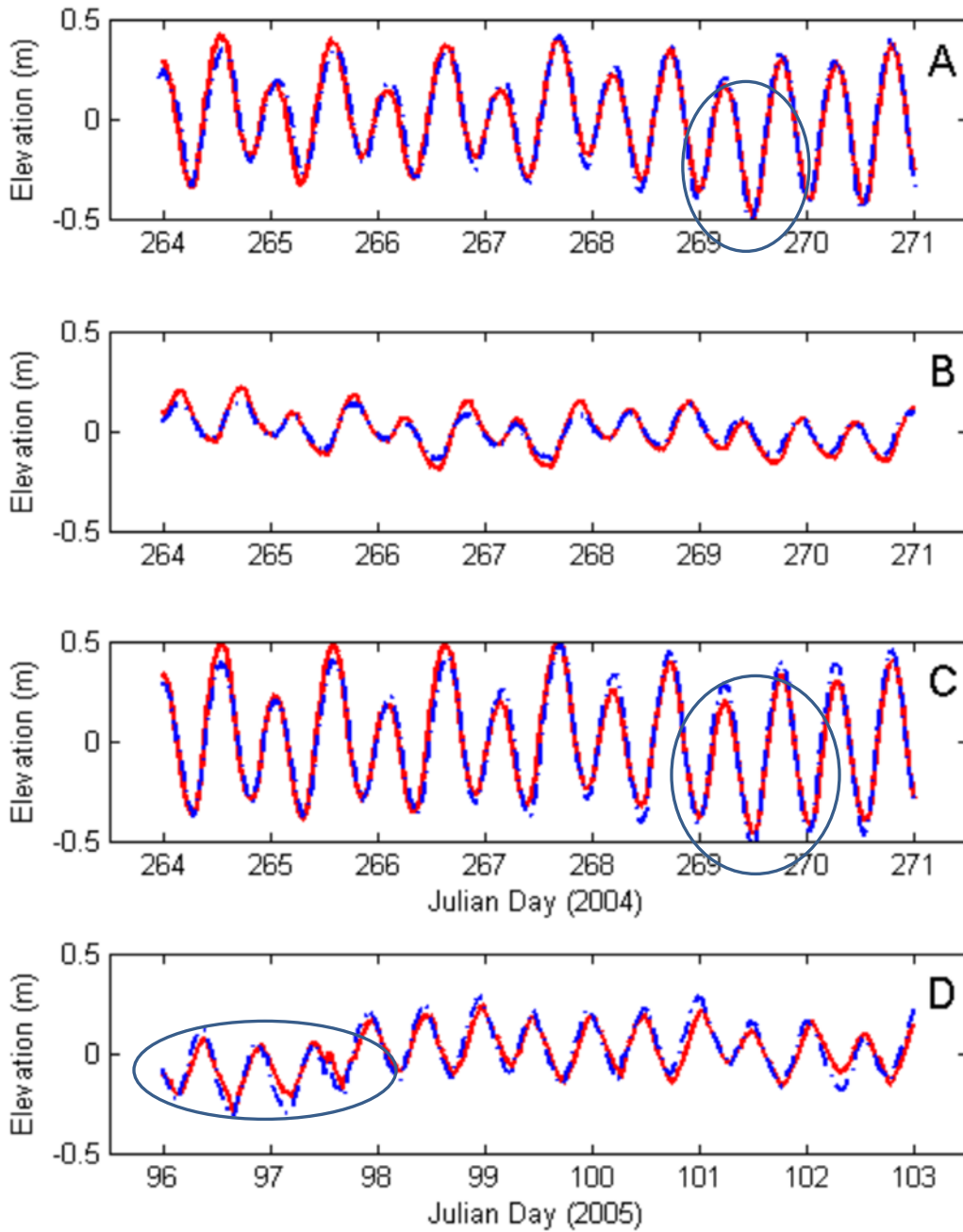
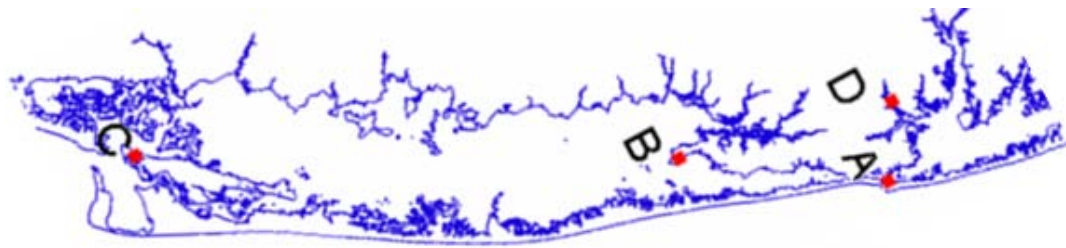


Figure 3.7: Water level verification at A) Ocean City Inlet; B) South Point; C) Harbor of Refuge, and D) Turville Creek.

3.4.2 Velocity calibration

The hydrodynamic model velocity calibration was also conducted during the year 2004, when simultaneous measurements of currents by Acoustic Doppler Current Profilers (ADCP) and water levels were available. The University of Maryland, Center for Environmental Science (UMCES) utilized ADCP to monitor velocities at two locations in the Ocean City Inlet and one site in the Chincoteague Bay (see Figure 3.1). The MGS recorded water levels at two locations. The current measurement locations are shown as U1, U2, U3 for current and W8 and W10 for tide. Detailed descriptions of the instrumentation and methods used by MGS can be found in: http://www.mgs.md.gov/coastal/pub/FR04_06.html

The ADCP deployed at the Ocean City Inlet was bottom mounted while the one deployed in the Chincoteague was a towed ADCP. The 1200-kHz ADCP manufactured by RD instruments has self-contained power supply and data recording and storage. ADCP data processing divides the measurement into uniform segments called depth cells or bins. Due to interference caused by side-lobe reflection from the surface and bottom, the cells for the top two meters and those within 1.5 m of the bottom were not be considered. Given nearly vertically homogeneous conditions at the inlets and the fact that the model uses sigma coordinate layer, which does not exactly match the vertical depth of the ADCP layer, it was decided to compare the vertically averaged velocity to avoid the potential error introduced by the interpolation of the exact vertical position, and thus achieve a more realistic result. In coastal waters, the data normally show a rotating current vector in the presence of the oscillating tide. Around the tidal inlet, because of its narrow width, the current is then dominated by the longitudinal component along the main axis of the local channel. Thus, the current velocity derived from the major axis of the scatter plot was convenient to compare with the modeled results. A spatial distribution of surface velocity distribution during flood tide was shown Figure 3.8 (a) near Ocean City Inlet. In Figure 3.8 (b), an un-filtered ADCP time series measured at the south of the Inlet was compared against the modeled current speed at a point location with reasonable comparison of current on the order of 0.6 m/sec range from flood to ebb. Figure 3.9 compares a 15-day model simulation of current velocities and the ADCP measured velocity at Stations A, B and C from 9/23/2004 – 10/08/2014. Station A is located slightly north of the Ocean City Inlet at the main channel in the Isle of Wight; Station B is located south of the Inlet at Sinexpent Bay. Both comparisons were satisfactory. Station A has higher maximum current of about 1 m/sec as compared to that of Station B at about 0.5 m/sec near the Ocean City Inlet. At Station C, the maximum current is larger than 1 m/sec and the model slightly over-estimated the velocity, presumably due to the complicated geometry and the abundant submerged aquatic vegetation (SAV) present at the mouth of Chincoteague Bay. The statistical measures of the comparison areas follow: $R^2 = 0.94, 0.81, 0.91$; and relative error = 8.96%, 12.94%, and 12.01% for Stations A, B, and C, respectively. These measures were shown in Figure 3.10.

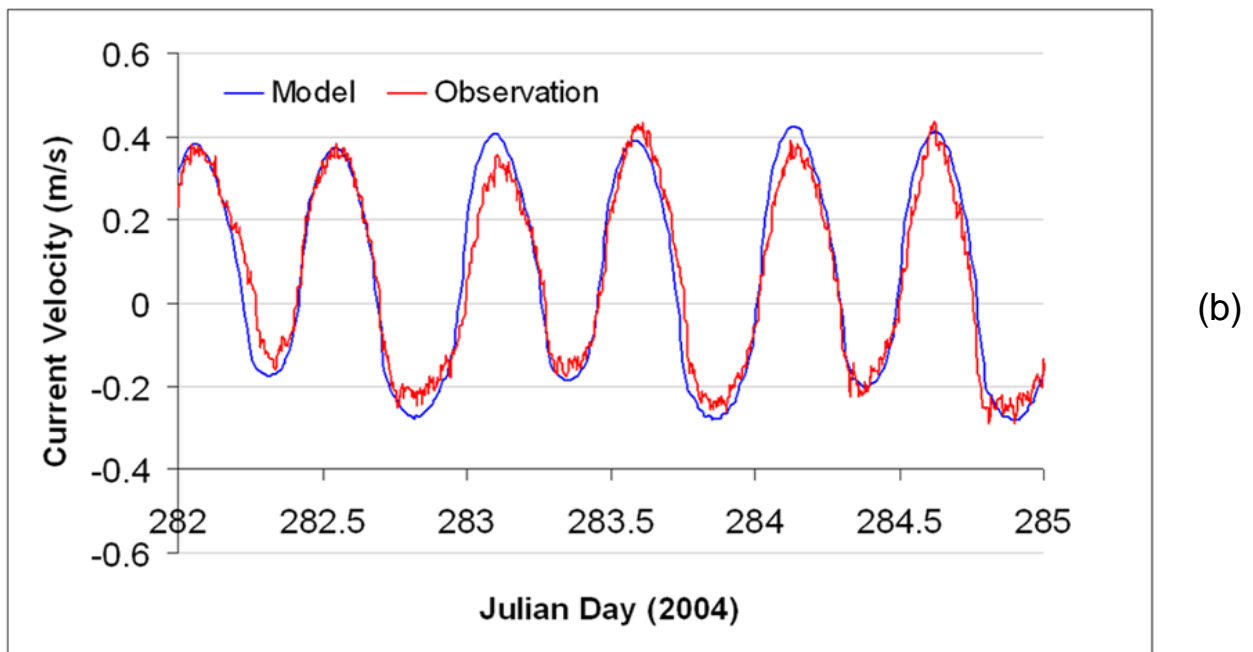
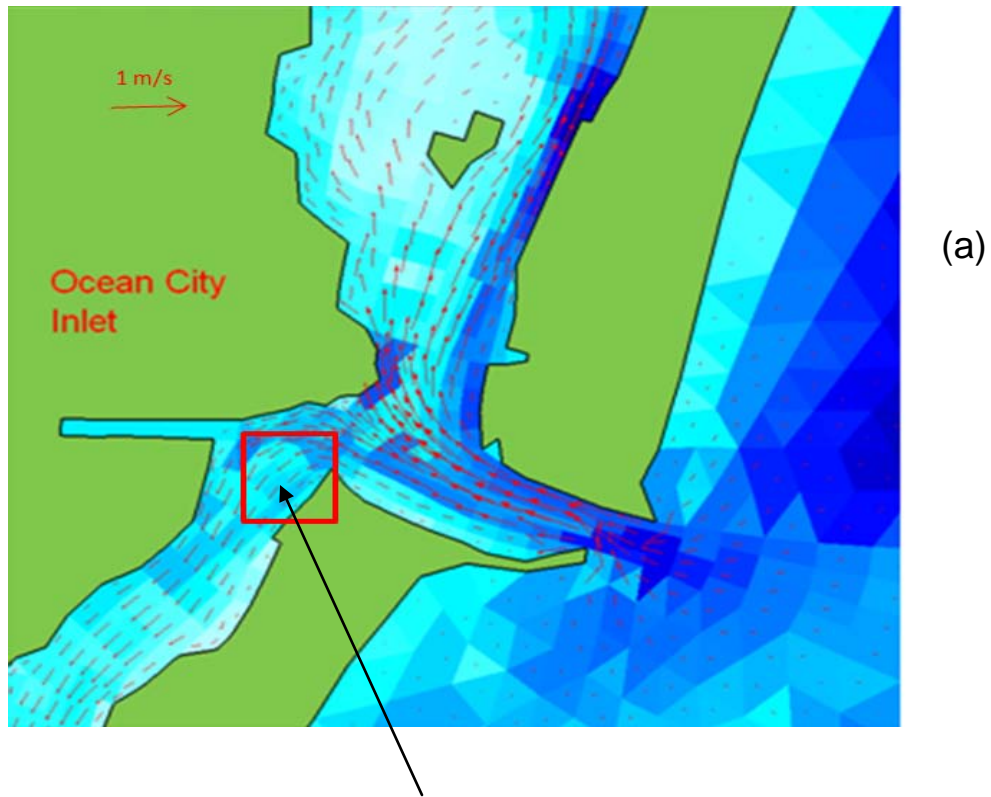


Figure 3.8: (a) Spatial distribution of surface velocities during maximum flood tide at Ocean City Inlet, October 2004; and (b) Current speed time series comparison along the major axis of the local channel; ADCP measurement (red) and model results (blue).

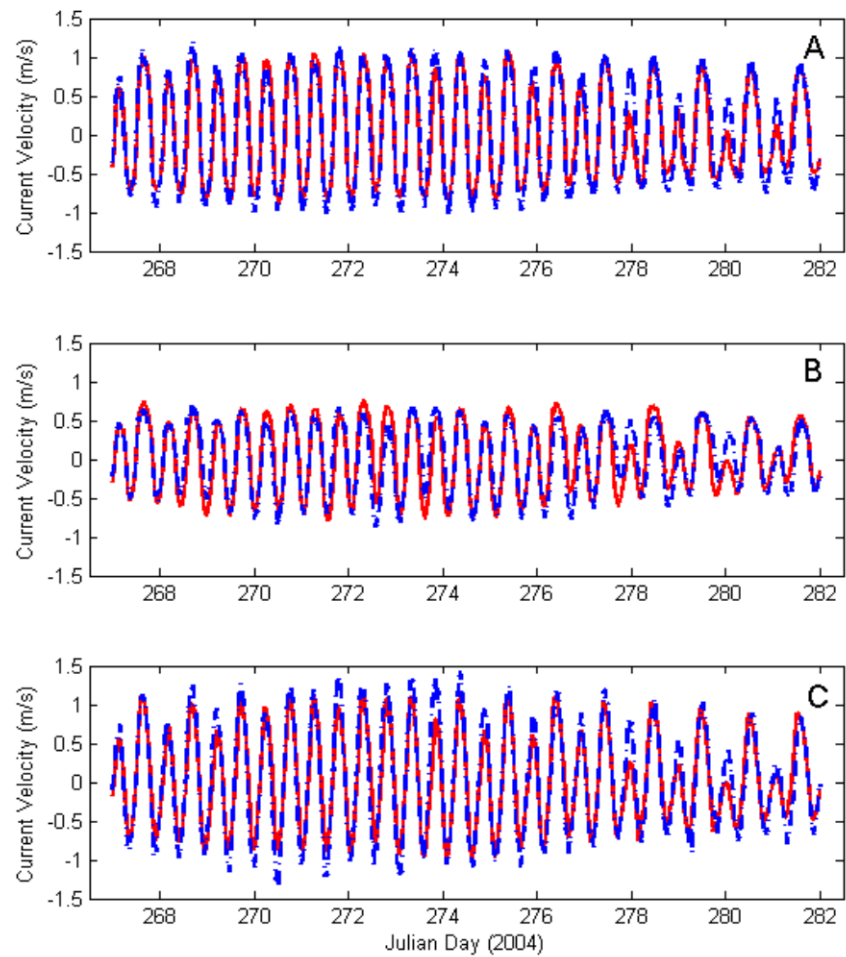
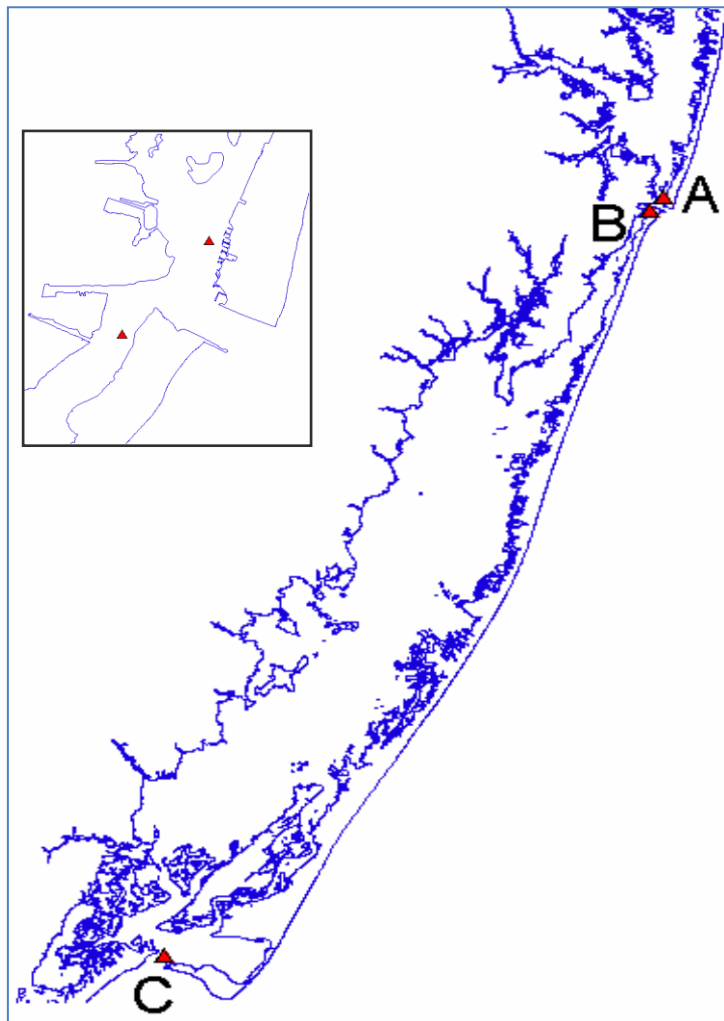
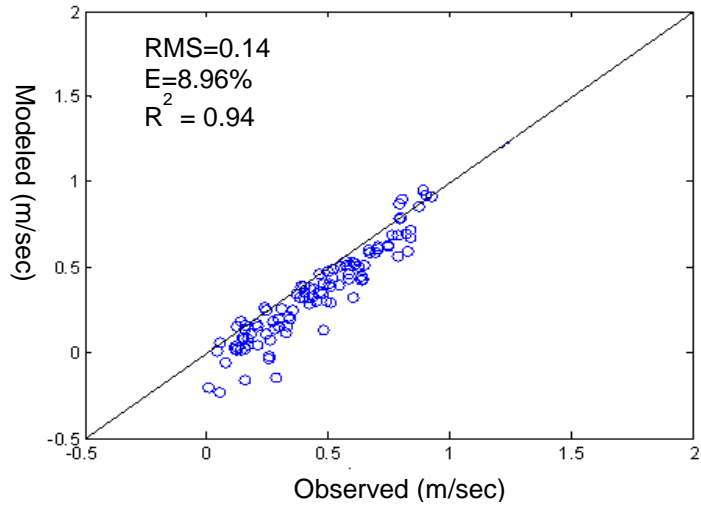
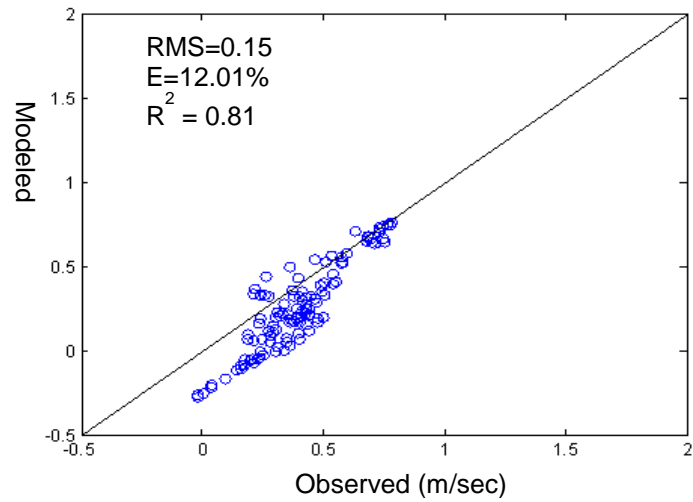


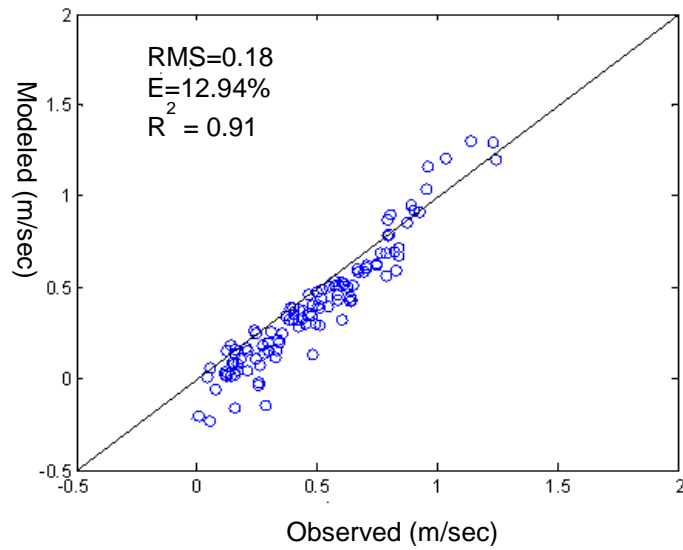
Figure 3.9: Current calibration results at A) Isle of Wight Channel; B) Sinepuxent Bay Channel; c) Chincoteague Channel; model (red solid line) and data (blue dash line).



(A)



(B)



(C)

Figure 3.10: Statistical measures for current comparison at calibration stations A, B, and C, respectively.

3.4.3 Salinity calibration

Salinity is a measure of the salt concentration in the water which can affect the density of water. Because the salinity satisfies the law of mass conservation, it is normally used as a conservative tracer to provide verification of the transport in the model. The saline waters from the coastal ocean, passing through Ocean City and Chincoteague Inlets, move into the MCBs and mixed with the fresher water discharged from the terrestrial inputs. These terrestrial inputs of the freshwater from 2001-2004 were generated by HSPF model, which is calibrated with measurements from USGS stream gauges at Birch Branch and Bassett Creek. Figure 3.11 (a) shows the daily discharge in 2004 for the Saint Martin River watershed, in which multiple freshwater input events in the form of pulsation can be clearly seen over the course of the year, for example, at Julian days 35, 105, 215, 230, 320, 330, and 345. Associated with the freshwater events are the low salinity regimes observed and simulated by the model, as shown in Figure 3.11 (b) in the northern MCBs' tributaries. It was seen that each freshwater event created a salinity drop whose top-to-bottom variation can be as large as 20 ppt, for example, at Saint Martin River (Station S5) and Turville Creek (Station S6), and with a lesser range at Greys Creek (Station S4). Similar trends were found at Stations S1 and S2 in the Assawoman Bay [see Figure 3.11(c)], but with lesser variation in Station S3, which is close to the Ocean City inlet, and more controlled by the ocean water, and thus shows less of a drop in salinity compared to the upstream stations. The observed and modeled salinities exhibit reasonable good agreement. Down to the southern Bay, observed and modeled salinities in the southern MCBs are compared at stations S7, S8 and S9, as shown in Figure 3.11 (d). For the station S7, one can see the effect of the freshwater pulse downstream of the Newport Bay can cause variation of salinity on the order of 10 ppt. The salinity in the middle and southern portions of the Chincoteague Bay, however, was less affected by the freshwater runoff and the range of the temporal variation of salinity is smaller. At station S9, model over-predicted the salinity in the spring and in the fall while under-predicted it in the early summer with mean absolute error around 2-2.5 ppt. The salinity variation in the southern Chincoteague Bay does not appear to be influenced directly by the freshwater discharge from the Newport Bay in the north, which suggests there are other processes at work. One possible mechanism is the ground water recharge studied by USGS (<http://soundwaves.usgs.gov/2002/06/research.html>). Overall, the modeled salinity compared well with the monthly measurement which reproduced field observations throughout the entire domain from the north to the south. Considering the total freshwater discharge in the MCBs system is small compared to other systems such as Chesapeake Bay, the episodic rainfall events still can have substantial impacts on the salinity field of the creeks in the tributaries. Because the fresh water influence, there is a clear salinity gradient pattern from the main stem of MCBs toward the upper tributaries - the saltier salinity near the inlets and main stem of MCBs and decreased as it moved toward upstream of the tributary, as shown in Figure 3.12. Both 2003 and 2004 are wet hydrological years with 2004 having a larger total amount of freshwater inputs and, thus, the salinity inside the MCBs was the lowest. The statistics of salinity comparison for 2001- 2003 at all 5 basins in MCBs are shown in Table 3.2. The relative errors were in the range of 2–5.4% with Sinepuxent having the lowest error. The highest relative error occurred in Isle of Wight Bay followed by Newport Bay due to the greater salinity change resulting from the larger freshwater

inputs in that basin. The salinity calibration and validation are considered satisfactory – the errors are within 5% for the majority of the stations - proved to be suitable for further use in coupling with the water quality model.

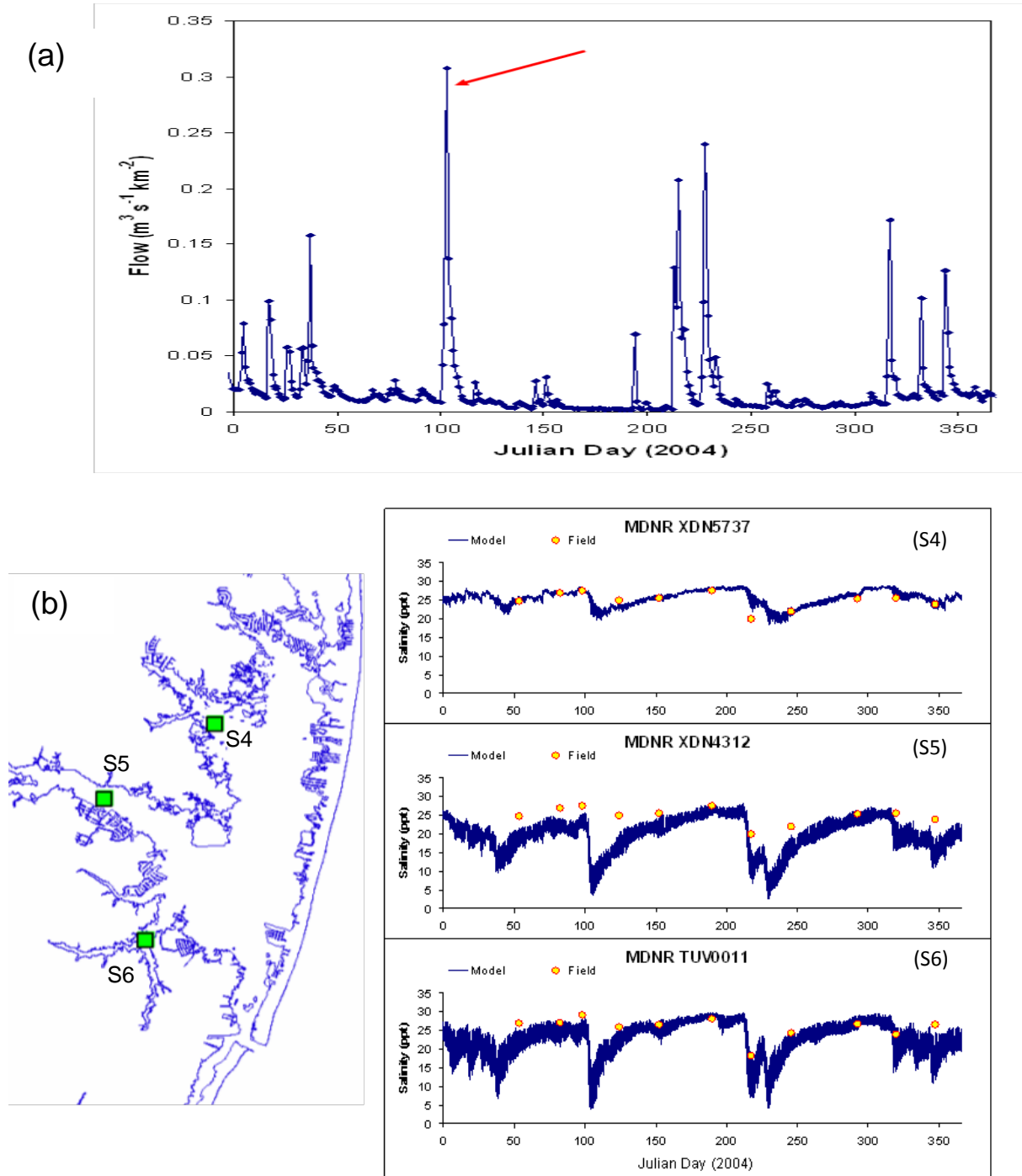


Figure 3.11 (a) Areally-weighted daily discharge from USGS flow gauges (01484719 and 0148471320) in MCBs, and (b) Salinity calibration in the tributaries of the northern MCBs.

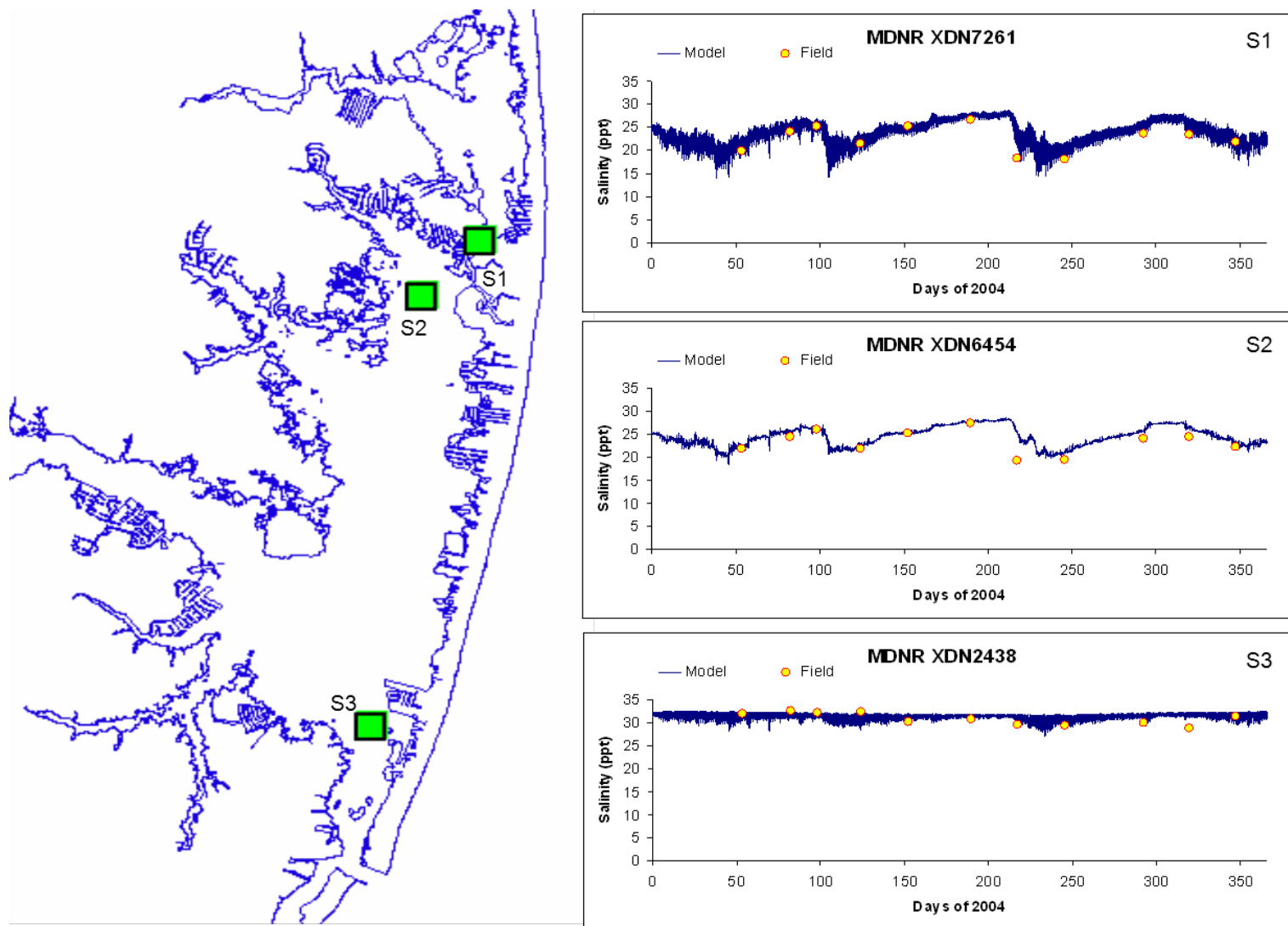


Figure 3.11 (c): Salinity calibration in the open waters of the northern MCBs.

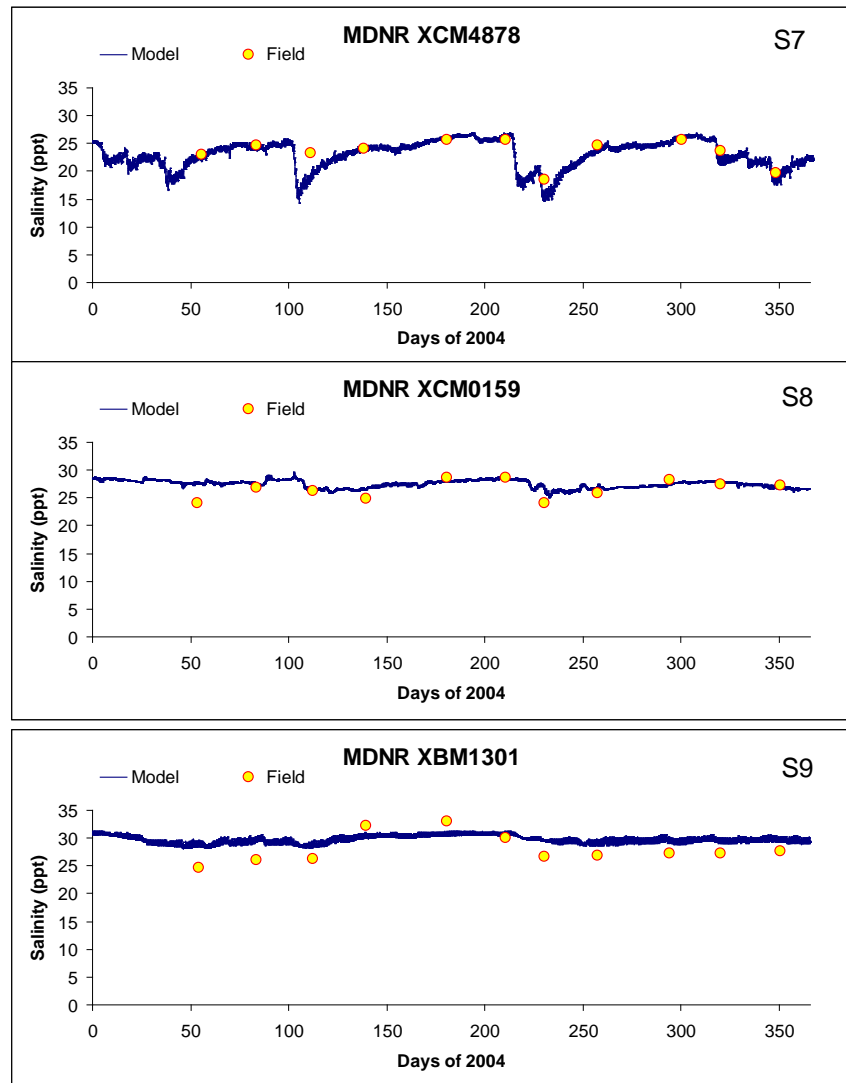
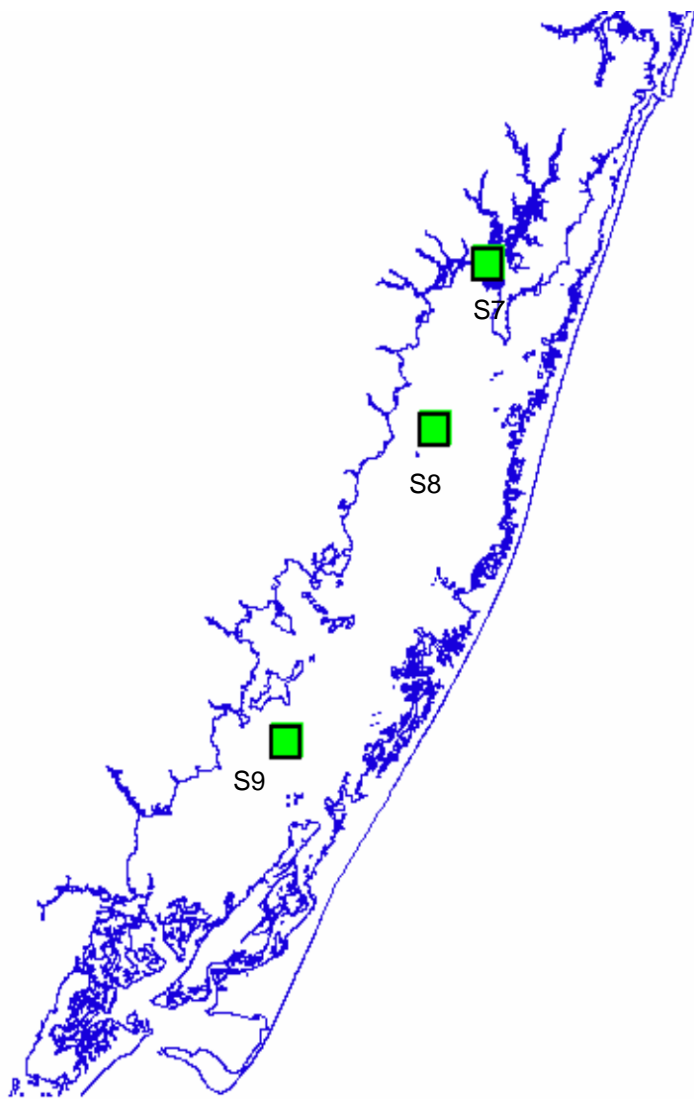


Figure 3.11 (d): Salinity calibration in the southern MCBs.

2004 Averaged Salinity Distribution



2005 Averaged Salinity Distribution



Figure 3.12: Spatial distribution of the averaged salinity contour in the MCBs over summers of (a) 2003 and (b) 2004.

Table 3.2: Statistical measures for modeled versus observed salinity at five basins in MCBs.

2001	Asswoman Bay	Isle of Wight Bay	Sinepuxent Bay	Newport Bay	Chincoteague Bay
Mean error	-0.72	-0.91	0.6	-0.8	0.8
Absolute Mean error	1.27	2.7	1.1	2.7	1.8
Relative error (%)	3%	5.00%	2%	4%	2.60%
2002	Asswoman Bay	Isle of Wight Bay	Sinepuxent Bay	Newport Bay	Chincoteague Bay
Mean error	-0.7	-0.8	0.5	-0.76	0.9
Absolute Mean error	1.17	2.5	0.9	2.5	1.9
Relative error	2.80%	4.80%	2%	3.70%	3.00%
2003	Asswoman Bay	Isle of Wight Bay	Sinepuxent Bay	Newport Bay	Chincoteague Bay
Mean error	-0.9	-1.1	0.8	-0.9	1.1
Absolute Mean error	1.4	2.9	1.4	2.9	2.1
Relative error	3.10%	5.40%	2.30%	4.50%	3.60%

CHAPTER 4: THE COUPLED WATER QUALITY AND SEDIMENT BENTHIC FLUX MODEL

The Maryland Coastal Bays (MCBs) are shallow water bodies situated behind barrier islands, with limited access to ocean exchange. They share many characteristics with coastal lagoons and are vulnerable to the excess anthropogenic nutrients leading to eutrophication (Dennison et al, 2012). A HEM3D (Hydrodynamic Eutrophication Model), which consists of a hydrodynamic model - SELFE, a water quality model ICM - (Integrated Compartment Model), and a sediment benthic flux model, was developed and coupled with the HSPF watershed model to simulate lagoon-type biogeochemical and water quality transport processes in the MCBs (Figure 4.1). The HSPF model furnished flows to hydrodynamic model and, at the same time, provided nutrient and carbon loads to the water column water quality model. The water column water quality model interacted with sediment benthic flux model by providing particulate organic matter and fed back with sediment fluxes and sediment oxygen demand.

4.1 The ICM Water Quality Model

The water quality model ICM (Integrated Compartment Model), originally developed by Cerco and Cole (1994), was used for simulating eutrophication in the water column. Fall-line load and below-fall line point and non-point source loads were supplied by the HSPF model. Computation of eutrophication process in ICM was coupled directly with hydrodynamic model on a time step of every 5 minutes. The ICM model simulates all the processes occurring in the water body from the sediment interface up to the surface of the water. It consists of 6 water quality variable groups as follows: (1) algae; (2) organic carbon; (3) nitrogen; (4) phosphorus, (5) silica and (6) dissolved oxygen. Each nutrient contains dissolved and particulate phases, and the particulate matter is further subdivided into refractory and labile particulate forms. Both refractory and labile particulate organics settle out of the water column and deposit onto the surface layer of benthic sediments. Refractory organic particulate has a longer degradation time, whereas labile organic particulate has a shorter degradation time. In terms of chemical processes, dissolved organic carbon, nitrogen and phosphorus are converted into inorganic forms by processes including hydrolysis and bacterially-mediated activities. Utilization of dissolved organic carbon during respiration of heterotrophic bacteria consumes dissolved oxygen. Similarly, dissolved organic nitrogen and phosphorus are converted by bacterial activity to ammonium nitrogen ($\text{NH}_4\text{-N}$) and orthophosphorus ($\text{PO}_4\text{-P}$). $\text{NH}_4\text{-N}$ is subsequently oxidized by bacteria to nitrate nitrogen ($\text{NO}_{23}\text{-N}$). This process, which is called nitrification, consumes dissolved oxygen. Under conditions of extremely low dissolved oxygen, $\text{NO}_3\text{-N}$ may be reduced by bacteria to dissolved nitrogen gas, which may subsequently be lost to the atmosphere at the air-water interface. Denitrification is the process whereby dissolved organic carbon is consumed. The schematic diagram is shown in Figure 4.2 (a).

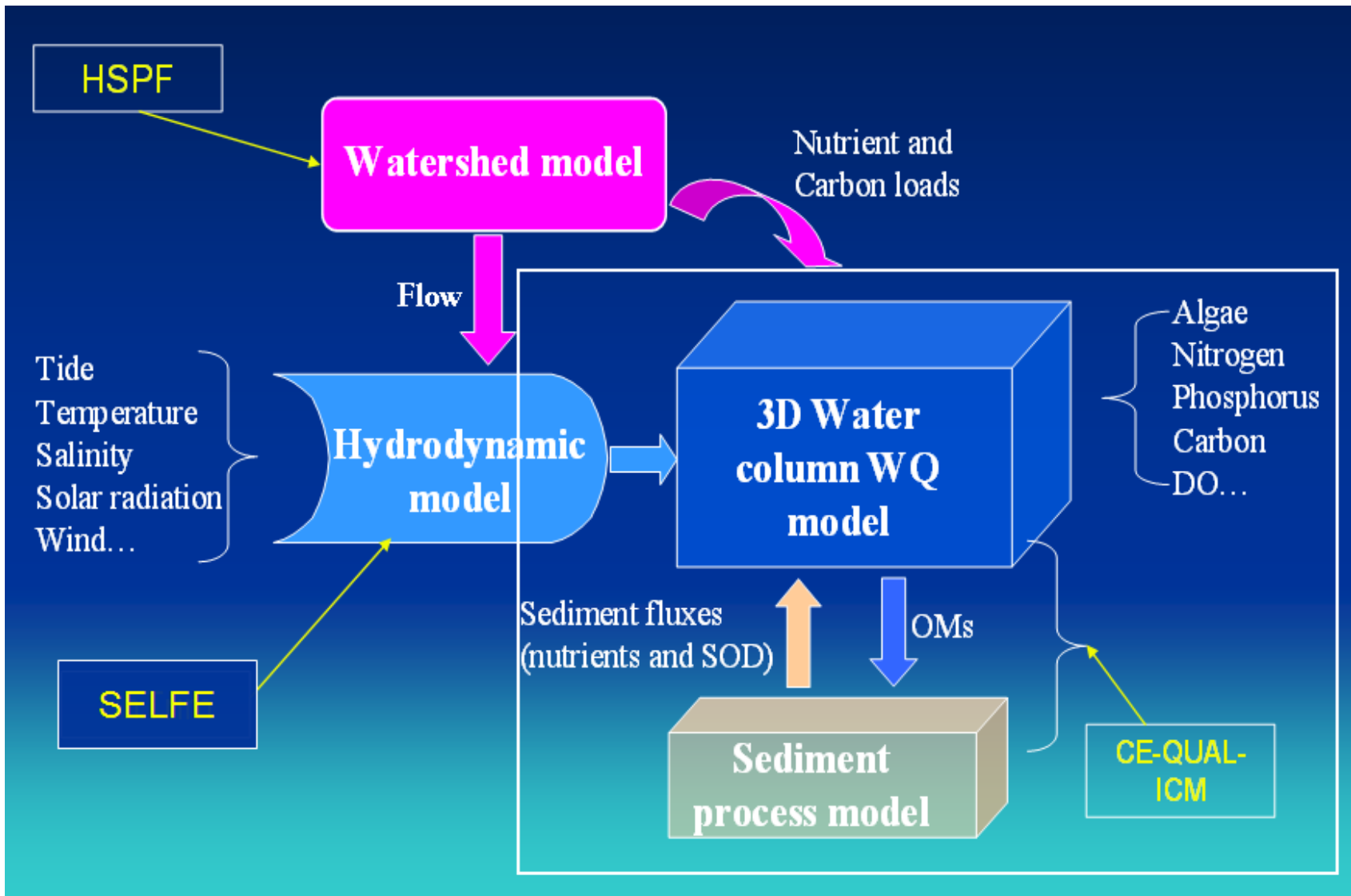


Figure 4.1 Schematic diagram of coupled HSPF watershed, SELFE hydrodynamic, ICM water quality, and sediment benthic models.

In the phytoplankton dynamics of the model, algae species are subdivided into three forms: diatoms, blue-green algae (cyanobacteria), and green algae (dinoflagellates). The growth, respiration, and mortality of each of these algal groups are controlled by optimal water temperature specified in the model. In the MCBs HEM3D model, algae are growth-limited in a multiplicative manner, based on the Liebig Law via ambient levels of light, water temperature, and concentrations of inorganic nitrogen ($\text{NH}_4\text{-N}$ and $\text{NO}_3\text{-N}$) and phosphorus (dissolved $\text{PO}_4\text{-P}$). All three algae forms consume nitrogen ($\text{NH}_4\text{-N}$ and $\text{NO}_3\text{-N}$) and phosphorus (dissolved $\text{PO}_4\text{-P}$) during growth. Similarly, due to respiration and mortality, algae release dissolved and particulate organic carbon, nitrogen, and phosphorus. Algae consume dissolved oxygen during respiration and release dissolved oxygen during photosynthetic activity. Blue-green algae exhibit a toxic response to salinity levels above one (1) part per thousand (ppt). Blue-green algae are not limited by low inorganic nitrogen concentrations, since they can alternatively utilize dissolved organic nitrogen in the water column. The particulate forms of the algae also settle out of the water column, contributing their organic carbon, nitrogen, and phosphorus contents to the surface layer of benthic sediments. For more details of the water column eutrophication model formulation, the reader can review Appendix B.

4.2. The Sediment Benthic Flux Model

The sediment benthic flux model was used to predict nutrient fluxes and sediment oxygen demand at the water-sediment interface. Water column eutrophication is coupled in real time with a benthic flux sub-model, which has twenty-seven water quality state variables associated with mass fluxes in a 2-layer sediment compartment (DiToro and Fitzpatrick, 1993). As shown in Figure 4.2 (b), the upper layer (layer 1) is in contact with the water column and may be oxic or anoxic depending on dissolved oxygen concentration in the overlying water. The lower layer (layer 2) is permanently anoxic. The upper layer depth, which is determined by the penetration of oxygen into the sediments, is at its maximum only about 1 centimeter (cm) thick. Layer 2 is much thicker, on the order of 10 cm to 1 meter. The sediment benthic flux sub-model incorporates three basic processes: (1) depositional flux of particulate organic matter (POM); (2) diagenesis flux; and (3) sediment flux. The settling of particulate organic matter (POM) from the overlying water is the main driver. POM fluxes include particulate organic carbon, nitrogen and phosphorus which are deposition to layer 2 sediments. Because of the negligible thickness of the upper layer, deposition is considered to be from the water column directly to the lower layer. Within the lower layer, the model simulates the diagenesis (mineralization or decay) of deposited POM, which produces inorganic nutrients flux (diagenesis flux). The third basic process is the flux of substances exchanged with the overlying water (sediment flux). The sediment fluxes include ammonium nitrogen, nitrate nitrogen, phosphate phosphorus and sediment oxygen.

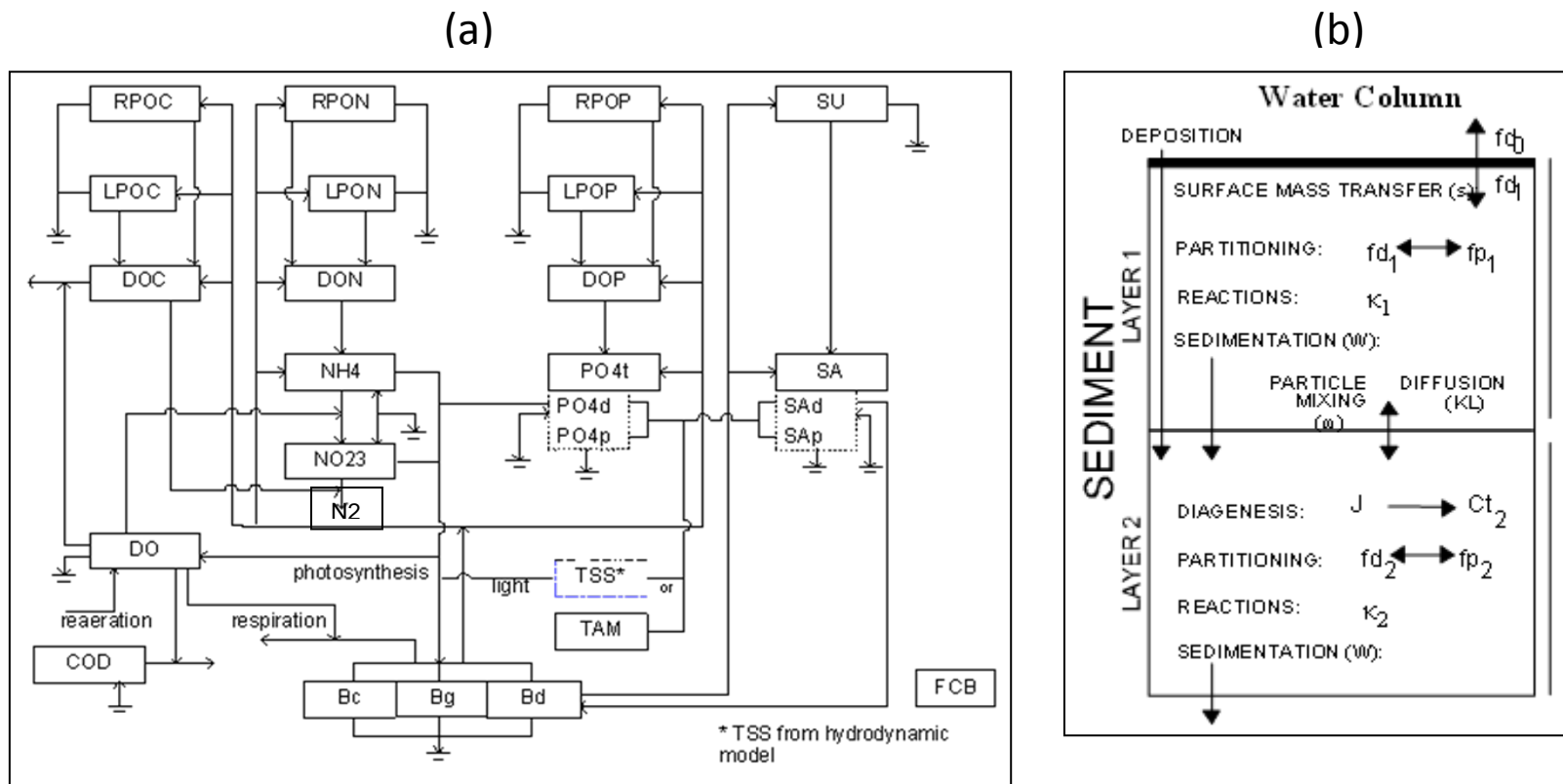


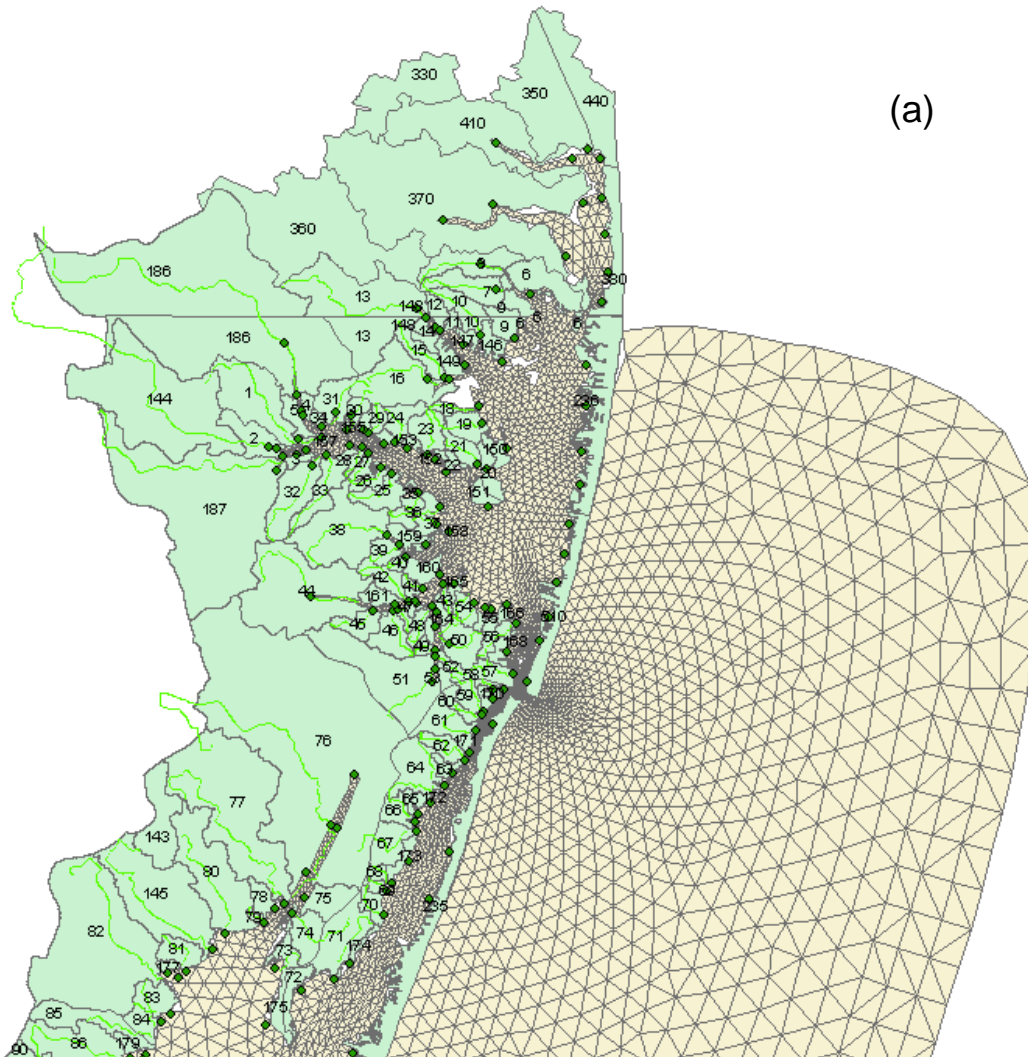
Figure 4.2 (a) Schematic diagrams for (a) ICM model water column processes and (b) sediment digenesis processes.

Oxygen demand takes three paths out of the sediments: (1) oxidation at the sediment-water interface as sediment oxygen demand; (2) export to the water column as chemical oxygen demand, or (3) burial to deep as inactive sediments. Inorganic nutrients produced by diagenesis take two paths out of the sediments: (1) release to the water column, or (2) burial to deep, inactive sediments. The state variables for describing above processes including: three separate classes (G1, G2, and G3) of particulate organic carbon, nitrogen and phosphorus, and sulfide/methane, ammonium nitrogen, nitrate nitrogen, phosphate phosphorus, and temperature in layers 1 and 2.

4.3 Water Quality Model Set-up

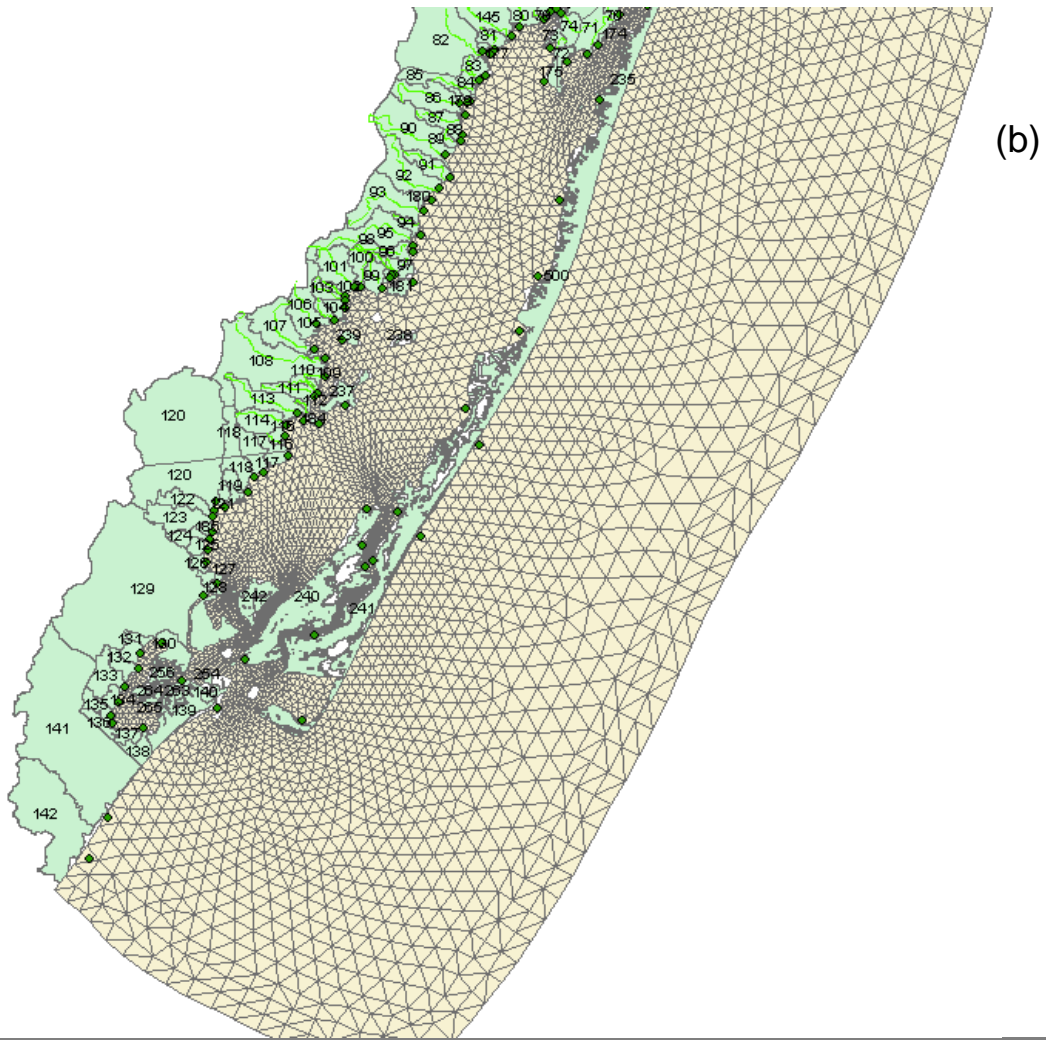
4.3.1 External loading

The water quality model receives nutrient loads from (1) non-point sources (2) point sources (3) shoreline erosion and (4) atmospheric deposition. The non-point source loads were provided from 225 watersheds delineated in the MCBs, as shown in Figure 4.3 (a) for the northern and Figure 4.3 (b) for the southern Bays. The water quality model grid was connected with the watersheds, with the green thin lines representing the major streams inside the watershed. These major streams include: (1) Greys Creek (in the Assawoman Bay); (2) Bishopville Prong, Shingle Landing Prong, St. Martin River, Herring Creek, Turville Creek and Manklin Creek (in the Isle of Wight Bay); (3) Kitts Branch/Ayer Creek, Newport Creek and Marshall Creek (in the Newport Bay). Examples of watershed segments, their Maryland 8 digit watershed codes, the 8-digit basin name, and the acreage of the segment are shown in the list table of Figures 4.3 (a) and (b). A complete list of segment list for the MCBs watershed can be found in VIMS (2013). In Figure 4.3, there are a total of 231 edge of stream loads points shown as diamond green symbols along the shoreline representing the point and nonpoint sources discharge points. The distribution is as follows: 36 in Assawoman Bay, 74 in Isle of Wight Bay, 25 in Sinepuxent Bay, 18 in Newport Bay and 78 in Chincoteague Bay. These discharge points are the direct linkage of flow and nutrient loading from the watershed into the water quality model. The shoreline erosional loads were determined by the total shoreline length multiplied by the TN and TP loads per unit shoreline length based on MGS' sediment erosion studies (Wells, 1998, 2002, 2003). The inputs for atmospheric loading were determined based on the water surface area of each of the basins multiplied by the unit loading of TN and TP per unit area. The determination of the unit loads was described in details in Chapter 2, Section 2.2.5.



SEGMENT	MDE8DIGIT	MDE8NAME	State	Area (m ²)	Acres
1	02130103	Isle of Wight Bay	MD	5877581.487	1452.366
2	02130103	Isle of Wight Bay	MD	2174529.604	537.3322
3	02130103	Isle of Wight Bay	MD	396413.9605	97.95497
4	02130103	Isle of Wight Bay	MD	440934.9881	108.9562
5	02130103	Isle of Wight Bay	MD	928127.7271	229.3429
6	02130102	Assawoman Bay	DE	4088756.294	1010.343
6	02130102	Assawoman Bay	MD	362549.3402	89.58693
7	02130102	Assawoman Bay	MD	2380970.667	588.3443
8	02130102	Assawoman Bay	MD	2923821.195	722.4842
9	02130102	Assawoman Bay	DE	414929.8449	102.5303
9	02130102	Assawoman Bay	MD	841858.0755	208.0254
10	02130102	Assawoman Bay	DE	1229176.32	303.7328

Figure 4.3 (a) Examples of the selected segments of HSPF Coastal Bays model segments in the Assawoman Bay, Isle of Wight Bay, Sinepuxent Bay and Newport Bays



SEGMENT	MDE8DIGT	MDE8NAME	STATE	Area(m ²)	Acres
132	02130106	Chincoteague Bay	VA	1664404.256	411.2788
133	02130106	Chincoteague Bay	VA	3698790.703	913.9812
134	02130106	Chincoteague Bay	VA	1112237.58	274.8369
135	02130106	Chincoteague Bay	VA	1783601.063	440.7327
136	02130106	Chincoteague Bay	VA	1454331.688	359.3693
137	02130106	Chincoteague Bay	VA	1124736.705	277.9255
138	02130106	Chincoteague Bay	VA	2081700	514.3937
139	02130106	Chincoteague Bay	VA	6290108.622	1554.303
140	02130106	Chincoteague Bay	VA	403200	99.63182
141	02130106	Chincoteague Bay	VA	42861600	10591.22
142	02130106	Chincoteague Bay	VA	19170900	4737.182

Figure 4.3 (b) Examples of the selected segments of HSPF Coastal Bays model segments in the Chincoteague Bay

4.3.2 Initial and boundary conditions

The initial condition was specified using January and February 2000 monitoring data of year 2000 conducted by DNR survey. The initial condition for each polygon within the MCBs was specified through linearly interpolating the survey data between adjacent stations. The polygons are horizontally variable but homogeneous vertically initially. The vertical variation was obtained by initializing the model for 5 years during which the vertical variation of concentration emerges as a result of the interaction with the sediment benthic model. The initial condition in the coastal ocean was specified based on the linear interpolation between concentrations at the Ocean City and Chincoteague Bay Inlets and the associated concentration specified at the open boundary condition. The model's open boundary conditions were specified approximately 7 miles offshore along the east boundary of the coast in addition to the two cross-shore boundaries - one at the north just south of Indian River, Delaware, and the other in the south, off of NASA Wallops Island Flight Center. The concentrations specified at these location are long-term nutrient mean conditions obtained from EPA's report "Criteria Development Guidance: Estuarine and Coastal Bay Waters" (see <http://www2.epa.gov/nutrient-policy-data/criteria-development-guidance-estuarine-and-coastal-waters>). The key variables assigned at the boundary are: Chlorophyll = 1 ug/l, DO = 5 mg/l, Salinity = 30 ppt, TN = 0.2 mg/l, TDN = 0.1mg/l, TP = 0.02 mg/l, TDP = 0.01 mg/l and Secchi depth = 4m. Because no sediment concentrations were measured, the initial condition for the sediment benthic flux model was not known *a priori*. Thus, the sediment concentration will be specified as clean sediments initially and executed along with the watershed loading into the system long enough until the depositional flux, diagenesis flux, and the sediment flux are in equilibrium. In a normal practice, the model is run to execute for five (5) years continuously until the loading and the sediment flux reaches a steady state. At the end of the five (5)-year simulation, the concentration values from sediment flux model, which characterize the sediment characteristics of each location, were then output and used as the initial condition for the different scenarios.

4.3.3 Estimation of parameters

Many parameters need to be specified in the water quality model. Most parameters in the water quality model CE-QUAL-ICM were adopted from the default parameters for the Chesapeake Bay (Cercio and Cole, 2004). However, there are a few parameters that which are re-calibrated because MCBs is a relatively shallow water system as compared to the Chesapeake Bay. During the testing, some parameters were changed in order to produce results that more closely simulate the field observations unique to the MCBs. The parameters that are specified differently from those of the Chesapeake Bay model are shown in Table 4.1. The parameters 1- 6 are related to algae in the water column, parameter 7 is related to heterotrophic respiration of DOC and parameter 8 is related to the critical oxygen concentration for releasing of PO₄ in the sediment benthic flux model. The final parameters used for the water quality model of this study are listed in of Appendix C.

Table 4.1: The parameter selected for phytoplankton dynamics

PARAMETER	DESCRIPTION	VALUE	UNIT
1. PMd	Maximum growth rate of diatoms	2.5	1/day
2. TMc	Optimum T for cyanobacteria	25	Degree
3. TMg	Optimum T for green algae	22.5	Degree
4. STOX	Salinity toxicity	5	Ppt
5. WSc	Settling velocity for diatoms	0.35	m/day
6. WScg	Settling velocity for green algae	0.25	m/day
7. Kdcalg	Constant relating respiration of DOC to algal	0.03	per g C m ³
	Biomass		per day
8. O2CRIT	Critical DO concentration for layer 1 incremental	2	mg/l
	PO4 sorption		

4.4 Water Quality Model Calibration and Verification

4.4.1 Model calibration

The primary means of calibrating the water quality model was through comparison of modeled and observed water quality variables. Calibration was an iterative process, in which algal growth and decay rates, chemical kinetic coefficients, partition coefficients, half saturation constants, and sediment mineralization rates were adjusted to improve model-observation comparison. For the calibration of the ICM model, the year 2004 was selected as the calibration period, as this is the year with intensive monitoring observations for both the hydrodynamic [surface water elevation, ADCP (Acoustic Doppler Current Profiler) measurement of currents], and water quality variables (DO, Chlorophyll, TN, TP, ammonia, nitrate, DON) as well as high spatial coverage. Figure 4.4 (a) displays six (6) intensive water quality monitoring stations in the Isle of Wight Bay: Stations 1, 2, 3 are located in Turville Creek and Stations 4, 5, 6 extend throughout Isle of Wight Bay approaching the Ocean City Inlet. Figure 4.4 (b) shows five (5) bay-wide stations: Station A at Assawoman Bay, Station B at the middle reach of the St. Martin River, Station C in northern Chincoteague Bay downstream of Newport Bay, and Stations D and E in middle and southern Chincoteague Bay. The hydrology of year 2004 in the Saint Martin River is shown in Figure 3-10 (a) in Chapter 3. Compared to the historical record, year 2004 is a wet hydrologic year with large spring freshwater inputs at about 200-300 cubic feet per second (cfs) in April, and greater than normal summer freshwater inputs in July and August. The model predicted water quality variables in 2004 for the five stations along the transect of Turville Creek in Isle of Wight Bay were compared to the DNR monthly survey data. Station 1 was not included due to

its location in the nontidal headwaters (and thus it is not included in the water quality model grid).

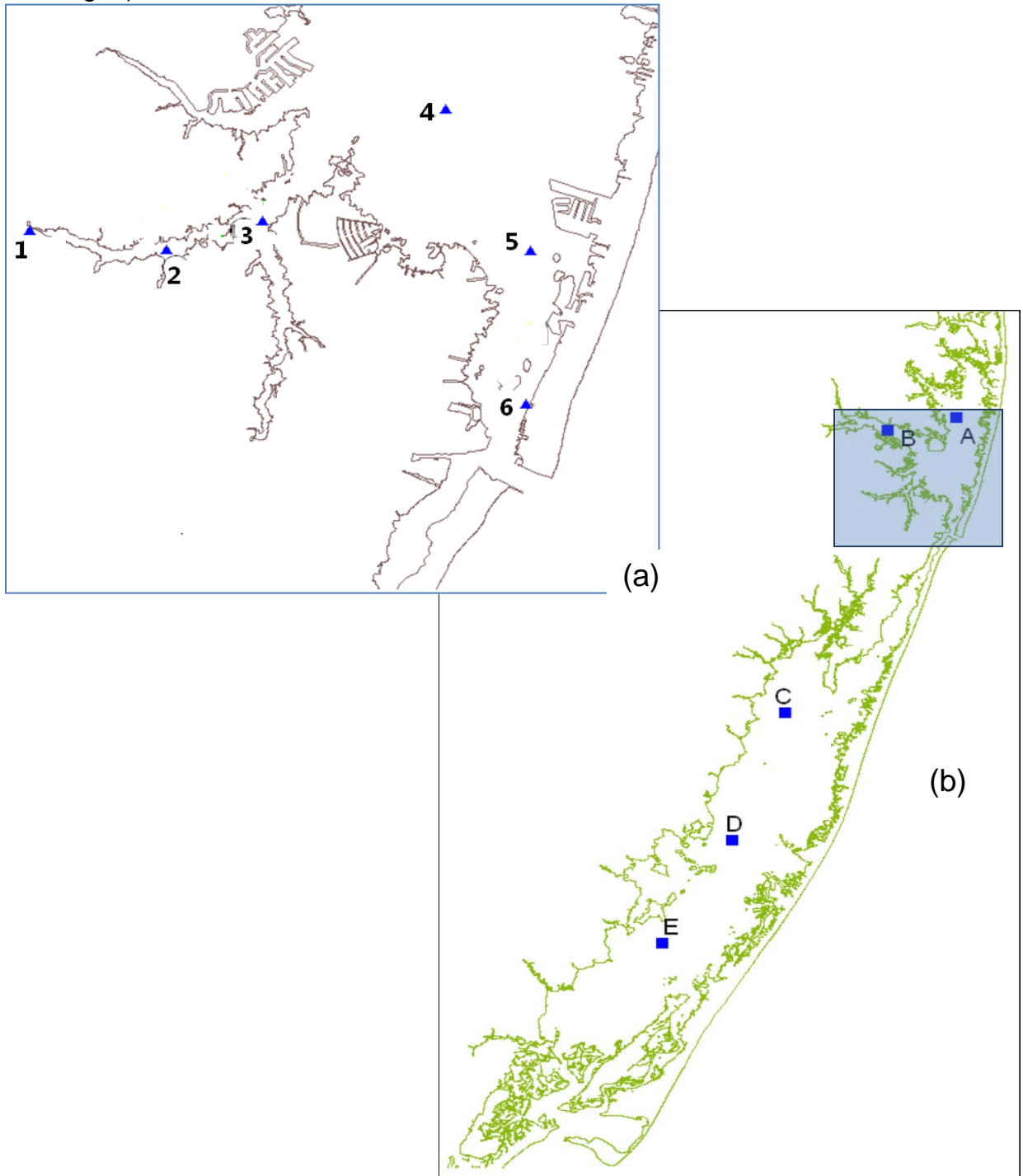


Figure 4.4 Intensive monitoring stations in (a) Isle of Wight Bay and (b) Maryland Coastal Bays.

Figure 4-5 (a) shows the results of the chlorophyll-a simulation, which capture both temporal and spatial features of chlorophyll-a along the transect of Turville Creek in the Isle of Wight Bay. Specifically, chlorophyll-a exhibits a strong longitudinal gradient from Station 2 to Station 6 from about 40 $\mu\text{g/l}$ at Station 2 (upper Turville Creek) to less than 10 $\mu\text{g/l}$ at Station 6 (lower Isle of Wight Bay). The model also captures the seasonal pattern well. For instance, at Station 2, the chlorophyll a levels remain low in winter and reach maximum in late summer. This general pattern has been well reproduced in the model. Additionally, the model also catches the spring phytoplankton bloom event around Day 90-120. An example of this is at Station 2, day 110, when chlorophyll a suddenly jumps above 40 $\mu\text{g/l}$. The same event was recorded at DNR's continuous monitoring site as well (not shown). Apparently, this phytoplankton bloom event was fueled by a large freshwater pulse and accompanied by a sharp salinity drop as shown in Chapter 3.

Figure 4.5(b) shows the model is capable of simulating the temporal and spatial variability of DO correctly as compared well with the observation data. In the upstream two stations of Turville Creek, the hypoxia and episodic, prolonged (days) low DO events does occur which is presumably driven by high nutrient load combined with respiration rate, suggested by the continuous monitoring data. Although the current model is not fully implemented to simulate diurnal DO diel cycle, the model does have the capability to capture variation of episodic hypoxic events on time scale of several days. For example, at Station 2, the monitoring data reveals a DO drop around Day 210 and the same event was also reasonably captured by the model. Lastly, along with field measurements, the model results reasonably reflect DO seasonality and the longitudinal gradient (e.g., low DO rarely occur at Stations 4-6 closer to the Ocean City Inlet). Chapter 5 discusses diurnal DO diel variation, which was reproduced by post-processing model results using a statistical relationship with the daily mean DO.

In terms of simulating nutrient variables including the nitrogen and phosphorus species, the model also performs satisfactorily. In Figure 4.5(c) and (d), the model captures the nutrients' seasonal pattern. For instance, NO_{23} , the most important land-originated N source has a distinct seasonal pattern that rose in winter-spring due to watershed inputs, and depleted in summer due to rapid uptake by autotrophs. This temporal variability is well produced by the model, as shown in Figure 4-5(d). On the other hand, NH_4 , which mainly derives from *in situ* recycling/regeneration processes in the sediment and water column, often increases in the summer/fall season, and the model captures this temporal trend. The PO_4 obtained from the watershed source can be used up in the spring by the phytoplankton bloom and subsequently deposited into sediment and re-mineralized. In the Chesapeake Bay, when the anoxic condition developed in the late summer, the stored phosphate will then be released back to the water column in large quantity and fuels the second peak of phytoplankton bloom. Figure 4.5(e) shows the seasonal pattern of PO_4 in the MCBs, in which, it doesn't seem to have release in pulsation like that in Chesapeake Bay presumably due to milder low DO condition in MCBs. Lastly, dissolved organic nutrients (e.g., DON), which are controlled by the balance between *in situ* production (source) and decomposition (sink) processes, were maintained at stable but higher concentrations as compared to inorganic nutrients. As can be seen from Figure 4.5(f), DON does not exhibit substantial variations in either

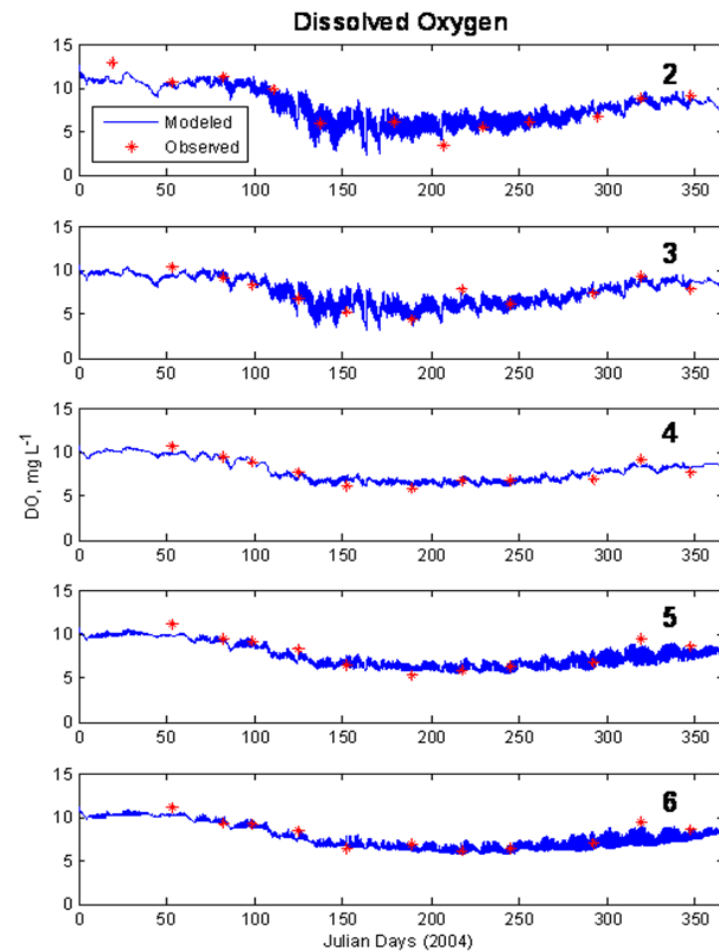
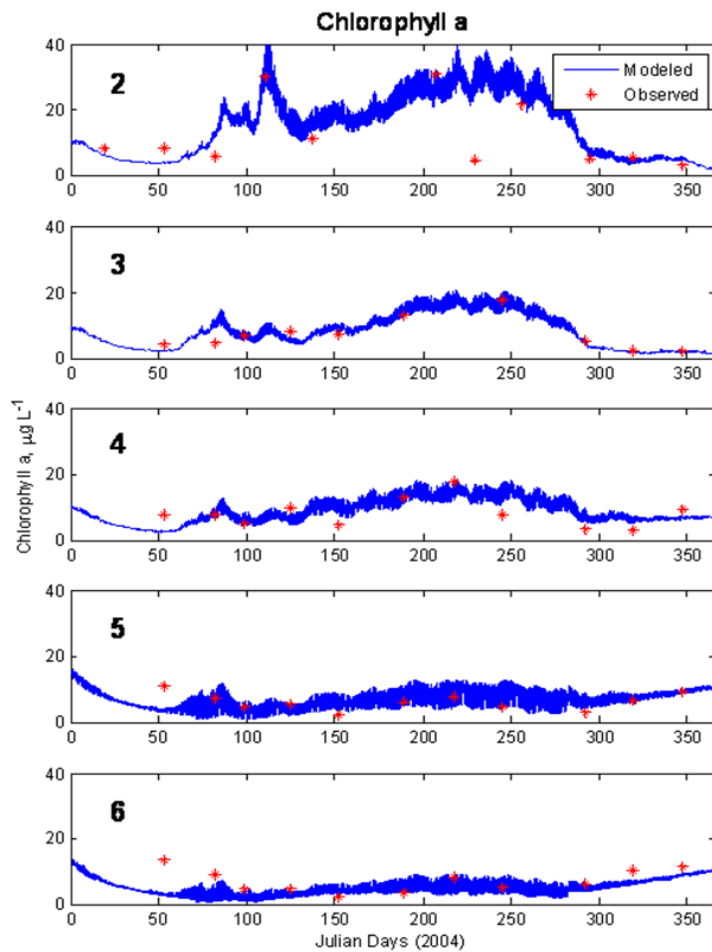


Figure 4.5 (a) and (b): Comparisons of model prediction and field measurement for chlorophyll-a and DO in the Isle of Wight Bay.

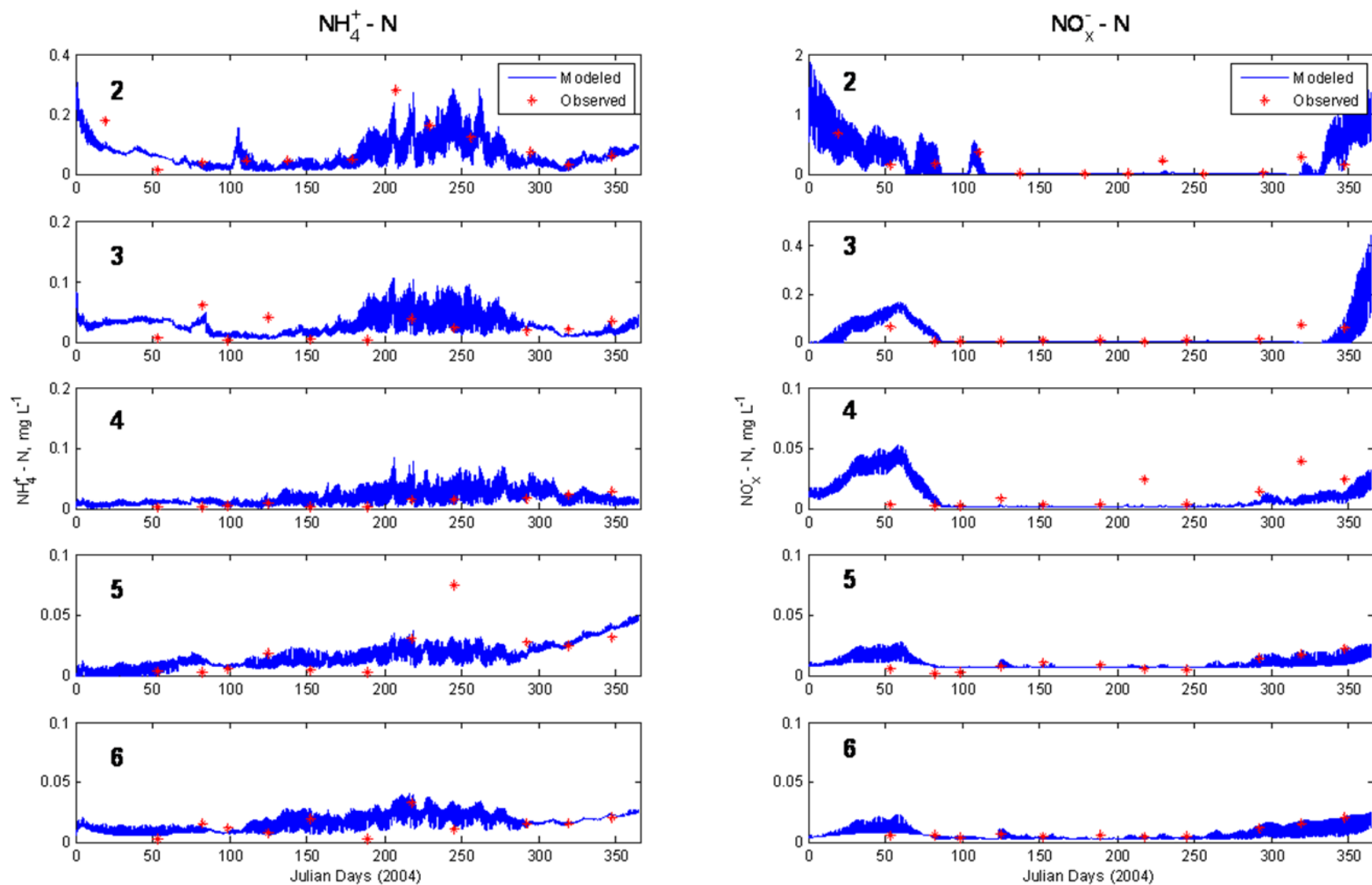


Figure 4.5 (c) and (d): Comparisons of model predictions and field measurement for NH_4 and NO_{23} in the Isle of Wight Bay.

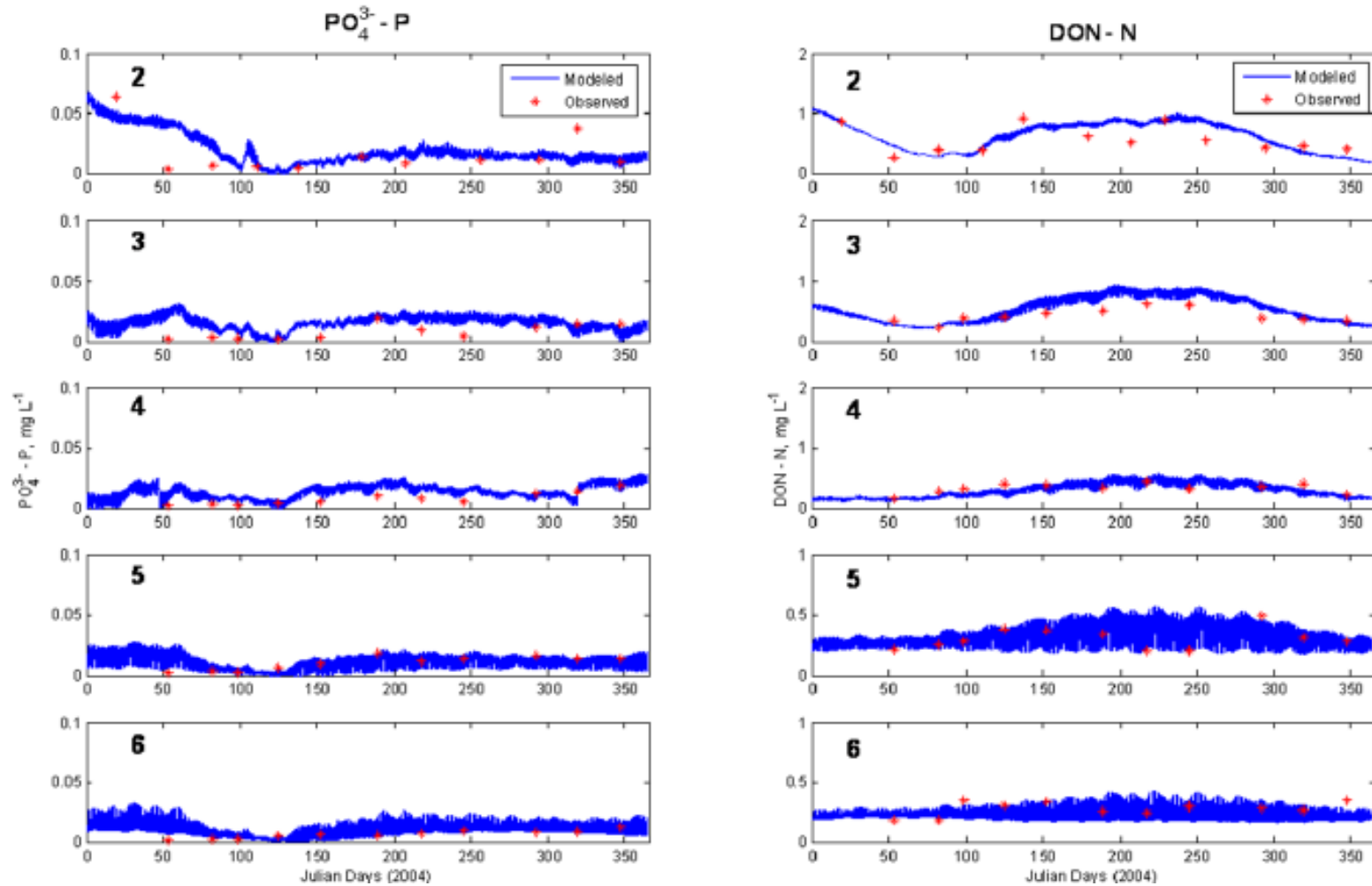


Figure 4.5 (e) and (f): Comparisons of model predictions and field measurement for PO_4 and DON in the Isle of Wight Bay.

temporal (seasonal) or spatial (at difference stations) scales unlike inorganic nutrients, which can change by an order of magnitude. Nevertheless, DON does have a seasonal trend, increasing in warmer months, presumably fueled by high primary production and respiration in the system. The model results agree well with field observations.

To expand the water quality calibration to the bay-wide scale, the model results were presented in five stations located in the open bay portion of the MCBs as shown in Figure 4.4 (b). These stations include Station A in Assawoman Bay, Station B in St. Martin River, Station C is in Newport Bay, Station D in mid-Chincoteague Bay and Station E in the southern Chincoteague bay. Figure 4.6 (a) shows that chlorophyll-a is consistently higher in the northern Bays (Stations A and B) than in the southern Bays (Stations C, D, and E). This is consistent with the fact that the northern Bays have a larger nutrient loading than do the southern Bays and thus supports higher concentration of algae. The high frequency variation of chlorophyll-a is also observed in the northern Bay stations, but not in the southern Bay stations. Figure 4.6 (b) shows DO concentration has a seasonal pattern, with the highest concentrations in the winter and the lowest in the summer. When compared with the previously generated DO results at the tributaries where DO can fall down to hypoxic levels (Figure 4.5 (b)), the DO at open Bay stations A, B, C, D, E does remains at or above 5 mg/l. It was observed that DO oscillation was more pronounced in the northern Bays, an indication of the effect of tidal currents which can induce semi-diurnal oscillation, as well as the manifestation of more photosynthetic activity during daytime and more cellular respiration at night due to greater algal biomass. Figure 4.6 (c) and 4.6 (d) show the temporal variation of nitrogen species NH_4 and NO_{23} , which have quite different seasonal patterns. NH_4 exhibits the highest concentrations in the late summer and early fall, whereas NO_{23} concentrations are highest in the winter and lowest in the late summer and early fall. This can be understood from the fact that most important source for NO_{23} is terrestrial and thus abundant in the winter due to watershed inputs; NO_{23} is depleted in the late spring and summer due to the uptake by phytoplankton. NH_4 is mainly maintained by *in situ* recycling and regeneration through sediment process. In the spring, NH_4 is quickly used up by the algal spring bloom, but is recycled back in the later summer and early fall into the water column through the sediment diagenesis process. Consistent with the chlorophyll-a concentrations, NH_4 concentrations are higher in the northern Bays than in the southern Bays. Figure 4.6(e) shows the seasonal pattern of phosphorus; lowest concentrations are in the spring due to the spring algae bloom, but, like NH_4 , concentrations can bounce back in the later summer through the sediment flux. In addition, phosphorus be delivered from the land in the winter. In the southern Bays, there is an apparent longitudinal gradient of NH_4 , NO_{23} and PO_4 , higher in the north and lower in the south along the axis of Stations C, D, and E; this suggests that it is derived from a source in the Newport Bay. Connecting cause and effect, it can be seen that the watershed loading, transport dynamics and bio-chemical processes are all linked together. The successful coupling of watershed, hydrodynamic and water quality models in this project, with good calibration, allows the model to produce excellent results that are consistent with the multi-phase measurements in MCBs.

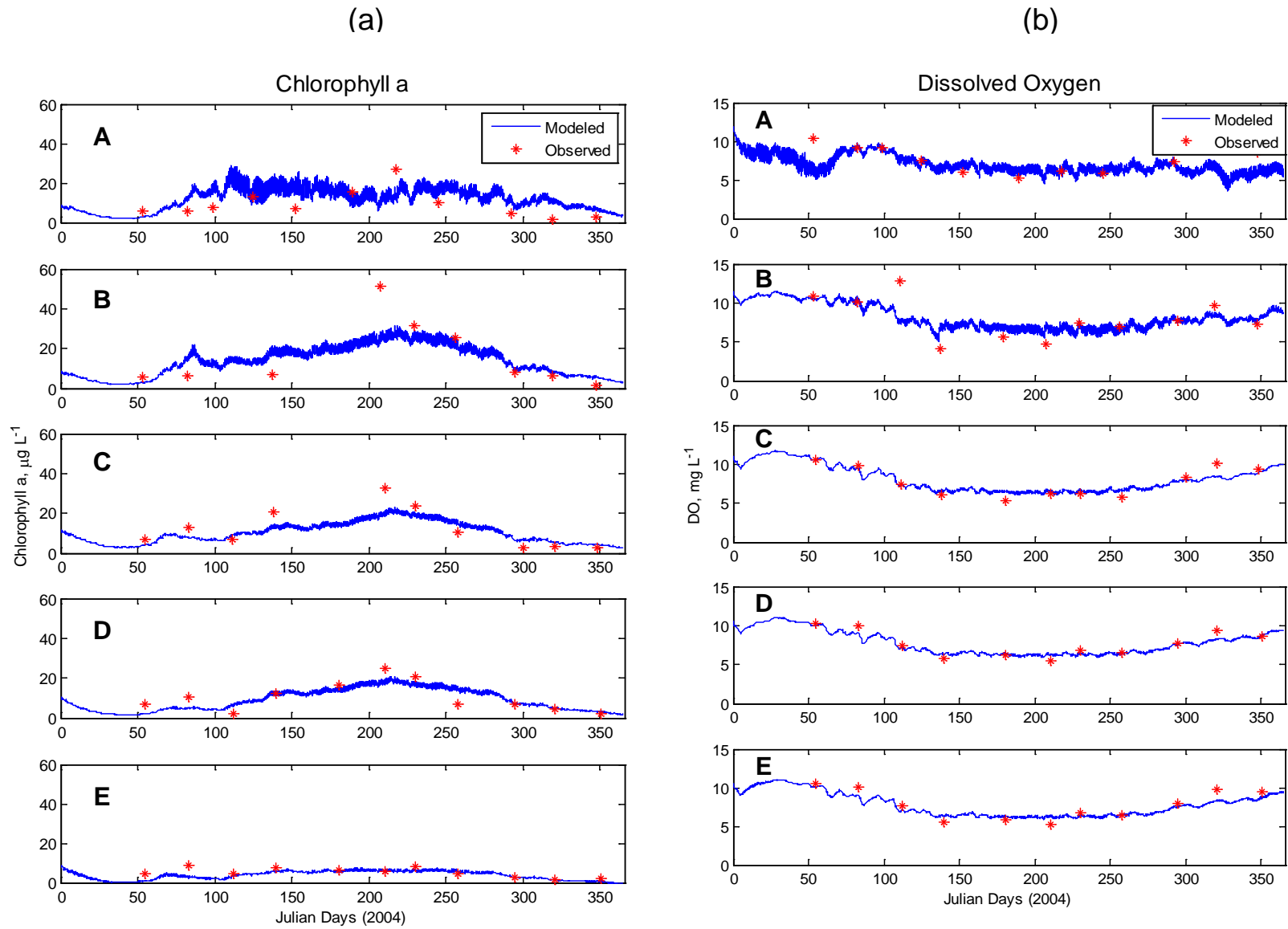


Figure 4.6 (a) and (b): Comparisons of model predictions and field measurement for Chlorophyll-a and DO in Bay-wide stations.

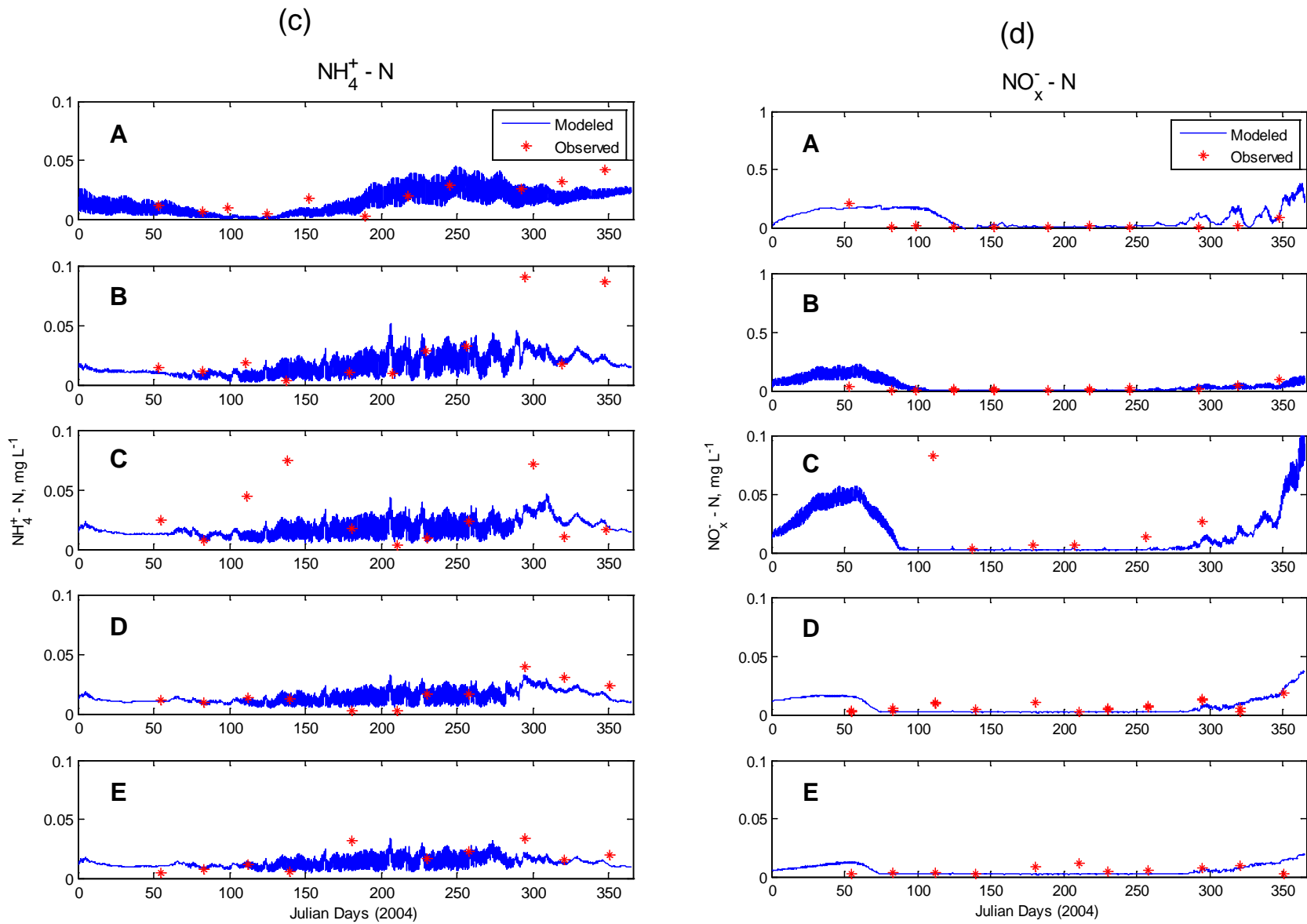


Figure 4.6 (c) and (d): Comparisons of model predictions and field measurements for NH_4 and NO_3 in Bay-wide stations.

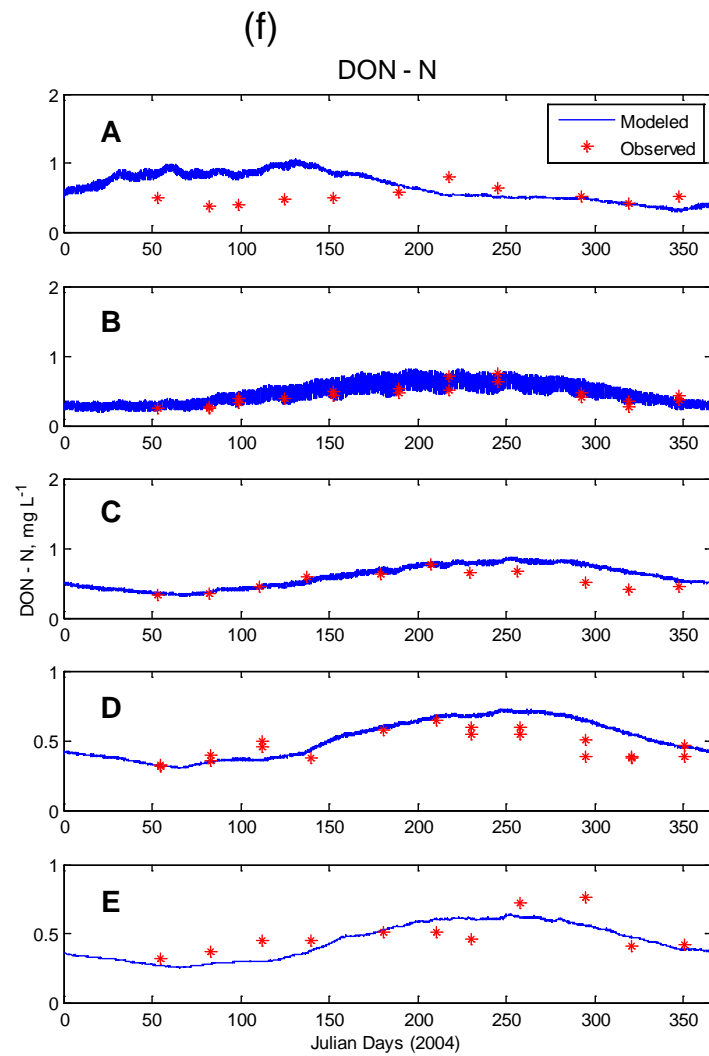
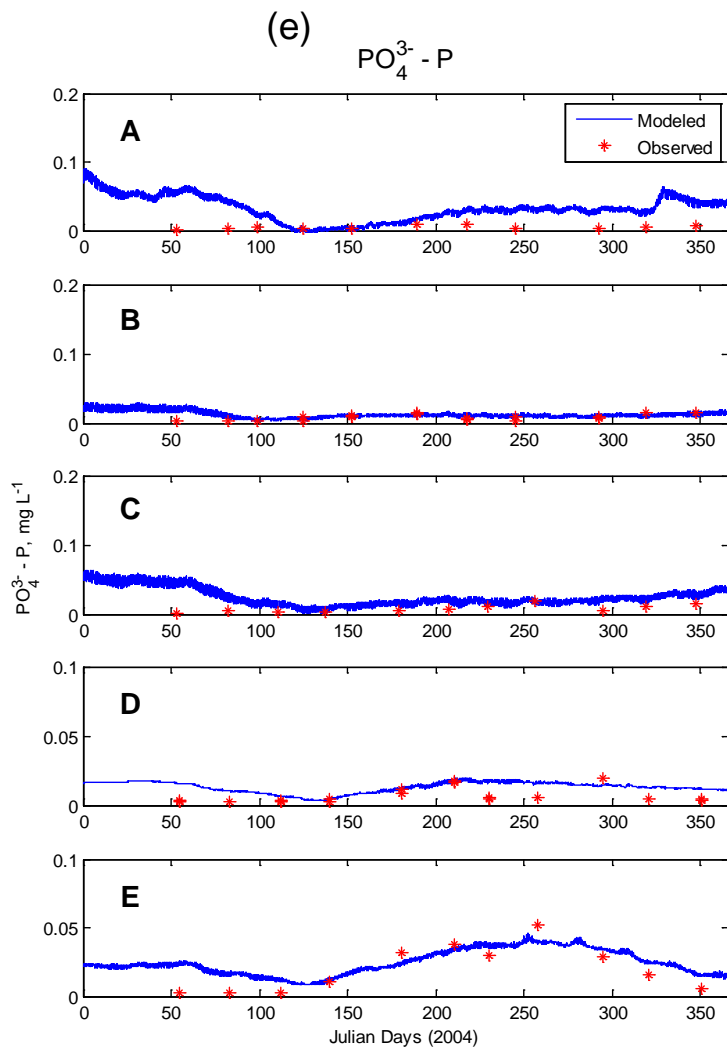


Figure 4.6 (e) and (f): Comparisons of model predictions and field measurement for PO_4 and DON in the Bay-wide stations.

4.4.2 Model verification

Since a water quality model typically requires using many coefficients to parameterize the ecosystem processes, a comparison of numerical model output with the observation data is an important and necessary step. Given that prediction capability is an important component of TMDLs, it is critical to assess the water quality model with an independent set of data and test the range of validity for the model. The process involves running the models with the calibrated parameters and comparing the results to verify that the coefficients used are self-consistent under various dynamic conditions. The calibration was conducted using intensive survey data collected in 2004; whereas for verification purposes, the water quality model was further compared with surveys conducted through 2001-2003 by Maryland DNR and Assateague Island Park Service (ASIS). With this step, the model is confirmed as valid for different hydrological and environmental conditions, and the model developed can be applied to investigate various operational and management scenarios. For the verification process, the external nutrient loadings, boundary conditions, and all the parameters of the water quality model were specified using identical values for the calibration. The initial condition was also specified to be the same at the beginning of both simulations. Figure 4.7 showed station locations where the monthly observed data were collected at the twenty-seven (27) DNR and eighteen (18) ASIS stations. The DNR stations cover most of the MCBs except Sinepuxent Bay whereas the ASIS stations only cover stations south of the Ocean City Inlet including Sinepuxent, Newport and Chincoteague Bays. An annual runoff cycle exists, with peak flow in the spring and minimum flow in the summer. However, floods and droughts frequently cause daily and monthly flow deviations from the long-term pattern. Figures 4.8 (a) show the flow discharge rate and Figure 4.8 (b) the chlorophyll-a calculated from January 2000 - August 2005 (note: for 2005, only a partial record, through August, was available) at the calibration site of Birch Branch watershed. The year of 2001 can be characterized as an average year, 2002 a dry year, and 2003 and 2004 were wet years. In 2002, the lower than normal spring flow was the result of the drought year and in 2003, the higher than normal flow in September was caused by Hurricane Isabel. As can be seen, the chlorophyll-a level is proportion to the hydrologic inputs: the larger the nutrient load inputs, the greater the phytoplankton biomass. The flushing effect of the fast moving stream on the phytoplankton biomass, which happens in other estuaries, does not seem to apply in the Maryland Coastal Bays.

The time series comparisons of water quality model results with the observations measured at DNR and ASIS stations are presented in Figures 4.9 through 4.15. Figure 4-9 (a) (b) and (c) show the dissolved oxygen comparison at all DNR stations from January 2001 to August 2005. The DO concentrations in Figure 4.9 (a) exhibit various degrees of hypoxia at the first 6 stations (4 stations in the left panel and the top 2 stations in the middle panel) located in the tributaries of the Saint Martin River. Among them, the Manklin Creek station demonstrates anoxic conditions in 2004 and 2005, which the model was able to capture by additional chemical oxygen demand. The model also simulated temporal variation of the hypoxia well for the other 5 stations. The DO at station XDM4486, located in the upstream of Saint Martin River, also showed similar signs of hypoxia both from both observations and model results (Figure 4.9 (b)).

For these stations, there are clear signs of increasing summer hypoxia from 2003 - 2005, coinciding with the high flow of these consecutive years. The rest of the 20 DNR stations, away from the aforementioned 7 stations in the Upper Saint Martin River tributaries, in general, do not exhibit persistent hypoxia issues. Figure 4.11 (a) – (c) shows the comparison of chlorophyll a for all the DNR stations. The pattern of high chlorophyll-a, in general, is correlated with that of low DO stations. For example, the 7 stations in the upper Saint Martin River tributaries (where hypoxia occurred) showed a consistent higher chlorophyll pattern. Three additional stations in the middle and lower Saint Martin River, XDN3724, XDN4312 and XDN4797, also have high chlorophyll a, exceeding 50 μg in 2004 and 2005. The reason for the correlation between low DO and high chlorophyll a can be partially explained by the sediment oxygen demand (SOD) as a result of the deposition of organic matter from phytoplankton blooms, as shown in Figures 4.13 (a) – (c). It was clear that hypoxia occurred at the stations whose SOD exceeds 0.5g C per m^2 . For stations with SOD less than 0.5 g C per m^2 , hypoxia rarely occurred. The DO and Chlorophyll a comparison for the ASIS stations is also shown in Figures 4.14 (a) – (b) and Figure 4.15 (a) – (b). For the stations south of the Ocean City Inlet, in general, there are no persistent low DO and high chlorophyll a problems.



Figure 4.7: MD DNR and ASIS monitoring stations in the Maryland Coastal Bays.

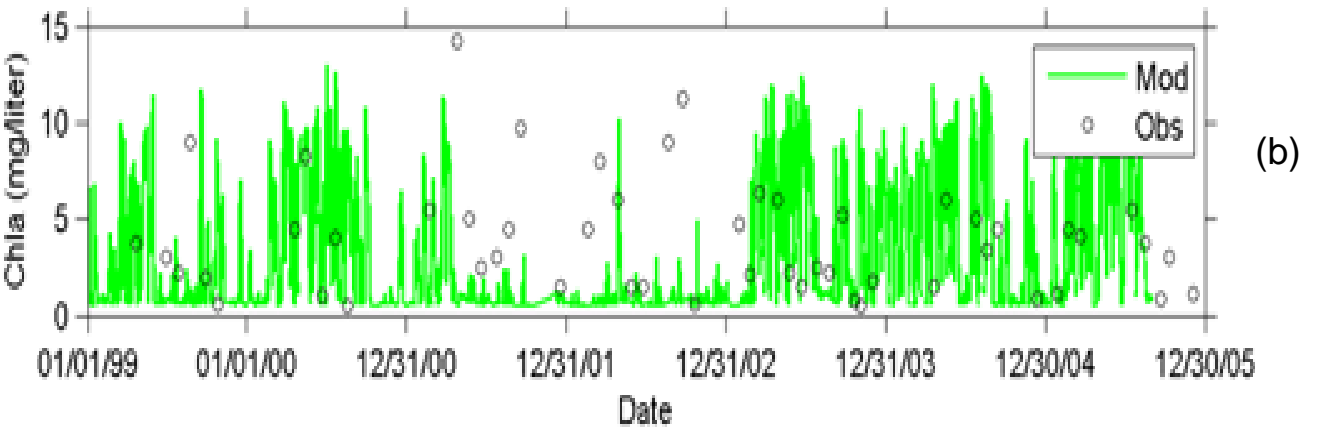
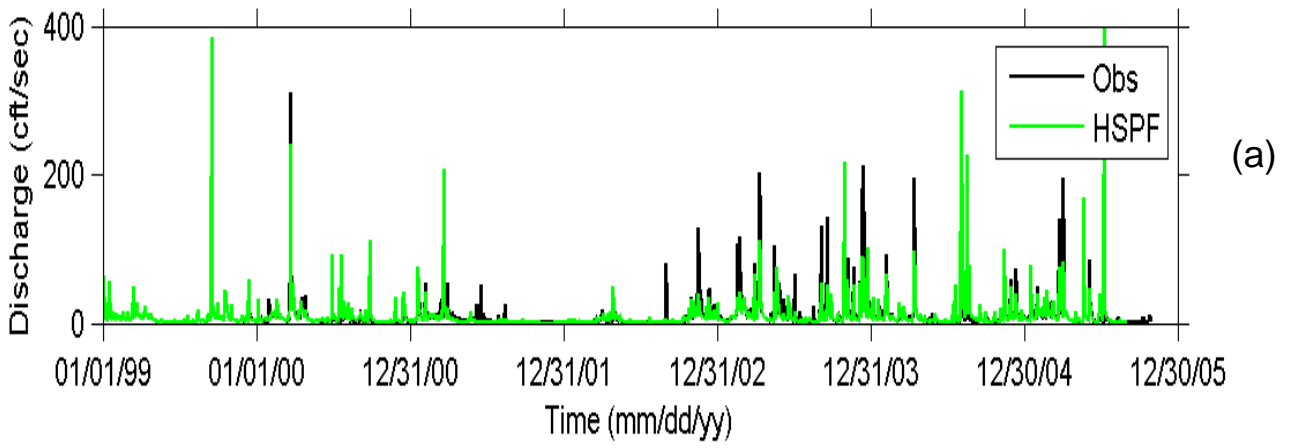


Figure 4.8 (a) The flow discharges and (b) Chlorophyll-a concentration from Birch Branch watersheds.

Evaluating model performance during the verification process requires statistical summaries of the comparison of many observations with model results. Summary statistics of mean error, absolute mean error, relative error and correlation coefficient are employed to assess the accuracy of the model. The mean error (ME) is defined as:

$$ME = \frac{1}{N} \sum_{n=1}^N (P_n - O_n)$$

Positive ME indicates the model's overestimation of the data on the average and negative ME indicates the model's underestimation of the data on the average, with zero ME being ideal. The mean absolute error (MAE), a measure of the absolute deviation of the model results from the data on the average, is defined as:

$$MAE = \frac{1}{N} \sum_{n=1}^N |P_n - O_n|$$

where P_n and O_n = corresponding model results and data; N = number of observations. The MAE of zero is ideal. Since the MAE cannot be used to discern the overestimation or underestimation, another measure is desirable. The relative error (RE) is defined as:

$$RE = \frac{\sum |P_n - O_n|}{\sum O_n}$$

The RE is the ratio of the MAE to the mean of the data, indicating the magnitude of the MAE relative to the data on the average. The correlation coefficient defined as:

$$r = \frac{\sum_{i=1}^N (P_{mod} - \bar{P}_{mod})(O_{obs} - \bar{O}_{obs})}{\left[\sum_{i=1}^N (P_{mod} - \bar{P}_{mod})^2 \sum_{i=1}^N (O_{obs} - \bar{O}_{obs})^2 \right]^{1/2}}$$

in which the model predictions were treated as independent variables and observations as dependent variables in a regression analysis.

The mean error describes whether the model over-estimates or under-estimates the observations, on average. The mean error can achieve its ideal value, zero, while large discrepancies exist between individual observations and computations. The absolute mean error is a measure of the characteristic difference between individual observations

and computations. An absolute mean error of zero indicates the model perfectly reproduces each observation. The relative error is the absolute mean error normalized by the mean concentration. Relative error provides a statistic suitable for comparison between different variables or systems. Quantitative statistics were determined through comparison of model results and observations for each of the basins in the MCBs sampled at approximately monthly intervals. For dissolved oxygen, the concentration measured at 1.5 meter above the bottom was compared and for chlorophyll a comparisons for surface samples were examined and presented.

The measure of correlation between modeled and observed DO were above 0.75, as shown in Figure 4.10, Tables 4.2 and 4.3. The bottom DO is within 1 mg/l of the observed range and the relative error is within 15%. Examination of relative error of chlorophyll-a indicating that chlorophyll a has the greatest error around 60-70%. The chlorophyll a error reflects the difficulty in computing this dynamic biological component which can attain a very large magnitude. The TN and TP statistics, as shown in Table 4.2, are in the mid-range of 30% to 45%, which total phosphorus, perhaps exhibiting slightly higher relative error. The higher error in phosphorus reflects the difficulties in evaluating loads, in simulating re-suspension and in representing particulate phosphorus transport (Cerco et al., 2004). This is particularly true for the Saint Martin River, where uncertain loads discharged into the constrained volumes of the tributaries, are the major reason for higher relative error in the Isle of Wight and Newport Bays.

No standard criteria exist for judging acceptable model performance. One approach is to compare performance with similar statistics from other model applications. Statistics comparable to other systems at least indicate the model is in the performance mainstream. The relative error was compared to the relative errors presented in the 2002 Chesapeake Bay application, Florida Bay (Cerco et al., 2000) and the lower St. Johns River, Florida (Tillman et al. 2004). Florida Bay is a shallow sub-tropical lagoon. The St. Johns River is a partially- to well-mixed estuary with a substantial tidal freshwater extent. When the relative error is inter-compared, as shown in Table 4.4, all models indicate chlorophyll a has the greatest relative error. Comparison of the parameters DO, TN and TP indicate that MCBs model results are comparable to the quality of other TMDL studies.

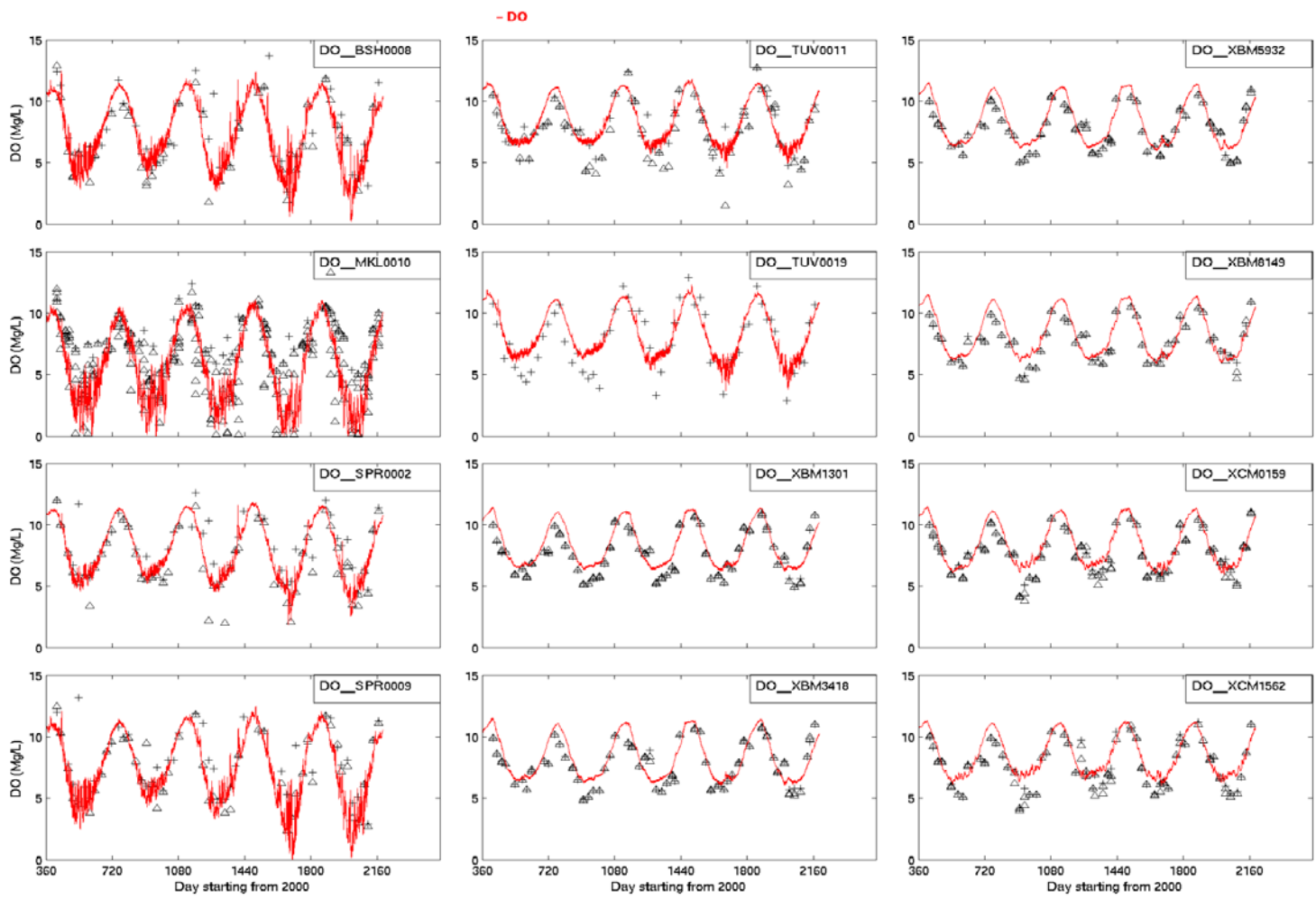


Figure 4.9 (a): DO verification with DNR data, Stations 1-12, 2001- 2005.

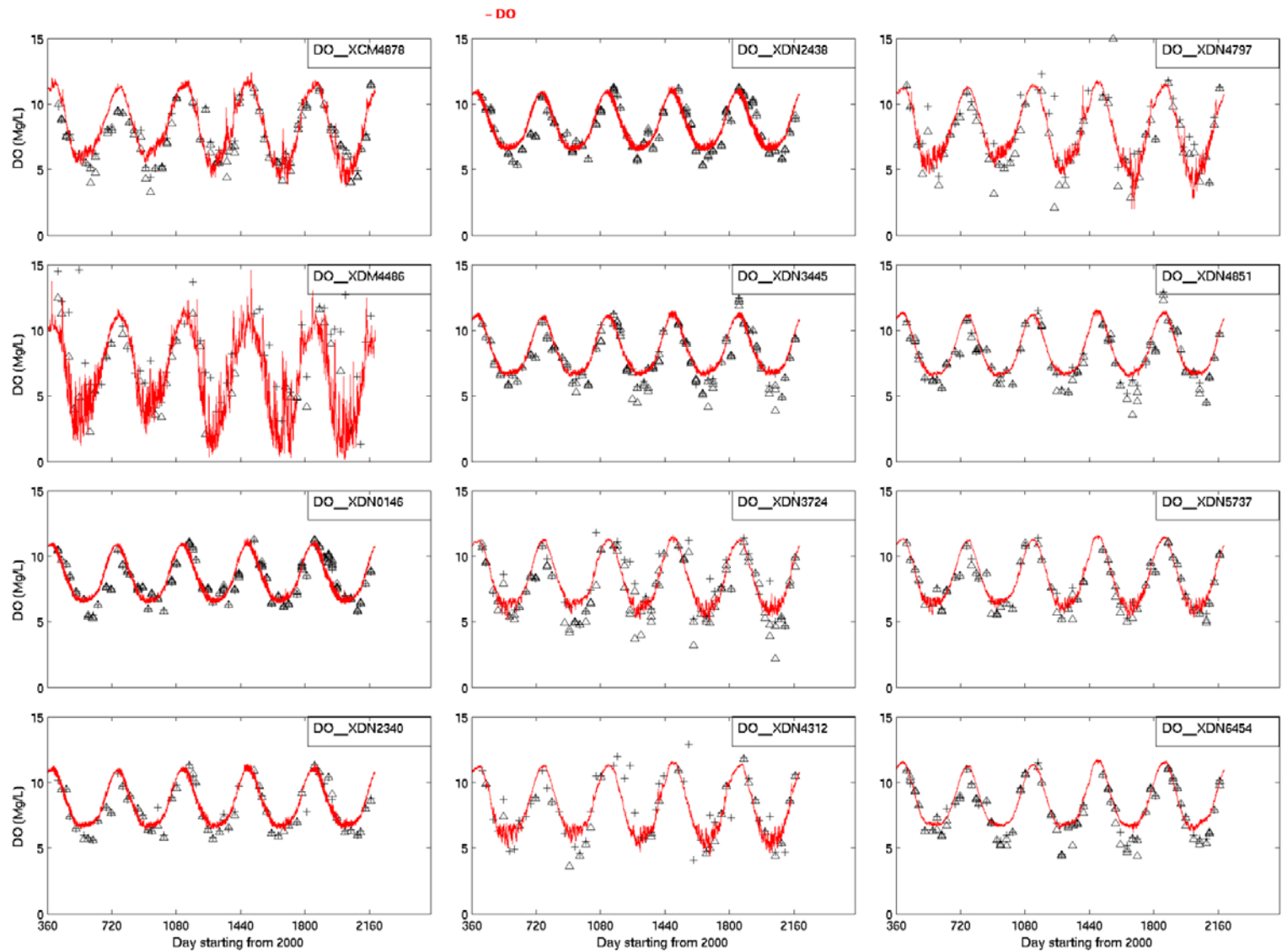


Figure 4.9 (b): DO verification with DNR data, Stations 13-24 2001-2005.

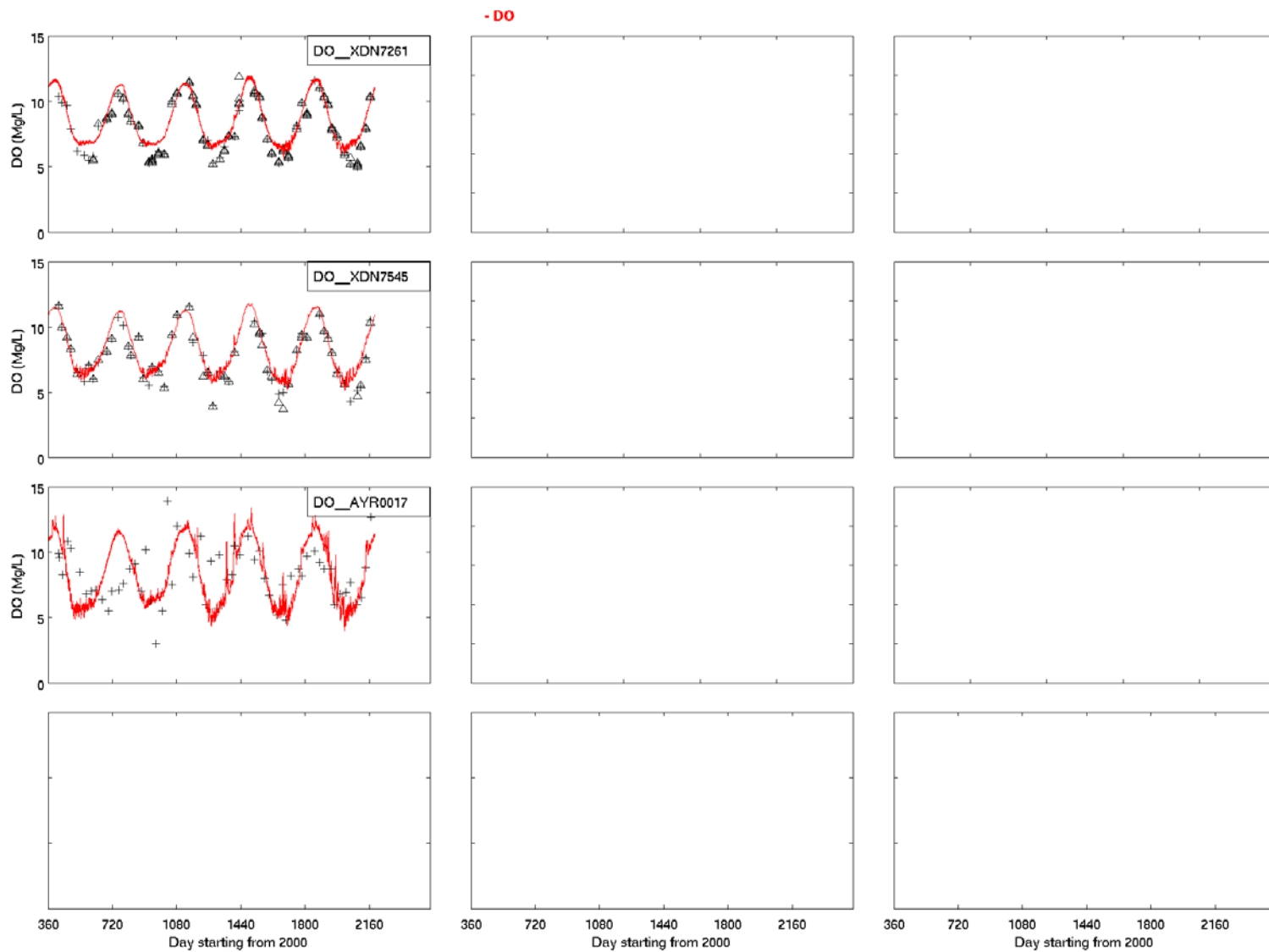


Figure 4.9 (c): DO verification with DNR data, Stations 25-27, 2001-2005.

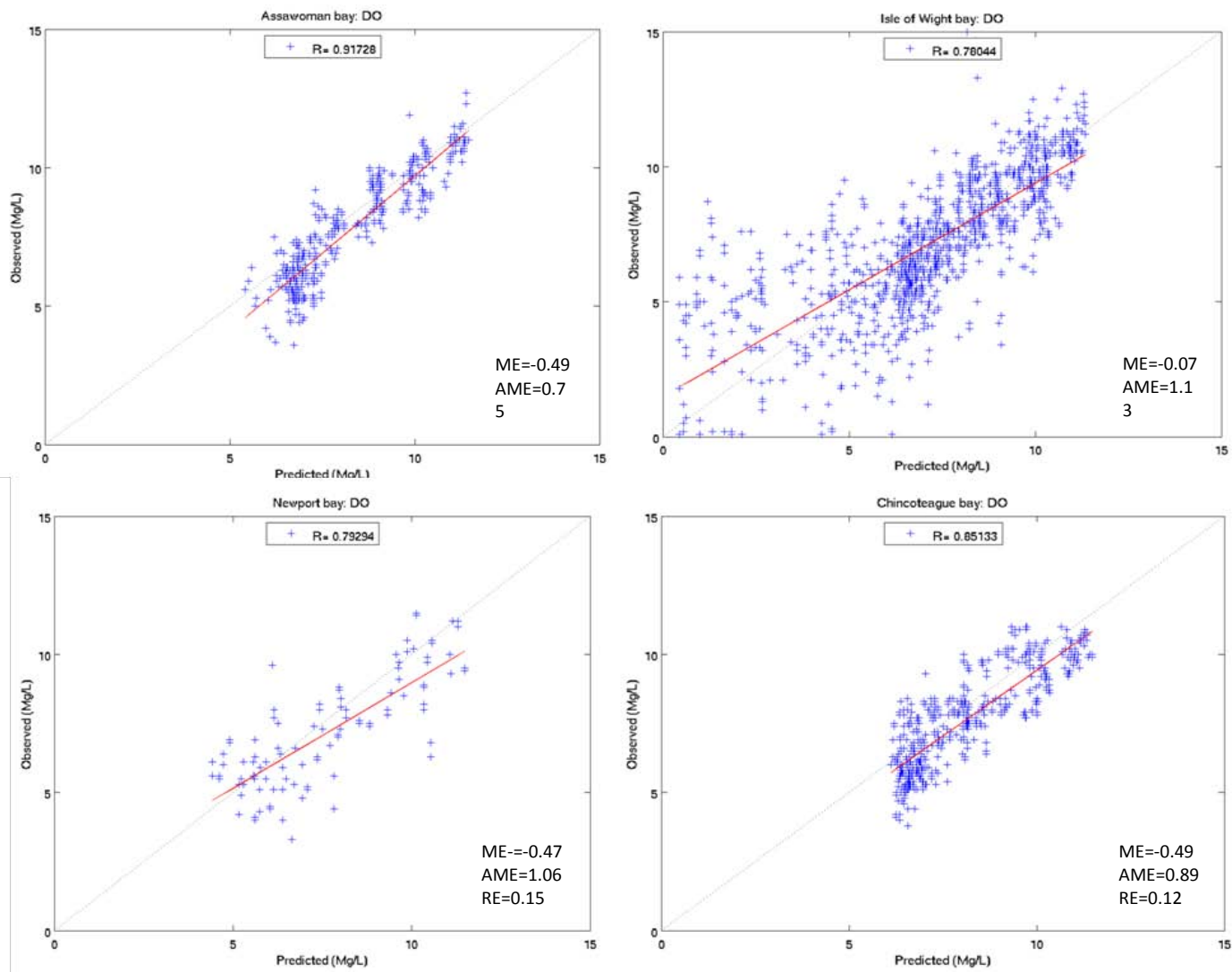


Figure 4.10: Statistical comparison of observed versus modeled DO; Assawoman, Isle of Wight, Newport, and Chincoteague Bays.

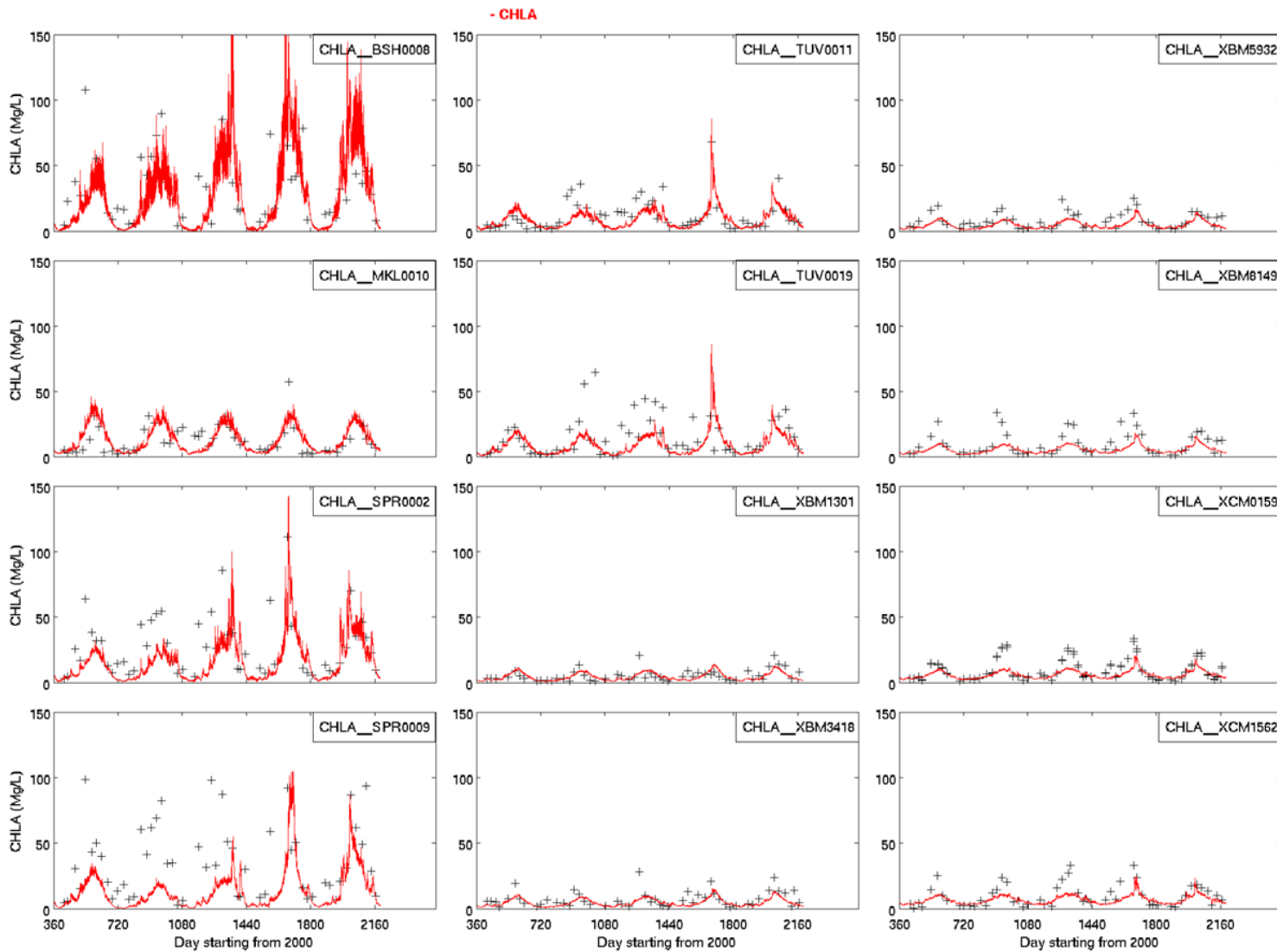


Figure 4.11 (a): Chlorophyll-a verification with DNR data Stations 1-12, 2001-2005.

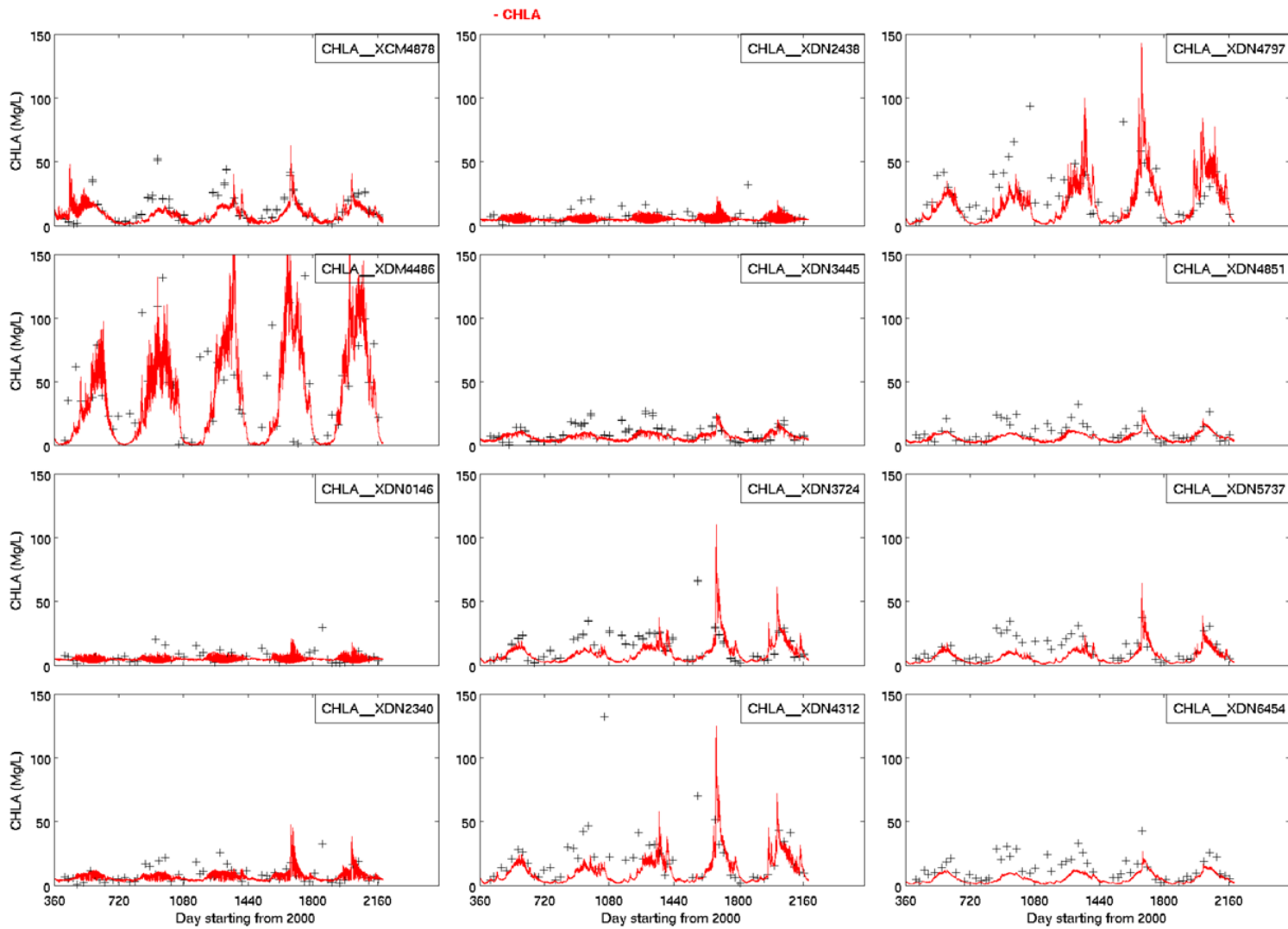


Figure 4.11(b): Chlorophyll-a verification with DNR data Stations 13-24, 2001-2005.

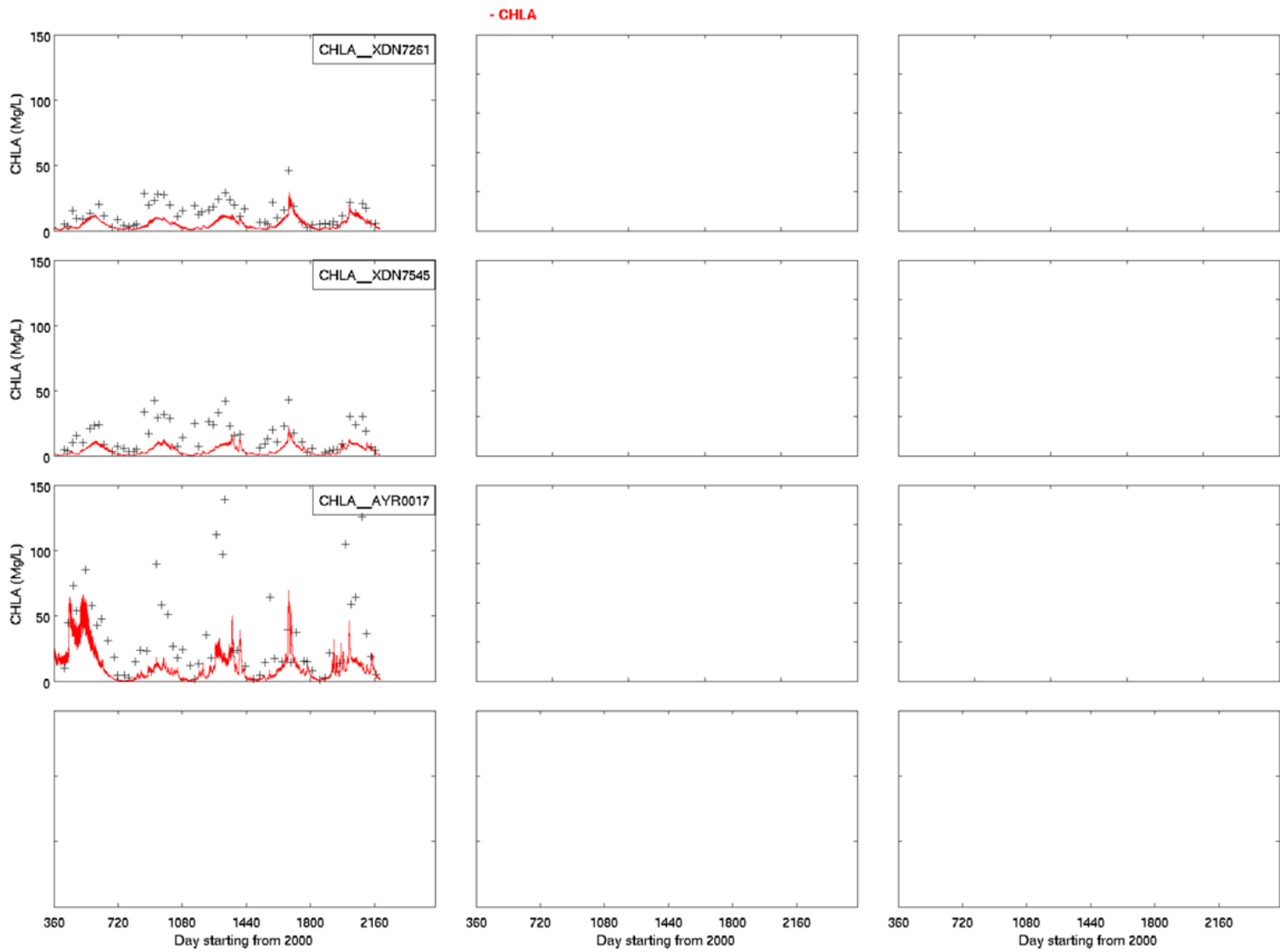


Figure 4.11 (c): Chlorophyll-a verification with DNR data Stations 25-27, 2001-2005.

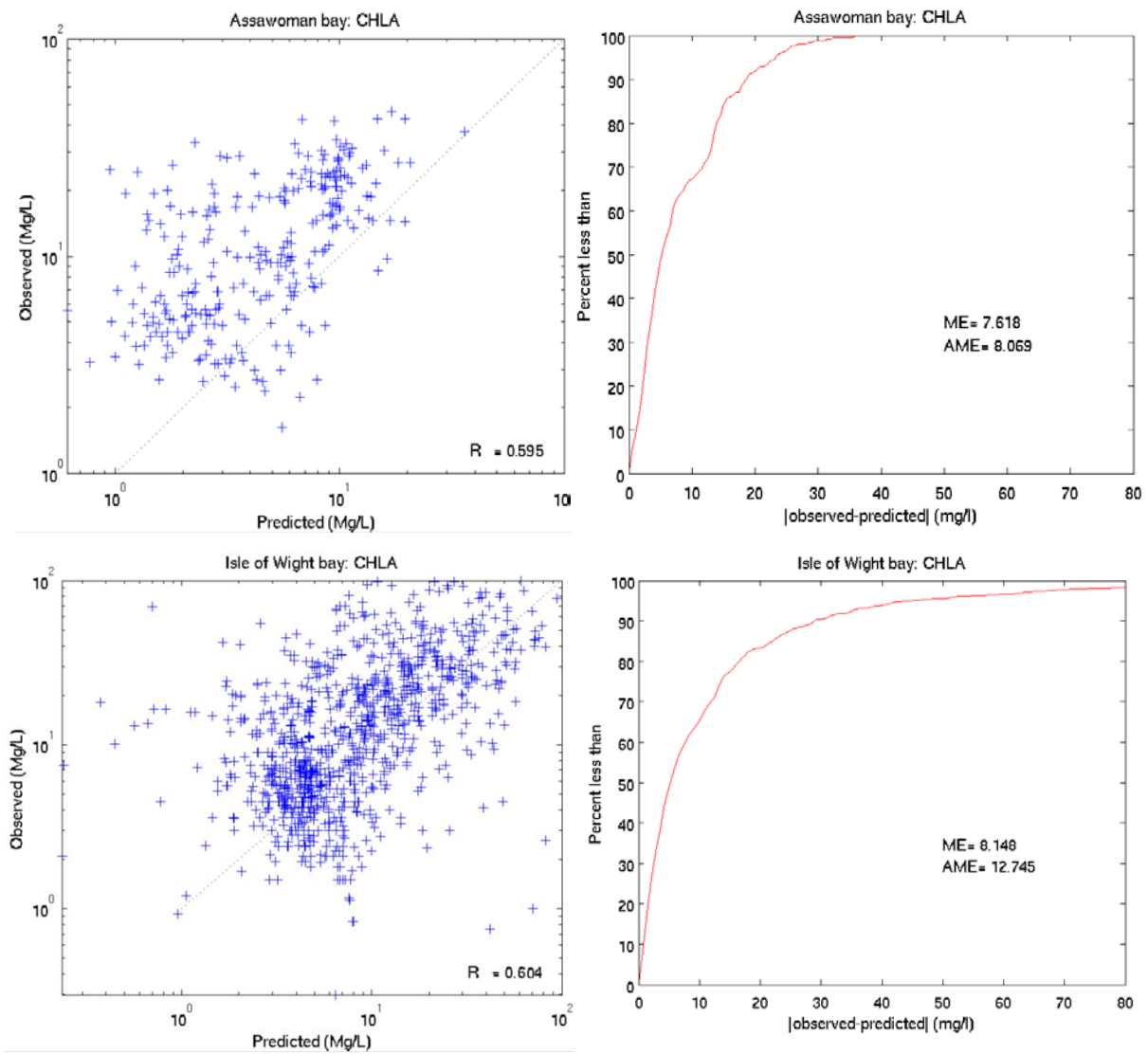


Figure 4.12 (a): Statistical comparison of observed versus modeled Chlorophyll-a data for Assawoman and Isle of Wight Bays.

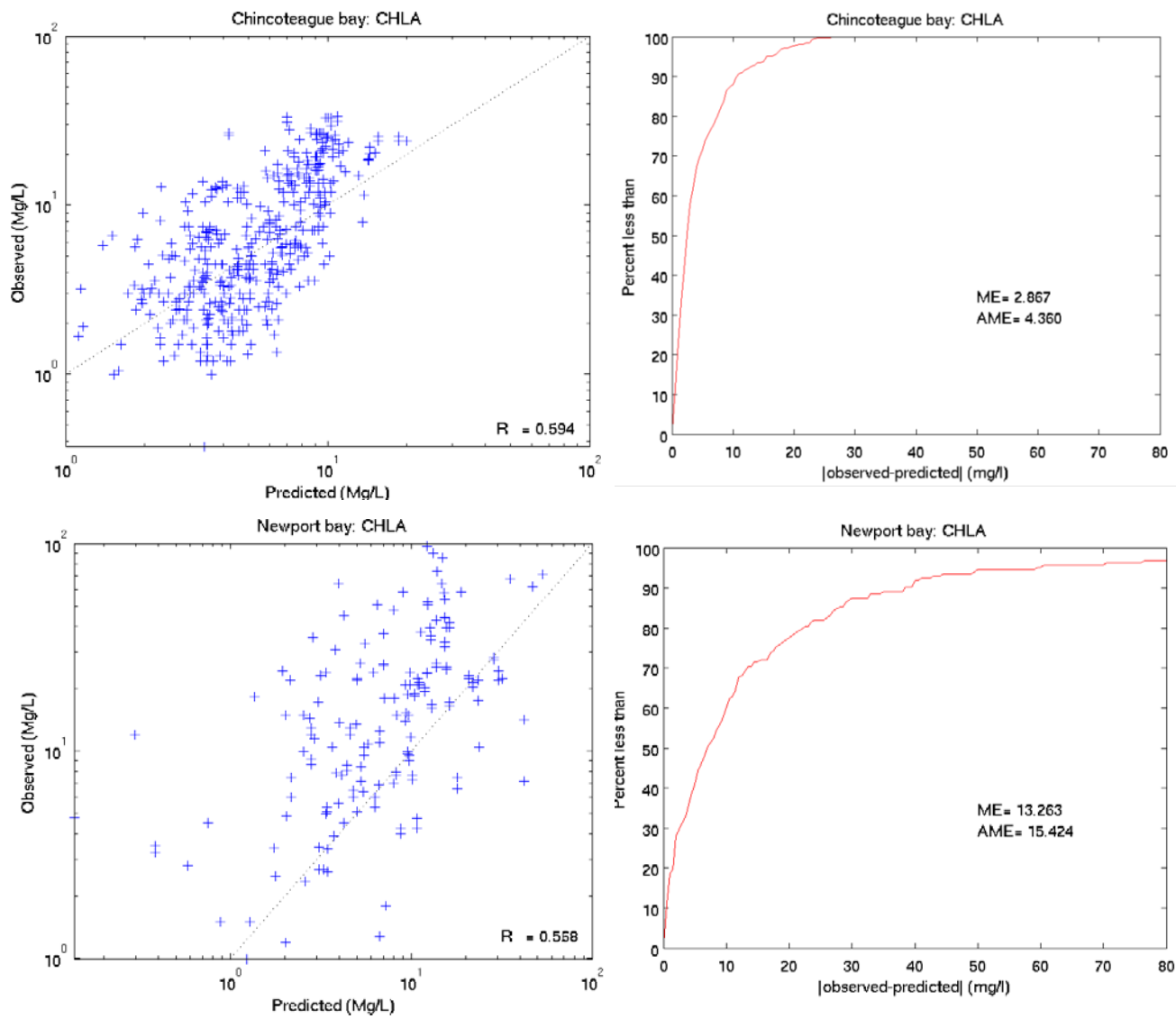


Figure 4.12 (b): Statistical comparison of observed versus modeled Chlorophyll-a data for Newport, and Chincoteague Bays.

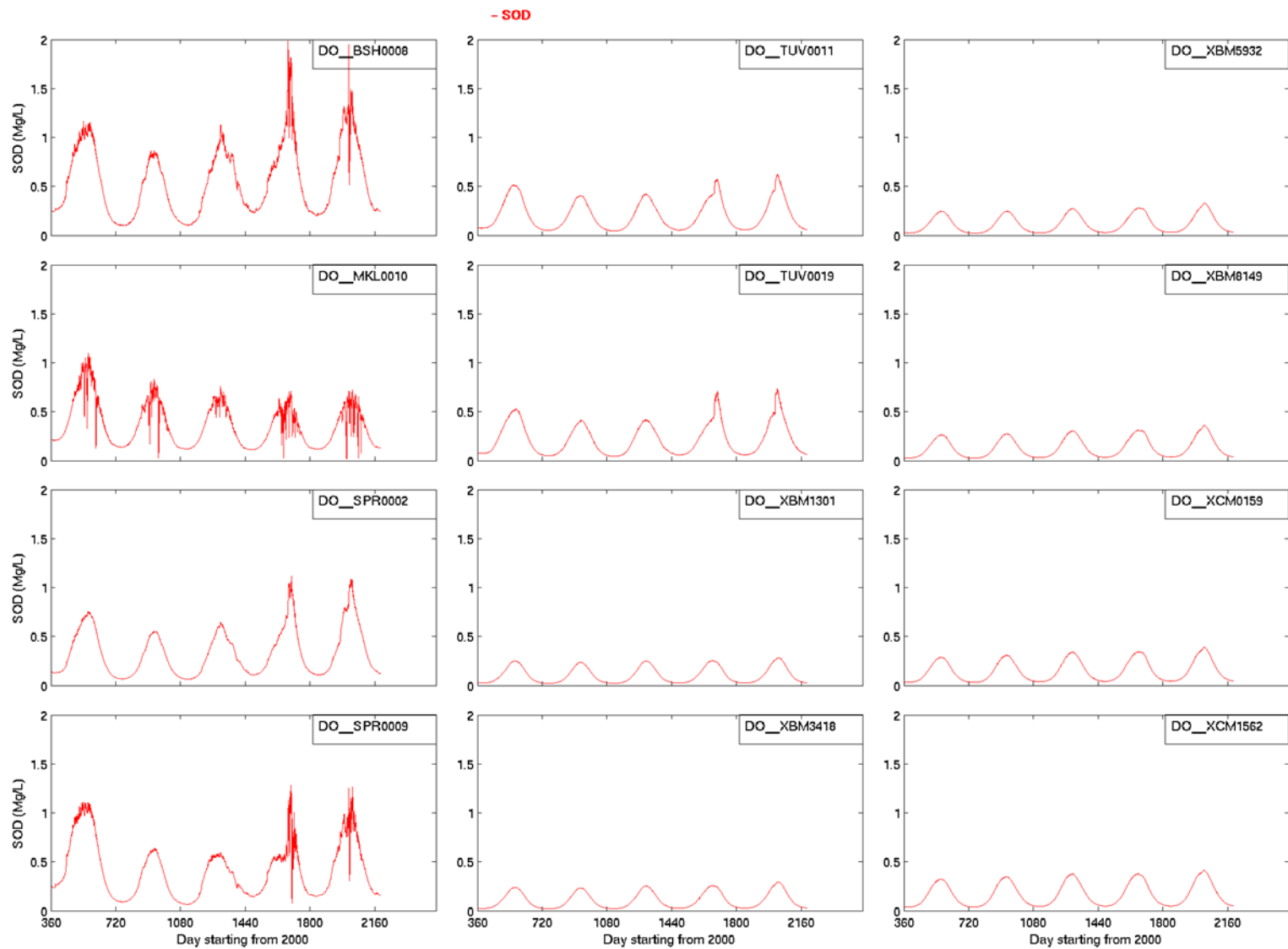


Figure 4.13 (a): SOD calculation at DNR Stations 1-12, 2001- August 2005.

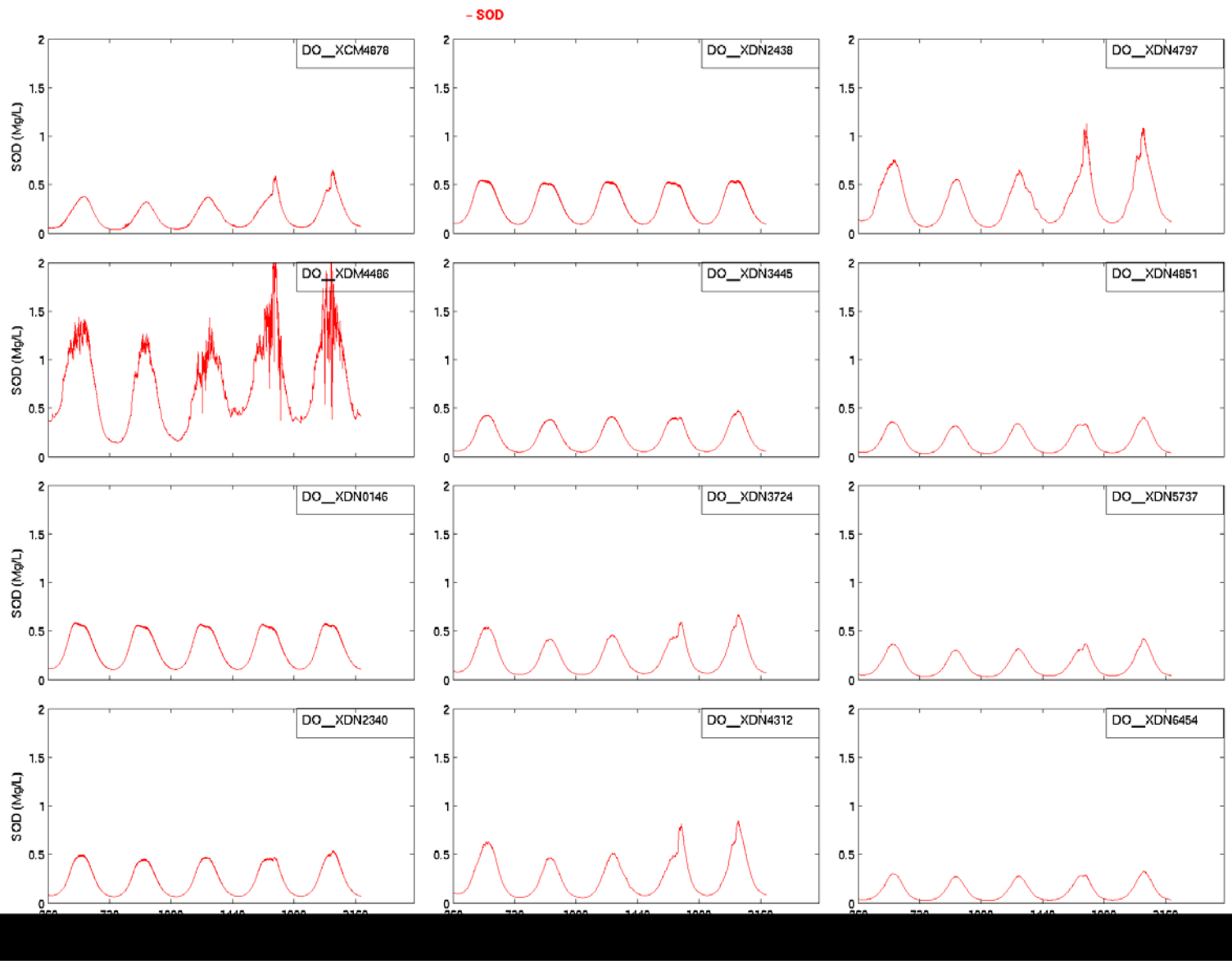


Figure 4.13 (b): SOD calculation at DNR Stations 13-24, 2001- August 2005.

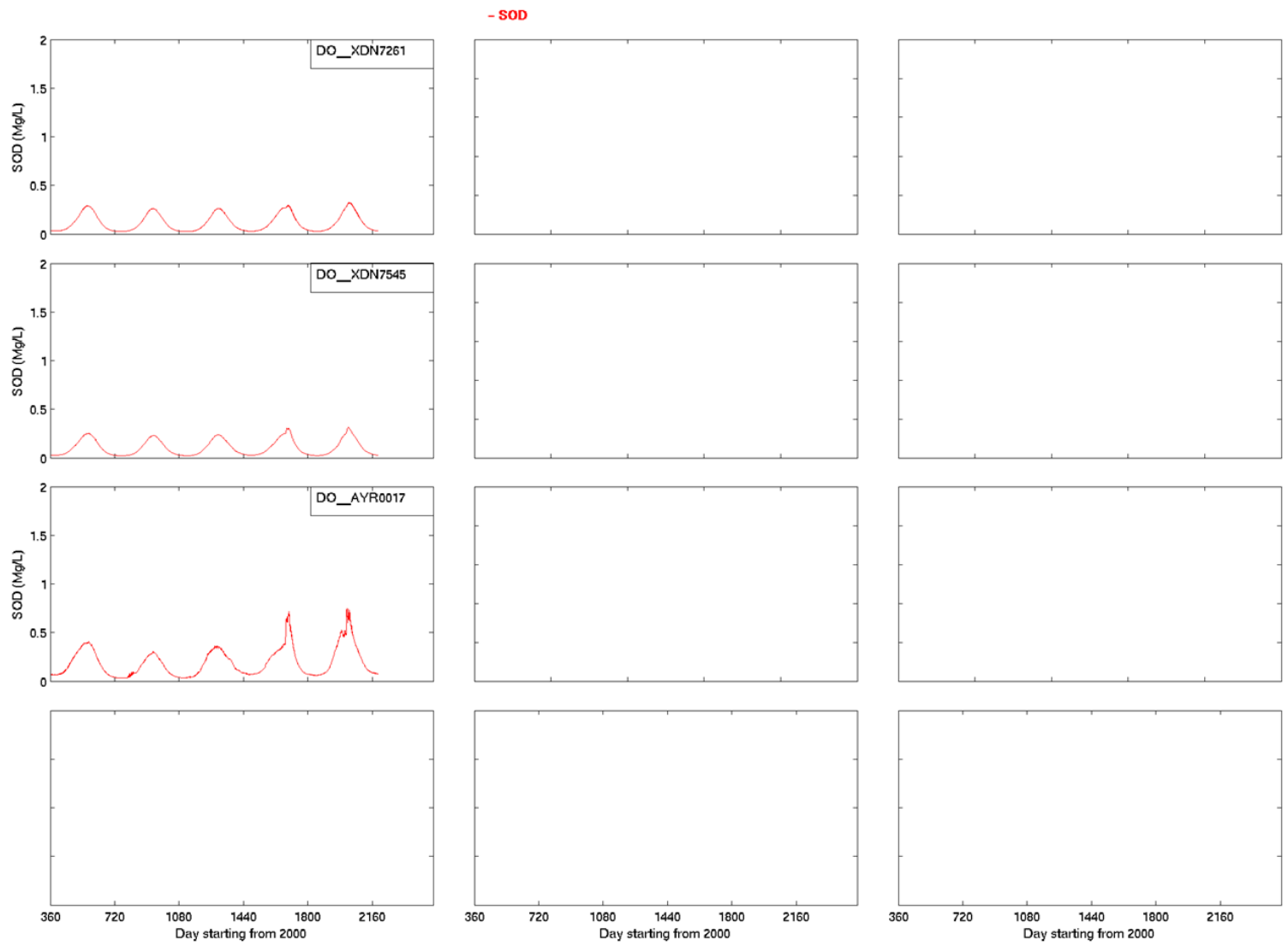


Figure 4.13 (c): SOD calculation at DNR Stations 25-27, 2001- August 2005.

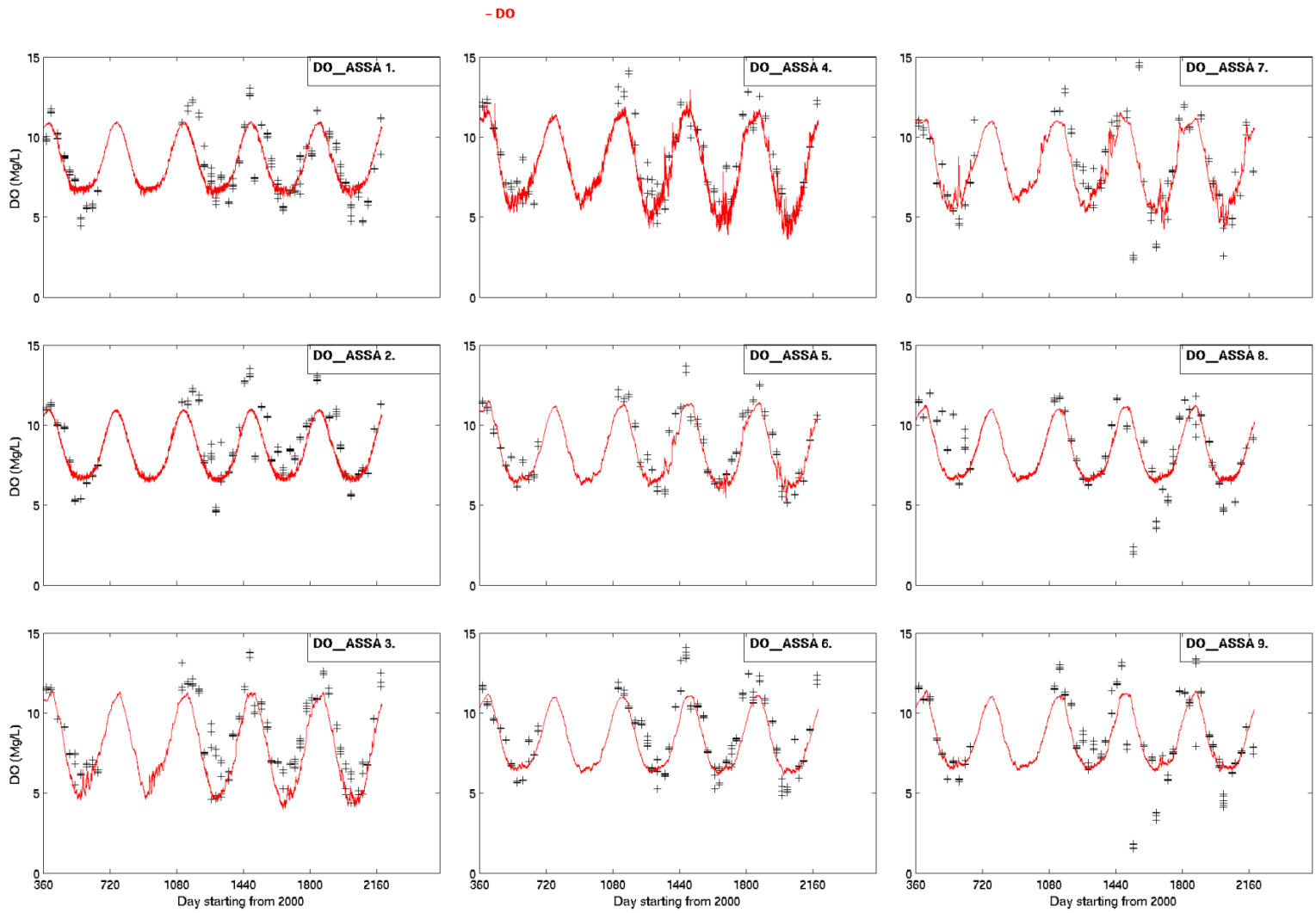


Figure 4.14 (a): DO verification at ASIS Stations 1-9, 2001- August 2005.

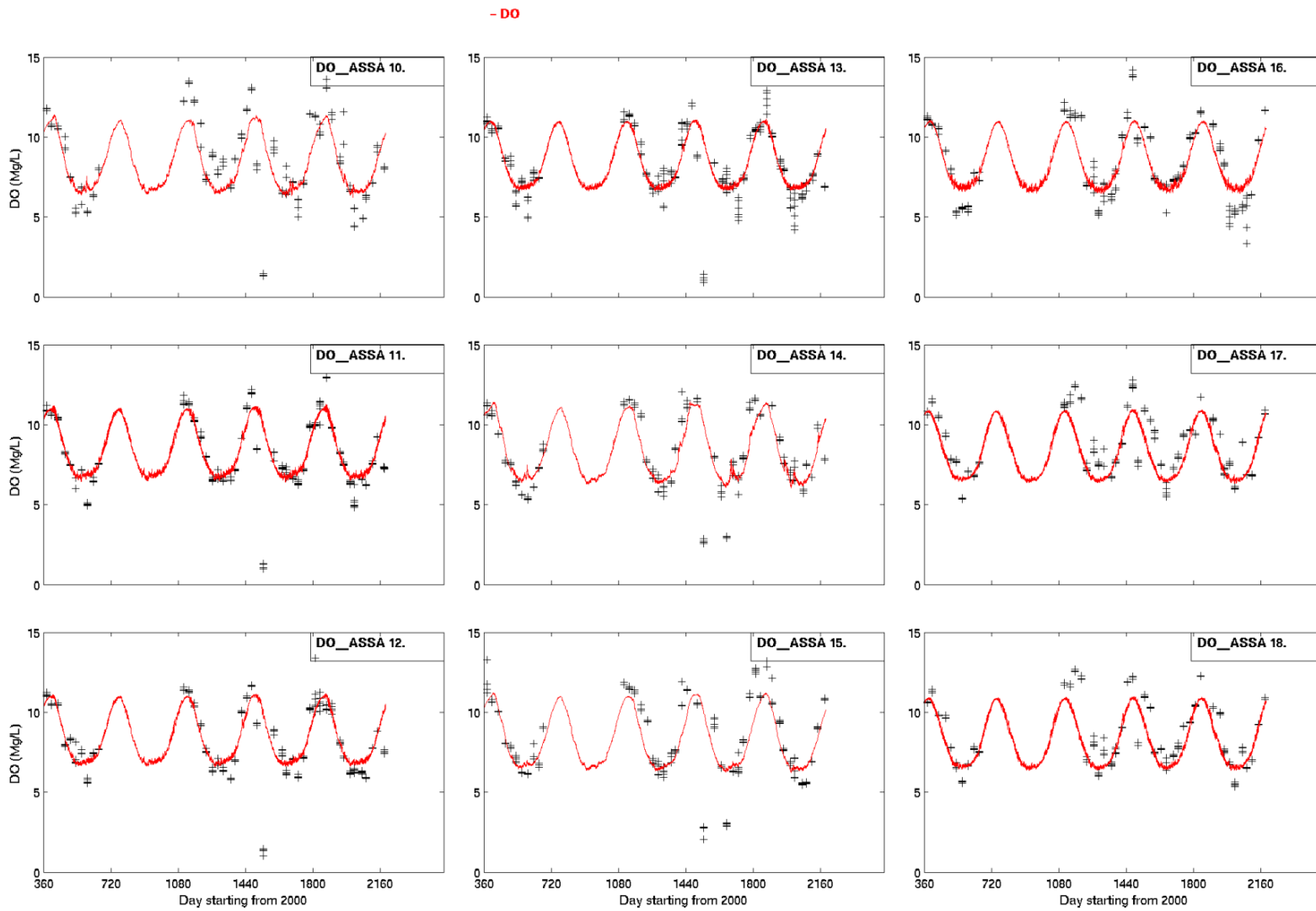


Figure 4.14 (b): DO verification at ASIS Stations 10-18, 2001- August 2005.

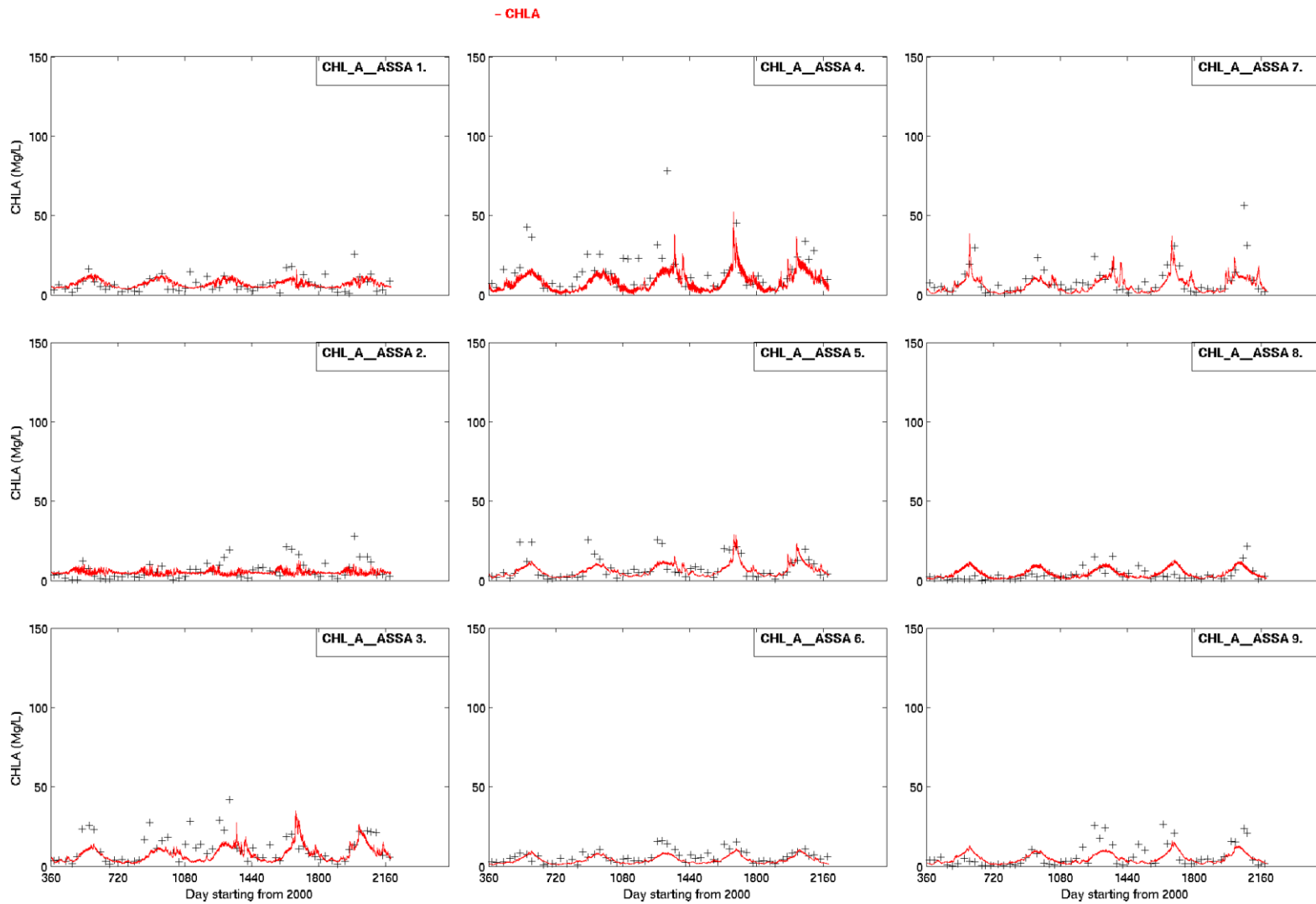


Figure 4.15 (a): Chlorophyll verification at ASIS Stations 1-9, 2001- August 2005.

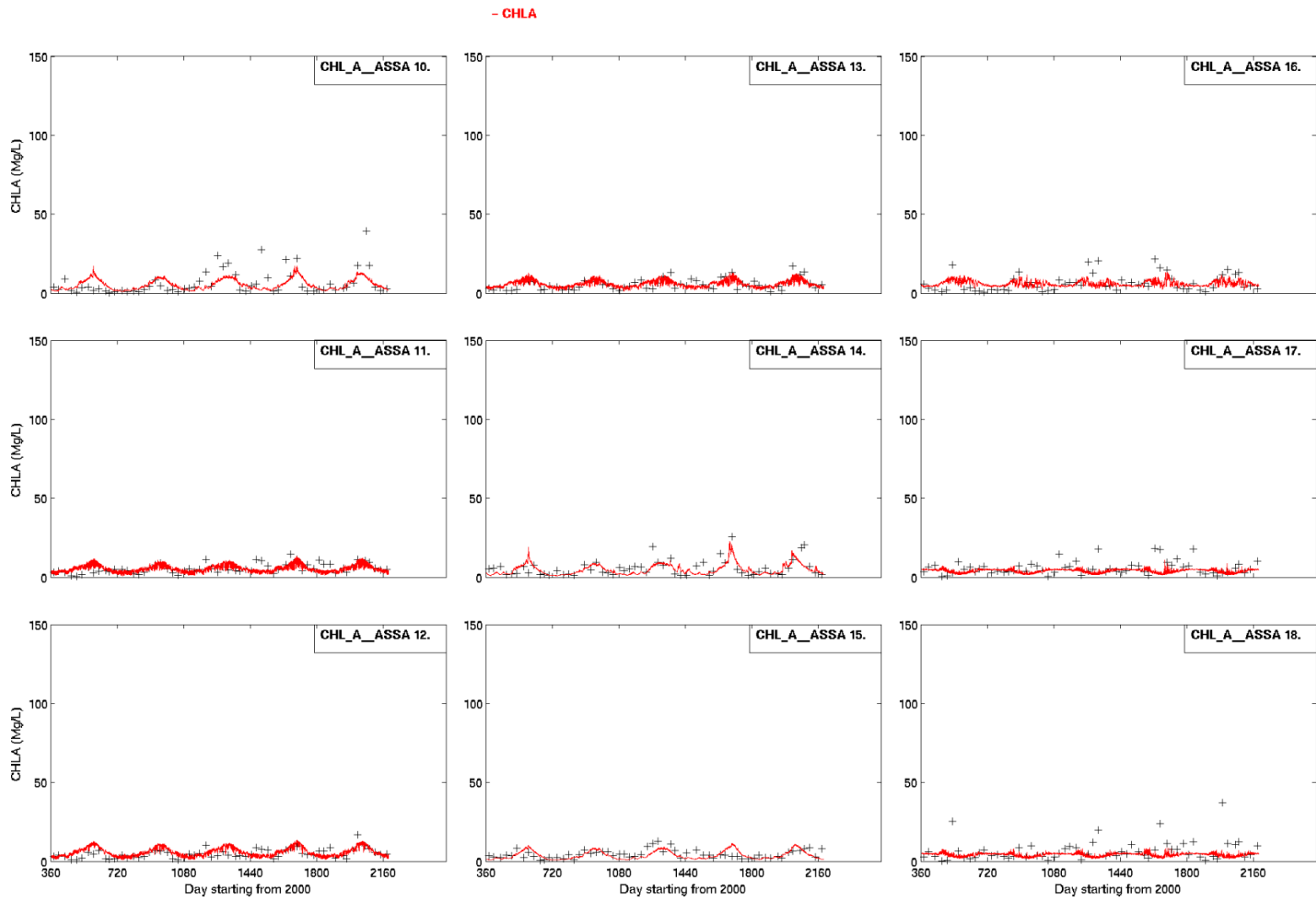


Figure 4-15 (b): Chlorophyll verification at ASIS Stations 10-18, 2001-August 2005

Table 4.2: Model and data comparison statistics for DNR stations.

DO statistics	R	RMS	ME	AME	RE
Assawoman Bay	0.92	0.93	-0.49	0.75	0.10
Isle of Wight Bay	0.78	1.55	-0.07	1.13	0.15
Newport Bay	0.79	1.37	-0.47	1.06	0.15
Chincoteague Bay	0.85	1.04	-0.49	0.89	0.12
TN statistics	R	RMS	ME	AME	RE
Assawoman Bay	0.60	0.41	0.29	0.32	0.32
Isle of Wight Bay	0.67	0.65	0.35	0.43	0.37
Newport Bay	0.60	0.75	0.41	0.51	0.37
Chincoteague Bay	0.65	0.30	0.22	0.25	0.32
TP statistics	R	RMS	ME	AME	RE
Assawoman Bay	0.73	0.02	0.00	0.01	0.26
Isle of Wight Bay	0.45	0.05	0.01	0.03	0.42
Newport Bay	0.49	0.07	0.03	0.04	0.43
Chincoteague Bay	0.67	0.02	0.00	0.02	0.35
CHLA statistics	R	RMS	ME	AME	RE
Assawoman Bay	0.60	10.84	7.62	8.07	0.61
Isle of Wight Bay	0.60	28.32	8.15	12.75	0.61
Newport Bay	0.56	30.33	13.26	15.42	0.67
Chincoteague Bay	0.69	6.62	2.87	4.36	0.49

Table 4.3: Model and data comparison statistics for ASIS stations.

DO statistics	R	RMS	ME	AME	RE
Sinepuxent Bay	0.83	1.20	0.35	0.95	0.11
Newport Bay	0.89	1.55	1.11	1.31	0.15
Chincoteague Bay	0.71	1.67	0.20	1.01	0.12
CHLA statistics	R	RMS	ME	AME	RE
Sinepuxent Bay	0.59	5.96	1.02	4.27	0.69
Newport Bay	0.55	5.85	-1.65	4.34	0.70
Chincoteague Bay	0.61	5.27	1.09	3.70	0.60

Table 4.4: Relative Error in the MCBs model compared with other modeled systems.

	Chesapeake Bay	St. Johns River	Florida Bay	MD Coastal Bays
Dissolved Oxygen (mg/l)	0.36	0.09	0.07	0.16
Chlorophyll-a (µg/l)	0.58	0.49	0.72	0.58
Total Nitrogen (mg/l)	0.24	0.29	0.39	0.34
Total Phosphorus (mg/l)	0.37	0.27	0.31	0.36

CHAPTER 5: ADDITIONAL MODEL ANALYSES

5.1 Adjustments to incorporate the DO Diel Cycle

One of the important considerations for the TMDL assessment with respect to hypoxia in the MCBs is diel (diurnal) cycle of dissolved oxygen (DO). Oxygen is a by-product of aquatic plant photosynthesis. Through photosynthesis and respiration, phytoplankton, periphyton, and rooted aquatic plants can significantly affect the DO levels in a waterbody with a profound effect on the variability of the DO throughout a day. This is because photosynthesis only occurs during daylight hours, whereas respiration and decomposition proceed at all times and are not dependent on solar energy. On a daily average basis, aquatic plants provide a net addition of DO to a water body through photosynthesis, yet respiration can cause low DO levels at night. This results in the diel cycle, whereby daily DO maximum occurs in mid-afternoon, during which time photosynthesis is the dominant mechanism and the daily DO minimum occurs in the early morning during which time respiration and decomposition have the greatest effect on DO. When algae are growing excessively, they can cause large diurnal DO variation, and lead to violations of DO standards. DO was monitored in the MCBs monthly at the fixed station network to provide information on the status of water quality condition for living resources. Traditional monitoring programs collected periodic data at a small number of fixed sampling locations, often in the deeper channel areas. Since the mid-2000s, new monitoring technology allows for continuous monitoring (ConMon) has become available, with which high frequency (every 15 minutes) temperature, salinity, DO, fluorescence (converted to chlorophyll), pH and turbidity can be continuously recorded. ConMon was implemented in the Maryland Coastal Bays in April 2002 and was reported by Wazniak et al. (2004) in details. Today, MD Department of Natural Resources (DNR), Delaware Natural Resource and Environmental Control (DNREC) and Virginia Estuarine and Coastal observation system are using it routinely as a real-time monitoring program; see <http://mddnr.chesapeakebay.net/eyesonthebay/index.cfm>. The ConMon data sondes usually are installed in shallow water sites, record data at approximately 0.5 m above the sediment surface, and thus can provide information for estimating the total production and respiration in shallow water ecosystems. Figure 5.1 shows an example of the ConMon data measured at Bishop's Landing in the MCBs in July and August, 2005. It has a record of 25 days of continuously measured depth, DO, salinity, temperature, turbidity, chlorophyll-a, and Photosynthetically Active Radiation (PAR). On the left panel, it can be seen that a daily swing of DO with amplitude 2-3 mg/l can vary between DO saturation and hypoxia within a single daily cycle. Typically, the diel pattern shows the lowest DO occurring in the early morning and rising through the day to reach a maximum in the later afternoon as the DO-producing chlorophyll of phytoplankton is activated by sunlight. It can also be seen that at day 12 and day 13, the diel cycle amplitude was suppressed by the low light condition by a storm with rain and cloud cover. On the right panel, the spectral magnitude at the diurnal frequency was clearly identified by the FFT (Fast Fourier Transform) analysis, indicative of signal of diel oscillation, followed by a weaker semi-diurnal signal presumably related to the tide.

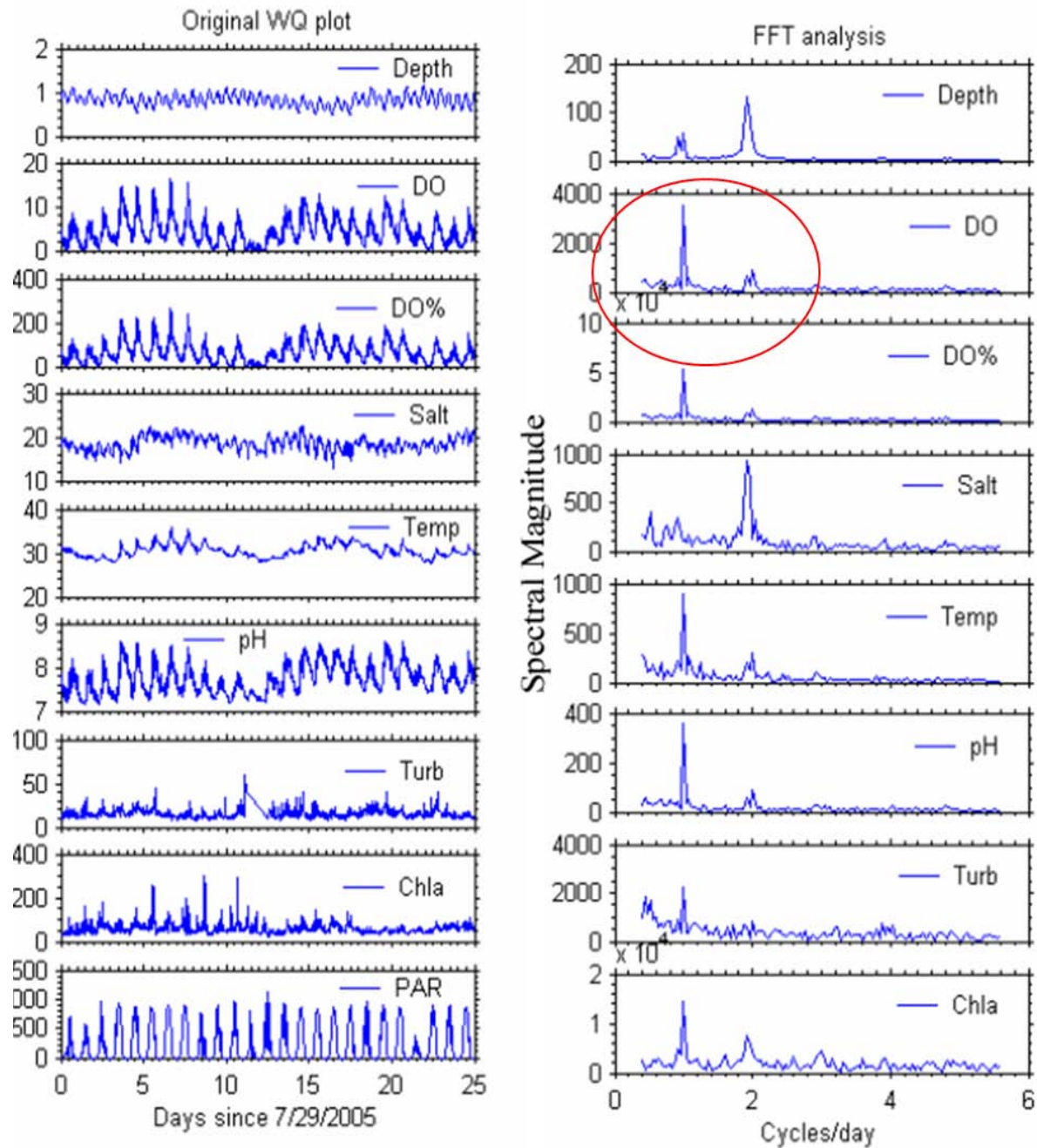


Figure 5.1: ConMon data measured at Bishop's Landing, July – August, 2005; before (left) and after (right) Fast Fourier transformation.

Both CH3D/ ICM and HEM3D models used for eutrophication studies in the Chesapeake Bay and MCBs, respectively, were most suitable for predicting daily average DO. Although higher frequency DO outputs can be made available in the current framework, the accuracy of its variation in short time scale is questionable because of the following reasons. First, the current technology is lacking full understanding of the short time scale of photosynthesis and respiration processes for phytoplankton dynamics. The best example is the harmful algal bloom, in which a rapid increase and accumulation of algae population can occur within very a short time (within a day). The cause is still an actively researched topic. Second, it lacks robust and accurate high frequency forcing functions and parameters to specify for growth rate and mortality. These forcing functions are high frequency PAR, wind speed and direction, air and water temperature, and wind wave sea state. The parameters include carbon to chlorophyll-a ratio, heterotrophic respiration, and the organic nitrogen uptake rate for certain species. Even the best available modeling technology today does not guarantee the prediction of DO diel cycle as accurate enough for TMDL implementation. In fact, a national research program, ECOHAB (The Ecology and Oceanography of Harmful Algal Blooms), is being launched to unlock the factors causing the harmful algal bloom and the consequence of it. As a result, new information and tools are being developed. Given the situation, the strategy adopted in this study was to use the process-based HEM3D model results and to combine with the empirically-derived statistical results. The empirical relation was developed by Elgin Perry et al. (2012) and used to incorporate the diel oscillation into the predicted daily DO. The diel adjustment was implemented in steps. First, a trigonometric time series model using the Sine and Cosine function of time was fitted to DNR ConMon data to determine the amplitude and phase of the diel cycle. Second, a separate regression equation was developed to obtain the amplitude and phase as a function of seasonal water temperature, daily water temperature, turbidity, salinity, chlorophyll concentration, and PAR. As a third step, the regression equation is used to estimate the diel cycle of DO for each day using daily conditions. The incorporation of the diel cycle can be used for adjusting the fixed station monthly DO measurements to a fixed time of day. Or it can be used for TMDL worst-case scenario evaluation. The idea behind the diel DO adjustment essentially is to take the total DO and split it into the daily mean and diel DO component (expressed as DO').

$$DO = \overline{DO} + DO'$$

Where \overline{DO} is the daily mean, and DO' is the diel component, which will be fitted by the Fourier series for its amplitude and the phase.

By the splitting and then fitting with Fourier series, the resultant formula is:

$$DO = \mu_i + \beta_1 \sin\left(\frac{t * 2\pi}{24}\right) + \beta_2 \cos\left(\frac{t * 2\pi}{24}\right)$$

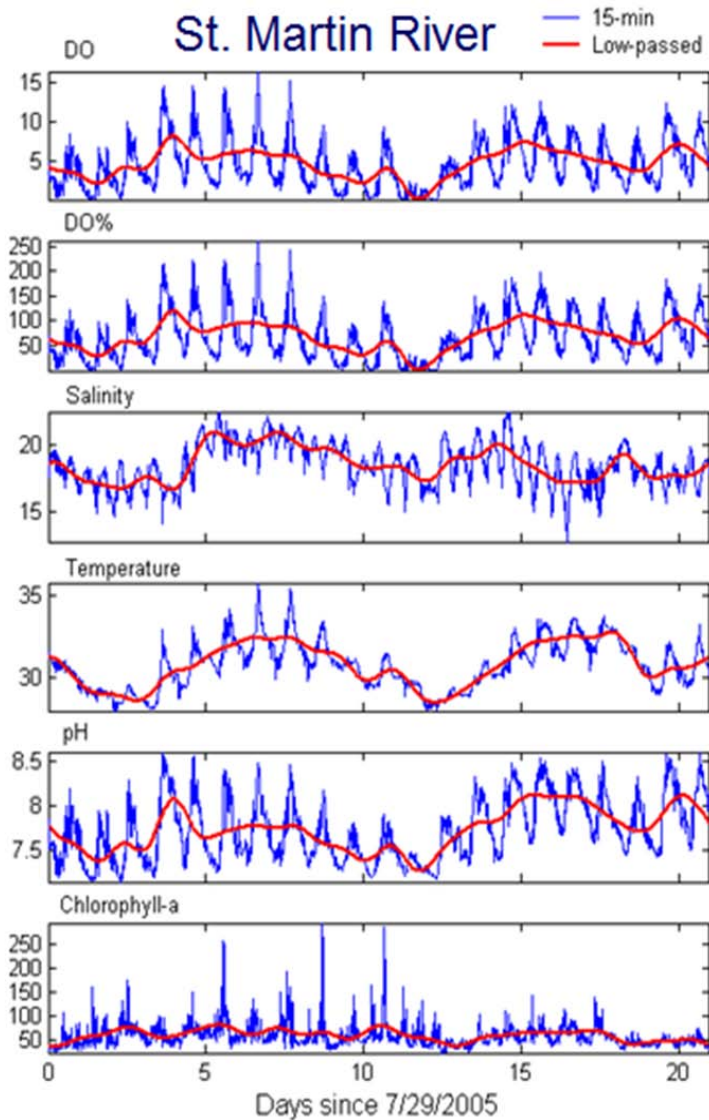
Where μ_i is mean DO for the 24 hour period, β_1 and β_2 are regression coefficients, t is time of the day and i is the day.

The phase and amplitude of the diel cycle are computed as:

$$\hat{a} = \sqrt{\beta_1^2 + \beta_2^2} \quad \text{and} \quad \hat{p} = \arctan\left[\frac{\beta_1}{\beta_2}\right] \times \frac{24}{2\pi}$$

based on the Fourier series formulation.

In practice, the diel DO measured each day was fitted with sinusoidal curves using a 24 hour period and with different amplitude and phase, as shown on the right panel of Figure 5.2. The amplitude measures how far the diel curve deviates from the mean line, while the phase measures shift in time between the beginning of the diel cycle on each day and the nominal start time of 6:00 am. Perry et al. (2012) used a 5-year dataset to fit all the amplitude and phase and relate them to the contributing variables. In many cases the fit was good (as in the right top panel in Figure 5.2) and in some cases the fit was poor (as in the right bottom panel in Figure 5.2). The amplitude tends to be skewed to the right and it was found that a 1/5th power transformation provides symmetric and approximately normal residuals distribution. Therefore, the amplitude was transformed by the 5th root first and then used by a linear regression model as dependent variable.



DO

DO'

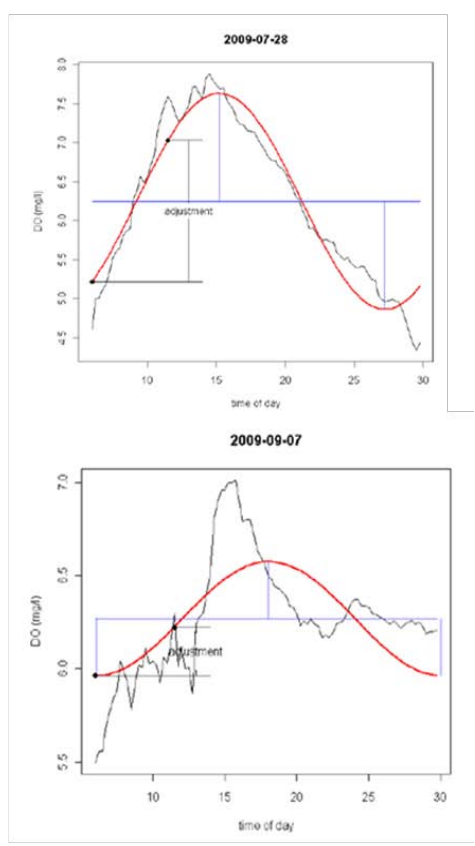


Figure 5.2: Low-pass-filtered daily DO, DO saturation, salinity, temperature, and chlorophyll-a data (left); measured (blue) and fitted sinusoidal curve (red) diel cycle of DO (right).

Different variables - seasonal water temperature, daily water temperature, turbidity, salinity, chlorophyll concentration, and PAR-were added as independent variables by the stepwise procedure to ensure that the linear regression model covers enough variables to adequately represent the cause-and-effect relationship. The final variables used for the linear regression model and the corresponding coefficients are listed in Table 5.1. Also shown are the associated parameters and their variance. As can be seen, the seasonal temperature has the largest variance, followed by daily temperature, turbidity, chlorophyll-a and PAR. It was observed that the variance of the seasonal temperature likely overlaps with the variance of PAR for both sharing a strong seasonal component.

Table 5.1: Variables, coefficient values and statistical test results for DO diel cycle linear regression model (Perry et al., 2012).

Source variables	Sum of squares	Mean square	F-stat	P-value
Seasonal temperature	6.18	0.8833	287.321	<0.0001
Daily temperature	1.17	1.1676	379.8237	<0.0001
Log turbidity	0.65	0.6546	212.9489	<0.0001
Log Chlorophyll	0.39	0.3857	125.4532	<0.0001
PAR (photosynthetic active radiation)	0.23	0.2332	75.8538	<0.0001
Residual	2.78	0.0031		

The amplitude adjustments for the seasonal temperature cycle are apportioned to the monthly mean temperature with the mean amplitude in the range of 0.5 – 2.5 mg/l depending on the season. It has the largest amplitude in July and August with 2.5 m/l in amplitude, and smallest in November and December with less than 1 m/l, as shown in Figure 5.3. An empirical relationship between light extinction coefficient:

Ke (ft⁻¹) and turbidity (NTU)

$$K_e = 0.543 + 0.0177 \text{ Turb}$$

was used to calculate the turbidity correction. The log transformation was made to the turbidity and chlorophyll-a for the amplitude adjustment in the regression equation. It should be noted that since the phase does not exhibit a systematic variation, the adjustment was not considered in this study. In the end, the diel adjustment was performed for the entire model calibration years from 2001-2004. Examples of diel adjustments were shown in Figure 5.4 (a)-(f) for stations located in Assawoman Bay, Isle of Wight Bay (inside St. Martin River), Isle of Wight Bay (outside St. Martin River), Sinepuxent Bay, Newport Bay, and Chincoteague Bay. It can be seen that the DO diel oscillation are embedded in the mean daily DO and with larger amplitude in the summer months and smaller amplitude in the winter, as expected. With the diel adjustment procedure, the skill score for the final calibration of the DO results for all DNR and Assateague Island National Seashore (ASIS) stations are presented in Figure 5.5 (a) - (e). The correlation coefficient (R²) for model and data comparison are mostly in the range of 0.8 - 0.9. This skill score for model and data comparison was improved using the modeled, adjusted DO (over that without the DO adjustment) because the adjusted DO now have a range of values within a day in comparing with the observed data. In other words, it was improved for the observed data can compare with a range of the simulated adjusted diel DO rather than just single comparison.

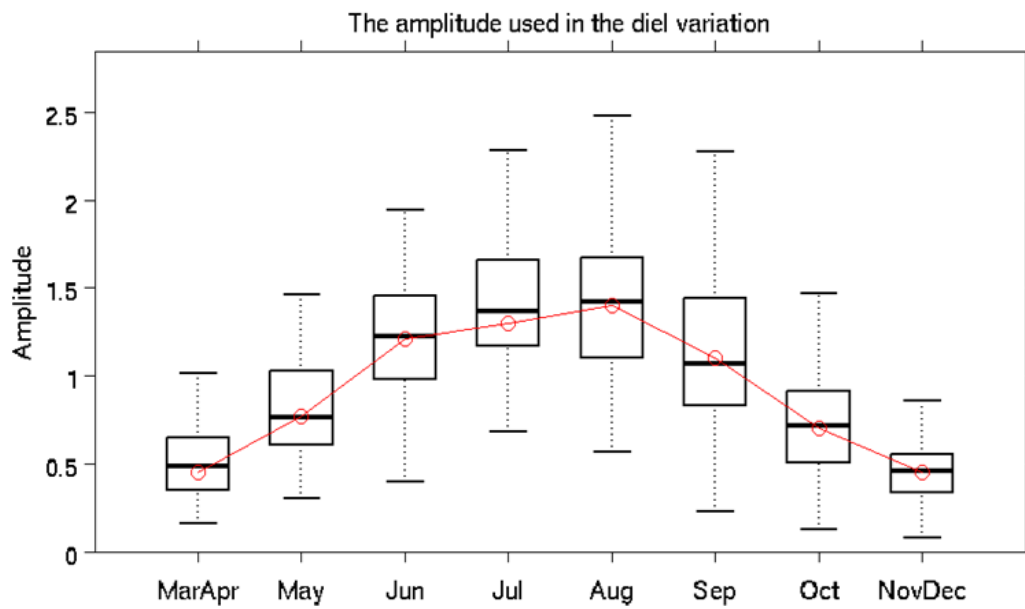
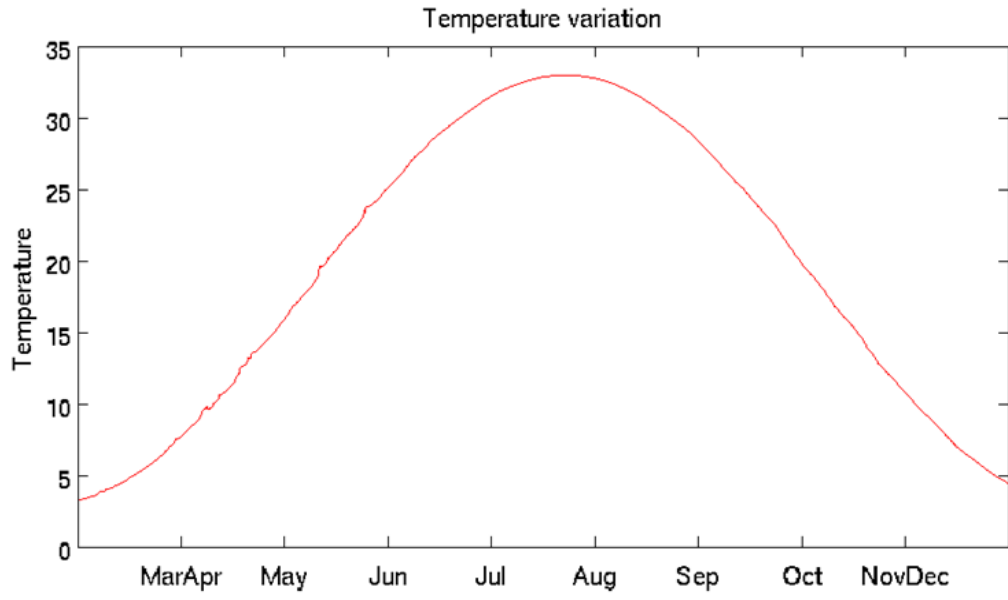


Figure 5.3: DO diel cycle amplitude adjustments for seasonal temperature cycle proportioned to monthly mean temperature.

Assawoman Bay

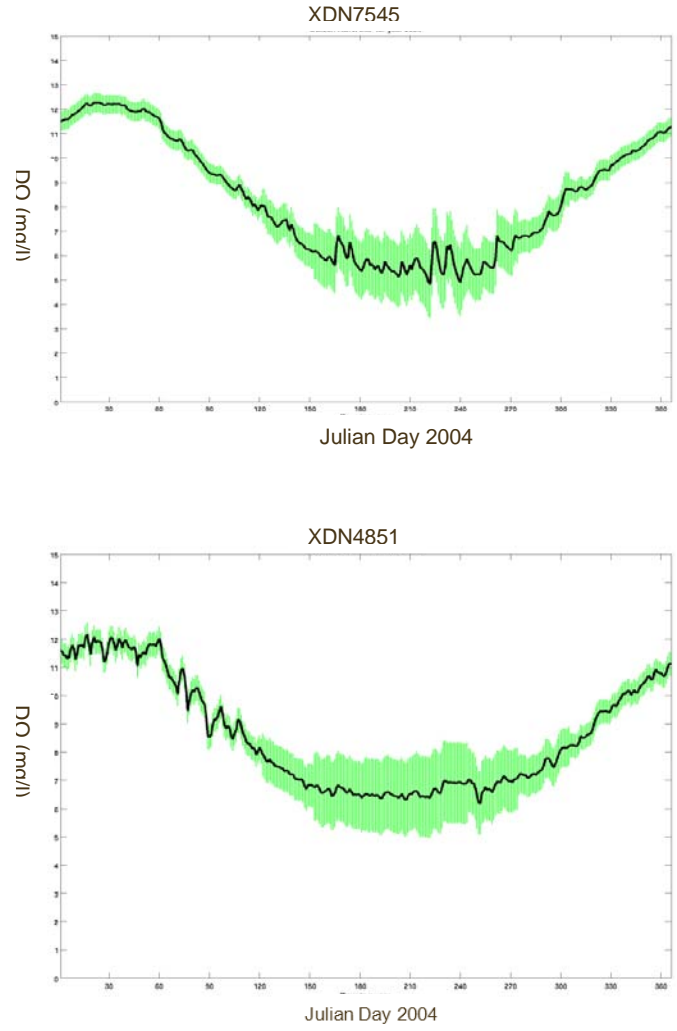
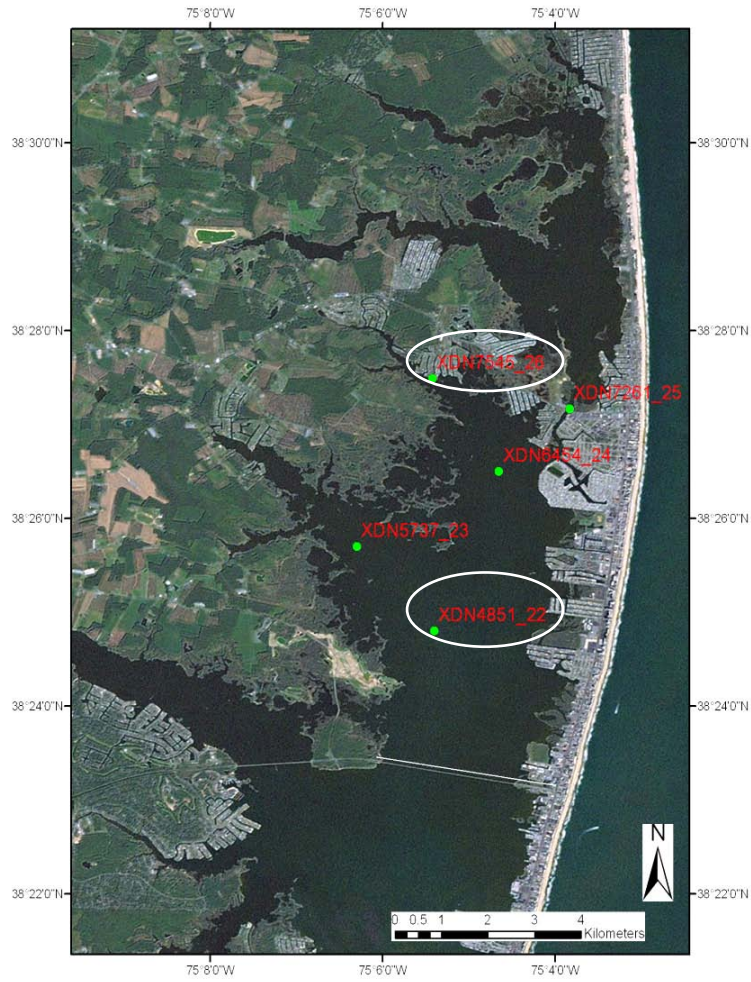


Figure 5.4 (a): DO daily average (black) and diel (green) time series, Stations XDN7545 and XDN4851, Assawoman Bay, January 1 – December 31 2004.

Isle of Wight Bay – inside St. Martin

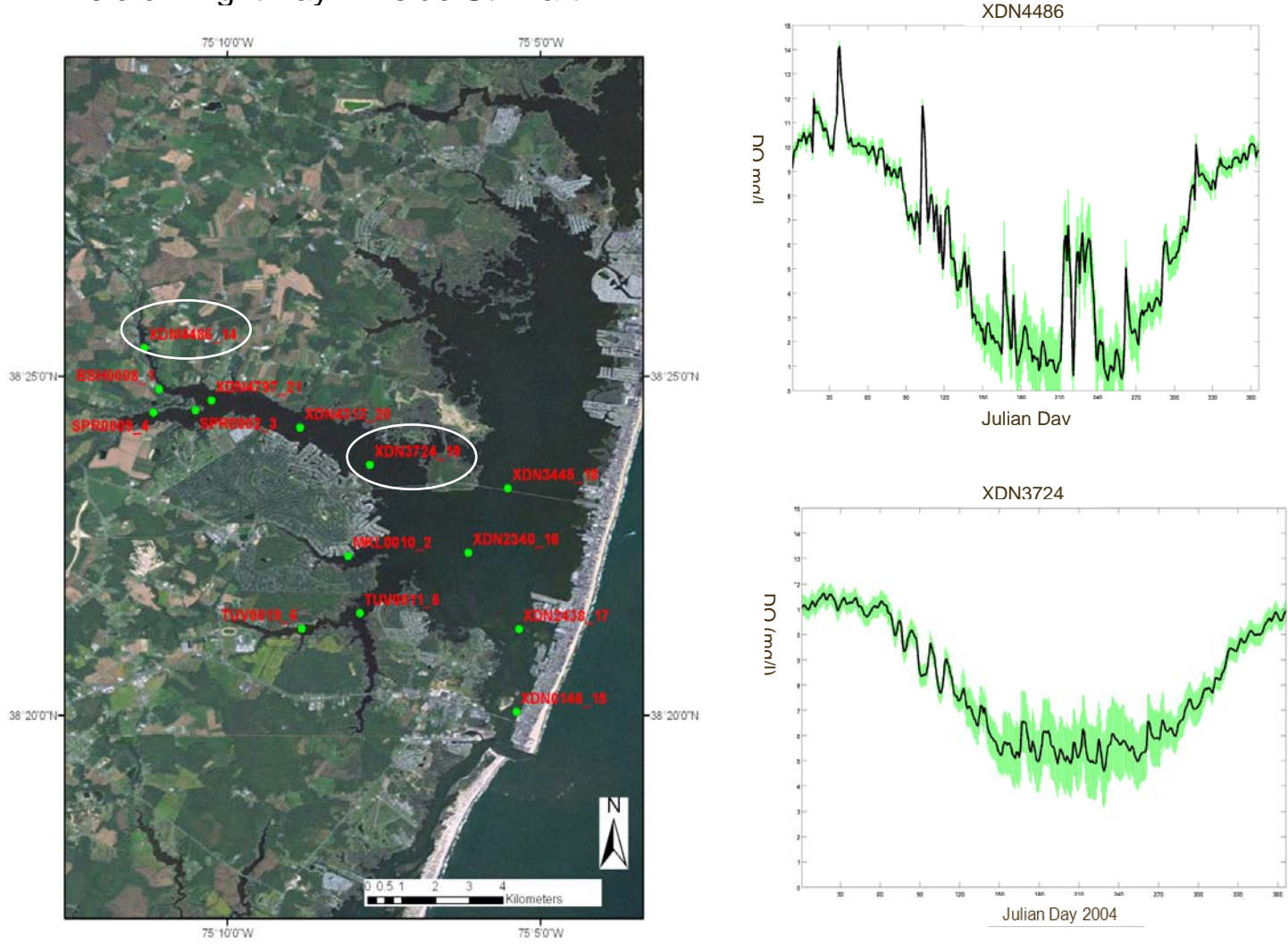


Figure 5.4 (b): DO daily average (black) and diel (green) time series, Stations XDN4486 and XDN3724, St. Martin River, Isle of Wight Bay, January 1 – December 31, 2004.

Isle of Wight Bay – outside St. Martin

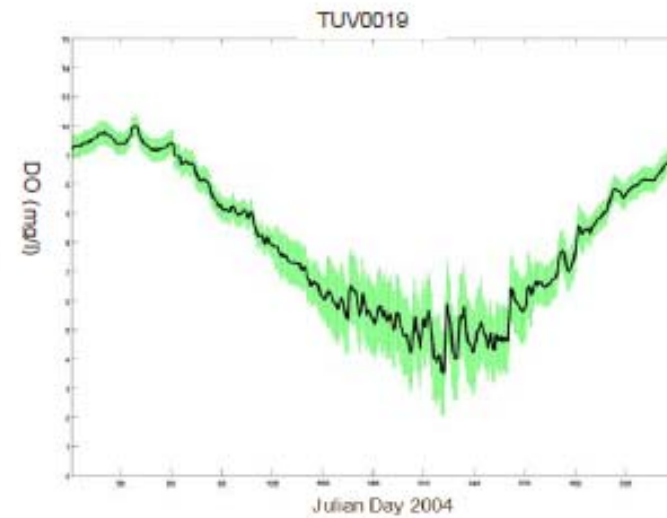
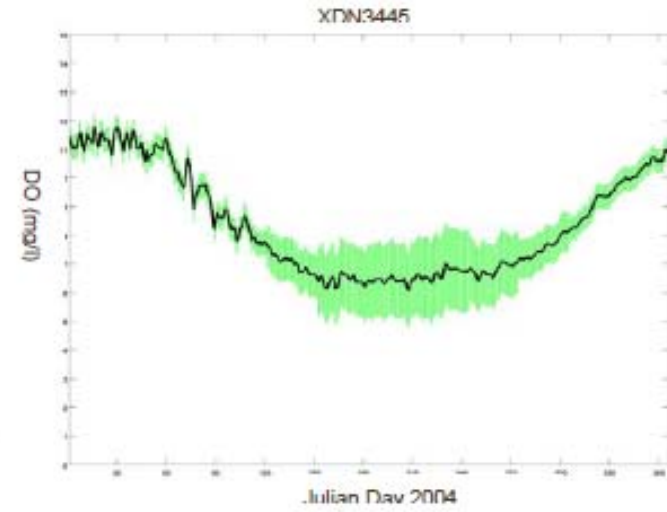
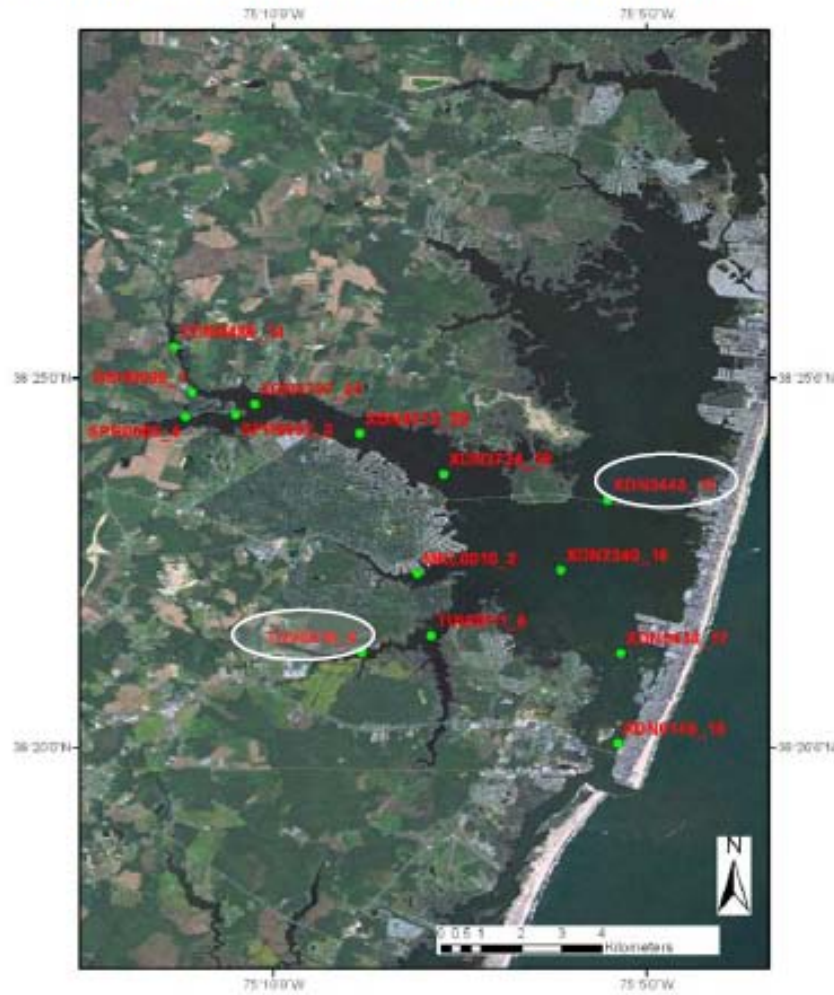


Figure 5.4 (c): DO daily average (black) and diel (green) time series, Stations XDN3445 and TUV0019, Isle of Wight Bay open waters, January 1 – December 31 2004.

Sinepuxent Bay

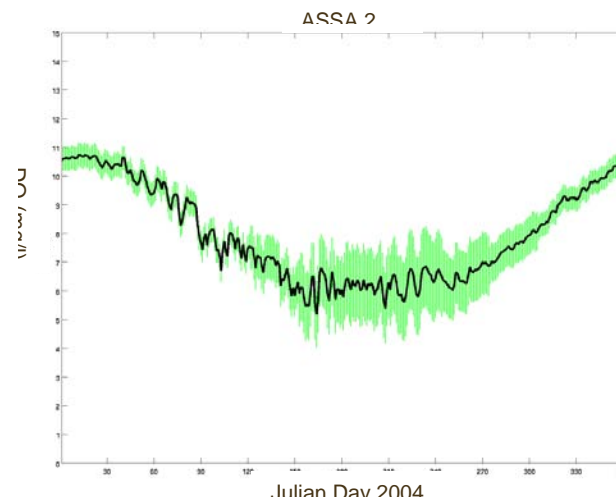
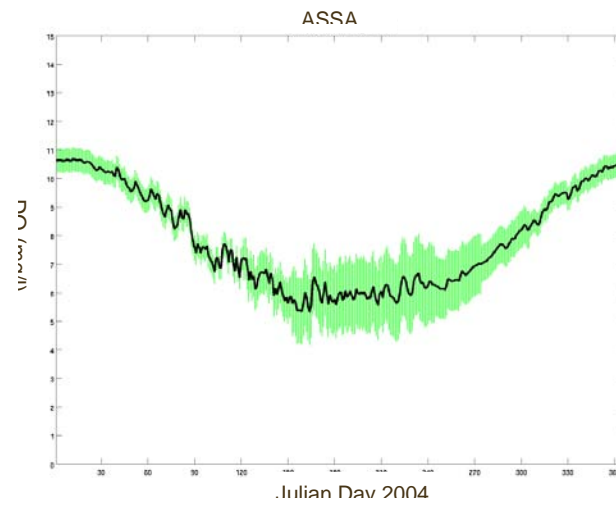
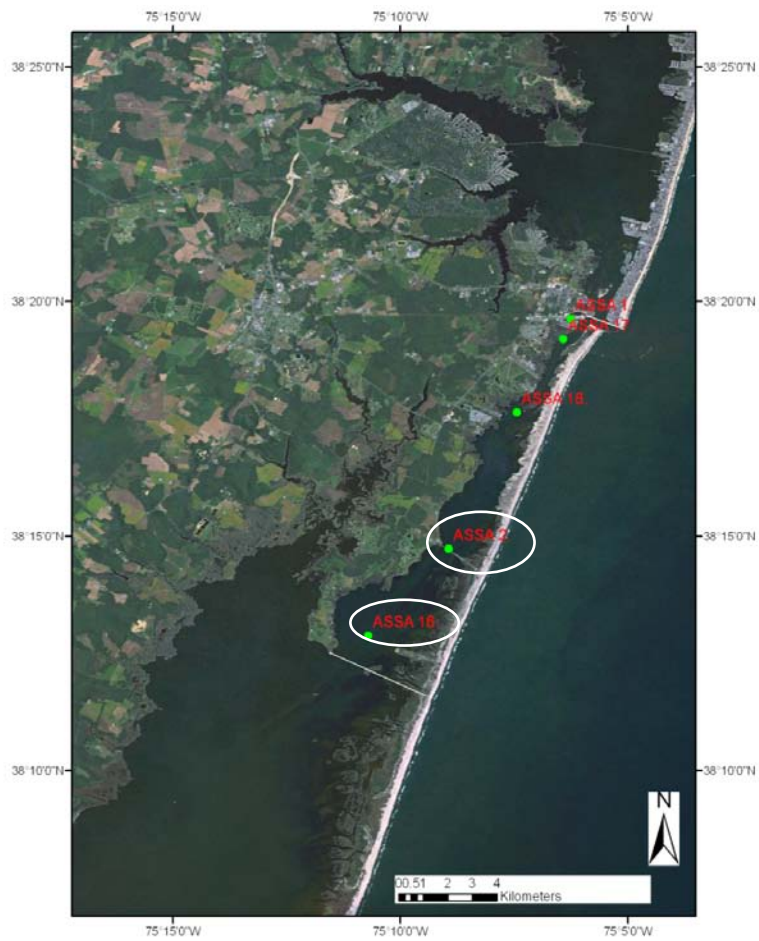


Figure 5.4 (d): DO daily average (black) and diel (green) time series, Stations ASSA 16 and ASSA 2, Sinepuxent Bay, January 1 – December 31, 2004.

Newport Bay

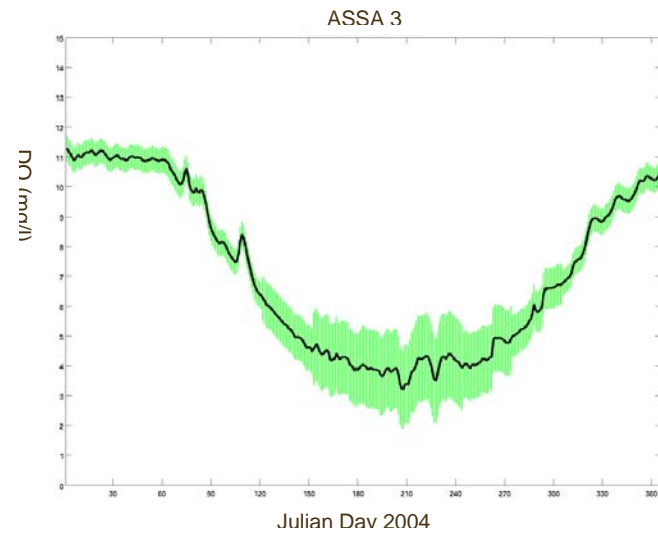
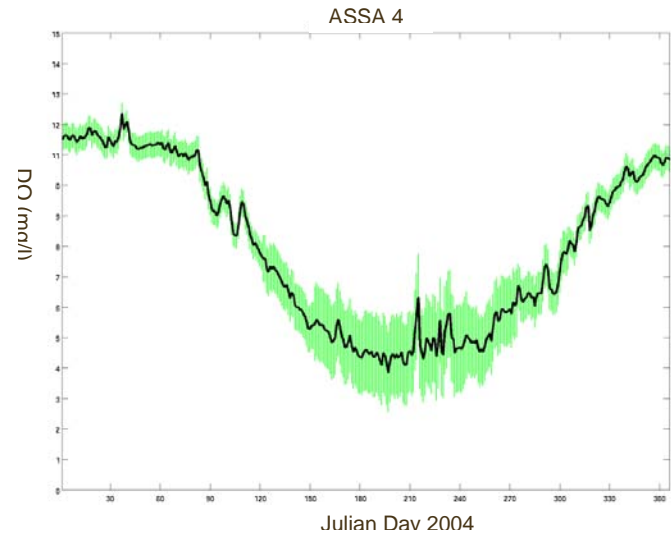
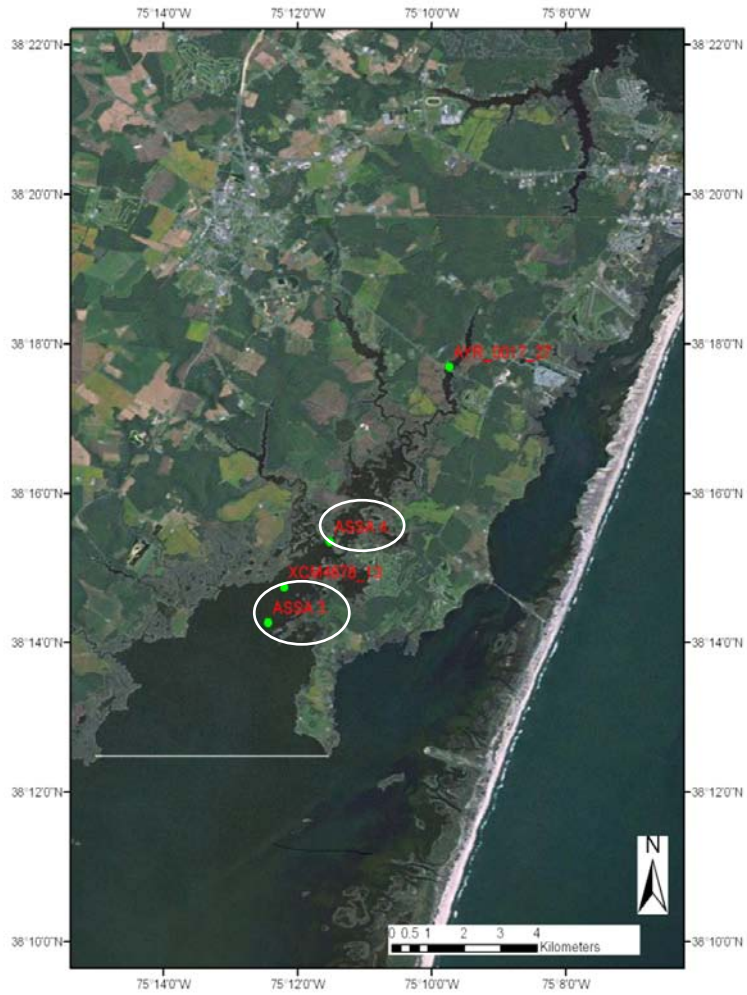


Figure 5.4 (e): DO daily average (black) and diel (green) time series, Stations ASSA 4 and ASSA 3, Newport Bay, January 1 – December 31, 2004.

Chincoteague Bay

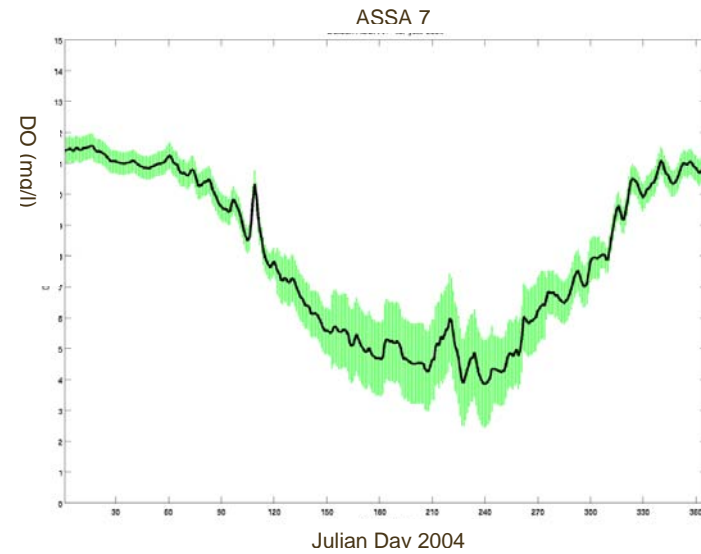
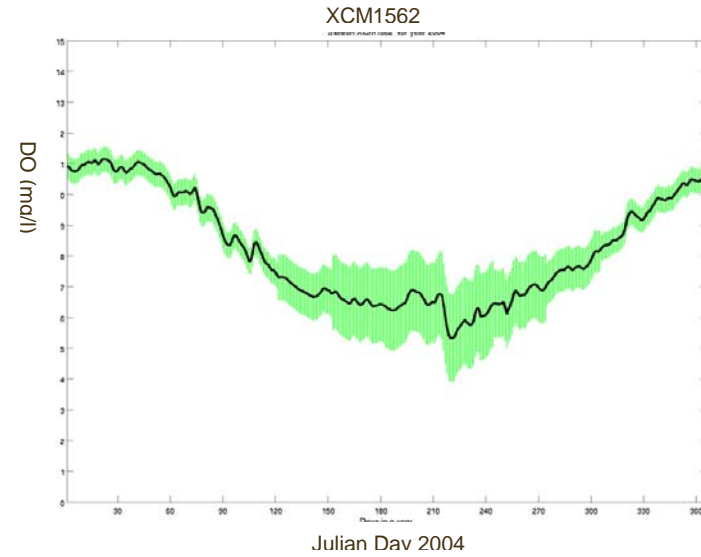


Figure 5.4 (f): Daily average (black) and diel (green) time series, Stations XCM1562 and ASSA 7, Chincoteague Bay, January 1 – December 31, 2004.

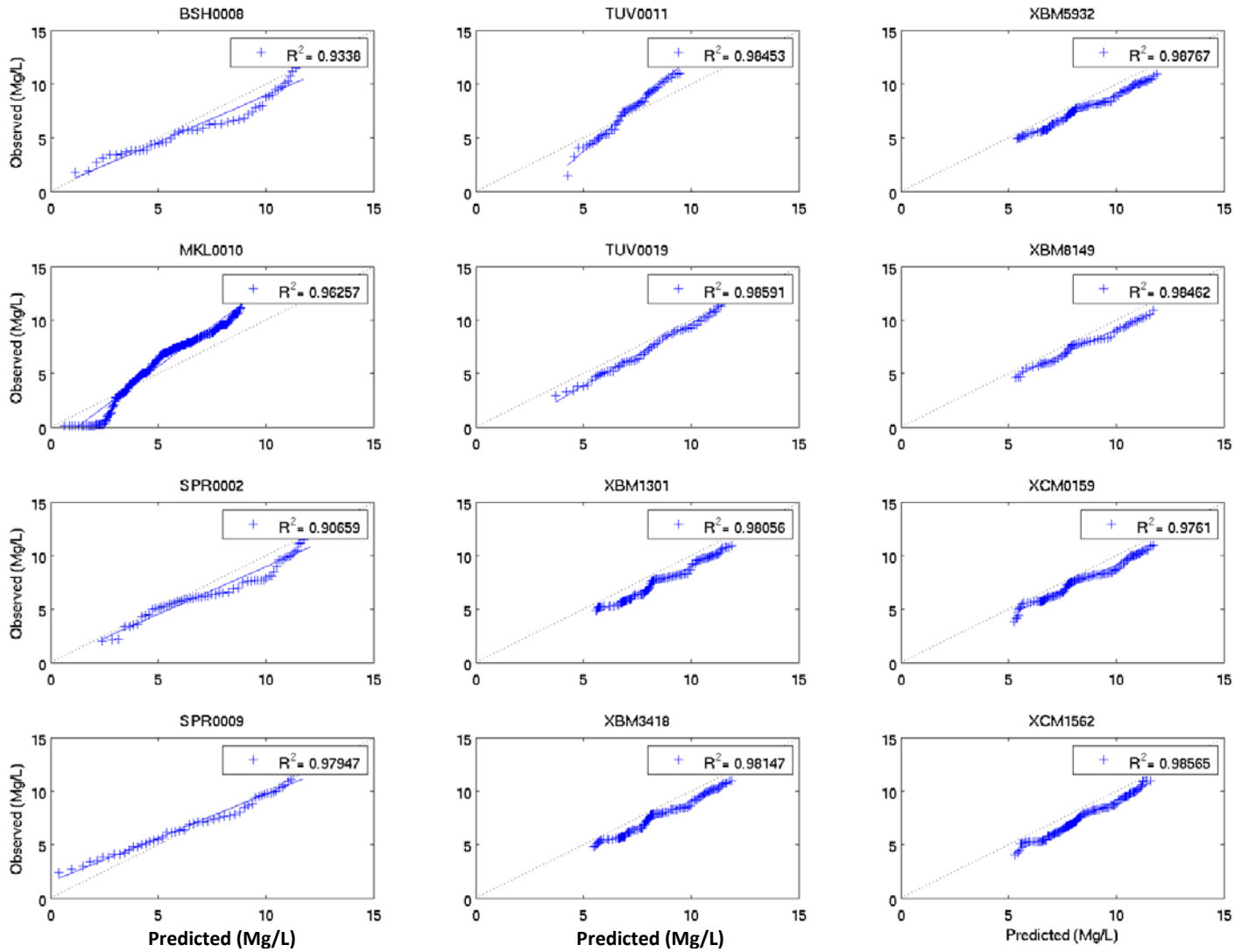


Figure 5.5 (a): Correlation coefficient (R^2) between diel-cycle-adjusted modeled and observed DO, DNR Stations 1-12, baseline conditions, January 2001- August 2005.

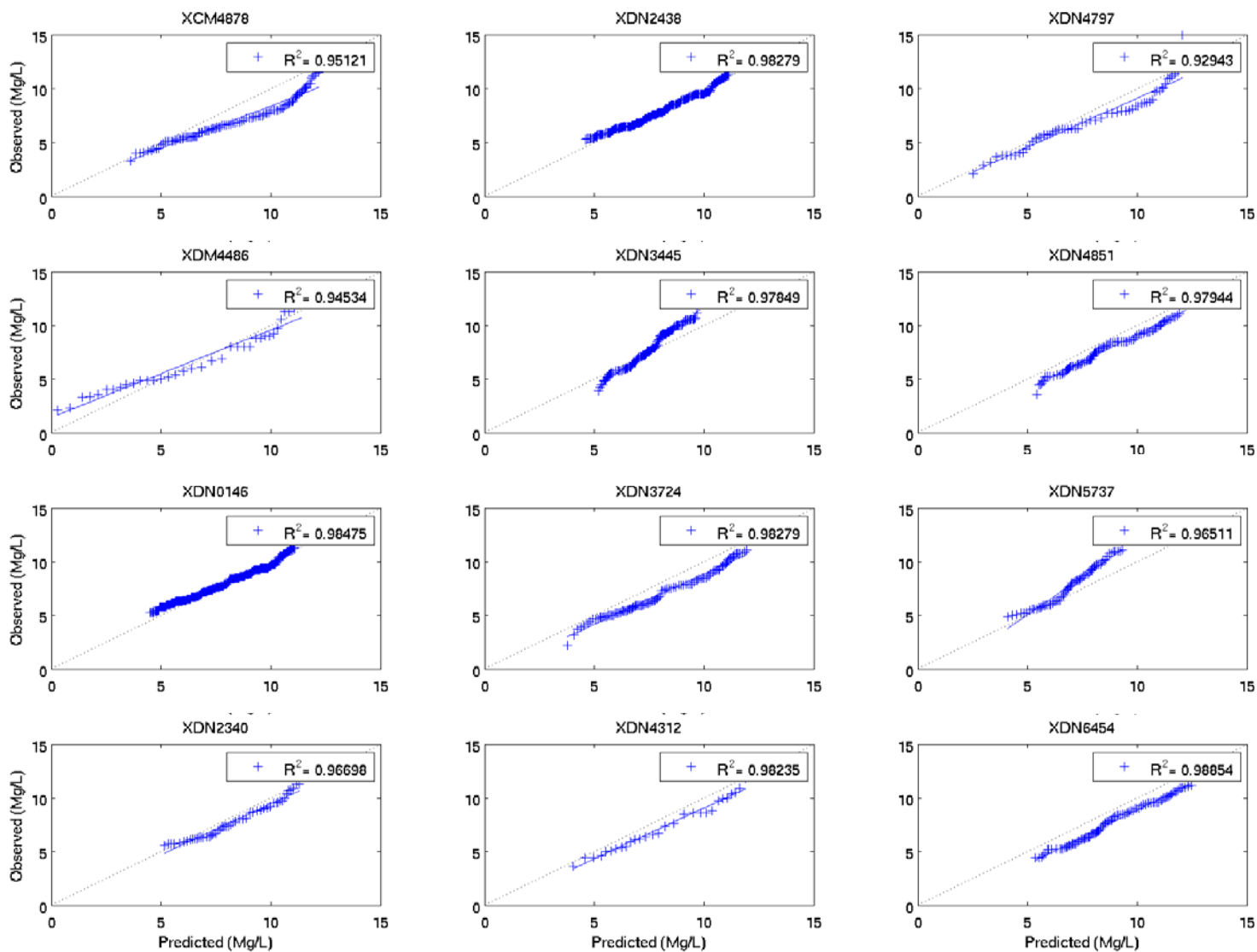


Figure 5.5 (b): Correlation coefficient (R^2) between diel-cycle-adjusted modeled and observed DO, DNR Stations 13-24, baseline conditions, January 2001- August 2005.

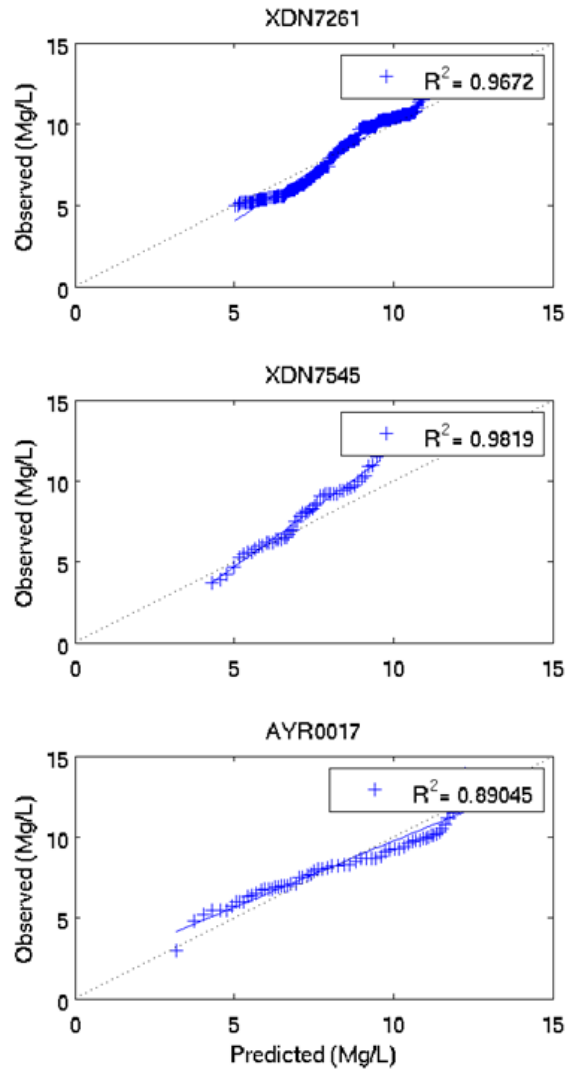


Figure 5.5 (c): Correlation coefficient (R^2) between diel-cycle-adjusted modeled and observed DO, DNR Stations 25-27, baseline conditions, January 2001- August 2005.

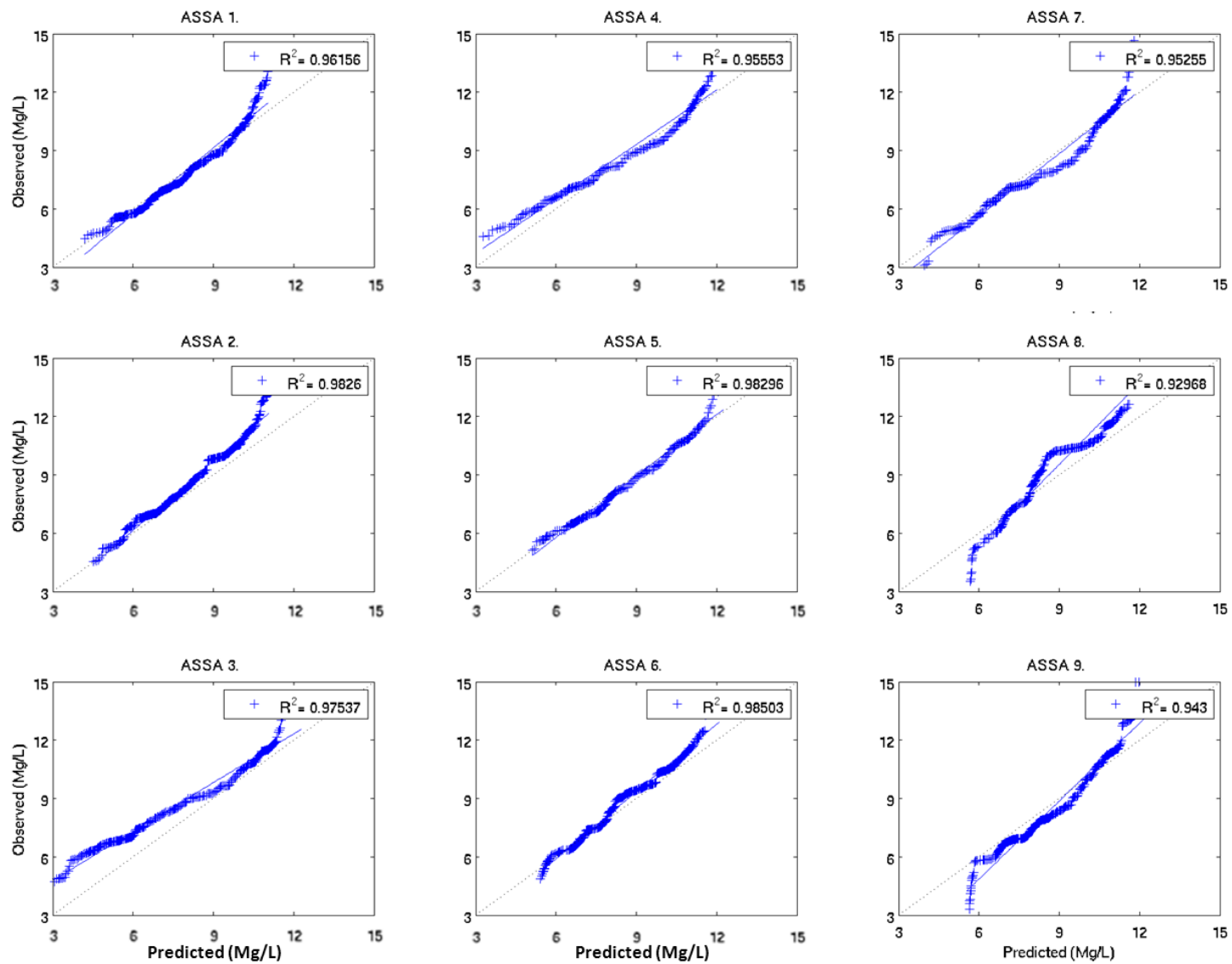


Figure 5.5 (d): Correlation coefficient (R^2) between diel-cycle-adjusted modeled and observed DO, ASIS Stations 1-9, baseline conditions, January 2001- August 2005.

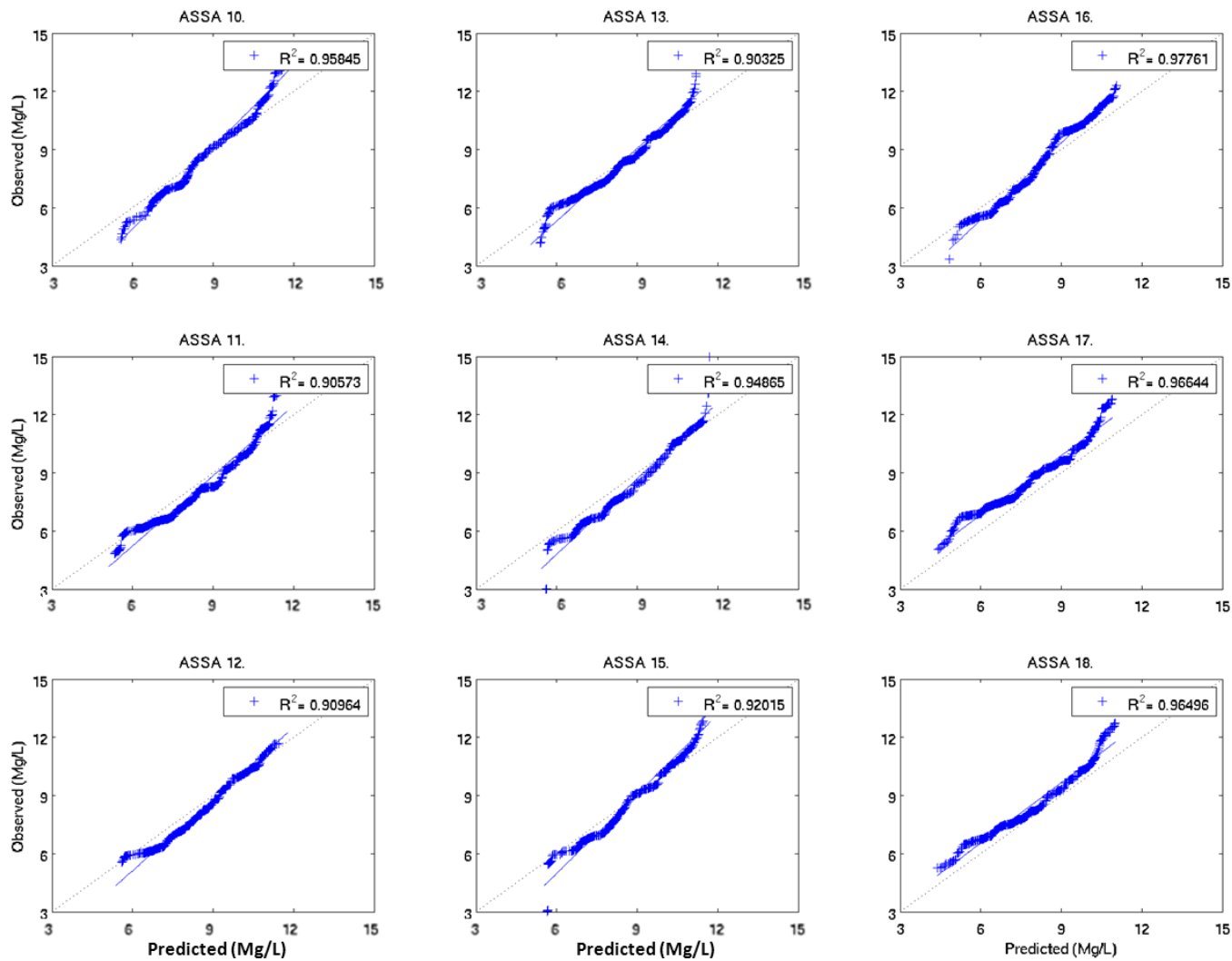


Figure 5.5 (e): Correlation coefficient (R²) between diel-cycle-adjusted modeled and observed DO, ASIS Stations 10-18, baseline conditions, January 2001- August 2005.

5.2 Sensitivity Analyses

Model sensitivity to variations in model parameters is an important characteristic of a model. Often, one needs to find out how model results vary as model parameters are changed and to identify the most influential parameters in determining the accuracy of model results. The accuracy of model output is influenced by a number of uncertainties from measured data, model formulations, and model parameters. Sensitivity analysis is a useful tool to clarify the relationship between uncertainty in parameter values and model results. With the efforts of HEM3D model calibration and verification, sensitivity analyses were conducted to test the following effects: (1) the Ocean City Wastewater Treatment Plant outfall (2) phytoplankton and organic nutrient settling rate and (3) the inputs of ground water discharge.

5.2.1 Ocean City Wastewater Treatment Plant outfall

Within the MCBs modeling domain, there is a major point source outfall offshore of the Ocean City Inlet -The Ocean City Wastewater Treatment Plant (OC WWTP). The outfall is approximately 4600 feet offshore of Ocean City Inlet in the Atlantic Ocean at the depth of 30 feet. This is a secondary treatment plant which treats the wastewater by biological method after the primary treatment. The NPDES (National Pollutant Discharge Elimination System) permitted flow is 14 MGD with a TN concentration of 19 mg/l, and a TP concentration of 3 mg/l. To be consistent with the most conservative approach, the flow rate and TN and TP concentrations were set at the permit level in all the HEM3D model runs conducted. This sensitivity analysis was conducted in order to test whether this facility has the potential to significantly affect the water quality condition inside the MCBs. The sensitivity tests were performed by reducing TN and TP loads by 20%, 40% and 60%, from the base condition over 2001-2004 with all other conditions remaining the same.

The chlorophyll-a modeling result for base and incremental reduction scenarios at DNR and ASIS stations were examined. The exceedance rates for criteria (15 $\mu\text{g/l}$ or 50 $\mu\text{g/l}$, depending on location) are shown in Table 5.2. When comparing exceedance rates of these criteria in both the baseline scenario and scenarios with reductions of 20%, 40% and 60% from the Ocean City WWTP, there is practically no change. When the actual chlorophyll concentrations were examined, the change is on the order of 0.0001 $\mu\text{g/l}$, which is within the numerical error and considered statistically no difference from baseline condition. The DO exceedance results displayed similar results (not shown). Thus, it is concluded that given the present setting of the model domain and the open boundary condition, the Ocean City WWTP outfall does not affect chlorophyll-a and DO inside the MCBs. It should be noted that the present modeling was conducted in a model domain limited by the cross-shore ocean extent, and the boundary conditions used are based on climatologically-averaged values, and thus do not explicitly account for event-driven coastal ocean phenomena.

Table 5.2: Exceedance rates for Chlorophyll-a under Ocean City WWTP 20%, 40% and 60% incremental reduction scenarios.

Percent Chla > 15		Grow Season 2001-2004				Annual average 2001-2004			
Station	TMDL-basin	Base	OCwwtp-20%	OCwwtp-40%	OCwwtp-60%	Base	OCwwtp-20%	OCwwtp-40%	OCwwtp-60%
(SAV growing stations)									
XBM1301	Chincoteague Bay	0.00%	0.00%	0.00%	0.00%	0.00%	0.00%	0.00%	0.00%
XBM8149	Chincoteague Bay	2.31%	2.31%	2.31%	2.31%	1.16%	1.16%	1.16%	1.16%
XCM0159	Chincoteague Bay	2.85%	2.72%	2.72%	2.72%	1.44%	1.37%	1.37%	1.37%
XDN0146	Isle of Wight Bay	0.00%	0.00%	0.00%	0.00%	0.00%	0.00%	0.00%	0.00%
XDN2340	Isle of Wight Bay	4.21%	4.21%	4.21%	4.21%	2.12%	2.12%	2.12%	2.12%
XDN2438	Isle of Wight Bay	0.00%	0.00%	0.00%	0.00%	0.00%	0.00%	0.00%	0.00%
XDN3445	Assawoman Bay	3.94%	3.94%	3.94%	3.94%	1.99%	1.99%	1.99%	1.99%
XDN4851	Assawoman Bay	4.48%	4.48%	4.48%	4.48%	2.26%	2.26%	2.26%	2.26%
XDN6454	Assawoman Bay	2.99%	2.99%	2.99%	2.99%	1.51%	1.51%	1.51%	1.51%
XDN7261	Assawoman Bay	3.26%	3.26%	3.26%	3.26%	1.64%	1.64%	1.64%	1.64%
XDN7545	Assawoman Bay	1.22%	1.22%	1.22%	1.22%	0.62%	0.62%	0.62%	0.62%
ASSA 1.	Sinepuxent Bay	0.00%	0.00%	0.00%	0.00%	0.00%	0.00%	0.00%	0.00%
ASSA 2.	Sinepuxent Bay	0.00%	0.00%	0.00%	0.00%	0.00%	0.00%	0.00%	0.00%
ASSA 3.	Newport Bay	8.83%	8.83%	8.83%	8.83%	4.73%	4.73%	4.73%	4.73%
ASSA 5.	Chincoteague Bay	4.48%	4.48%	4.48%	4.48%	2.26%	2.26%	2.26%	2.26%
ASSA 6.	Chincoteague Bay	0.00%	0.00%	0.00%	0.00%	0.00%	0.00%	0.00%	0.00%
ASSA 7.	Chincoteague Bay	8.15%	8.15%	8.15%	8.15%	4.79%	4.79%	4.79%	4.79%
ASSA 8.	Chincoteague Bay	0.00%	0.00%	0.00%	0.00%	0.00%	0.00%	0.00%	0.00%
ASSA 9.	Chincoteague Bay	0.00%	0.00%	0.00%	0.00%	0.00%	0.00%	0.00%	0.00%
ASSA 11.	Chincoteague Bay	0.00%	0.00%	0.00%	0.00%	0.00%	0.00%	0.00%	0.00%
ASSA 12.	Chincoteague Bay	0.00%	0.00%	0.00%	0.00%	0.00%	0.00%	0.00%	0.00%
ASSA 13.	Chincoteague Bay	0.00%	0.00%	0.00%	0.00%	0.00%	0.00%	0.00%	0.00%
ASSA 14.	Chincoteague Bay	3.53%	3.53%	3.53%	3.53%	1.78%	1.78%	1.78%	1.78%
ASSA 15.	Chincoteague Bay	0.00%	0.00%	0.00%	0.00%	0.00%	0.00%	0.00%	0.00%
ASSA 16.	Sinepuxent Bay	0.00%	0.00%	0.00%	0.00%	0.00%	0.00%	0.00%	0.00%
ASSA 17.	Sinepuxent Bay	0.00%	0.00%	0.00%	0.00%	0.00%	0.00%	0.00%	0.00%
ASSA 18.	Sinepuxent Bay	0.00%	0.00%	0.00%	0.00%	0.00%	0.00%	0.00%	0.00%
Percent Chla>50 (Non-SAV growing stations)		Grow Season 2001-2004				Annual average 2001-2004			
Station	TMDL-basin	Base	OCwwtp-20%	OCwwtp-40%	OCwwtp-60%	Base	OCwwtp-20%	OCwwtp-40%	OCwwtp-60%
BSH0008	Bishopville Prong	19.43%	19.43%	19.43%	19.43%	10.00%	10.00%	10.00%	10.00%
MKL0010	Manklin Creek	2.45%	2.45%	2.45%	2.31%	1.23%	1.23%	1.23%	1.16%
SPR0002	Shingle Landing Prong	5.57%	5.57%	5.57%	5.57%	2.81%	2.81%	2.81%	2.81%
SPR0009	Shingle Landing Prong	6.66%	6.66%	6.66%	6.66%	3.36%	3.36%	3.36%	3.36%
TUV0011	Turville Creek	0.54%	0.54%	0.54%	0.54%	0.27%	0.27%	0.27%	0.27%
TUV0019	Turville Creek	1.36%	1.36%	1.36%	1.36%	0.68%	0.68%	0.68%	0.68%
XBM3418	Chincoteague Bay	0.00%	0.00%	0.00%	0.00%	0.00%	0.00%	0.00%	0.00%
XBM5932	Chincoteague Bay	0.00%	0.00%	0.00%	0.00%	0.00%	0.00%	0.00%	0.00%
XCM1562	Chincoteague Bay	0.00%	0.00%	0.00%	0.00%	0.00%	0.00%	0.00%	0.00%
XCM4878	Newport Bay	0.00%	0.00%	0.00%	0.00%	0.00%	0.00%	0.00%	0.00%
XDM4486	Bishopville Prong	38.59%	38.59%	38.59%	38.59%	19.66%	19.66%	19.66%	19.66%
XDN3724	St. Martin River	1.36%	1.36%	1.36%	1.36%	0.68%	0.68%	0.68%	0.68%
XDN4312	St. Martin River	2.72%	2.72%	2.72%	2.72%	1.37%	1.37%	1.37%	1.37%
XDN4797	St. Martin River	5.98%	5.98%	5.98%	5.98%	3.01%	3.01%	3.01%	3.01%
XDN5737	Assawoman Bay	0.00%	0.00%	0.00%	0.00%	0.00%	0.00%	0.00%	0.00%
AYR0017	Ayer Creek	0.14%	0.14%	0.14%	0.14%	0.07%	0.07%	0.07%	0.07%
ASSA 4.	Newport Bay	0.00%	0.00%	0.00%	0.00%	0.00%	0.00%	0.00%	0.00%
ASSA 10.	Chincoteague Bay	0.00%	0.00%	0.00%	0.00%	0.00%	0.00%	0.00%	0.00%

5.2.2 Effect of phytoplankton and organic nutrient settling rate

The settling velocity is the fundamental property governing the motion of the particles in water. The settling rate (the product of settling velocity and the concentration) of phytoplankton and organic matter links the particulate matter in the water column with the sediment processes. For TN, TP and total carbon (TC), approximately 40% of the nonliving organic components are in the particulate forms. There are also the living organic TN, TP and TC, which are part of the phytoplankton biomass. The living and nonliving particulate TN, TP and TC are the primary source of deposition flux into the sediment. Once settled in the sediment, the particulate organic nitrogen (PON) and phosphorus (POP), and POC are transformed into dissolved forms through the sediment diagenesis process. The ammonia, nitrate, phosphorus, SOD and methane fluxes are generated as a result of interactions between sediment and the overlying water column. When nutrient loads are reduced as the TMDL is implemented, in the MCBs, the reduced particulate portion of the load will have effects on the settling rate and in turn affect the SOD and nutrient fluxes. Since settling velocity is extremely difficult to measure and the exact forms are not known, it is normal practice to specify them as constants. In the HEM3D model, the phytoplankton's settling velocities are set at 0.25, 0.15 and 0.01 m/day for diatoms, green algae and cyanobacteria respectively. For organic carbon, nitrogen and phosphorus, the settling velocities are set at 1 m/day.

It is well known that the diatom component of phytoplankton can change the settling velocity appreciably by orders of magnitude (Collins and Wlosinski, 1983; Jorgensen, 1979). A sensitivity test was conducted by varying the diatom settling velocity from 0.25 m/day to 0.50 m/day, 100% larger than the prescribed value. The results at station AYR0017 for 2004 are shown in Figure 5.6. Due to the high settling velocity (0.5 m/day), the phytoplankton are not retained in the water column long enough to undergo net growth. As a consequence, the chlorophyll-a concentration became lower, which is not reflective of the observed value. In this case, by increasing the settling velocity of diatoms by 100%, the spring chlorophyll-a concentration was reduced by about 50% (from 36 µg/l to 18 µg/l). In general, concentrations of chlorophyll-a, total N, P and C reduced when the settling velocity increased as an inversely relationship. For different phytoplankton species, the responses to changes in settling velocities vary through the different seasons. For example, green algae and cyanobacteria tend to be affected more in the summer and fall while diatoms are affected in the spring.

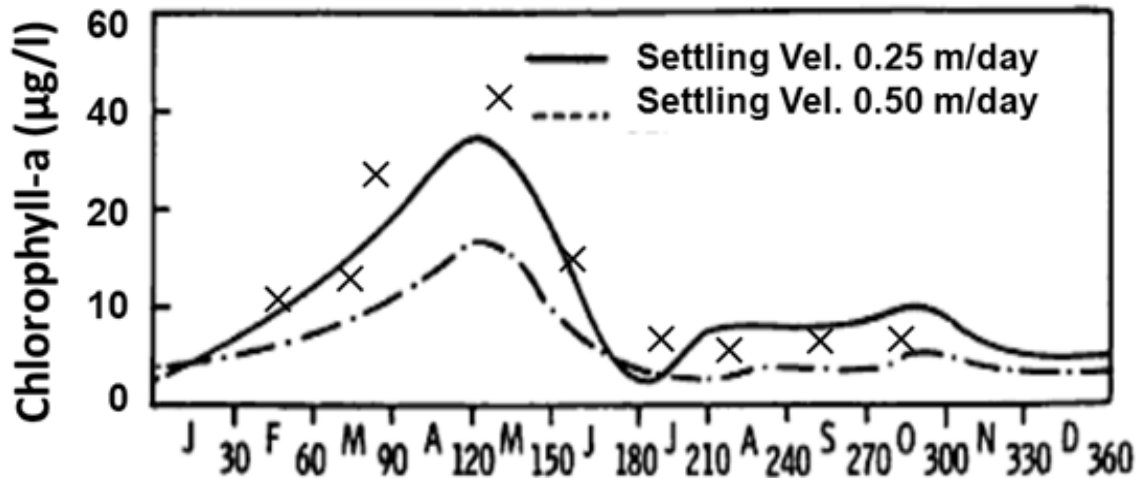


Figure 5.6: Sensitivity test comparing the effect of settling velocities of diatom species on Chlorophyll-a concentration at station AYR0017 in 2004.

Nine sensitivity runs were conducted by changing the settling velocities for phytoplankton, organic carbon, organic nitrogen, and organic phosphorus one each at a time. Table 5.3 summarizes the results of changing the settling velocities on chlorophyll-a concentration. Overall, the chlorophyll-a concentrations are sensitive to the phytoplankton settling velocities. The change of organic N, P and C particulate settling velocity has less effect on the chlorophyll-a concentration. The effect of labile organic component on chlorophyll concentration is slightly higher, while the refractory component has almost no effect. Thomann et al. (1975) reported that phytoplankton settling velocity can have an effect on the nutrient limitation function and thus on the nutrient uptake, which has more of a nonlinear effect. An important question for the sensitivity analysis is: when the TMDL scenarios are implemented, does the settling velocities need to be changed? The answer is no. When the TMDL reduction scenarios were conducted, the settling velocity does not change, but the settling "rate" will be changed due to the change of the concentration in the water column. During the TMDL reduction scenario, if the load reduction leads to concentration reduction, the settling rate (the product of settling velocity and the concentration) will be reduced accordingly and approximately in proportion to the change of the particulate concentration in the water column. This is one of the ways that sediment concentration will be gradually improved.

Table 5.3: Effect of changing settling velocities of phytoplankton and organic nutrients on chlorophyll-a concentration.

Parameter Description	Settling velocity	Net settling velocity	Actual Settling velocity	Input Change	Response of ChlA at MCBs stations (%)			
					BUSH0008	SPR0009	XDM4486	AYR0017
in unit m/day	(Base)		(Sensitivity test)					
Algal settling rate								
Diatom	0.25	0.25	0.5	100%	-41%	-49%	-51%	-46%
Green algae	0.15	0.15	0.075	-50%	25%	23%	21%	18%
Cyanobacteria	0.01	0.01	0.005	-50%	15%	13%	12%	10%
Organic carbon settling rate								
labile	1	1	0.5	-50%	1%	1%	1%	0%
refractory	1	1	0.5	-50%	0%	0%	0%	0%
Organic nitrogen settling rate								
labile	1	1	2	100%	-6%	-7%	-7%	-9%
refractory	1	1	2	100%	0%	1%	1%	0%
Organic phosphorus settling rate								
labile	1	1	2	100%	-4%	-3%	-3%	-2%
refractory	1	1	0.5	-50%	0%	0%	0%	0%

5.2.3 Effects of groundwater discharge

In the Maryland Coastal Bays, it was reported that groundwater discharge in the Atlantic Coastal Bays basin can enhance nitrogen load (Dillow and Greene, 1999). The pathways that groundwater can deliver nitrogen from the land to the Bay are either through direct discharge of groundwater or through base flow to streams that discharge to the Bays. Recently, Fertig et al. (2013) suggested that there is terrestrial nutrient source discharge into the Chincoteague Bay near Johnson Bay, as shown in Figure 5.7 (a); the source is unknown. Cornwell and Owens (2013) further suggested that sediments are the key source and have strong seasonality. They hypothesize that nitrate can be de-nitrified or converted to ammonium at the groundwater/ wetland interface, and subsequently released from the underlying aquifer into Chincoteague Bay proper, with a seasonal switch mechanism in the later summer. For the present water quality model setup, the watershed model input has already generated the interflows, which discharge into the edge of the stream. Thus, the component of groundwater that was not considered is the groundwater discharge directly from the aquifer underneath the Bay into the surface water. In order to test how sensitive the present water quality calibration is to the nitrogen directly discharged from the groundwater to surface water, the interflow from the edge of the land-water margin was re-distributed to the open water of Johnson Bay. The model was re-run and the total nitrogen concentrations were compared at XBM5932 and XBM3418 for before-and-after conditions. The left panel of the Figure 5.7 (b) shows the results before re-distribution, and the right panel of Figure 5.7 (b) shows the result after the interflow was re-distributed to the open water.

It was recognized that the right panel results, which mimic the groundwater release from the underneath of the open bay, has slightly better comparison with observed data in terms of magnitude and phase, especially at the maximum in later summer. This suggests that direct groundwater discharge through under-the-Bay aquifers to the Bay is a plausible hypothesis, which is suggested by the field experiment. From the TMDL point of view, while this is of scientific interest, the full understanding of the process is yet to be uncovered to answer the questions as to actual ammonia release mechanism, the amount of release, and the extent to which it affects the MCBs. The percentage difference in Figure 5.7 (b) is on the order of 5-7%, which is not substantial and also may be localized in the vicinity of Johnson Bay only.

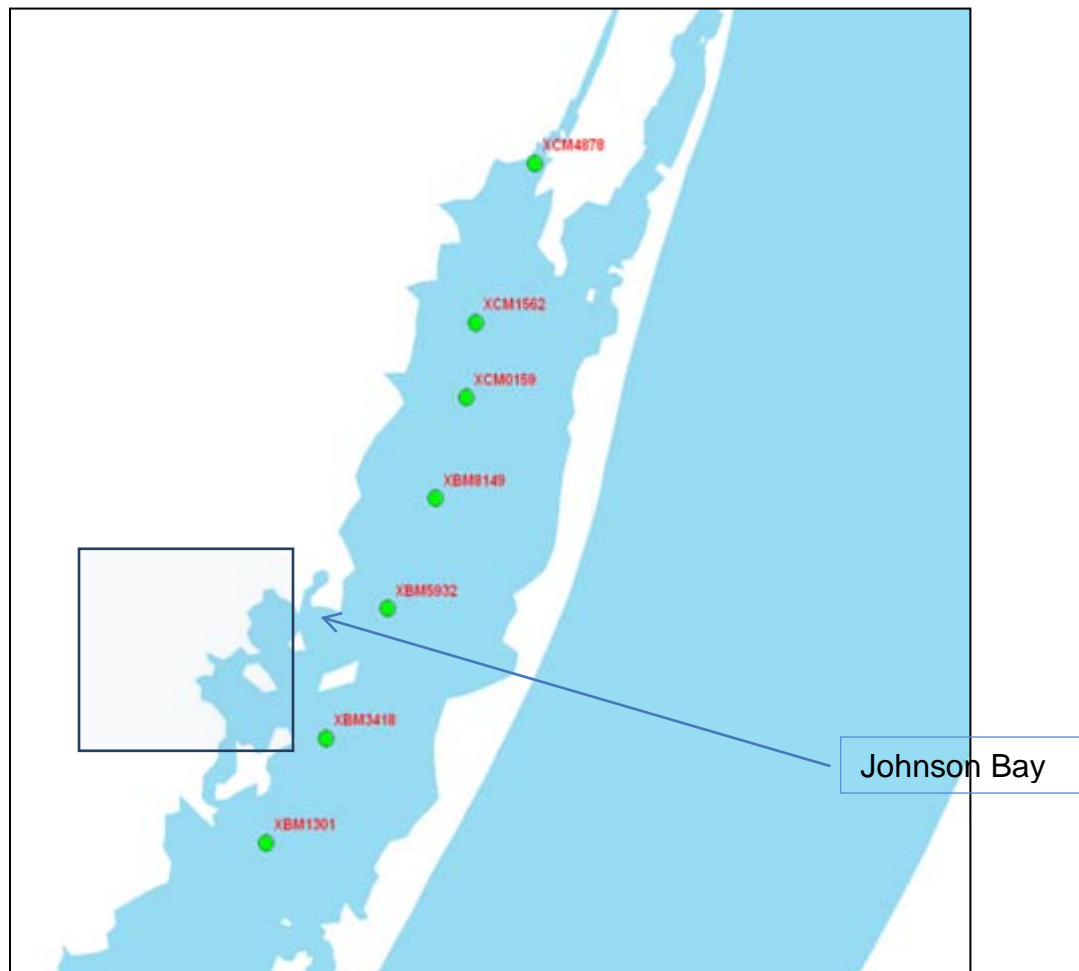


Figure 5.7 (a): Location of Johnson Bay in the middle of the Chincoteague Bay and the nearby DNR stations XBM5932 and XBM3418.

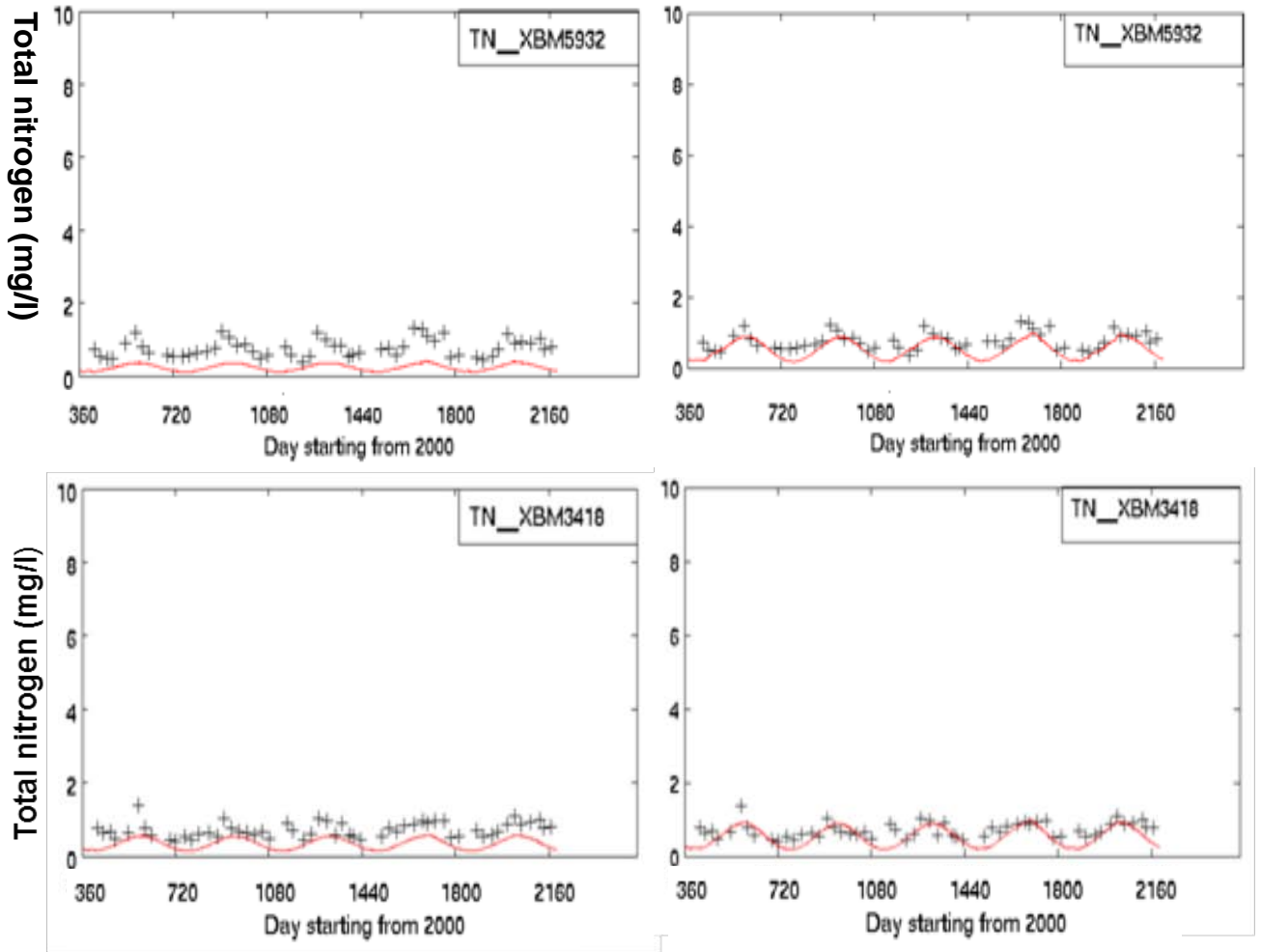


Figure 5.7(b): Comparison of modeled total nitrogen concentrations under groundwater release at edge-of-stream vs. bay-floor release, Johnson Bay area, Chincoteague Bay, 2001-2005.

CHAPTER 6: TMDL SCENARIO DEVELOPMENT

The purpose for developing coupled hydrodynamic and water quality models, which link with the watershed model, was to determine the total load of nutrients that the MCBs could assimilate while maintaining the State's water quality standards (WQS). To support the TMDL analysis, the calibrated model was used to simulate the effect of reduced nutrient loading on DO and chlorophyll concentrations, and the exceedance frequency of relevant water quality criteria. The base condition was conducted from January 2000 through December 2004, while the load reduction analysis time period was calendar years 2001 – 2004.

6.1. Developing nutrient load reduction scenario

6.1.1 Critical conditions

One of the primary concerns in the MCBs is its recurring hypoxia in the bottom waters. Upon completion of the calibrated model from 2000 to 2004 as described in Chapters 4 and 5, the model was used to develop the TMDL that would attain water quality standards under the critical conditions. Estuaries and coastal waters are complex systems and present a challenge for defining the critical conditions. The goal is to estimate the loading capacity during periods when estuaries and coastal waters are most vulnerable to pollutant sources. Based on data analysis and model runs, the factors contributing to low DO and high chlorophyll-a in MCBs are (1) nutrient loads entering into the Bays; (2) hydrodynamic residence time and vertical stratification as a result of freshwater and tides; (3) water temperature and plant respiration; (4) sediment oxygen demand and (5) carbonaceous oxygen demand. All these factors can contribute to low DO and high chlorophyll in MCBs, but not all contribute equally, depending on the time, locations and the associated mechanisms. In terms of temporal variation of DO and chlorophyll-a, it has been found that as flow and nitrogen and phosphorus loads increase, the DO levels decrease and chlorophyll-a level increase. This is clearly demonstrated in Chapter 4; DO is lower and chlorophyll-a is higher in the wet years (2003-2004) versus the average and low flow years (2001-2002). Therefore, high-flow years are the critical periods. A strong spatial gradient exists for both physical characteristics and water quality condition. For example, Allen et al. (2007) showed the gradient of tidal range, salinity, and wave energy from the south to the north of Chincoteague Bay to reach Newport Bay where it has relatively low salinity, low tide, and low wave energy. The water quality condition in the MCBs also has a spatial gradient with the worst condition generally occurring in the head water of the streams as part of the tributaries of the open Bay, and the best condition generally near the inlets (DNR, 2004). There are two basins in the MCBs where hypoxia was consistently observed: Saint Martin River of the Isle of Wight Bay and Newport Bay. The high non-point source loads from the upper reach of the St. Martin River and headwater of the tributaries are believed to be the dominant causes of low DO. On the other hand, in Newport Bay, the combination of the moderately high nutrient load coupled with the long residence time is believed to be the root cause. Hypoxia and anoxia occur most commonly in systems that are seasonally stratified, such as Chesapeake Bay. For a shallow, well mixed water column, the reaeration from the air-water exchange would tend to be sufficient to prevent the development of hypoxic conditions. In metabolically active aquatic systems such as the MCBs, however, a dissolved oxygen diel cycle can

develop due to the presence of large concentrations of algae (Boynton, 1996; Dennison et al, 2012). Under diel oscillation, hypoxia can develop in the early morning and swing to the DO saturation condition in the afternoon within a diel time scale. The diel oxygen change was found to be correlated closely with the chlorophyll concentration, an indication that hypoxia is largely controlled by the algal concentration. In terms of nutrient limitation, N:P ratios tend to be low in the MCBs with nitrogen tending to be limiting in most of the open waters. In the isolated headwaters of some tributaries, phosphorus can be limiting. The nitrogen and phosphorus limitations can vary with the season and the flow as well.

6.1.2 Margin of Safety (MOS)

In the development of a TMDL, a Margin of Safety (MOS) is required to account for the uncertainties involved. In general this uncertainty can be caused by insufficient or poor quality data, a lack of knowledge about the pollution effects, and errors in estimating the loading of the water body. In this approach in the MCBs, the uncertainties were accounted for implicitly by using conservative assumptions. Specifically, the conservative modeling assumptions used include: (1) incorporating a wide range of meteorological conditions - extremely dry to extremely wet—for continuous simulation; (2) the organic material originated from the land was directly transported into the stream, without considering the loss of organic material from the land surface on the way to the stream; (3) all land areas are considered directly connected to streams; (4) nutrient sequestration or transformation occurring in retention ponds or wetlands is not considered; (5) point sources discharges and concentrations were set at the permit value; and (6) the DO diel cycle was incorporated. The effect of DO diel cycle was discussed in detail in Chapter 5.1.

6.1.3 Seasonal variation

The seasonal variations of the phytoplankton optimal growth rate and the bio-chemical reactions are important factor affecting the water quality. These rates in general are a function of water temperature and light condition, both of which change daily and the seasonally. The hydrology in the region also exhibits a seasonal cycle, with the spring having the largest runoff, followed by the winter, with less runoff during the summer and fall seasons. In developing the TMDLs, the seasonal variation was considered for four periods: December through February for winter, March through May for spring, June through August for summer, and September through November for fall. Model runs were performed with direct inputs of temperature, light as well as various hydrologic, meteorological, and loading conditions to simulate the water quality conditions, thus fully evaluating the response to the seasonal variations. A key aspect of nitrogen and phosphorus dynamics in the MCBs modeling system is that daily loads were generated and used as a forcing function to the ecosystem simulated in the HEM3D model. The model can thus be viewed as an integrator of the day-to-day nutrient variation, which incorporated the temperature dependent physical bio-chemical processes, described above, and presented the results in a seasonal-dependent time scale. Problems associated with eutrophication are most likely to occur during the growing season, during which there is typically less stream flow available to flush the system, more sunlight to grow aquatic plants, and warmer temperature, which are favorable conditions

for the biological processes of plant growth and decay of dead plant matter. Therefore, the load reduction scenarios based on the temporal analysis were broken into annual average as well as growing seasons (May 1 – October 31).

6.2 Developing the TMDL scenario

In the watershed load analysis (Chapter 2.2), it was shown that the nutrient loads of MCBs are from five major sources: (1) atmospheric deposition; (2) non-point sources loading (including those from different land uses and the interflow from the shallow groundwater aquifer); (3) point sources; (4) shoreline erosion and (5) septic tanks. Among these sources, the non-point source was the most significant portion of loads that caused the high algal concentration and hypoxia in the MCBs. Therefore, the management strategies for the MCBs is to incrementally reduce the non-point source nutrient loading and to find out to what extent the modeled DO concentration will satisfy the TMDL target. Thus, the TMDL development requires the identification and evaluation by model of various management alternatives for achieving water quality goals. The HEM3D model is used to determine the relationships between changing pollutant loads and the water quality response, and to project the future water quality conditions under “what-if” scenario condition. For the scenario model set up, the water quality boundary condition remained unchanged for various scenarios, which was reasonable since open boundary condition is located 7-9 km away from the open coast (and the inlet), and the concentration is much less than the riverine boundaries in the upstream. The effects of changes in nutrient fluxes from the sediment were incorporated by using the results of the benthic sediment flux model. For each scenario, the load reduction was simulated by running a 5-year simulation three times to achieve equilibrium condition for the concentration in the sediment and overlaying water. The reductions were then applied to all of the simulated years (calendar years 2001-2004) during the TMDL analysis. To represent the simulated DO and chlorophyll-a concentration for each of the Water Quality Limited Segments (WQLS), a volume-weighted calculation was made with chlorophyll-a and DO for each grid cell. In order to encompass a wide range of hydrologic conditions during the TMDL analysis period, the full data set was divided into three hydrology years: 2001 - an average year; 2002 - a dry year; and 2003-2004, wet years.

In developing the TMDL scenario, multiple reduction scenarios were run to determine the assimilative capacity of the waterbody. These scenarios include baseline conditions, natural conditions, incremental reduction and geographic isolation scenarios to determine the best possible combination of load- and source-reduction to attain water quality standards. A set of model scenarios were developed based on the percentage reduction to simulate the changes of chlorophyll-a and DO as the nitrogen and phosphorus loads coming into the MCBs were reduced. The natural conditions scenario was also conducted to check whether there are areas where the water quality endpoints would not be met even if the watershed was returned to a natural state of all-forested and beach areas. In the natural conditions scenario, the atmospheric deposition was reduced to 10% of the baseline atmospheric load, all land uses except beach were changed to forest, and septic loads as well as all point sources were removed. Incremental load reduction scenarios were conducted by reducing the

loading of dissolved inorganic nitrogen: ammonia, nitrate and nitrite, particulate organic nitrogen, dissolved organic nitrogen, phosphate, and organic phosphorus by 20%, 40%, 60% and Maximum Practicable Anthropogenic Reduction (MPAR) to determine which loading conditions in these watersheds would result in the attainment of water quality standards (WQS). The 20%, 40% and 60% scenario are reductions straight from the total loading of the base condition. For the MPAR scenario, percent reductions are calculated from CBP-P5 scenario results for the Eastern Shore for total nitrogen and total phosphorus. CBP-P5 scenario results are available for the following scenarios: no-action (no reductions applied to the baseline); E-3 (Everyone, Everything, Everywhere – maximum reductions from all sources); 2009 Progress (incorporates reductions from implementation through 2009); and 2010 progress (incorporates reductions from implementation through 2010). For each land use sector, the mean percent reduction from the baseline and the three available reduction scenarios was used to calculate the reduction rate for the Coastal Bays watershed model: no-action to E3; 2009 progress to E3; and 2010 progress to E3. The MPAR reductions from specific non-point source sectors are shown in Table 6.1.

Table 6.1: Maximum Practicable Anthropogenic Reduction (MPAR) Percentages for each non-point source sector based on CBP-Phase 5.3.2 scenario results.

Non-Point Source Sector	TN Reduction	TP Reduction	TSS Reduction
Animal Feeding Operations (AFO)	67%	69%	29%
Crop	64%	34%	50%
Pasture	45%	46%	54%
Urban	51%	68%	73%
Septic	57%	0%	0%
Forest	0%	0%	0%

The model results, showing WQS exceedance rates under baseline and incremental scenarios: 20%, 40%, 60%, natural condition, and MPAR are presented in Table 6.2 for all 27 DNR and 18 ASIS stations. The exceedance rate was determined for growing season as well as annual average conditions, and spatially aggregated into five assessment basins—Assawoman Bay, Isle of Wight Bay, Sinepuxent Bay, Newport Bay and Chincoteague Bay (in columns 2 and 3), consistent with Maryland’s WQLS listing. Table 6.2 demonstrates that there are 6 stations: MKL0010, XDM4486, BSH0008, SPR0009, AYR0017 and ASSA4, located in the Isle of Wight Bay and in Newport Bay, having the highest exceedance rate during both growing season and average annual conditions. Among these six stations, the first four stations are in the Saint Martin River of the Isle of Wight; and the other two stations are in the Newport Bay. The response of these 6 stations to the incremental reductions of 20%, 40%, 60%, MPAR and natural conditions are shown in Figure 6.1, which shows a decreasing trend of the exceedance rate as the reduction increases, with an asymptotic approach to the natural condition. It can be seen that DO exceedance rates are below 10% criteria for all 6 stations when 60% incremental reduction is executed. The 60% is, thus, considered to be the theoretical maximum reduction that is required for any place within the MCBs. To demonstrate that the ideal 60% reduction would improve the water quality condition in real time, the time

series results for DO base condition and 60% reduction from 2001-2004 are shown in Figure 6.2 (a)–(e). In these figures, the time series with 60% reduction (represented by magenta) and without 60% reduction (represented by blue) were directly compared. It can be seen that under the 60% reduction scenario all of the stations were improved and meet the DO criteria. The improvements were particularly obvious for the 6 most severely impaired stations identified in Figure 6.1.

Table 6.2: DO exceedance rate under baseline conditions and reduction scenarios of 20%, 40%, 60%, natural conditions and MPAR for all DNR and ASIS stations.

Stations	TMDL-basin	MD-8digit-basin	DO exceedance rate (Growing Season 2001-2004)						DO exceedance rate (Annual 2001-2004)					
			Base	20%	40%	60%	natural C	MPAR	Base	20%	40%	60%	natural C	MPAR
BSH0008	Bishopville Prong	Isle of Wight Bay	20.79%	11.55%	3.53%	1.77%	1.77%	2.72%	10.48%	5.82%	1.78%	0.89%	1.03%	1.37%
MKL0010	Manklin Creek	Isle of Wight Bay	54.18%	32.20%	17.80%	5.16%	0.27%	1.36%	40.89%	36.99%	17.81%	5.32%	0.14%	9.32%
SPR0002	Shingle Landing Prong	Isle of Wight Bay	1.90%	0.95%	0.41%	0.27%	0.68%	0.00%	0.96%	0.48%	0.21%	0.14%	0.34%	0.00%
SPR0009	Shingle Landing Prong	Isle of Wight Bay	19.84%	13.32%	8.42%	2.99%	1.63%	6.11%	10.00%	6.71%	4.25%	1.51%	0.82%	3.08%
TUV0011	Turville Creek	Isle of Wight Bay	0.00%	0.00%	0.00%	0.00%	0.00%	0.00%	0.00%	0.00%	0.00%	0.00%	0.00%	0.00%
TUV0019	Turville Creek	Isle of Wight Bay	0.54%	0.00%	0.00%	0.41%	0.68%	0.00%	0.27%	0.00%	0.00%	0.21%	0.34%	0.00%
XBM1301	Chincoteague Bay	Chincoteague Bay	0.00%	0.00%	0.00%	0.00%	0.00%	0.00%	0.00%	0.00%	0.00%	0.00%	0.00%	0.00%
XBM3418	Chincoteague Bay	Chincoteague Bay	0.00%	0.00%	0.00%	0.00%	0.00%	0.00%	0.00%	0.00%	0.00%	0.00%	0.00%	0.00%
XBM5932	Chincoteague Bay	Chincoteague Bay	0.00%	0.00%	0.00%	0.00%	0.00%	0.00%	0.00%	0.00%	0.00%	0.00%	0.00%	0.00%
XBM8149	Chincoteague Bay	Chincoteague Bay	0.00%	0.00%	0.00%	0.00%	0.00%	0.00%	0.00%	0.00%	0.00%	0.00%	0.00%	0.00%
XCM0159	Chincoteague Bay	Chincoteague Bay	0.00%	0.00%	0.00%	0.00%	0.00%	0.00%	0.00%	0.00%	0.00%	0.00%	0.00%	0.00%
XCM1562	Chincoteague Bay	Chincoteague Bay	0.00%	0.00%	0.00%	0.00%	0.00%	0.00%	0.00%	0.00%	0.00%	0.00%	0.00%	0.00%
XCM4878	Newport Bay	Newport Bay	5.03%	0.68%	0.00%	0.14%	0.82%	0.00%	2.53%	0.34%	0.00%	0.07%	0.41%	0.00%
XDM4486	Bishopville Prong	Isle of Wight Bay	42.66%	34.38%	20.79%	5.03%	2.58%	18.48%	21.51%	17.33%	10.48%	2.53%	2.26%	9.32%
XDN0146	Isle of Wight Bay	Isle of Wight Bay	0.00%	0.00%	0.00%	0.00%	0.00%	0.00%	0.00%	0.00%	0.00%	0.00%	0.00%	0.00%
XDN2340	Isle of Wight Bay	Isle of Wight Bay	0.00%	0.00%	0.00%	0.00%	0.00%	0.00%	0.00%	0.00%	0.00%	0.00%	0.00%	0.00%
XDN2438	Isle of Wight Bay	Isle of Wight Bay	0.00%	0.00%	0.00%	0.00%	0.00%	0.00%	0.00%	0.00%	0.00%	0.00%	0.00%	0.00%
XDN3445	Assawoman Bay	Asswoman Bay	0.00%	0.00%	0.00%	0.00%	0.00%	0.00%	0.00%	0.00%	0.00%	0.00%	0.00%	0.00%
XDN3724	St. Martin River	Isle of Wight Bay	0.00%	0.00%	0.00%	0.00%	0.00%	0.00%	0.00%	0.00%	0.00%	0.00%	0.00%	0.00%
XDN4312	St. Martin River	Isle of Wight Bay	0.00%	0.00%	0.00%	0.00%	0.00%	0.00%	0.00%	0.00%	0.00%	0.00%	0.00%	0.00%
XDN4797	St. Martin River	Isle of Wight Bay	2.04%	1.09%	0.54%	0.41%	0.68%	0.00%	1.03%	0.55%	0.27%	0.21%	0.34%	0.00%
XDN4851	Assawoman Bay	Asswoman Bay	0.00%	0.00%	0.00%	0.00%	0.00%	0.00%	0.00%	0.00%	0.00%	0.00%	0.00%	0.00%
XDN5737	Assawoman Bay	Asswoman Bay	0.00%	0.00%	0.00%	0.00%	0.00%	0.00%	0.00%	0.00%	0.00%	0.00%	0.00%	0.00%
XDN6454	Assawoman Bay	Asswoman Bay	0.00%	0.00%	0.00%	0.00%	0.00%	0.00%	0.00%	0.00%	0.00%	0.00%	0.00%	0.00%
XDN7261	Assawoman Bay	Asswoman Bay	0.00%	0.00%	0.00%	0.00%	0.00%	0.00%	0.00%	0.00%	0.00%	0.00%	0.00%	0.00%
XDN7545	Assawoman Bay	Asswoman Bay	0.00%	0.00%	0.00%	0.00%	0.00%	0.00%	0.00%	0.00%	0.00%	0.00%	0.00%	0.00%
AYR0017	Ayer Creek	Newport Bay	8.42%	3.67%	0.54%	0.82%	1.36%	0.68%	4.25%	1.85%	0.27%	0.41%	0.68%	0.34%
ASSA 1.	Sinepuxent Bay	Sinepuxent Bay	0.00%	0.00%	0.00%	0.00%	0.00%	0.00%	0.00%	0.00%	0.00%	0.00%	0.00%	0.00%
ASSA 2.	Sinepuxent Bay	Sinepuxent Bay	0.00%	0.00%	0.00%	0.00%	0.00%	0.00%	0.00%	0.00%	0.00%	0.00%	0.00%	0.00%
ASSA 3.	Newport Bay	Newport Bay	0.27%	0.00%	0.00%	0.00%	0.00%	0.00%	0.14%	0.00%	0.00%	0.00%	0.00%	0.00%
ASSA 4.	Newport Bay	Newport Bay	5.57%	1.09%	0.27%	0.54%	0.95%	0.00%	2.81%	0.55%	0.14%	0.27%	0.48%	0.00%
ASSA 5.	Chincoteague Bay	Chincoteague Bay	0.00%	0.00%	0.00%	0.00%	0.00%	0.00%	0.00%	0.00%	0.00%	0.00%	0.00%	0.00%
ASSA 6.	Chincoteague Bay	Chincoteague Bay	0.00%	0.00%	0.00%	0.00%	0.00%	0.00%	0.00%	0.00%	0.00%	0.00%	0.00%	0.00%
ASSA 7.	Chincoteague Bay	Chincoteague Bay	0.00%	0.00%	0.00%	0.00%	0.00%	0.00%	0.00%	0.00%	0.00%	0.00%	0.00%	0.00%
ASSA 8.	Chincoteague Bay	Chincoteague Bay	0.00%	0.00%	0.00%	0.00%	0.00%	0.00%	0.00%	0.00%	0.00%	0.00%	0.00%	0.00%
ASSA 9.	Chincoteague Bay	Chincoteague Bay	0.00%	0.00%	0.00%	0.00%	0.00%	0.00%	0.00%	0.00%	0.00%	0.00%	0.00%	0.00%
ASSA 10.	Chincoteague Bay	Chincoteague Bay	0.00%	0.00%	0.00%	0.00%	0.00%	0.00%	0.00%	0.00%	0.00%	0.00%	0.00%	0.00%
ASSA 11.	Chincoteague Bay	Chincoteague Bay	0.00%	0.00%	0.00%	0.00%	0.00%	0.00%	0.00%	0.00%	0.00%	0.00%	0.00%	0.00%
ASSA 12.	Chincoteague Bay	Chincoteague Bay	0.00%	0.00%	0.00%	0.00%	0.00%	0.00%	0.00%	0.00%	0.00%	0.00%	0.00%	0.00%
ASSA 13.	Chincoteague Bay	Chincoteague Bay	0.00%	0.00%	0.00%	0.00%	0.00%	0.00%	0.00%	0.00%	0.00%	0.00%	0.00%	0.00%
ASSA 14.	Chincoteague Bay	Chincoteague Bay	0.00%	0.00%	0.00%	0.00%	0.00%	0.00%	0.00%	0.00%	0.00%	0.00%	0.00%	0.00%
ASSA 15.	Chincoteague Bay	Chincoteague Bay	0.00%	0.00%	0.00%	0.00%	0.00%	0.00%	0.00%	0.00%	0.00%	0.00%	0.00%	0.00%
ASSA 16.	Sinepuxent Bay	Sinepuxent Bay	0.00%	0.00%	0.00%	0.00%	0.00%	0.00%	0.00%	0.00%	0.00%	0.00%	0.00%	0.00%
ASSA 17.	Sinepuxent Bay	Sinepuxent Bay	0.00%	0.00%	0.00%	0.00%	0.00%	0.00%	0.00%	0.00%	0.00%	0.00%	0.00%	0.00%
ASSA 18.	Sinepuxent Bay	Sinepuxent Bay	0.00%	0.00%	0.00%	0.00%	0.00%	0.00%	0.00%	0.00%	0.00%	0.00%	0.00%	0.00%

DO Growing Season 2001-2004

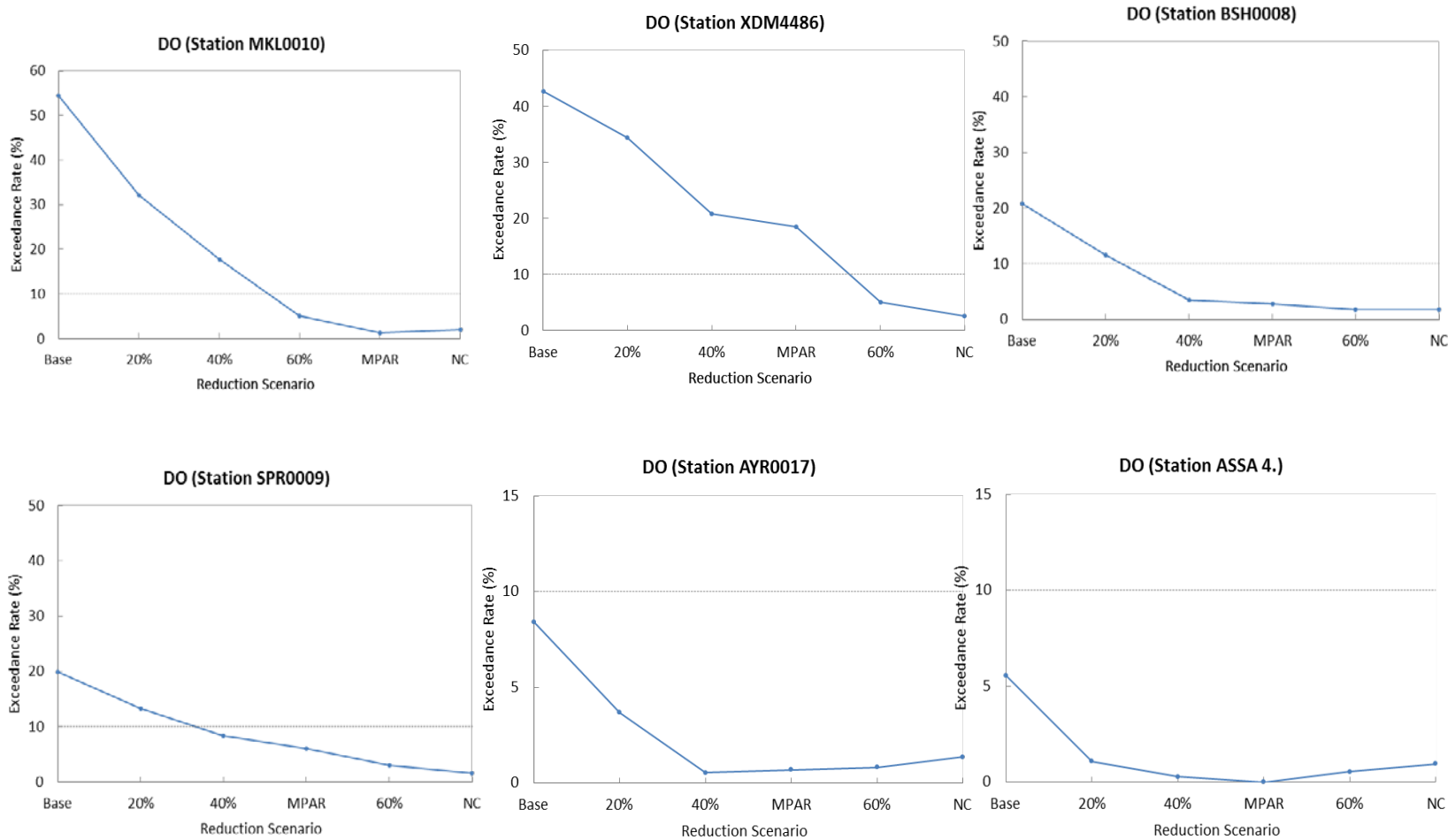


Figure 6.1: Response of six stations having the highest DO exceedance rates to the incremental reductions, MPAR and natural conditions scenarios.

In addition to the DO criteria, Table 6.3 (a) and (b) present the chlorophyll-a exceedance rates under baseline, reductions of 20%, 40% and 60%, MPAR, natural conditions, growing season TMDL, and average annual TMDL scenarios. There are two endpoints for the chlorophyll-a concentration: 50 µg/l for the non-SAV growing area, and 15µg/l for the SAV growing area. Tables 6.3 (a) and (b) show the exceedance rates for all of the stations in the MCBs under non-SAV growing and SAV growing areas chlorophyll-a endpoint respectively. From Table 6.3 (a), it was identified that there were two stations: BSH008 and XDM4488, both located near Bishopville Prong of the Isle of Wight Bay, exceeded the 50ug/l chlorophyll-a concentration endpoint in the non-SAV growing areas. For the 4 year time period simulated, the model predicted that a 40% reduction in nutrient loading would have eliminated the water quality impairment for chlorophyll-a in all of the basins in MCBs, as the frequency of chlorophyll-a exceedances fell below 10% in each area during the growing season. It is noted that the two stations that exceeded the chlorophyll-a endpoint were also the stations corresponding to the lower DO condition and thus reducing nutrient loading will produce lower chlorophyll-a concentrations as well as improving the daily oxygen concentration. It was estimated that the 40% nutrient reduction reduced average chlorophyll a concentrations by approximately 60 ug/l. For the SAV growing areas (and the surrounding 2500-ft buffer zone), the more stringent endpoint, a maximum chlorophyll-a concentration not to exceed 15ug/l is applied. Table 6.3 (b) shows that the highest exceedance rates under base conditions were 8.83% and 8.15% in the ASIS Stations 3 and 7, located near Newport Bay and Johnson Bay, respectively. MDE's assessment methodology requires that the chlorophyll-a concentration not exceed 15µg/l more than 10 percent of the time under both average annual and growing season conditions. Therefore, no TMDL action was required to meet the chlorophyll a TMDL endpoint with respect to SAV grow zones.

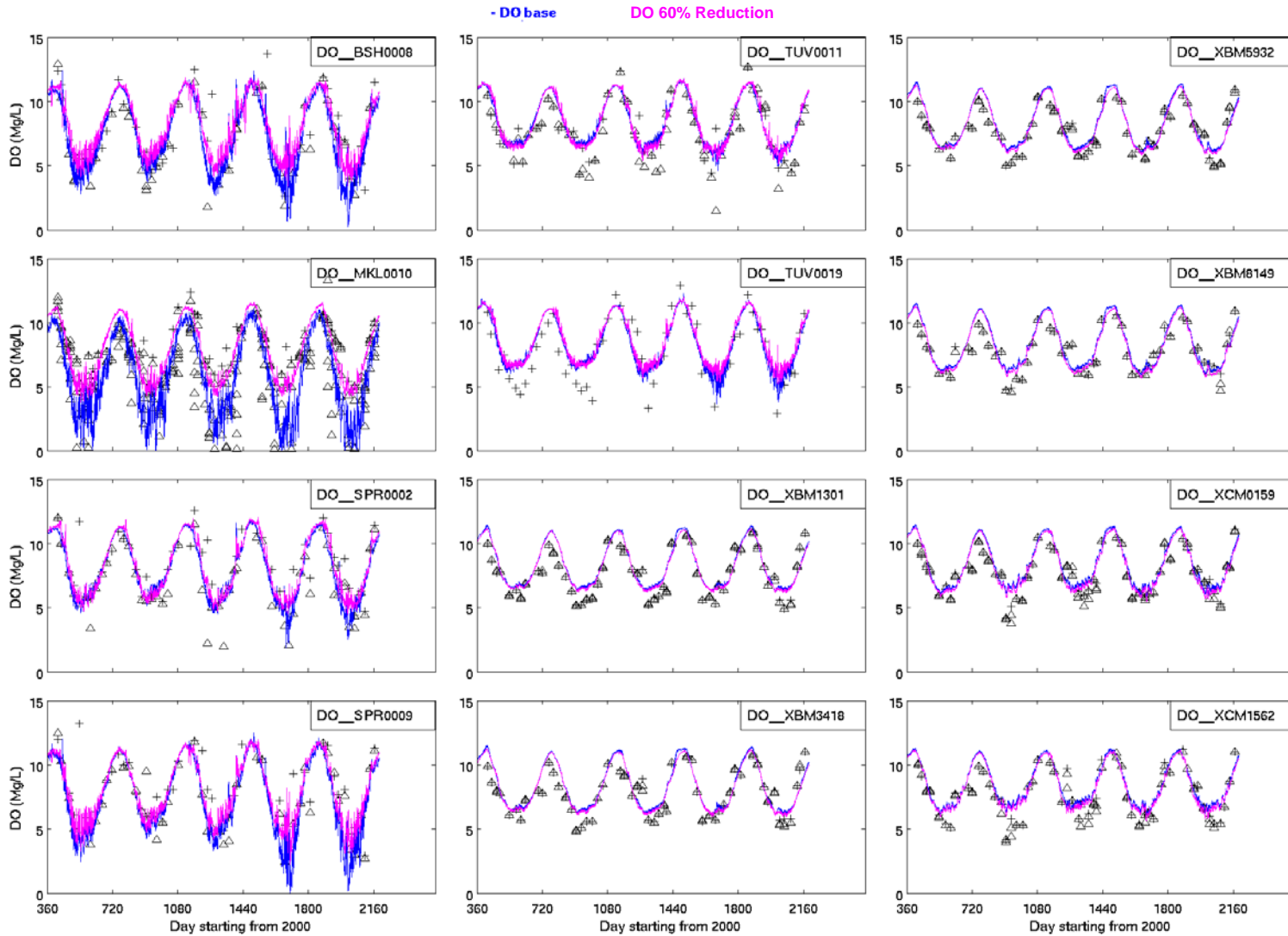


Figure 6.2 (a): DO time series, 2001- August 2005, baseline conditions (blue), 60% reduction scenario (magenta), and observed (symbol) at DNR Stations 1-12.

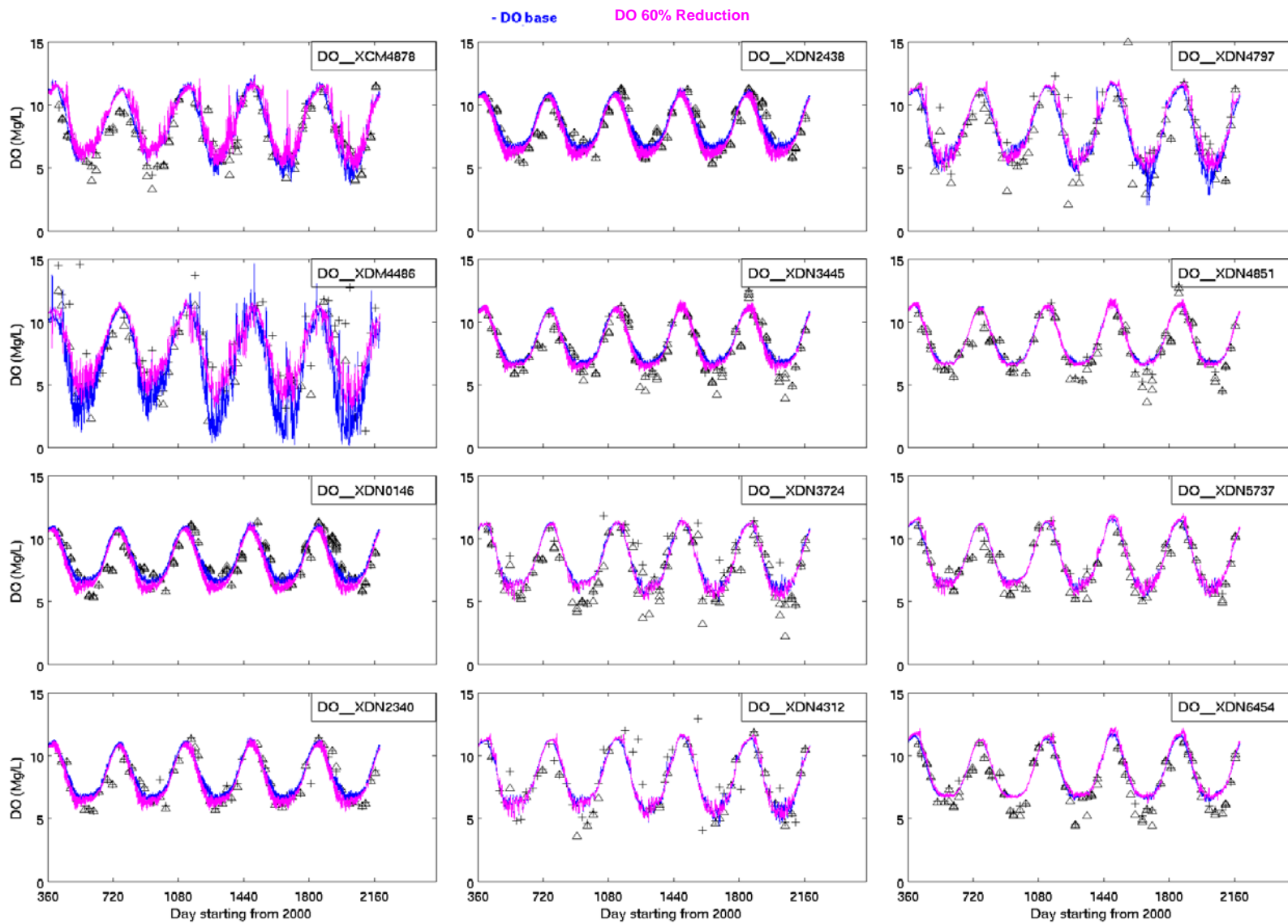


Figure 6.2 (b): DO time series, 2001- August 2005, for baseline conditions (blue), 60% reduction scenario(magenta), and observed (symbol) at DNR Stations: 13 -24.

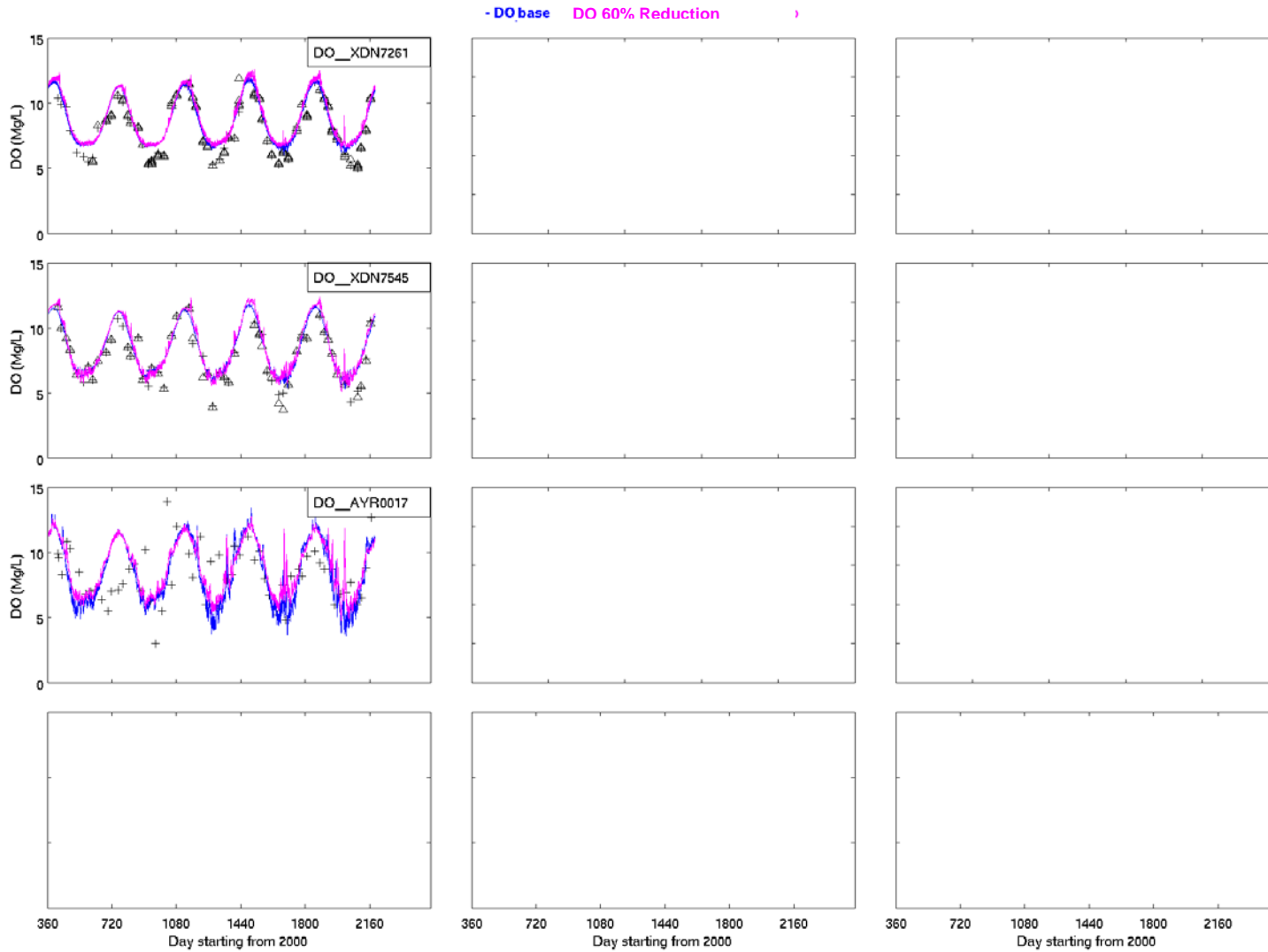


Figure 6.2 (c): DO time series, 2001-August 2005 for baseline conditions (blue), and 60% reduction scenario (magenta), and observed (symbol) at DNR Stations 25 - 27.

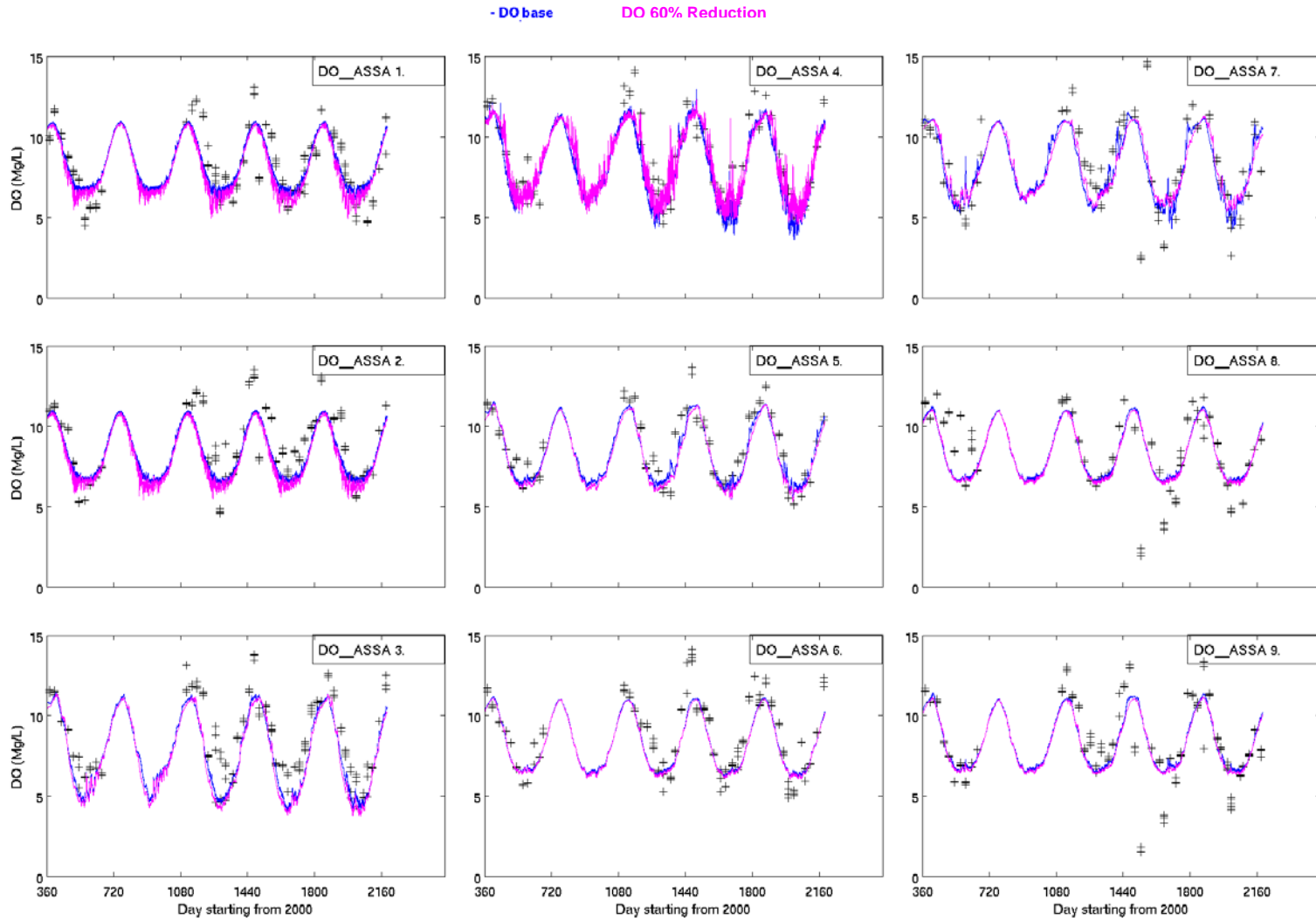


Figure 6.2 (d): DO time series, 2001-August 2005, baseline conditions (blue), 60% reduction scenario (magenta) and observed data (symbol) at ASIS Stations 1-9.

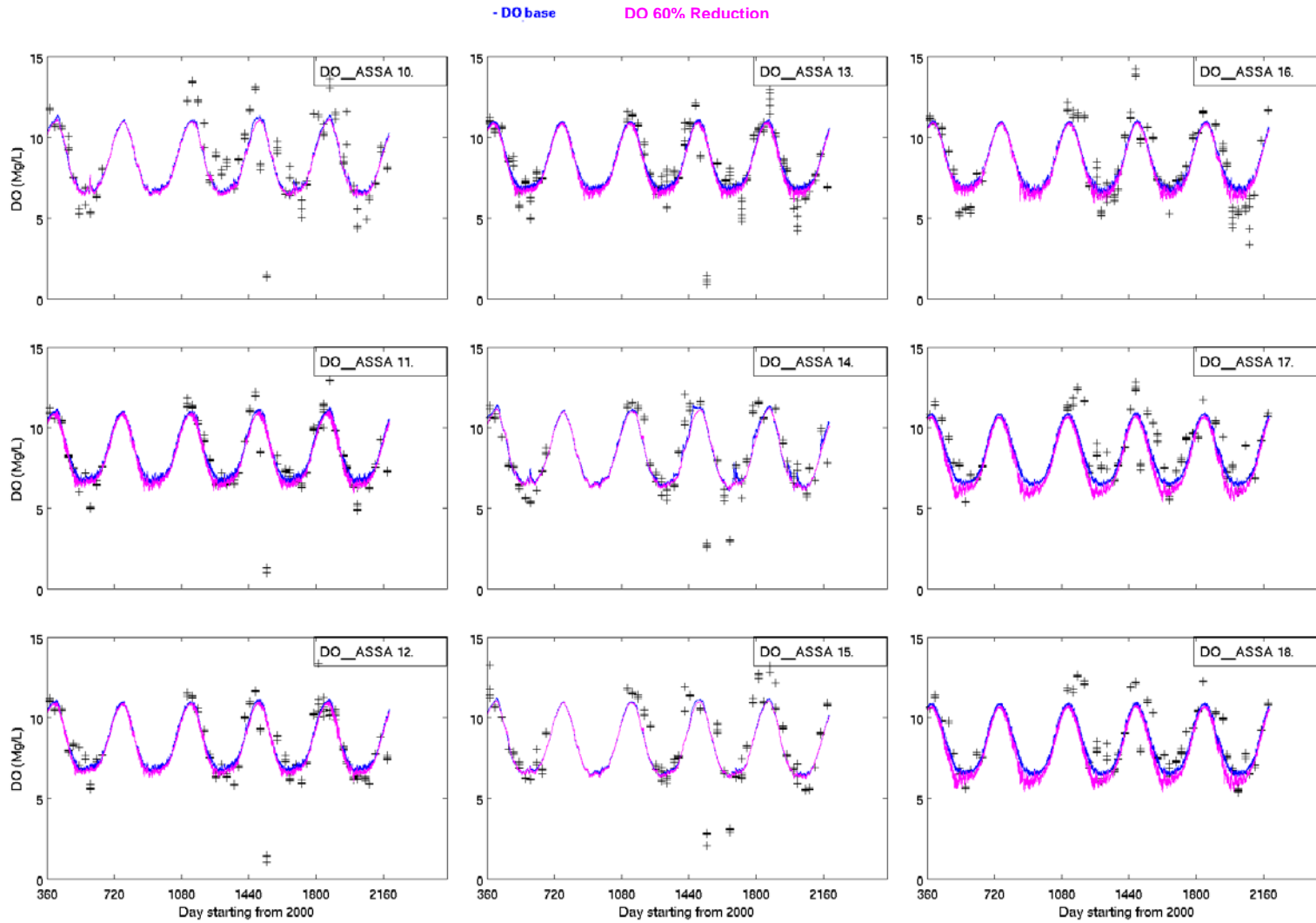


Figure 6.2 (e): DO time series, 2001-August 2005, baseline conditions (blue), 60% reduction scenario (magenta), and observed data (symbol) at ASIS Stations 10 -18.

Table 6.3 (a): Modeled chlorophyll-a exceedance rates under baseline conditions and reduction scenarios of 20%, 40%, 60%, natural and MPAR conditions for non-SAV growing zone with Chl-a endpoint greater than 50 µg/l.

Percent Chla > 50			Chla exceedance rate (Growing Season 2001-2004)						Chla exceedance rate (Annual 2001-2004)					
Station	TMDL-basin	MD-8digit-basin	Base	20%	40%	60%	natural C	MPAR	base	20%	40%	60%	natural	MPAR
BSH0008	Bishopville Prong	Isle of Wight Bay	19.43%	8.70%	3.40%	0.82%	0.00%	6.66%	10.00%	4.38%	1.71%	0.41%	0.00%	3.36%
MKL0010	Manklin Creek	Isle of Wight Bay	2.45%	0.00%	0.00%	0.00%	0.00%	0.00%	1.23%	0.00%	0.00%	0.00%	0.00%	0.00%
SPR0002	Shingle Landing Prong	Isle of Wight Bay	5.57%	2.72%	0.68%	0.00%	0.00%	2.58%	2.81%	1.37%	0.34%	0.00%	0.00%	1.30%
SPR0009	Shingle Landing Prong	Isle of Wight Bay	6.66%	4.08%	0.00%	0.00%	0.00%	2.04%	3.36%	2.05%	0.00%	0.00%	0.00%	1.03%
TUV0011	Turville Creek	Isle of Wight Bay	0.54%	0.00%	0.00%	0.00%	0.00%	0.00%	0.27%	0.00%	0.00%	0.00%	0.00%	0.00%
TUV0019	Turville Creek	Isle of Wight Bay	1.36%	0.00%	0.00%	0.00%	0.00%	0.00%	0.68%	0.00%	0.00%	0.00%	0.00%	0.00%
XBM3418	Chincoteague Bay	Chincoteague Bay	0.00%	0.00%	0.00%	0.00%	0.00%	0.00%	0.00%	0.00%	0.00%	0.00%	0.00%	0.00%
XBM5932	Chincoteague Bay	Chincoteague Bay	0.00%	0.00%	0.00%	0.00%	0.00%	0.00%	0.00%	0.00%	0.00%	0.00%	0.00%	0.00%
XCM1562	Chincoteague Bay	Chincoteague Bay	0.00%	0.00%	0.00%	0.00%	0.00%	0.00%	0.00%	0.00%	0.00%	0.00%	0.00%	0.00%
XCM4878	Newport Bay	Newport Bay	0.00%	0.00%	0.00%	0.00%	0.00%	0.00%	0.00%	0.00%	0.00%	0.00%	0.00%	0.00%
XDM4486	Bishopville Prong	Isle of Wight Bay	38.59%	18.07%	5.16%	1.49%	0.00%	10.05%	19.66%	9.18%	2.60%	0.75%	0.00%	5.21%
XDN3724	St. Martin River	Isle of Wight Bay	1.36%	0.54%	0.00%	0.00%	0.00%	0.41%	0.68%	0.27%	0.00%	0.00%	0.00%	0.21%
XDN4312	St. Martin River	Isle of Wight Bay	2.72%	0.95%	0.27%	0.00%	0.00%	0.82%	1.37%	0.48%	0.14%	0.00%	0.00%	0.41%
XDN4797	St. Martin River	Isle of Wight Bay	5.98%	3.53%	0.68%	0.00%	0.00%	2.85%	3.01%	1.78%	0.34%	0.00%	0.00%	1.44%
XDN5737	Assawoman Bay	Asswoman Bay	0.00%	0.00%	0.00%	0.00%	0.00%	0.00%	0.00%	0.00%	0.00%	0.00%	0.00%	0.00%
AYR0017	Ayer Creek	Newport Bay	0.14%	0.00%	0.00%	0.00%	0.00%	0.00%	0.07%	0.00%	0.00%	0.00%	0.00%	0.00%
ASSA 4.	Newport Bay	Newport Bay	0.00%	0.00%	0.00%	0.00%	0.00%	0.00%	0.00%	0.00%	0.00%	0.00%	0.00%	0.00%
ASSA 10.	Chincoteague Bay	Chincoteague Bay	0.00%	0.00%	0.00%	0.00%	0.00%	0.00%	0.00%	0.00%	0.00%	0.00%	0.00%	0.00%

Table 6.3 (b): Modeled chlorophyll-a exceedance rates under baseline conditions and reduction scenarios of 20%, 40%, 60%, natural and MPAR conditions for SAV growing zone with Chl-a endpoint greater than 15µg/l.

Percent Chla >15															
Station	TMDL-basin	MD-8digit-basin	Chla exceedance rate (Growing Season 2001-2004)						Chla exceedance rate (Annual 2001-2004)						
			Base	20%	40%	60%	natural C	MPAR	Base	20%	40%	60%	natural C	MPAR	
XBM1301	Chincoteague Bay	Chincoteague Bay	0.00%	0.00%	0.00%	0.00%	0.00%	0.00%	0.00%	0.00%	0.00%	0.00%	0.00%	0.00%	0.00%
XBM8149	Chincoteague Bay	Chincoteague Bay	2.31%	0.00%	0.00%	0.00%	0.00%	0.54%	1.16%	0.00%	0.00%	0.00%	0.00%	0.00%	0.27%
XCM0159	Chincoteague Bay	Chincoteague Bay	2.85%	1.36%	0.00%	0.00%	0.00%	2.31%	1.44%	0.68%	0.00%	0.00%	0.00%	0.00%	1.16%
XDN0146	Isle of Wight Bay	Isle of Wight Bay	0.00%	0.00%	0.00%	0.00%	0.00%	0.00%	0.00%	0.00%	0.00%	0.00%	0.00%	0.00%	0.00%
XDN2340	Isle of Wight Bay	Isle of Wight Bay	4.21%	3.53%	2.04%	0.14%	0.00%	3.67%	2.12%	1.78%	1.03%	0.07%	0.00%	1.85%	
XDN2438	Isle of Wight Bay	Isle of Wight Bay	0.00%	0.00%	0.00%	0.00%	0.00%	0.00%	0.00%	0.00%	0.00%	0.00%	0.00%	0.00%	0.00%
XDN3445	Assawoman Bay	Asswoman Bay	3.94%	2.45%	0.00%	0.00%	0.00%	3.53%	1.99%	1.23%	0.00%	0.00%	0.00%	0.00%	1.78%
XDN4851	Assawoman Bay	Asswoman Bay	4.48%	2.72%	0.00%	0.00%	0.00%	0.82%	2.26%	1.37%	0.00%	0.00%	0.00%	0.00%	0.41%
XDN6454	Assawoman Bay	Asswoman Bay	2.99%	0.41%	0.00%	0.00%	0.00%	0.00%	1.51%	0.21%	0.00%	0.00%	0.00%	0.00%	0.00%
XDN7261	Assawoman Bay	Asswoman Bay	3.26%	1.09%	0.00%	0.00%	0.00%	0.00%	1.64%	0.55%	0.00%	0.00%	0.00%	0.00%	0.00%
XDN7545	Assawoman Bay	Asswoman Bay	1.22%	0.54%	0.00%	0.00%	0.00%	0.00%	0.62%	0.27%	0.00%	0.00%	0.00%	0.00%	0.00%
ASSA 1.	Sinepuxent Bay	Sinepuxent Bay	0.00%	0.00%	0.00%	0.00%	0.00%	0.00%	0.00%	0.00%	0.00%	0.00%	0.00%	0.00%	0.00%
ASSA 2.	Sinepuxent Bay	Sinepuxent Bay	0.00%	0.00%	0.00%	0.00%	0.00%	0.00%	0.00%	0.00%	0.00%	0.00%	0.00%	0.00%	0.00%
ASSA 3.	Newport Bay	Newport Bay	8.83%	4.89%	3.26%	0.27%	0.00%	5.43%	4.73%	2.47%	1.64%	0.14%	0.00%	3.22%	
ASSA 5.	Chincoteague Bay	Chincoteague Bay	4.48%	3.40%	1.49%	0.00%	0.00%	3.67%	2.26%	1.71%	0.75%	0.00%	0.00%	1.85%	
ASSA 6.	Chincoteague Bay	Chincoteague Bay	0.00%	0.00%	0.00%	0.00%	0.00%	0.00%	0.00%	0.00%	0.00%	0.00%	0.00%	0.00%	0.00%
ASSA 7.	Chincoteague Bay	Chincoteague Bay	8.15%	6.66%	3.40%	0.54%	0.00%	4.62%	4.79%	3.49%	1.71%	0.27%	0.00%	2.95%	
ASSA 8.	Chincoteague Bay	Chincoteague Bay	0.00%	0.00%	0.00%	0.00%	0.00%	0.00%	0.00%	0.00%	0.00%	0.00%	0.00%	0.00%	0.00%
ASSA 9.	Chincoteague Bay	Chincoteague Bay	0.00%	0.00%	0.00%	0.00%	0.00%	0.00%	0.00%	0.00%	0.00%	0.00%	0.00%	0.00%	0.00%
ASSA 11.	Chincoteague Bay	Chincoteague Bay	0.00%	0.00%	0.00%	0.00%	0.00%	0.00%	0.00%	0.00%	0.00%	0.00%	0.00%	0.00%	0.00%
ASSA 12.	Chincoteague Bay	Chincoteague Bay	0.00%	0.00%	0.00%	0.00%	0.00%	0.00%	0.00%	0.00%	0.00%	0.00%	0.00%	0.00%	0.00%
ASSA 13.	Chincoteague Bay	Chincoteague Bay	0.00%	0.00%	0.00%	0.00%	0.00%	0.00%	0.00%	0.00%	0.00%	0.00%	0.00%	0.00%	0.00%
ASSA 14.	Chincoteague Bay	Chincoteague Bay	3.53%	1.49%	0.00%	0.00%	0.00%	0.41%	1.78%	0.75%	0.00%	0.00%	0.00%	0.21%	
ASSA 15.	Chincoteague Bay	Chincoteague Bay	0.00%	0.00%	0.00%	0.00%	0.00%	0.00%	0.00%	0.00%	0.00%	0.00%	0.00%	0.00%	0.00%
ASSA 16.	Sinepuxent Bay	Sinepuxent Bay	0.00%	0.00%	0.00%	0.00%	0.00%	0.00%	0.00%	0.00%	0.00%	0.00%	0.00%	0.00%	0.00%
ASSA 17.	Sinepuxent Bay	Sinepuxent Bay	0.00%	0.00%	0.00%	0.00%	0.00%	0.00%	0.00%	0.00%	0.00%	0.00%	0.00%	0.00%	0.00%
ASSA 18.	Sinepuxent Bay	Sinepuxent Bay	0.00%	0.00%	0.00%	0.00%	0.00%	0.00%	0.00%	0.00%	0.00%	0.00%	0.00%	0.00%	0.00%

6.3 Final TMDL scenario for MD Coastal Bays – geographic isolation method

In the MCBs, different basins have different assimilation capacities and respond differently to the inputs of nutrient loading. Based on the incremental reduction studies in Section 6.1, it is apparent that an across-the-board 60% reduction is sufficient to bring all stations into attainment. On the other hand, many of the stations in different basins do not (or only slightly) exceed DO or chlorophyll-a endpoints; so they do not need (or only need minor) reductions. This geographic difference may be due to various factors such as in-stream transport, geographic location of the nutrient source, the estuarine transport, the residence time, different phytoplankton response, and variations in the nitrogen to phosphorus ratio. For example, upper reaches of the Saint Martin River in Isle of Wight Bay have the highest chlorophyll-a and lowest DO, because large nutrient loads are discharged into a narrow headstream of the river where there is very limited transport and dilution capacity leading, to high chlorophyll-a and low DO. In contrast, the areas close to the inlets have much larger transport and mixing leading to the lower chlorophyll-a and higher DO conditions. In determining final TMDL scenario for management action in the MCBs, it is necessary to consider incremental reductions in the context of these differing geographic characteristics. To determine the magnitude of the load reductions needed in six basins due to different variability in each of the basins, the “geographic isolation method” was used. The essence of geographic isolation reductions is to hold the target basin in MPAR and all other basin at calibration levels. In doing so, the spatial impact of loads on water quality was revealed. Based on the analysis, the stations in the headwater areas of the Saint Martin River require a significantly higher reduction (55%-58% or MPAR) than the other watersheds, followed by 40% reduction in the open water of the Isle of Wight Bay in order to achieve the DO criteria. This is mainly because Isle of Wight Bay has a relatively low assimilative capacity, especially in the headwater stream, the Saint Martin River.

Combining the incremental reduction, namely the base, 20%, 40%, and 60% with the geographic isolation reduction, it was determined that Assawoman Bay, Newport Bay and Chincoteague Bay require 20% reduction while Sinepuxent Bay requires no reduction. In the case of Chincoteague Bay, the final TMDL scenario entailed a 20% reduction applied to Maryland’s portion of the watershed, with assessment of attainment conducted at stations within Maryland’s waters. Final TMDL scenarios are shown in Table 6.4. For the final TMDL, the reductions in Bishopville Prong and Shingle Landing Prong used MPAR, which is approximately 55 – 58%. The resulting exceedances associated with the final TMDL are shown in Table 6.5. Under the final TMDL incorporating geographic isolation scenarios (TMDL-GI in the tables), the projected DO exceedance for all stations under growing season condition are under 1% except for Bishopville Prong and Shingle Landing Prong, which are 8.56% and 6.66 %, respectively. Under the average annual conditions, the exceedance is reduced to 4.32% and 3.36%, respectively. The model-simulated DO and chlorophyll-a concentration under the final TMDL are shown in Figures 6.3 (a) – (c) and Figures 6.4 (a)-(c). Both figures show the time series from January 2001-August 2005 for baseline versus final TMDL conditions over spatially distributed individual stations in the MCBs. The TMDL reduction clearly results in improving conditions and in meeting the water quality standards. The geographic isolation method combined with incremental reductions thus

provides a way to address temporal and spatial variation of loading capacity for achieving both DO and chlorophyll-a endpoints in the MCBs.

Table 6.4: Final TMDL reductions needed to meet WQS incorporating Geographic Isolation Scenarios.

Water Body/Water Quality Limited Segment	TMDL - IR	TMDL – GI
	(Incremental Reduction)	(Geographic Isolation)
	The incremental reductions needed to meet WQS using Incremental Reduction Scenarios	Final TMDL -- Reduction needed to meet WQS incorporating Geographic Isolation Scenarios
Sinepuxent Bay (All)	0%	0%
Newport Bay (All)	20%	20%
Bishopville Prong/Shingle Landing Prong	60%	MPAR (55-58%)
Assawoman Bay (Open Waters)	20%	20%
Isle of Wight Bay (All areas except those identified above)	40%	40%
Chincoteague Bay (Maryland portion only)	20%	20%

Table 6.5: DO exceedance rates for TMDL IR (Incremental Reduction) and final TMDL (TMDL GI, incorporating Geographic Isolation Scenario).

Station	TMDL-basin	MD-8digit-basin	Percent DO less than 5mg/l			Percent DO less than 5mg/l		
			Growing Season (2001-2004)			Average Annual (2001-2004)		
			Base	TMDL IR (Increment Reduction)	TMDL GI (Geographic Isolation)	Base	TMDL IR (Increment Reduction)	TMDL GI (Geographic Isolation)
BSH0008	Bishopville Prong	Isle of Wight Bay	15.49%	0.41%	0.00%	7.81%	0.21%	0.00%
MKL0010	Manklin Creek	Isle of Wight Bay	78.26%	0.00%	0.27%	39.45%	0.00%	0.14%
SPR0002	Shingle Landing Prong	Isle of Wight Bay	1.36%	0.00%	0.00%	0.68%	0.00%	0.00%
SPR0009	Shingle Landing Prong	Isle of Wight Bay	15.76%	1.77%	6.66%	7.95%	0.89%	3.36%
TUV0011	Turville Creek	Isle of Wight Bay	0.00%	0.00%	0.00%	0.00%	0.00%	0.00%
TUV0019	Turville Creek	Isle of Wight Bay	0.00%	0.00%	0.00%	0.00%	0.00%	0.00%
XBM1301	Chincoteague Bay	Chincoteague Bay	0.00%	0.00%	0.00%	0.00%	0.00%	0.00%
XBM3418	Chincoteague Bay	Chincoteague Bay	0.00%	0.00%	0.00%	0.00%	0.00%	0.00%
XBM5932	Chincoteague Bay	Chincoteague Bay	0.00%	0.00%	0.00%	0.00%	0.00%	0.00%
XBM8149	Chincoteague Bay	Chincoteague Bay	0.00%	0.00%	0.00%	0.00%	0.00%	0.00%
XCM0159	Chincoteague Bay	Chincoteague Bay	0.00%	0.00%	0.00%	0.00%	0.00%	0.00%
XCM1562	Chincoteague Bay	Chincoteague Bay	0.00%	0.00%	0.00%	0.00%	0.00%	0.00%
XCM4878	Newport Bay	Newport Bay	1.77%	0.00%	0.00%	0.89%	0.00%	0.00%
XDM4486	Bishopville Prong	Isle of Wight Bay	37.09%	2.72%	8.56%	18.70%	1.37%	4.32%
XDN0146	Isle of Wight Bay	Isle of Wight Bay	0.00%	0.00%	0.00%	0.00%	0.00%	0.00%
XDN2340	Isle of Wight Bay	Isle of Wight Bay	0.00%	0.00%	0.00%	0.00%	0.00%	0.00%
XDN2438	Isle of Wight Bay	Isle of Wight Bay	0.00%	0.00%	0.00%	0.00%	0.00%	0.00%
XDN3445	Assawoman Bay	Asswaman Bay	0.00%	0.00%	0.00%	0.00%	0.00%	0.00%
XDN3724	St. Martin River	Isle of Wight Bay	0.00%	0.00%	0.00%	0.00%	0.00%	0.00%
XDN4312	St. Martin River	Isle of Wight Bay	0.00%	0.00%	0.00%	0.00%	0.00%	0.00%
XDN4797	St. Martin River	Isle of Wight Bay	1.63%	0.00%	0.00%	0.82%	0.00%	0.00%
XDN4851	Assawoman Bay	Asswaman Bay	0.00%	0.00%	0.00%	0.00%	0.00%	0.00%
XDN5737	Assawoman Bay	Asswaman Bay	0.00%	0.00%	0.00%	0.00%	0.00%	0.00%
XDN6454	Assawoman Bay	Asswaman Bay	0.00%	0.00%	0.00%	0.00%	0.00%	0.00%
XDN7261	Assawoman Bay	Asswaman Bay	0.00%	0.00%	0.00%	0.00%	0.00%	0.00%
XDN7545	Assawoman Bay	Asswaman Bay	0.00%	0.00%	0.00%	0.00%	0.00%	0.00%
AYR0017	Ayer Creek	Newport Bay	5.98%	0.00%	0.00%	3.01%	0.00%	0.00%
ASSA 1.	Sinepuxent Bay	Sinepuxent Bay	0.00%	0.00%	0.00%	0.00%	0.00%	0.00%
ASSA 2.	Sinepuxent Bay	Sinepuxent Bay	0.00%	0.00%	0.00%	0.00%	0.00%	0.00%
ASSA 3.	Newport Bay	Newport Bay	0.00%	0.00%	0.00%	0.00%	0.00%	0.00%
ASSA 4.	Newport Bay	Newport Bay	2.58%	0.00%	0.00%	1.30%	0.00%	0.00%
ASSA 5.	Chincoteague Bay	Chincoteague Bay	0.00%	0.00%	0.00%	0.00%	0.00%	0.00%
ASSA 6.	Chincoteague Bay	Chincoteague Bay	0.00%	0.00%	0.00%	0.00%	0.00%	0.00%
ASSA 7.	Chincoteague Bay	Chincoteague Bay	0.00%	0.00%	0.00%	0.00%	0.00%	0.00%
ASSA 8.	Chincoteague Bay	Chincoteague Bay	0.00%	0.00%	0.00%	0.00%	0.00%	0.00%
ASSA 9.	Chincoteague Bay	Chincoteague Bay	0.00%	0.00%	0.00%	0.00%	0.00%	0.00%
ASSA 10.	Chincoteague Bay	Chincoteague Bay	0.00%	0.00%	0.00%	0.00%	0.00%	0.00%
ASSA 11.	Chincoteague Bay	Chincoteague Bay	0.00%	0.00%	0.00%	0.00%	0.00%	0.00%
ASSA 12.	Chincoteague Bay	Chincoteague Bay	0.00%	0.00%	0.00%	0.00%	0.00%	0.00%
ASSA 13.	Chincoteague Bay	Chincoteague Bay	0.00%	0.00%	0.00%	0.00%	0.00%	0.00%
ASSA 14.	Chincoteague Bay	Chincoteague Bay	0.00%	0.00%	0.00%	0.00%	0.00%	0.00%
ASSA 15.	Chincoteague Bay	Chincoteague Bay	0.00%	0.00%	0.00%	0.00%	0.00%	0.00%
ASSA 16.	Sinepuxent Bay	Sinepuxent Bay	0.00%	0.00%	0.00%	0.00%	0.00%	0.00%
ASSA 17.	Sinepuxent Bay	Sinepuxent Bay	0.00%	0.00%	0.00%	0.00%	0.00%	0.00%
ASSA 18.	Sinepuxent Bay	Sinepuxent Bay	0.00%	0.00%	0.00%	0.00%	0.00%	0.00%

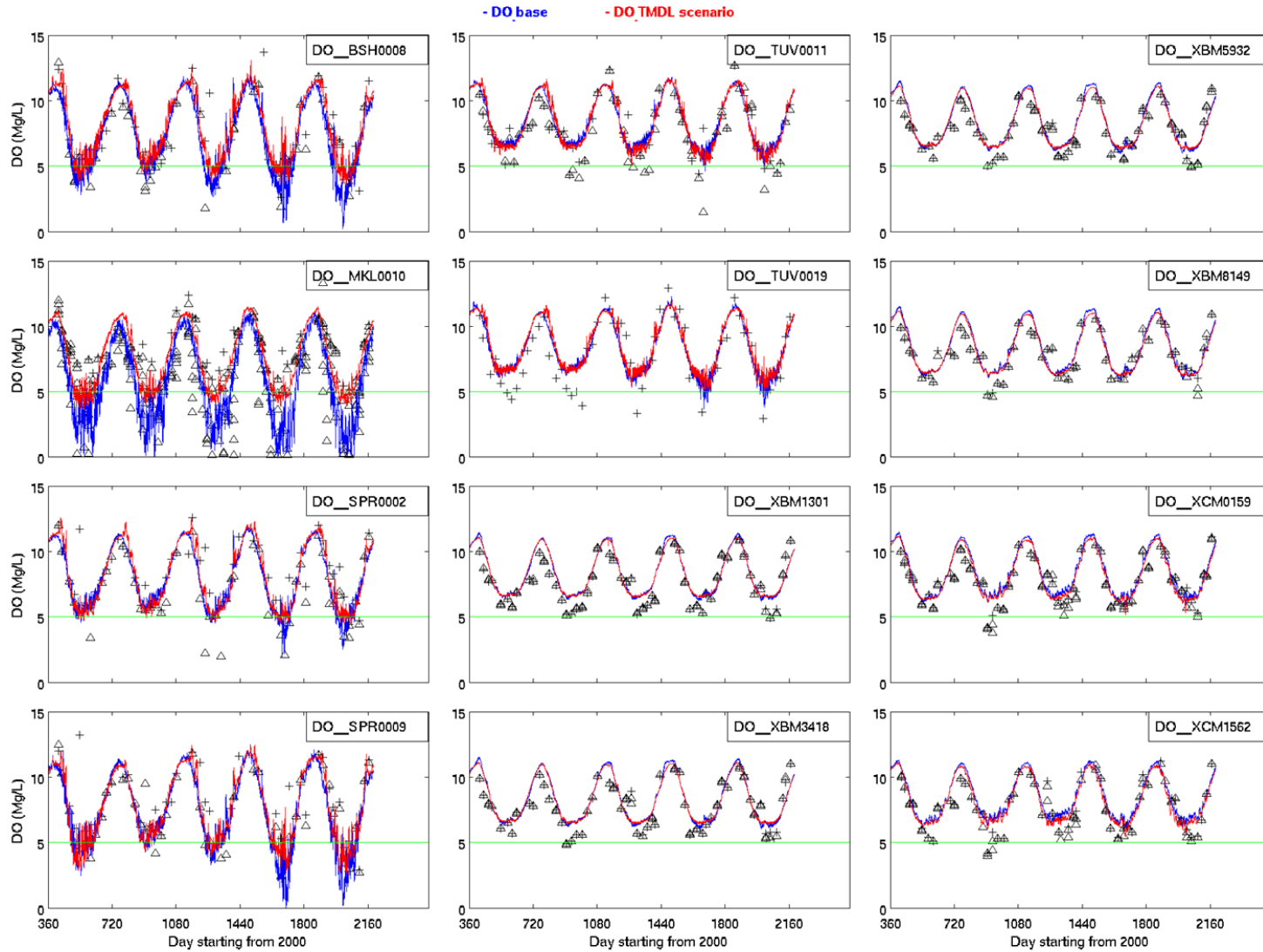


Figure 6.3 (a): DO time series, 2001-August 2005, baseline conditions (blue), final TMDL (red) and observed (symbol) at DNR Stations 1 -12.

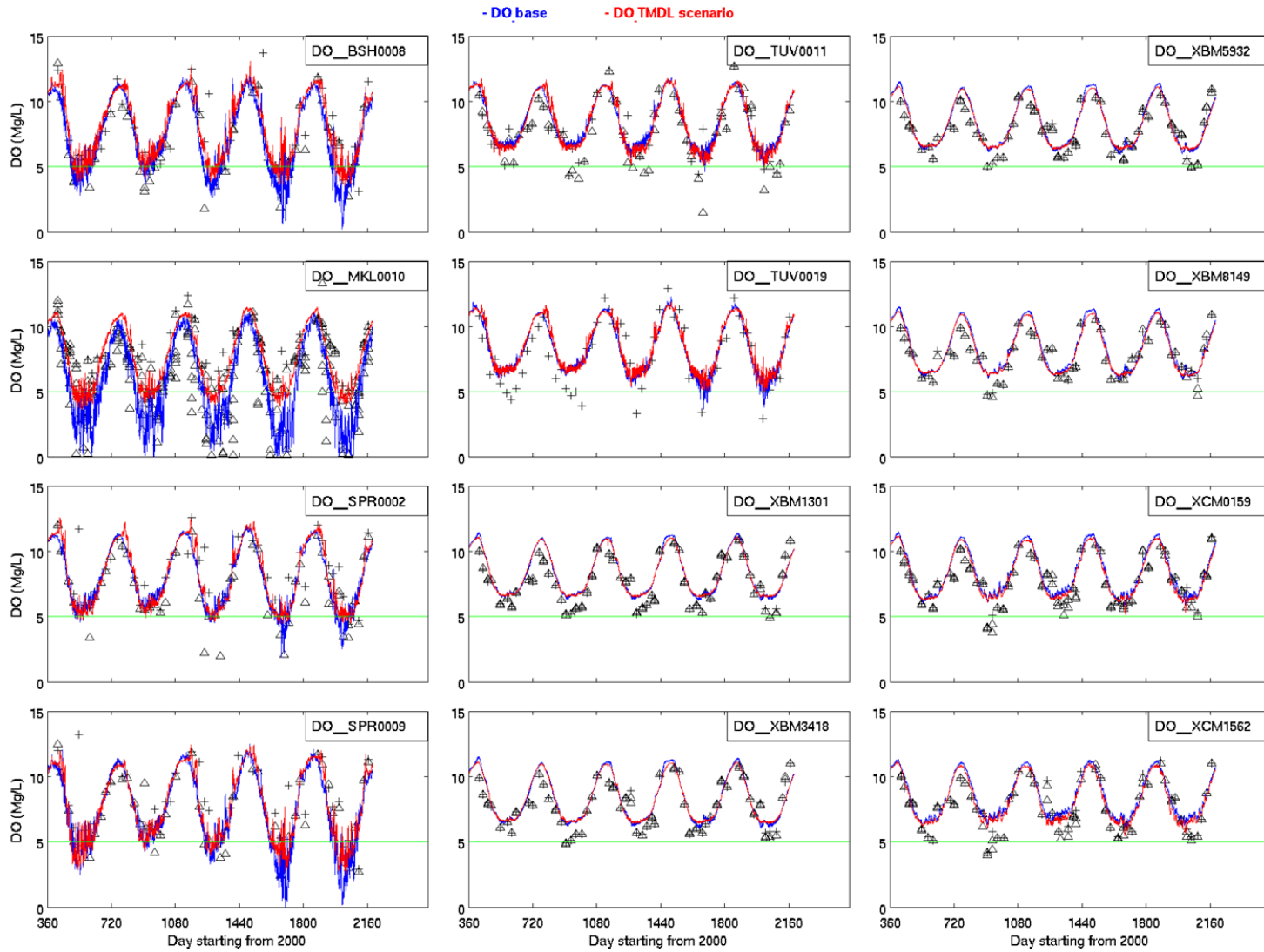


Figure 6.3 (b): DO time series, 2001-August 2005, baseline conditions (blue), final TMDL (red) and observed (symbol) at DNR Stations 13 -24.

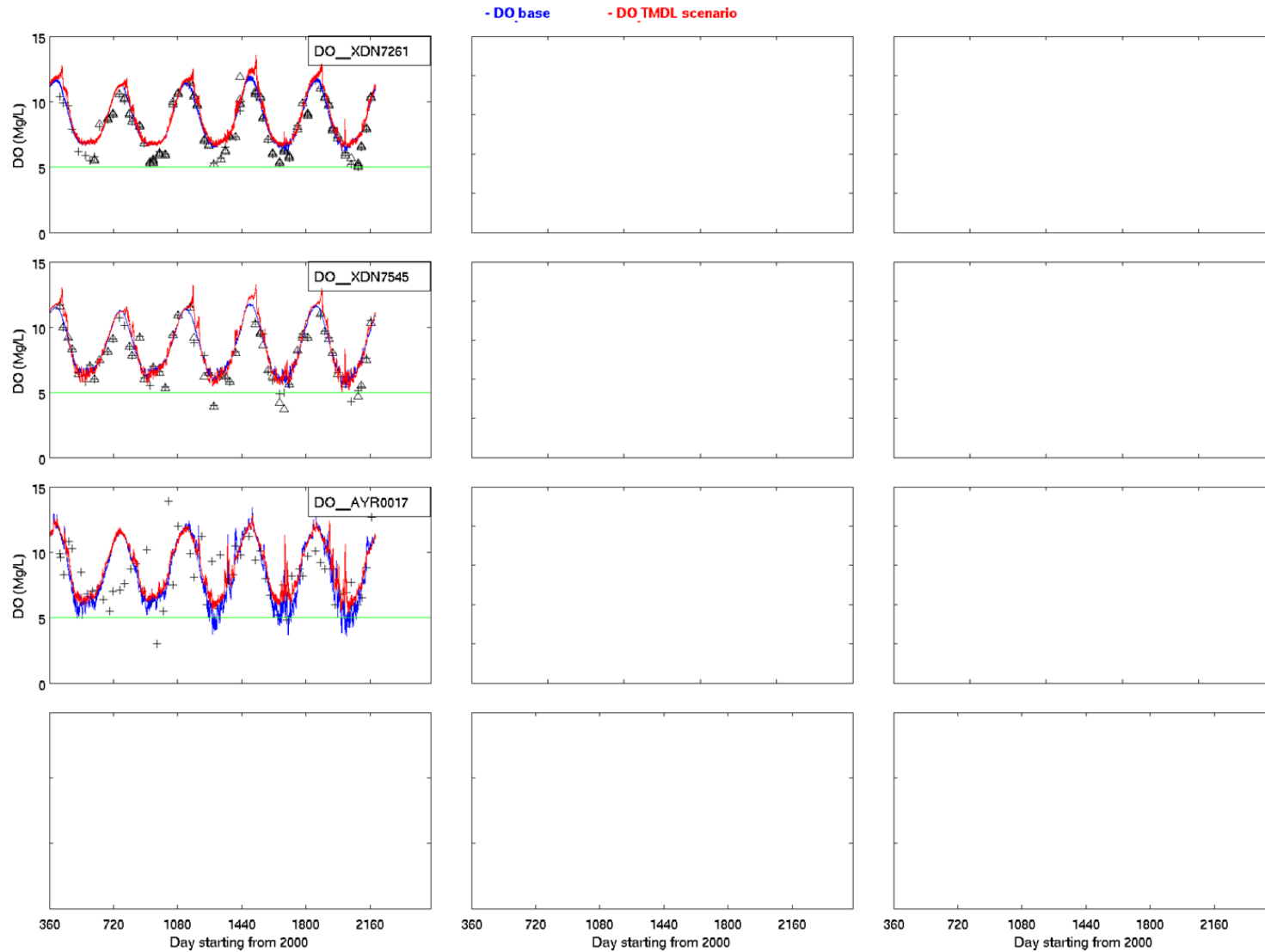


Figure 6.3 (c): DO time series, 2001-August 2005, baseline conditions (blue), final TMDL (red) and observed (symbol) at DNR Stations 25-27.

Table 6.6(a): Chla greater than 50 ug/l exceedance rates for TMDL IR (Incremental Reduction) and final TMDL (TMDL GI, incorporating Geographic Isolation Scenario).

Station	TMDL-basin	MD-8digit-basin	Percent Chla greater than 50 ug/l			Percent Chla greater than 50 ug/l		
			Growing Season (2001-2004)			Average Annual (2001-2004)		
			Base	TMDL IR	TMDL GI	Base	TMDL IR	TMDL GI
			(Increment	(Geographic		(Increment	(Geographic	
			Reduction)	Isolation)		Reduction)	Isolation)	
BSH0008	Bishopville Prong	Isle of Wight Bay	19.43%	3.40%	3.40%	10.00%	1.71%	1.71%
MKL0010	Manklin Creek	Isle of Wight Bay	2.45%	0.00%	0.00%	1.23%	0.00%	0.00%
SPR0002	Shingle Landing Prong	Isle of Wight Bay	5.57%	0.82%	0.82%	2.81%	0.41%	0.41%
SPR0009	Shingle Landing Prong	Isle of Wight Bay	6.66%	3.40%	3.40%	3.36%	1.71%	1.71%
TUV0011	Turville Creek	Isle of Wight Bay	0.54%	0.00%	0.00%	0.27%	0.00%	0.00%
TUV0019	Turville Creek	Isle of Wight Bay	1.36%	0.00%	0.00%	0.68%	0.00%	0.00%
XBM3418	Chincoteague Bay	Chincoteague Bay	0.00%	0.00%	0.00%	0.00%	0.00%	0.00%
XBM5932	Chincoteague Bay	Chincoteague Bay	0.00%	0.00%	0.00%	0.00%	0.00%	0.00%
XCM1562	Chincoteague Bay	Chincoteague Bay	0.00%	0.00%	0.00%	0.00%	0.00%	0.00%
XCM4878	Newport Bay	Newport Bay	0.00%	0.00%	0.00%	0.00%	0.00%	0.00%
XDM4486	Bishopville Prong	Isle of Wight Bay	38.59%	5.57%	5.57%	19.66%	2.81%	2.81%
XDN3724	St. Martin River	Isle of Wight Bay	1.36%	0.00%	0.00%	0.68%	0.00%	0.00%
XDN4312	St. Martin River	Isle of Wight Bay	2.72%	0.00%	0.00%	1.37%	0.00%	0.00%
XDN4797	St. Martin River	Isle of Wight Bay	5.98%	0.95%	0.95%	3.01%	0.48%	0.48%
XDN5737	Assawoman Bay	Asswoman Bay	0.00%	0.00%	0.00%	0.00%	0.00%	0.00%
AYR0017	Ayer Creek	Newport Bay	0.14%	0.14%	0.14%	0.07%	0.07%	0.07%
ASSA 4.	Newport Bay	Newport Bay	0.00%	0.00%	0.00%	0.00%	0.00%	0.00%
ASSA 10.	Chincoteague Bay	Chincoteague Bay	0.00%	0.00%	0.00%	0.00%	0.00%	0.00%

Table 6.6(b): Chla greater than 15 ug/l exceedance rates for TMDL IR (Incremental Reduction) and final TMDL (TMDL GI, incorporating Geographic Isolation Scenario).

Station	TMDL-basin	MD-8digit-basin	Percent Chla greater than 15 ug/l			Percent Chla greater than 15 ug/l		
			Growing Season (2001-2004)			Average Annual (2001-2004)		
			Base	TMDL IR (Increment Reduction)	TMDL GI (Geographic Isolation)	Base	TMDL IR (Increment Reduction)	TMDL GI (Geographic Isolation)
XBM1301	Chincoteague Bay	Chincoteague Bay	0.00%	0.00%	0.00%	0.00%	0.00%	0.00%
XBM8149	Chincoteague Bay	Chincoteague Bay	2.31%	0.00%	0.00%	1.16%	0.00%	0.00%
XCM0159	Chincoteague Bay	Chincoteague Bay	2.85%	0.00%	0.00%	1.44%	0.00%	0.00%
XDN0146	Isle of Wight Bay	Isle of Wight Bay	0.00%	0.00%	0.00%	0.00%	0.00%	0.00%
XDN2340	Isle of Wight Bay	Isle of Wight Bay	4.21%	1.22%	1.22%	2.12%	0.62%	0.62%
XDN2438	Isle of Wight Bay	Isle of Wight Bay	0.00%	0.00%	0.00%	0.00%	0.00%	0.00%
XDN3445	Assawoman Bay	Asswoman Bay	3.94%	0.00%	0.00%	1.99%	0.00%	0.00%
XDN4851	Assawoman Bay	Asswoman Bay	4.48%	1.36%	1.36%	2.26%	0.68%	0.68%
XDN6454	Assawoman Bay	Asswoman Bay	2.99%	1.22%	1.22%	1.51%	0.62%	0.62%
XDN7261	Assawoman Bay	Asswoman Bay	3.26%	3.13%	3.13%	1.64%	1.58%	1.58%
XDN7545	Assawoman Bay	Asswoman Bay	1.22%	5.03%	5.03%	0.62%	2.74%	2.74%
ASSA 1.	Sinepuxent Bay	Sinepuxent Bay	0.00%	0.00%	0.00%	0.00%	0.00%	0.00%
ASSA 2.	Sinepuxent Bay	Sinepuxent Bay	0.00%	0.00%	0.00%	0.00%	0.00%	0.00%
ASSA 3.	Newport Bay	Newport Bay	8.83%	4.62%	4.62%	4.73%	2.74%	2.74%
ASSA 5.	Chincoteague Bay	Chincoteague Bay	4.48%	0.00%	0.00%	2.26%	0.00%	0.00%
ASSA 6.	Chincoteague Bay	Chincoteague Bay	0.00%	0.00%	0.00%	0.00%	0.00%	0.00%
ASSA 7.	Chincoteague Bay	Chincoteague Bay	8.15%	0.14%	0.14%	4.79%	0.07%	0.07%
ASSA 8.	Chincoteague Bay	Chincoteague Bay	0.00%	0.00%	0.00%	0.00%	0.00%	0.00%
ASSA 9.	Chincoteague Bay	Chincoteague Bay	0.00%	0.00%	0.00%	0.00%	0.00%	0.00%
ASSA 11.	Chincoteague Bay	Chincoteague Bay	0.00%	0.00%	0.00%	0.00%	0.00%	0.00%
ASSA 12.	Chincoteague Bay	Chincoteague Bay	0.00%	0.00%	0.00%	0.00%	0.00%	0.00%
ASSA 13.	Chincoteague Bay	Chincoteague Bay	0.00%	0.00%	0.00%	0.00%	0.00%	0.00%
ASSA 14.	Chincoteague Bay	Chincoteague Bay	3.53%	0.00%	0.00%	1.78%	0.00%	0.00%
ASSA 15.	Chincoteague Bay	Chincoteague Bay	0.00%	0.00%	0.00%	0.00%	0.00%	0.00%
ASSA 16.	Sinepuxent Bay	Sinepuxent Bay	0.00%	0.00%	0.00%	0.00%	0.00%	0.00%
ASSA 17.	Sinepuxent Bay	Sinepuxent Bay	0.00%	0.00%	0.00%	0.00%	0.00%	0.00%
ASSA 18.	Sinepuxent Bay	Sinepuxent Bay	0.00%	0.00%	0.00%	0.00%	0.00%	0.00%

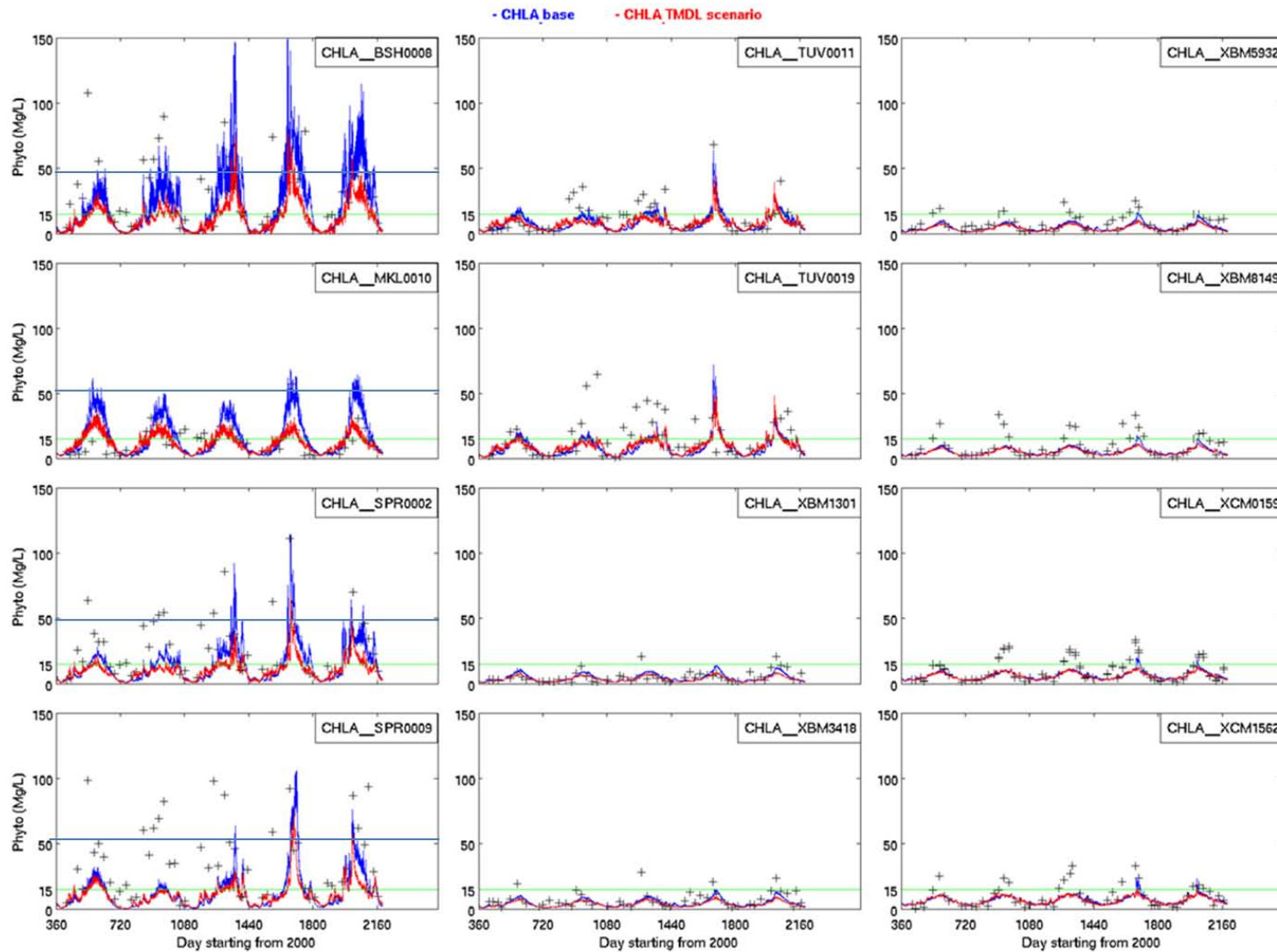


Figure 6.4 (a): Chlorophyll-a time series, 2001-August 2005, baseline conditions (blue), final TMDL (red) and observed (symbol) at DNR Stations 1-12.

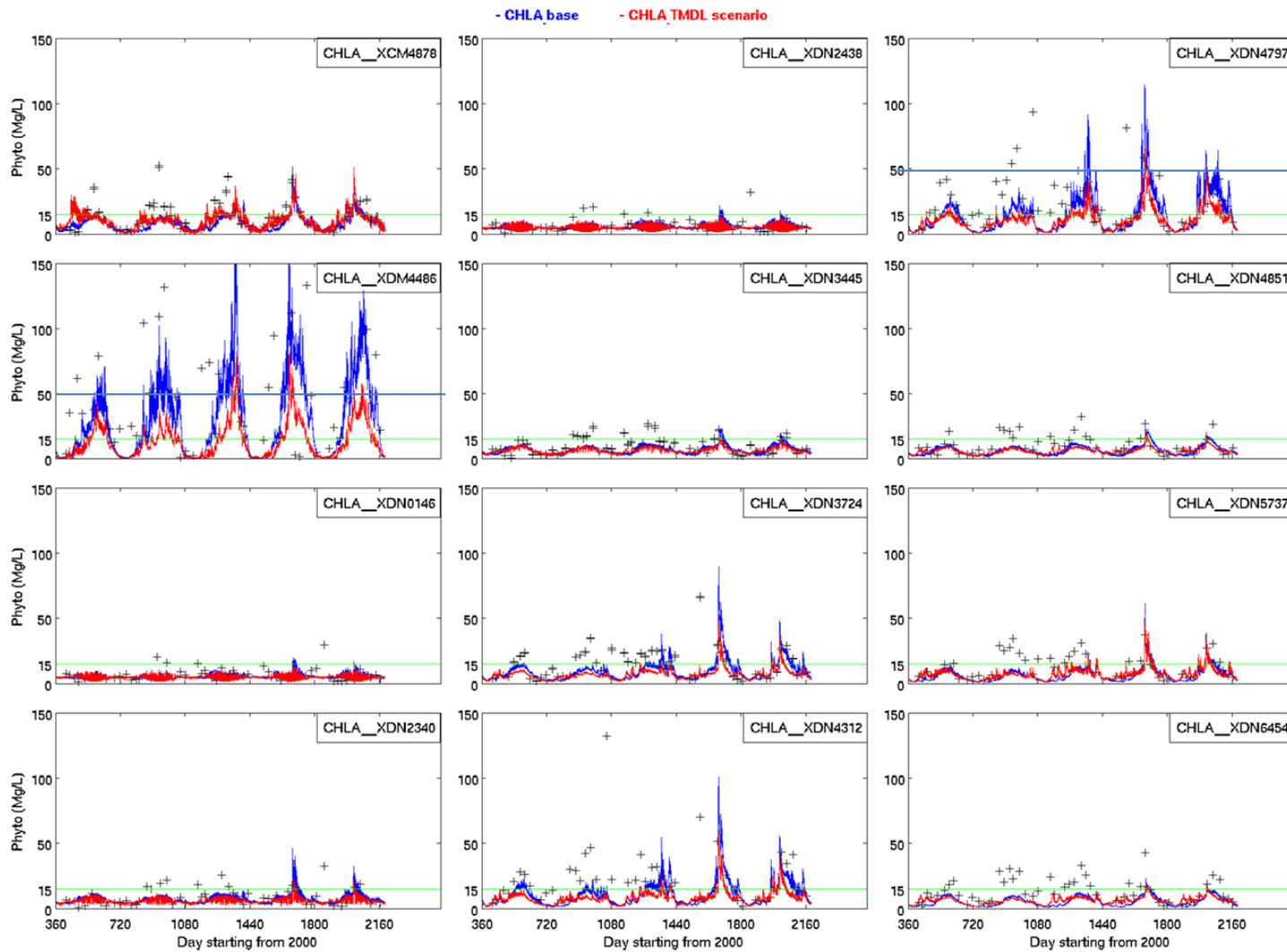


Figure 6.4 (b): Chlorophyll-a time series, 2001-August 2005, baseline conditions (blue), final TMDL (red) and observed (symbol) at DNR Stations 13-24.

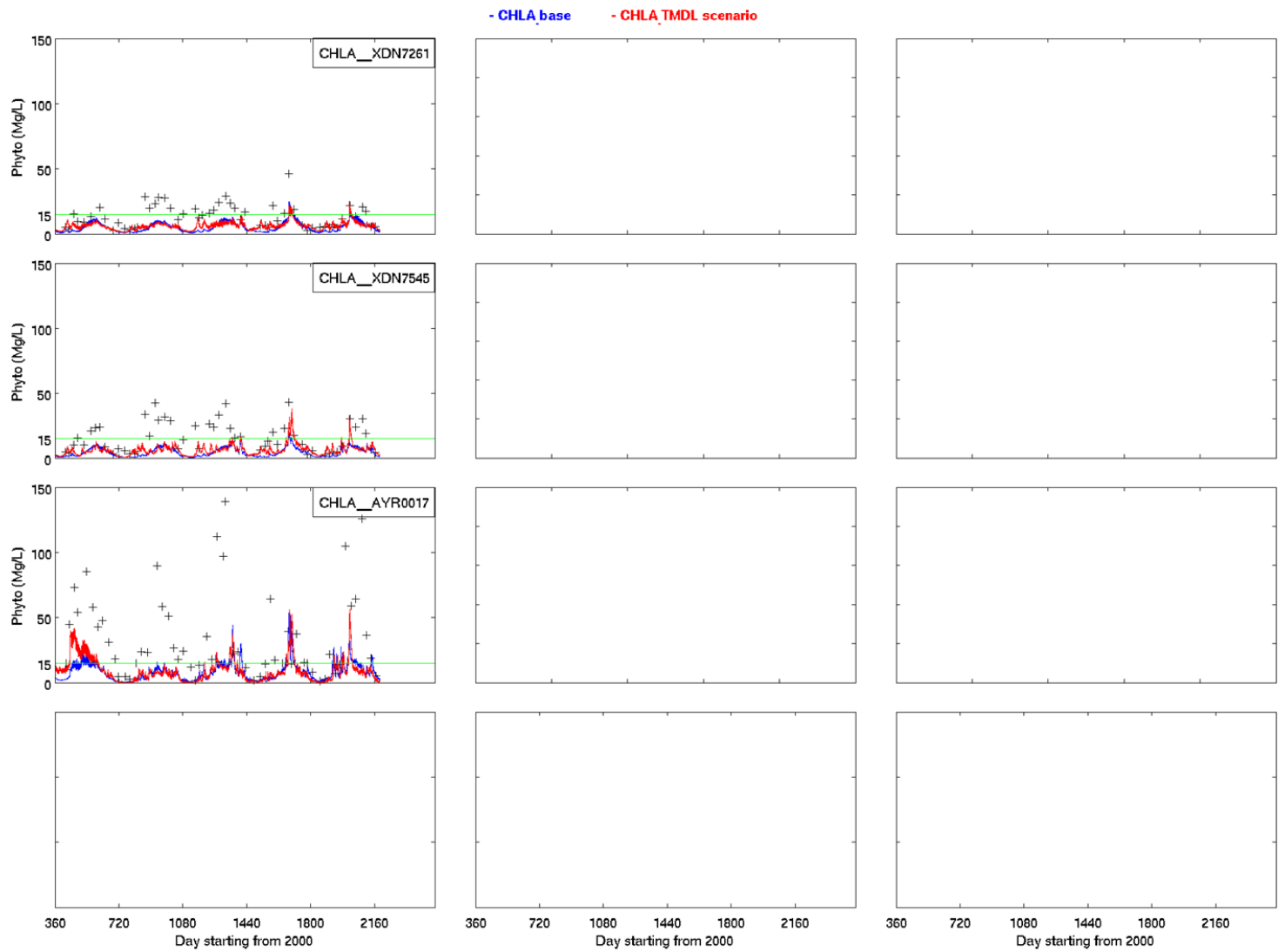


Figure 6.4 (c): Chlorophyll-a time series, 2001-August 2005, baseline conditions (blue), final TMDL (red) and observed (symbol) at DNR Stations 25-27.

CHAPTER 7: DISCUSSION AND CONCLUSION

The MCBs are subject to anthropogenic impacts from the agricultural practices and expanding population in the coastal watersheds. As a result, the individual bays are showing signs of increasing eutrophication. In particular, the hypoxic conditions in the tributaries pose the most serious threat to the long-term health and function of the bays. As a component of developing the MCB TMDLs, a HEM3D (Hydrodynamic Eutrophication Model) was developed, consisting of a hydrodynamic model SELFE (Semi-implicit, Eulerian-Lagrangian Finite Element model), a water quality model ICM (Integral Compartment Model), and a sediment benthic flux model. The HEM3D was coupled with an HSPF watershed model to simulate water quality transport and biochemical ecosystem processes in the MCBs.

In terms of nutrient loading generated by the HSPF watershed model, the non-point source and atmospheric loads dominate the total loads with point-source loads comprising only a small portion. Based on the areal loading rate defined as the total loading divided by the total water surface area, it is clear that the Isle of Wight sub-watershed has the largest TN and TP unit loads (per water surface water area), followed by Newport Bay, Assawoman Bay, Sinepuxent and Chincoteague Bays. The relatively larger drainage areas lead to the greater non-point source loads, causing the receiving waterbody to be vulnerable to eutrophication problems. By contrast, waterbodies with relatively smaller drainage areas receive correspondingly less non-point source loading, and are less susceptible to eutrophication problems. Each component of the HEM3D is calibrated and verified with field measured data collected in the MCBs. The hydrodynamic model was calibrated with astronomical tide, the measured water level, the intensive ADCP current velocities (measurement conducted in 2004), and salinity observations across MCB stations. Although the total freshwater discharge in the MCBs system is small as compared to other systems (for example, the Chesapeake Bay), episodic rainfall events can still have substantial impacts on the runoff and salinity distribution in the creeks and tributaries. The model captured the large rainfall-induced salinity variability as large as 10-20 ppt. For the water quality model calibration, the chlorophyll-a, dissolved oxygen, ammonia, nitrite and nitrate, phosphate and DON data compared well with the model result over a transect in the Isle of Wight Bay. For validation, this analysis was extended throughout the MCBs, and comparison with data at all 27 DNR and 18 ASIS stations yielding reasonable results with satisfactory skill scores.

It should be noted that a stand-alone macroalgae sub-model in the MCBs has been developed (Wang, Taiping, 2009). The model includes two macroalgae species, *Ulva lactuca* and *Gracilaria vermiculophylla*, and the Droop formulation was used to account for the luxury uptake. Using a vertical one-dimensional box model, the well-known boom-and-bust life cycle of macroalgae was qualitatively simulated. The macroalgae sub-model, however, was used primarily in a research capacity; it was not included in the current TMDL, for with the current technology, a thorough understanding of the macroalgae life cycle is still lacking. For example, little is known about a suite of factors contributing to the boom-and-bust life cycle, the fate of the macroalgae biomass after

the bust, and the species interaction of macroalgae with other phytoplankton species. These gaps in knowledge about macroalgae hampered the ability of the model to formulate a proper relationship between phosphorus and nitrogen loading to the macroalgae sub-model, and hence the model was not implemented in this study. However, the micro-algae, a single-celled 'plant-like' organism was included by imbedding it in the benthic sediment flux model which acted as proxies for macrobenthos. As a result, some effects of the macroalgae, such as its interaction with the overlying water column, are partially simulated.

After the calibration and verification of the HEM3D model, additional modeling analyses were conducted to substantiate the effect of diel DO cycle and perform the sensitivity analysis in the MCBs. First, the daily mean DO (from HEM3D) was adjusted to incorporate diel oscillation based on the work of Elgin Perry (2012). The empirical corrections were made based on monthly temperature, daily temperature, daily Photosynthetically Active Radiation (PAR), and daily chlorophyll. In doing so, the DO variation includes the diel oscillation, providing a better representation of the full spectrum of DO in the MCBs. Secondly, sensitivity analyses were conducted to test the effects of (a) the Ocean City wastewater treatment plant outfall, (b) phytoplankton and organic nutrient settling rate and (c) ground water discharge so their potential effects are checked and measured.

For the TMDL scenario development, the target is such that the daily mean DO concentration everywhere shall not be below 5 mg/l more than 10 percent of the time, both annually and during the growing season (May 1 – October 31). The TN and TP sources were assessed for the five impaired basins in the MCBs. It was found that for Assawoman, Isle of Wight, and Newport Bays, the terrestrial sources are the dominant source of loading, whereas in the Sinepuxent and Chincoteague Bays the terrestrial source loading are about equal to that of atmospheric loading. To further determine the assimilative capacity of the MCBs for nutrients, incremental reductions of 20%, 40%, 60%, natural conditions and MPAR (Maximum Practicable Anthropogenic Reduction) of the total loading were conducted. It was revealed that there is a large difference in the response from the different basins given the similar amount of reduction. In the end, the final TMDL scenario was determined by the geographic isolation method to reflect the relative impact of source sectors from different basin in the Maryland Coastal Bays to meet the TMDL endpoints. A spatial pattern emerges that Bishopville Prong of the Upper Saint Martin River watershed requires the most reduction (55-60%) followed by the other areas of the Isle of Wight Bay watershed (40%). Assawoman Bay, Newport Bay and Chincoteague Bay only require only a 20% reduction to meet the water quality targets. It was determined that Sinepuxent Bay does not require a reduction from the baseline loading in order to meet the water quality endpoints.

Acknowledgements:

The work was supported by Maryland Department of the Environment TMDL Technical Development Program. The water quality data was provided by Maryland Coastal Bay Program, Maryland Department of Natural Resources, and Assateague Island National Seashore, US National Park Services. Additionally, Maryland Geological Survey provided the assistance on processing the shoreline erosion data and University of Maryland Horn Point Laboratory the ADCP data. During the course of the project, we appreciated the valuable inputs and comments by the members of the Maryland Coastal Bays Program Scientific and Technical Advisory Committee (STAC). Lastly, but not least, the authors are grateful to Ms. Rou Shi, Ms. Melissa Chatham and Mr. Tim Rule for their technical guidance and project development.

REFERENCES

- Allan, Thomas R., H. T. Tolvanen, G. F. Oertel, and G. M. McLeod (2007): Spatial characterization of environmental gradients in a coastal lagoon. Chincoteague Bay. *Estuaries and Coasts*, Vol. 30. No.6, pp. 959-977.
- Ambrose, R. B., T. A. Wool, and J. L. Martin (1992): The water quality Analysis and Simulation Program, WASP5; Part A, Model Documentation. US EPA Athens, Environmental Research Laboratory, 2010 pp.
- Azevedo, A., Oliveira, A., Fortunato, A.B. and Bertin, X. (2009): Application of an Eulerian-Lagrangian oil spill modeling system to the Prestige accident: trajectory analysis. *J. Coastal Res.*, SI 56, 777-781.
- Banks, R.B. & Herrera, F.F. (1977): Effect of wind and rain on surface reaeration. *J. of the Environmental Engineering Division, ASCE*, 103(EE3): 489-504.
- Bertin, X., N. Bruneau, J.-F. Breilh, A.B. Fortunato, and M. Karpytchev (2012): Importance of wave age and resonance in storm surges: The case Xynthia, Bay of Biscay, *Ocean Modelling*, 42(0), 16-30.
- Blumberg, A.F. and G.L. Mellor (1987): A description of a three-dimensional coastal ocean circulation model. In: *Three-Dimensional Coastal Ocean Models*, vol. 4, Coastal and Estuarine Studies, N. Heaps, editor, Washington, D.C.: AGU, pp. 1-16.
- Boynton, W. R. (1996): A comparative analysis of eutrophication patterns in a temperate coastal lagoon. *Estuaries*, Vol. 10, No. 2B, p408-421.
- Brovchenko I., V. Maderich, and K. Terletska (2011): Numerical simulations of 3D structure of currents in the region of deep canyons on the east coast of the Black Sea. *International Journal for Computational Civil and Structural Engineering*, 7 (2): 47-53.
- Canuto, V.M., A. Howard, Y. Cheng and M.S. Dubovikov (2001): Ocean turbulence I: one-point closure model. Momentum and heat vertical diffusivities. *J. Phys. Ocean.*, 31, pp. 1413-1426.
- Casulli, V. and P. Zanolli (2005): High resolution methods for multidimensional advection-diffusion problems in free-surface hydrodynamics. *Ocean Modelling*, 10, pp.137-151.
- Casulli, V. and E. Cattani (1994): Stability, accuracy and efficiency of a semi-implicit method for 3D shallow water flow. *Computers & Mathematics with Applications*, 27, pp. 99-112.

- Cerco, C. F. and Mark Noel (2004): The 2002 Chesapeake Bay eutrophication model . Contract report EPA-903-R-04-004 to Chesapeake Bay Program Office, US Environmental Protection Agency, 410 Severn Avenue, Annapolis, MD 21401, administrated by the Baltimore District, US Army Corps of Engineers.
- Cerco, C. F. and T. Cole (1994): Three-dimensional eutrophication model of Chesapeake Bay/ Volume 1: Main report. Technical report EL-94-4, U. S. Army Corps of Engineers, Waterways Experiment Stations, Vicksburg, MS.
- Cerco, C. F. B Bunch, A. Teeter, and M. Dortch (2000): Water quality model of Florida Bay: Technical report ERDC/EL-00-10, U. S. Army Corps of Engineers, Waterways Experiment Stations, Vicksburg, MS.
- Collins, C. D. and J. H. Wlosinski (1983): Coefficients for Use in the U.S. Army Corps of Engineers Reservoir Model, CE-QUAL-R1. Tech. Rept. E-83-15, Environmental Laboratory, U.S. Army Engineer Waterways Experiment Station, Vicksburg, MS.
- Cornwell, J. and M. Owens (2013): Benthic nutrient cycling at the coastal bays land-sea interface: investigation of ammonium sources. Maryland Coastal Bay STAC meeting presentation, January, 2013.
- Dennison, W. C. J. E. Thomas, C. J. Cain, T, U. B. Carruthers, M. R. Hall, R. V. Jesien, C. E. Wazniak, D. E. Wilson (2009): Shifting Sands, Environmental and cultural change in Maryland's coastal Bays. pp396, IAN press, University of Maryland, Center for Environmental Science.
- Di Toro, D. M. (2001): Sediment flux modeling. John Wiley and Sons, Inc. New York. pp624.
- Di Toro, D. M. and J. Fitzpatrick (1993): Chesapeake Bay sediment flux model. Contract report EL-93-2, U. S. Army Corps of Engineers, Waterways Experiment Stations, Vicksburg, MS.
- Dillow, J.J.A. and E.A. Greene (1999): Groundwater Discharge and Nitrate Loadings to the Coastal Bays of Maryland. U.S. Geological Survey Water-Resources Investigations Report 99-4167.
- Department of Natural Resources (2004): State of the Maryland Coastal Bays. Maryland Department of Natural Resources, Maryland Coastal Bays Program, C. E. Wazniak, C., M. Hall, C. Cain, D. Wilson, R., Jesien, J. Thomas, T. Carruthers, W. Dennison. 2004. and University of Maryland Center for Environmental Science.
<http://dnrweb.dnr.state.md.us/pressroom/MCB.pdf>
- EPA Chesapeake Bay Program (2009): Bay barometer: A health and restoration assessment of the Chesapeake Bay and watershed in 2008. Chesapeake Bay Program report TRS 293-09: US EPA-903-R-09-001, March 2009.

- Fertig, B. M, J. O'Neil , K. A. Beckert , C. J. Cain, D. M. Needham, T. J. B. Carruthers, W. C. Dennison WC (2013): Elucidating terrestrial nutrient sources to a coastal lagoon, Chincoteague Bay, Maryland, USA. *Estuarine, Coast. Shelf Sci.* 116:1–10.
- Flather, R.A. (1987): A tidal model of Northeast Pacific. *Atmosphere–Ocean*. Vol. 25, 22–45.
- Fortunato, A.B. and A.M. Baptista (1996): Evaluation of Horizontal Gradients in Sigma-Coordinate Shallow Water Models. *Atmosphere-Ocean*, 34, pp. 489-514.
- Galperin, B., L. H. Kantha, S. Hassid and A. Rosati (1988): A quasi-equilibrium turbulent energy model for geophysical flows. *J. Atmos. Sci.*, 45, pp. 55-62.
- Ham, D.A., J. Pietrzak, J. and G.S. Stelling (2005): A scalable unstructured grid 3-dimensional finite volume model for the shallow water equations. *Ocean Modelling*, 10, pp. 153-169.
- HydroQual (1995): A water quality model for Massachusetts and Cape Cod Bays: Calibration of the Bays eutrophication model (BEM). Technical report, HydroQual, Inc. Mahwah, NJ.
- Ji, Zhen-Gang (2008): Hydrodynamics and water quality modeling rivers, lakes, and estuaries. Wiley-Interscience, John Wiley and Sons, Inc. pp676.
- Jørgensen, S. E., editor. (1979): *Handbook of Environmental Data and Ecological Parameters*. Pergamon Press, Oxford.
- July O'Neil, C. Wazniak, C. McCollough, D. McKay, K. Meyer, B. Walsh (2013): Offshore nutrient sampling R/V Rachel Carson: August 2012. Maryland Coastal Bay STAC meeting presentation, January, 2013.
- Kantha, L.H. and C.A. Clayson (1994): An improved mixed layer model for geophysical applications. *J. Geophys. Res*, 99(25), pp. 235-266.
- Le Roux, D. Y., C. A. Lin, and A. Staniforth (1997): An accurate interpolating scheme for semi-Lagrangian advection on an unstructured mesh for ocean modelling, *Tellus A*, 49(1), 119-138.
- Luetich, R.A., J.C. Muccino and M.G.G. Foreman (2002): Considerations in the calculation of vertical velocity in three-dimensional circulation models. *Journal of Atmospheric and Oceanic Technology*, 19, pp. 2063-2076.
- Mellor, G.L. and T. Yamada (1982): Development of a turbulence closure model for geophysical fluid problems. *Rev. Geophys.*, 20, pp. 851-875.

- Maryland Department of the Environment (1993): An assessment of aquatic ecosystems, pollutant loadings and management options. University of Maryland System Centers for Environmental and Estuarine Studies and Coastal Environmental Services Inc.
- Maryland Department of the Environment (2001): Total maximum daily loads of nitrogen and phosphorus for 5 tidal tributaries in the Northern Coastal Bays, Worcester County, MD. Final report submitted to EPA Region III, Watershed Protection Division, Philadelphia, PA. http://www.mde.state.md.us/assets/document/NCB_main_final.pdf.
- Maryland Department of the Environment (2004): Priority areas for wetland restoration, preservation, and mitigation in Maryland's Coastal Bays. Final report submitted to US Environmental Protection Agency, State Wetland Program development grant.
- Maryland Department of the Environment (2010): Final integrated report of surface water quality in Maryland. Baltimore, MD: Maryland Department of the Environment.
- Morel, F. (1983): Principles of Aquatic Chemistry. John Wiley & Sons, N.Y, NY, 446 pp.
- NTHMP (2011): NTHMP MMS Tsunami Inundation Model Validation Workshop, Galveston, April 2011. NOAA internal report (in press).
- O'Connor, D.J. & Dobbins, W.E. (1958): Mechanism of reaeration in natural streams. Transactions of the American Society of Civil Engineers, 123(2934): 641-684
- Oliveira, A. and A.M. Baptista (1998): On the role of tracking on Eulerian-Lagrangian solutions of the transport equation. Advances in Water Resources, 21, pp. 539-554.
- Park, K., A. Y. Kuo, J. Shen, and J. M. Hamrick (1995): A three-dimensional hydrodynamic eutrophication model (HEM3D): description of water quality and sediment processes submodels. The College of William and Mary, Virginia Institute of Marine Science. Special Report 327, 113pp.
- Perry, Elgin (2012): Adjustment of dissolved oxygen observations for diel cycles in Maryland Coastal Bays; contract report submitted to Maryland Department of natural Resources, Tidewater Ecosystem Assessment, administered by Catherine E. Wazniak and Carol B. McCollough.
- Pietrzak, J., J.B. Jakobson, H. Burchard, H.J. Vested and O. Petersen (2002): A three-dimensional hydrostatic model for coastal and ocean modelling using a generalised topography following coordinate system. Ocean Modelling, 4, pp. 173-205.
- Pond, S. and G.L. Pickard (1998): Introductory Dynamical Oceanography, Butterworth-Heinemann.
- Pritchard, D. W. (1960). Salt balance and exchange rate for Chincoteague Bay. Chesapeake Science 1:48-57.

- Rodi, W. (1984): Turbulence models and their applications in hydraulics: a state of the art review. Delft, The Netherlands, International Association for Hydraulics Research.
- Rodrigues M., A. Oliveira, H. Queiroga, A.B. Fortunato, Y. Zhang (2009): Three-dimensional modeling of the lower trophic levels in the Ria de Aveiro (Portugal), *Ecological Modelling*, 220(9-10), 1274-1290.
- Shapiro, R. (1970): Smoothing, filtering and boundary effects. *Rev. Geophys. and Space Physics*, 8(2), pp. 359-387.
- Shchepetkin, A.F. and J.C. McWilliams (2005): The regional oceanic modeling system (ROMS): a split-explicit, free-surface, topography-following-coordinate, oceanic model. *Ocean Modelling*, 9, pp. 347-404.
- Song, Y., Haidvogel, D. (1994). A semi-implicit ocean circulation model using a generalized topography-following coordinate system. *J. Comput. Phys.* 115, 228–244.
- Sweby, P.K. (1984): High resolution schemes using flux limiters for hyperbolic conservation laws. *SIAM J. Num. Analysis*, 21(5), pp. 995-1011.
- Thomann, Robert V., D. M. Di Toro, R. P. Winfield, D. J. O'Connor (1975): Mathematical modeling of phytoplankton in Lake Ontario. Part 1: Model development and verification.
- Tillman, Dottie H., Carl F. Cerco, Mark R. Noel, J. L. Martin, and John Hamrick (2004): Three-dimensional eutrophication model of the lower St. Johns River, Florida. Environmental Lab. ERDC/EL TR-04-13, US Army Corps of Engineering Research and Development Center.
- Umlauf, L. and H. Burchard (2003): A generic length-scale equation for geophysical turbulence models. *J. Mar. Res.*, 6, pp. 235-265.
- VIMS (Virginia Institute of Marine Science), (2013): Maryland Coastal Bays Watershed Modeling Report conducted by Hongzhou Xu and Jian Shen, submitted to MDE on February 2013.
- Walters, Roy, A. (2005): Coastal ocean models: two useful finite element methods. *Continental Shelf Research*, Vol. 25, p775-793.
- Wang, Taiping (2009): Numerical modeling of eutrophication dynamics in the shallow coastal ecosystem: a case study in the Maryland and Virginia Coastal Bays. Virginia Institute of Marine Sciences, Ph.D. thesis, pp236.

- Wazniak, C.E., and P.M. Glibert. (2004): Potential impacts of brown tide, *Aureococcus anophagefferens*, on juvenile hard clams, *Mercenaria mercenaria*, in the Coastal Bays of Maryland, USA. *Harmful Algae* 3:321-329.
- Wazniak, C., M. Trice, B. Sturgis, W. Romano, and M. Hall. (2004): Status and trends of phytoplankton abundance in the Maryland Coastal Bays. In: Wazniak, C. and M. Hall [eds.] *Maryland's Coastal Bays: Ecosystem health assessment 2004*. Maryland Department of Natural Resources, document number: DNR-12-1202-0009.
- Wazniak, C.E. and M.R. Hall [Ed]. (2005): *Maryland's Coastal Bays: Ecosystem Health Assessment 2004*. DNR-12-1202-0009. Maryland Department of Natural Resources, Tidewater Ecosystem Assessment, Annapolis, MD.
- Wazniak, C.E., M.R. Hall, T. Carruthers, and R. Sturgis (2007): Linking water quality to living resources in a mid-Atlantic lagoon system, USA. *Ecological Applications*. 17(5):S64-S78.
- Wezernak, C. T. and Gannon, J. J. (1968): Evaluation of nitrification in streams. *Journal of the Sanitary Engineering Division, ASCE*, 94(SA5): p883-895.
- Wells, Darlene V., J. M. Hill, M. J. Park, and C. P. Williams (1998): The shallow sediments of the middle Chincoteague Bay area in Maryland: physical and chemical characteristics. *Coastal and estuarine geology*, file report no. 98-1. Maryland Geological Survey.
- Wells, Darlene. V. 2002, E. L. Hennessee, and J. M. Hill (2002): Shoreline erosion as a source of sediments and nutrients, Northern Coastal Bay, Maryland. *Coastal and estuarine geology*, file report no. 02-05. Maryland Geological Survey.
- Wells, Darlene. V. 2003, E. L. Hennessee, and J. M. Hill (2003): Shoreline erosion as a source of sediments and nutrients, Middle Coastal Bays, Maryland. *Coastal and estuarine geology*, file report no. 03-07. Maryland Geological Survey.
- Wicker, L.J. and Skamarock, W.C. (1998). A time-splitting scheme for the elastic equations incorporating second-order Runge–Kutta time differencing. *Monthly Weather Rev.* 126, 1992–1999.
- Wilcox, D.C. (1998): Reassessment of scale determining equation for advance turbulence models. *AIAA J.*, 26, pp. 1299-1310.
- Zeng, X., M. Zhao and R.E. Dickinson (1998): Intercomparison of bulk aerodynamic algorithms for the computation of sea surface fluxes using TOGA COARE and TAO data. *J. Clim.*, 11, pp. 2628-2644.

- Zhang, Y.L., A.M. Baptista and E.P. Myers (2004): A cross-scale model for 3D baroclinic circulation in estuary-plume-shelf systems: I. Formulation and skill assessment. *Continental Shelf Research*, 24, pp. 2187-2214.
- Zhang, Y., and A. M. Baptista (2008a): SELFE: A semi-implicit Eulerian–Lagrangian finite-element model for cross-scale ocean circulation, *Ocean Modelling*, 21(3–4), 71-96.
- Zhang, Y., R. C. Witter, and G. R. Priest (2011): Tsunami–tide interaction in 1964 Prince William Sound tsunami, *Ocean Modelling*, 40(3–4), 246-259.
- Zhang, Y., and A. Baptista (2008b). An efficient and robust tsunami model on unstructured grids. Part I: inundation benchmarks, *Pure and Applied Geophysics*, 165(11), 2229-2248.

APPENDIX A: Summary of SELFE hydrodynamic model formulations

A1. Physical formulation of SELFE

SELFE solves the 3D shallow-water equations, with hydrostatic and Boussinesq approximations, and transport equations for salt and heat. The primary variables that SELFE solves are free-surface elevation, 3D velocity, 3D salinity, and 3D temperature of the water. In a Cartesian frame, the equations read:

$$(1) \nabla \cdot \mathbf{u} + \frac{\partial w}{\partial z} = 0$$

$$(2) \frac{\partial \eta}{\partial t} + \nabla \cdot \int_{-h}^{\eta} \mathbf{u} dz = 0$$

$$(3) \frac{D\mathbf{u}}{Dt} = \mathbf{f} - g \nabla \eta + \frac{\partial}{\partial z} \left(\nu \frac{\partial \mathbf{u}}{\partial z} \right); \quad \mathbf{f} = -f \mathbf{k} \times \mathbf{u} + \alpha g \nabla \hat{\psi} - \frac{1}{\rho_0} \nabla p_A - \frac{g}{\rho_0} \int_z^{\eta} \nabla \rho dz + \nabla \cdot (\mu \nabla \mathbf{u})$$

$$(4) \frac{DS}{Dt} = \frac{\partial}{\partial z} \left(\kappa \frac{\partial S}{\partial z} \right) + F_s$$

$$(5) \frac{DT}{Dt} = \frac{\partial}{\partial z} \left(\kappa \frac{\partial T}{\partial z} \right) + \frac{\dot{Q}}{\rho_0 C_p} + F_h$$

where

(x, y) horizontal Cartesian coordinates, in [m]

z vertical coordinate, positive upward, in [m]

∇ $\left(\frac{\partial}{\partial x}, \frac{\partial}{\partial y} \right)$

t time [s]

$\eta(x, y, t)$ free-surface elevation, in [m]

$h(x, y)$ bathymetric depth, in [m]

$\mathbf{u}(x, y, z, t)$ horizontal velocity, with Cartesian components (u, v) , in [ms^{-1}]

w vertical velocity, in [ms^{-1}]

f Coriolis factor, in [s^{-1}] (Section 2.5)

g acceleration of gravity, in [ms^{-2}]

$\hat{\psi}(\phi, \lambda)$ earth-tidal potential, in [m] (Section 2.5)

α effective earth-elasticity factor

$\rho(\mathbf{x},t)$	water density; by default, reference value ρ_0 is set as 1025 kgm^{-3}
$p_A(x, y, t)$	atmospheric pressure at the free surface, in $[\text{Nm}^{-2}]$
S, T	salinity and temperature of the water [<i>practical salinity units (psu)</i> , $^{\circ}\text{C}$]
ν	vertical eddy viscosity, in $[\text{m}^2\text{s}^{-1}]$
μ	horizontal eddy viscosity, in $[\text{m}^2\text{s}^{-1}]$
κ	vertical eddy diffusivity, for salt and heat, in $[\text{m}^2\text{s}^{-1}]$
F_s, F_h	horizontal diffusion for transport equations (neglected in SELFE)
\dot{Q}	rate of absorption of solar radiation $[\text{Wm}^{-2}]$
C_p	specific heat of water $[\text{JKg}^{-1}\text{K}^{-1}]$

The differential system Eqs. (1-5) are closed with: (a) the equation of state describing the water density as a function of salinity and temperature, (b) the definition of the tidal potential and Coriolis factor; (c) parameterizations for horizontal and vertical mixing, via turbulence closure equations, and (d) appropriate initial and boundary conditions. Further details can be found in Zhang et al. (2004).

A1.1 Turbulence closure model

SELFE uses the Generic Length Scale (GLS) turbulence closure of Umlauf and Burchard (2003), which has the advantage of encompassing most of the 2.5-equation closure models: k - ε (Rodi 1984); k - ω (Wilcox 1998); k - ℓ (Mellor and Yamada 1982). In this framework, the transport, production, and dissipation of the turbulent kinetic energy (K) and of a generic length-scale variable (ψ) are governed by:

$$(6) \quad \frac{DK}{Dt} = \frac{\partial}{\partial z} \left(\nu_k^{\psi} \frac{\partial K}{\partial z} \right) + \nu M^2 + \mu N^2 - \varepsilon,$$

$$(7) \quad \frac{D\psi}{Dt} = \frac{\partial}{\partial z} \left(\nu_{\psi} \frac{\partial \psi}{\partial z} \right) + \frac{\psi}{K} (c_{\psi 1} \nu M^2 + c_{\psi 3} \mu N^2 - c_{\psi 2} F_w \varepsilon),$$

where ν_k^{ψ} and ν_{ψ} are vertical turbulent diffusivities, $c_{\psi 1}$, $c_{\psi 2}$ and $c_{\psi 3}$ are model-specific constants (Umlauf and Burchard 2003; Zhang et al. 2004), F_w is a wall proximity function, M and N are shear and buoyancy frequencies, and ε is a dissipation rate. The generic length-scale is defined as

$$(8) \quad \psi = (c_{\mu}^0)^p K^m \ell^n,$$

where $c_\mu^0 = 0.3^{1/2}$ and ℓ is the turbulence mixing length. The specific choices of the constants p , m and n lead to the different closure models mentioned above. Finally, vertical viscosities and diffusivities as appeared in Eqs. (3-5) are related to K , ℓ and stability functions:

$$\begin{aligned} \nu &= \sqrt{2} s_m K^{1/2} \ell \\ \mu &= \sqrt{2} s_h K^{1/2} \ell \\ (9) \quad \nu_k^\psi &= \frac{\nu}{\sigma_k^\psi} \quad , \\ \nu_\psi &= \frac{\nu}{\sigma_\psi} \end{aligned}$$

where the Schmidt numbers σ_k^ψ and σ_ψ are model-specific constants. The stability functions (s_m and s_h) are given by an Algebraic Stress Model (e.g.: Kantha and Clayson 1994, Canuto et al. 2001, or Galperin et al. 1988).

At the free surface and at the bottom of rivers and oceans, the turbulent kinetic energy and the mixing length are specified as Dirichlet boundary conditions:

$$(10) \quad K = \frac{1}{2} B_1^{2/3} |\tau_b|^2,$$

$$(11) \quad \ell = \kappa_0 d_b \text{ or } \kappa_0 d_s,$$

where τ_b is a bottom frictional stress (Eq. (14)), $\kappa_0 = 0.4$ is the von Karman's constant, B_1 is a constant, and d_b and d_s are the distances to the bottom and the free surface, respectively.

A1.2 Vertical boundary conditions for the momentum equation

The vertical boundary conditions for the momentum equation – especially the bottom boundary condition - play an important role in the SELFE numerical formulation, as it involves the unknown velocity (see Section A2). In fact, as a crucial step in solving the differential system, SELFE uses the bottom boundary condition to decouple the free-surface Eq. (2) from the momentum Eq. (3).

At the sea surface, SELFE enforces the balance between the internal Reynolds stress and the applied shear stress:

$$(12) \quad \nu \frac{\partial \mathbf{u}}{\partial z} = \tau_w, \quad \text{at } z = \eta$$

where the stress τ_w can be parameterized using the approach of Zeng et al. (1998) or the simpler approach of Pond and Pickard (1998).

Because the bottom boundary layer is usually not well resolved in ocean models, the no-slip condition at the sea or river bottom ($\mathbf{u} = \mathbf{w} = 0$) is replaced by a balance between the internal Reynolds stress and the bottom frictional stress,

$$(13) \quad \nu \frac{\partial \mathbf{u}}{\partial z} = \boldsymbol{\tau}_b, \text{ at } z = -h.$$

The specific form of the bottom stress τ_b depends on the type of boundary layer used. While the numerical method for SELFE as outlined in Section A2 can be applied to other types of bottom boundary layer (e.g., laminar boundary layer), only the turbulent boundary layer below (Blumberg and Mellor 1987) is discussed, given its prevalent usage in ocean modeling. The bottom stress in Eq. (13) is then:

$$(14) \quad \boldsymbol{\tau}_b = C_D |\mathbf{u}_b| \mathbf{u}_b.$$

The velocity profile in the interior of the bottom boundary layer obeys the logarithmic law:

$$(15) \quad \mathbf{u} = \frac{\ln[(z+h)/z_0]}{\ln(\delta_b/z_0)} \mathbf{u}_b, \quad (z_0 - h \leq z \leq \delta_b - h),$$

which is smoothly matched to the exterior flow at the top of the boundary layer. In Eq. (15), δ_b is the thickness of the bottom computational cell (assuming that the bottom is sufficiently resolved in SELFE that the bottom cell is inside the boundary layer), z_0 is the bottom roughness, and \mathbf{u}_b is the velocity measured at the top of the bottom computational cell. Therefore, the Reynolds stress inside the boundary layer is derived from Eq. (15) as:

$$(16) \quad \nu \frac{\partial \mathbf{u}}{\partial z} = \frac{\nu}{(z+h) \ln(\delta_b/z_0)} \mathbf{u}_b.$$

Utilizing the turbulence closure theory discussed in Section 2.1, the eddy viscosity can be found from Eq. (9), with the stability function, the turbulent kinetic energy, and the meso-scale mixing length given by:

$$(17) \quad \begin{aligned} s_m &= g_2, \\ K &= \frac{1}{2} B_1^{2/3} C_D |\mathbf{u}_b|^2, \\ \ell &= \kappa_0 (z+h) \end{aligned}$$

where g_2 and B_1 are constants with $g_2 B_1^{1/3} = 1$. Therefore, the Reynolds stress is constant inside the boundary layer:

$$(18) \quad \nu \frac{\partial \mathbf{u}}{\partial z} = \frac{\kappa_0}{\ln(\delta_b / z_0)} C_D^{1/2} |\mathbf{u}_b| \mathbf{u}_b, \quad (z_0 - h \leq z \leq \delta_b - h),$$

and the drag coefficient is calculated from Eqs. (13), (14), and (18) as:

$$(19) \quad C_D = \left(\frac{1}{\kappa_0} \ln \frac{\delta_b}{z_0} \right)^{-2},$$

a drag coefficient formula as discussed in Blumberg and Mellor (1987). Eq. (18) also shows that the vertical viscosity term in the momentum equation Eq. (3) vanishes inside the boundary layer. This fact will be utilized in the numerical model of SELFE in Section A2.

A2. Numerical formulation of SELFE

Numerical efficiency and accuracy consideration dictates the numerical formulation of SELFE. SELFE solves the differential equation system described in Section 2 with finite-element and finite-volume schemes. No mode splitting is used in SELFE, thus eliminating the errors associated with the splitting between internal and external modes (Shchepetkin and McWilliams 2005). Semi-implicit schemes are applied to all equations; the continuity and momentum equations (Eqs. (2-3)) are solved simultaneously, thus bypassing the most severe stability restrictions (e.g. CFL). A key step in SELFE is to decouple the continuity and momentum equations (Eqs. (2-3)) via the bottom boundary layer, as shown in Section A2.2. SELFE uses an Eulerian-Lagrangian method (ELM) to treat the advection in the momentum equation, thus further relaxing the numerical stability constraints. The advection terms in the transport equations (Eqs. (4-5)) are treated with either ELM or a finite-volume upwind method (FVUM), the latter being mass conservative.

A2.1. Domain discretization

In SELFE, unstructured triangular grids are used in the horizontal direction, while hybrid vertical coordinates – partly terrain-following S coordinates and partly Z coordinates – are used in the vertical direction. The origin of the z-axis is at the undisturbed Mean Sea Level (MSL). The terrain-following S layers (Song and Haidvogel 1994) are placed on top of a series of Z layers with the demarcation line between S and Z layers located at level k^z ($z=-h_s$). That is to say, the vertical grid is allowed to follow the terrain up to a maximum depth of h_s . The free surface is at level N_z throughout the domain (for all wet points), but the bottom level indices, k^b , may vary in space due to the staircase representation of the bottom in Z layers. Note that $k^b < \text{or equal } k^z$ and the equality occurs when the local depth $h < \text{or equal } h_s$. A "pure S" representation is a special case with $k^b=k^z=1$ and h_s greater than the maximum depth in the domain, but a "pure Z" model is not a special case in SELFE. The details of the terrain-following coordinates used in SELFE can be found in Appendix A. The rationale for using such a hybrid coordinate system is discussed below.

The "pure S" representation of SELFE was initially chosen by the authors to avoid the staircase representation of the bottom and surface, and thus loss of accuracy commonly associated with the Z coordinates. While sufficient and preferable for some applications, "pure S" SELFE suffers from the so-called hydrostatic inconsistency commonly associated with the terrain-following coordinate models, and fails in applications involving steep bathymetry and strong stratification, as found in freshwater plumes of large rivers like the Columbia River. The inclusion of Z layers effectively alleviates the hydrostatic inconsistency and results in a physically more realistic plume. Therefore, the hybrid vertical coordinate system has the benefits of both S and Z coordinates: the S layers used in the shallow region resolves the bottom efficiently and the Z layers, which are only used in the deep region with $h > h_s$, fend off the hydrostatic inconsistency. The effects of the staircase representation of the bottom are arguably small in the deep region because the velocities there are small; the effects can also be minimized by choosing the largest possible value for h_s for a given application.

The use of a hybrid vertical coordinate system raises the issue of in which coordinate system the equations should be solved. All equations are solved in their original forms in the untransformed Z coordinates and use the transformation only to generate a vertical grid and to evaluate the horizontal derivatives (such as the horizontal viscosity). The main reason for not transforming the equations into S coordinates is that the transformation degenerates under the special circumstances described. Therefore, the role of vertical coordinates is mostly hidden in SELFE; all equations but one (the integrated continuity equation) are solved along the vertical direction only, which can be done in any vertical grid (including, in theory, an unstructured grid). The liberal treatment of the vertical coordinates makes the implementation of the hybrid vertical coordinates (SZ) system easier. A similar approach was also used by Shchepetkin and McWilliams (2005), who solved the equations in the Z space, despite the S coordinates being used in the vertical direction.

Strictly speaking, since the free surface is moving and so are the upper S levels (in the original Z space), all variables need to be re-interpolated onto the new vertical grid after the levels are updated at the end of each time step. However, the effects of movement of the S levels from one time step to the next are negligible, as long as the vertical movement of the free surface within a step is much smaller than the minimum layer thickness. This condition is easily satisfied in most practical applications; for example, in typical tidal-driven circulations, the maximum displacement of the free surface in a time step as large as five (5) minutes is only a few centimeters or less, which is much smaller than a typical top layer thickness of a few meters or more. Therefore, this interpolation step was skipped in SELFE, as a linear interpolation would introduce additional numerical diffusion, and a higher-order interpolation would introduce numerical dispersion into the solution. Note that a similar omission also occurs in many Z coordinate models, where the top layers also change with time.

In many parts of SELFE, interpolation at an arbitrary location in 3D space is necessary; examples include the interpolation at the foot of the characteristic line and the conversion of velocity from element sides to nodes. The horizontal interpolation is

usually done on a fixed Z plane (instead of along an S plane). One problem with this approach is the loss of accuracy near the bottom and the free surface (Fortunato and Baptista 1996). Therefore, in SELFE, the interpolation can be optionally done in the transformed S space in regions where no Z layers are used ("pure S region" with $h \leq h_s$). The latter approach is more accurate in shallow regions where rapid changes in bathymetry are common.

In the horizontal dimension, unstructured triangular grids are used, and the connectivity of the grid is defined as follows: the three sides of an element i are enumerated as $js(i,l)$ ($l = 1,2,3$). The surrounding elements of a particular node i are enumerated as $ine(i,l)$ ($l = 1, \dots, nne(i)$), where $nne(i)$ is the total number of elements in the "ball" of the node. After the domain is discretized horizontally and vertically, the basic 3D computational units of SELFE are triangular prisms. In the original Z space, the prisms may not have level bottom and top surfaces. A staggering scheme is used to define variables. The surface elevations are defined at the nodes. The horizontal velocities are defined at the side centers and whole levels. The vertical velocities are defined at the element centers and whole levels as the equations are solved with a finite-volume method. The linear shape functions are used for elevations and velocities; note, however, that for velocities, shape functions are only used for interpolation at the feet of characteristic lines. Note that the shape functions used here are different from those in a lowest-order Raviart-Thomas element (Walters 2005), in that the elevations are not constant within an element but continuous across elements. The locations where salinities and temperatures are defined depend on the method used to solve the transport equations; they are defined at the prism centers if the FVUM is used, and at both nodes and side centers, at whole levels, if the ELM is used.

A2.2 Barotropic module

SELFE solves the barotropic Eqs. (1-3) first, as the transport and turbulent closure equations lag one time step behind (in other words, the baroclinic pressure gradient term in the momentum equation is treated explicitly in SELFE). Due to the hydrostatic approximation, the vertical velocity w is solved from Eq. (1) after the horizontal velocity is found. To solve the coupled Eqs. (2-3), it was first discretized and combined with the vertical boundary conditions Eqs. (12-13) to be solved semi-implicitly in time as:

$$(20) \quad \frac{\eta^{n+1} - \eta^n}{\Delta t} + \theta \nabla \cdot \int_{-h}^{\eta^n} \mathbf{u}^{n+1} dz + (1-\theta) \nabla \cdot \int_{-h}^{\eta^n} \mathbf{u}^n dz = 0$$

$$(21) \quad \frac{\mathbf{u}^{n+1} - \mathbf{u}^*}{\Delta t} = \mathbf{f}^n - g \theta \nabla \eta^{n+1} - g(1-\theta) \nabla \eta^n + \frac{\partial}{\partial z} \left(\nu^n \frac{\partial \mathbf{u}^{n+1}}{\partial z} \right),$$

$$(22) \quad \begin{cases} \nu^n \frac{\partial \mathbf{u}^{n+1}}{\partial z} = \boldsymbol{\tau}_w^{n+1}, & \text{at } z = \eta^n; \\ \nu^n \frac{\partial \mathbf{u}^{n+1}}{\partial z} = \chi^n \mathbf{u}_b^{n+1}, & \text{at } z = -h, \end{cases}$$

where superscripts denote the time step, $0 \leq \theta \leq 1$ is the implicitness factor, $\mathbf{u}_*(x, y, z, t^n)$ is the back-tracked value calculated with ELM, and $\chi^n = C_D |\mathbf{u}_b^n|$. The elevations in the 2nd and 3rd terms of Eq. (20) are treated explicitly, which effectively amounts to a linearization procedure.

A Galerkin weighted residual statement in the weak form for Eq. (20) reads:

$$(23) \quad \int_{\Omega} \phi_i \frac{\eta^{n+1} - \eta^n}{\Delta t} d\Omega + \theta \left[-\int_{\Omega} \nabla \phi_i \square \mathbf{U}^{n+1} d\Omega + \int_{\Gamma_v} \phi_i \hat{U}_n^{n+1} d\Gamma_v + \int_{\bar{\Gamma}_v} \phi_i U_n^{n+1} d\bar{\Gamma}_v \right] + (1 - \theta) \left[-\int_{\Omega} \nabla \phi_i \square \mathbf{U}^n d\Omega + \int_{\Gamma} \phi_i U_n^n d\Gamma \right] = 0, \quad (i = 1, \dots, N_p)$$

where N_p is the total number of nodes, $\square \Gamma \equiv \Gamma_v + \bar{\Gamma}_v$ is the boundary of the entire domain \square , with Γ_v corresponding to the boundary segments where natural boundary conditions are specified, $\mathbf{U} = \int_{-h}^{\eta} \mathbf{u} dz$ is the depth-integrated velocity, U_n is its normal component along the boundary, and \hat{U}_n is the boundary condition. In SELFE, linear shape functions are used; thus, ϕ_i are conventional “hat” functions.

Integrating the momentum Eq. (21) along the vertical direction leads to:

$$(24) \quad \mathbf{U}^{n+1} = \mathbf{G}^n - g\theta H^n \Delta t \nabla \eta^{n+1} - \chi^n \Delta t \mathbf{u}_b^{n+1}$$

with

$$(25) \quad \mathbf{G}^n = \mathbf{U}_* + \Delta t \left[\mathbf{F}^n + \frac{n+1}{w} - g(1 - \theta) H^n \nabla \eta^n \right],$$

$$H^n = h + \eta^n, \quad \mathbf{F}^n = \int_{-h}^{\eta^n} \mathbf{f} dz, \quad \mathbf{U}_* = \int_{-h}^{\eta^n} \mathbf{u}_* dz$$

Note that Eq. (24) involves no vertical discretization as it is merely an analytical integration of Eq. (21).

To eliminate the unknown \mathbf{u}_b^{n+1} in Eq. (24), the discretized momentum equation form was invoked, as applied to the top of the bottom cell:

(26)

$$\frac{\mathbf{u}_b^{n+1} - \mathbf{u}_{*b}}{\Delta t} = \mathbf{f}_b^n - g\theta\nabla\eta^{n+1} - g(1-\theta)\nabla\eta^n + \frac{\partial}{\partial z}\left(v^n \frac{\partial\mathbf{u}^{n+1}}{\partial z}\right), \quad \text{at } z = \delta_b - h$$

However, since the viscosity term vanishes inside the bottom boundary layer (Eq. (18)), the bottom velocity can be formally solved as:

(27)

$$\mathbf{u}_b^{n+1} = \hat{\mathbf{f}}_b^n - g\theta\Delta t\nabla\eta^{n+1},$$

where:

(28)

$$\hat{\mathbf{f}}_b^n = \mathbf{u}_{*b} + \mathbf{f}_b^n\Delta t - g\Delta t(1-\theta)\nabla\eta^n.$$

Note that although the vertical viscosity is not explicitly present in Eq. (27), it is indirectly involved through terms \mathbf{u}_{*b} and the Coriolis term in \mathbf{f}_b^n .

Substituting Eq. (27) into (24) results in:

(29)

$$\mathbf{U}^{n+1} = \hat{\mathbf{G}}^n - g\theta\hat{H}^n\Delta t\nabla\eta^{n+1},$$

where:

(30)

$$\hat{\mathbf{G}}^n = \mathbf{G}^n - \chi^n\Delta t\hat{\mathbf{f}}_b^n, \quad \hat{H}^n = H^n - \chi^n\Delta t.$$

It is interesting to note from Eq. (30) that the bottom friction reduces the total depth by an amount that is proportional to the drag coefficient and the bottom velocity. For simplicity the Coriolis terms are treated explicitly in SELFE. It is well known that the explicit treatment of the Coriolis terms is stable but introduces damping (Wicker and Skamarock 1998). SELFE could have instead been formulated to treat the Coriolis terms implicitly, in which case, the two components of \mathbf{U} would become coupled in Eq. (29), but could still be solved simultaneously from this equation.

Since SELFE uses linear shape functions for the elevations, the two components of the horizontal velocity, u and v , are solved from the momentum equation independently from each other after the elevations are found. This approach has important implications as far as the Coriolis is concerned, and is different from that used in ELCIRC (Eulerian Lagrangian Circulation). As a matter of fact, special treatment must be made to find the tangential velocity components in UnTRIM-like models after the normal velocities are found, as discussed in Zhang et al. (2004) and Ham et al. (2005).

Finally, substitution of Eq. (29) into (23) leads to an equation for elevations alone:

$$(31) \int_{\Omega} \left[\phi_i \eta^{n+1} + g \theta^2 \Delta t^2 \hat{H}^n \nabla \phi_i \cdot \nabla \eta^{n+1} \right] d\Omega - g \theta^2 \Delta t^2 \int_{\bar{\Gamma}_v} \phi_i \hat{H}^n \frac{\partial \eta^{n+1}}{\partial n} d\bar{\Gamma}_v + \theta \Delta t \int_{\Gamma_v} \phi_i \hat{U}_n^{n+1} d\Gamma_v = I^n$$

where I^n consists of some explicit terms:

$$(32) I^n = \int_{\Omega} \left[\phi_i \eta^n + (1-\theta) \Delta t \nabla \phi_i \cdot \mathbf{U}^n + \theta \Delta t \nabla \phi_i \cdot \hat{\mathbf{G}}^n \right] d\Omega - (1-\theta) \Delta t \int_{\Gamma} \phi_i U_n^n d\Gamma - \theta \Delta t \int_{\bar{\Gamma}_v} \phi_i \mathbf{n} \cdot \hat{\mathbf{G}}^n d\bar{\Gamma}_v$$

Following standard finite-element procedures, and using appropriate essential and natural boundary conditions, SELFE solves Eq. (31) to determine the elevations at all nodes. For example, the integrals on $\bar{\Gamma}_v$ need not be evaluated if the essential boundary conditions are imposed by eliminating corresponding rows and columns of the matrix. Natural boundary conditions are used to evaluate the integral on Γ_v on the left-hand side of Eq. (31). If a Flather-type radiation condition (Flather 1987) needs to be applied, it can be done in the following fashion:

$$(33) \hat{U}_n^{n+1} - \bar{U}_n = \sqrt{g/H} (\eta^{n+1} - \bar{\eta}),$$

where \bar{U}_n and $\bar{\eta}$ are specified incoming current.

The matrix resulting from Eq. (31) is sparse and symmetric. It is also positive-definite if a mild restriction is placed on the friction-reduced depth in the form of $\hat{H}^n \geq 0$. Numerical experiments (not shown) indicated that even this restriction can be relaxed for many practical applications that include shallow areas. The matrix can be efficiently solved using a pre-conditioned Conjugate Gradient method (Casulli and Cattani 1994).

After the elevations are found, SELFE solves the momentum Eq. (3) along each vertical column at side centers. A semi-implicit Galerkin finite-element method is used, with the pressure gradient and the vertical viscosity terms being treated implicitly, and other terms treated explicitly:

(34)

$$\int_{-h}^{\eta} \gamma_k \left[\mathbf{u} - \Delta t \frac{\partial}{\partial z} \left(\nu \frac{\partial \mathbf{u}}{\partial z} \right) \right]_{j,k}^{n+1} dz = \int_{-h}^{\eta} \gamma_k \left\{ \mathbf{u}_* + \Delta t \left[\mathbf{f}_{j,k}^n - g \theta \nabla \eta_j^{n+1} - g(1-\theta) \nabla \eta_j^n \right] \right\} dz,$$

where $\gamma_k(z)$ is the hat function in the vertical dimension. The two terms that are treated implicitly would have imposed the most severe stability constraints. The explicit treatment of the baroclinic pressure gradient and the horizontal viscosity terms, however, does impose mild stability constraints.

After the velocities at all sides are found, the velocity at a node, which is needed in ELM, is evaluated by a weighted average of all surrounding sides in its ball, aided by proper interpolation in the vertical. The procedure to average the velocities (or alternatively calculating the velocity at a node based on a least-square fit from all surrounding sides) introduces numerical diffusion of the same order as the ELM. This is because the velocities at nodes are not used anywhere else in the model except in ELM tracking and interpolation. As an alternative to the averaging procedure, the velocity at a node is computed within each element from the three sides using the linear shape function and is kept discontinuous between elements. This approach leads to parasitic oscillations, but a Shapiro filter (Shapiro 1970) can be used to suppress the noise, with minimum distortion of physical features. The preliminary results indicate that the filter approach induces less numerical diffusion.

The vertical velocity serves as a diagnostic variable for local volume conservation, but is a physically important quantity, especially when a steep slope is present (Zhang et al. 2004). To solve the vertical velocity, we apply a finite-volume method to a typical prism, assuming that w is constant within an element i , and obtain:

$$(35) \quad \hat{S}_{k+1} (\bar{u}_{k+1}^{n+1} n_{k+1}^x + \bar{v}_{k+1}^{n+1} n_{k+1}^y + w_{i,k+1}^{n+1} n_{k+1}^z) - \hat{S}_k (\bar{u}_k^{n+1} n_k^x + \bar{v}_k^{n+1} n_k^y + w_{i,k}^{n+1} n_k^z) + \sum_{m=1}^3 \hat{P}_{js(i,m)} (\hat{q}_{js(i,m),k}^{n+1} + \hat{q}_{js(i,m),k+1}^{n+1}) / 2 = 0, \quad (k = k^b, \dots, N_z - 1)$$

where \hat{S} and \hat{P} are the areas of the five prism surfaces, (n_x, n_y, n_z) , are the normal vector (pointing upward), \bar{u} and \bar{v} the averaged horizontal velocities at the top and bottom surfaces, and \hat{q} is the outward normal velocity at each side center. The vertical velocity is then solved from the bottom to the surface, in conjunction with the bottom boundary condition. The closure error between the calculated w at the free surface and the surface kinematic boundary condition is an indication of the local

volume conservation error (Luettich et al. 2002). Because the primitive form of the continuity equation is solved in the model, this closure error is in general negligible.

A2.3 Baroclinic module

The barotropic module is one of the core parts of SELFE. To complete the model, SELFE solves two more sets of equations: transport and turbulence closure equations.

The advection in the transport equations is usually a dominant process. SELFE treats the advection in the transport equations with either an ELM or FVUM. If the ELM is used, the transport equations are solved at nodes and side centers along each vertical column using a finite-element method, with the lumping of the mass matrix to minimize numerical dispersion (in the form of under- or over-shoots). In order to interpolation used in ELM is important since linear interpolation leads to excessive numerical diffusion. To reduce the numerical diffusion, element-splitting or quadratic interpolation is used in ELM (Zhang et al. 2004).

Despite its efficiency, one of the main drawbacks of the ELM approach is its disregard for mass conservation (Oliveira and Baptista 1998). On the other hand, FVUM guarantees mass conservation. In FVUM, the scalar variables (salinity or temperature) are defined at the center of a prism, (i,k) , which has 5 exterior faces (top and bottom with areas $\hat{S}_{i,k}$ and $\hat{S}_{i,k-1}$, and 3 vertical faces with areas $\hat{P}_{jsj,k}$; The discretized temperature equation reads:

$$(36) \quad T_{i,k}^{n+1} V_{i,k}^n + \Delta t (u_n)_{i,k}^{n+1} \hat{S}_{i,k} T_{up(i,k)}^{n+1} + \Delta t (u_n)_{i,k-1}^{n+1} \hat{S}_{i,k-1} T_{up(i,k-1)}^{n+1} =$$

$$\Delta t A_i \left[\kappa_{i,k}^n \frac{T_{i,k+1}^{n+1} - T_{i,k}^{n+1}}{\Delta z_{i,k+1/2}^n} - \kappa_{i,k-1}^n \frac{T_{i,k}^{n+1} - T_{i,k-1}^{n+1}}{\Delta z_{i,k-1/2}^n} \right] +$$

$$V_{i,k}^n \left(T_{i,k}^n + \frac{\dot{Q}}{\rho_0 C_p} \Delta t \right) - \Delta t \sum_{l=1}^3 q_l^{n+1} T_{up(jsj,k)}^n, \quad (k = k^b + 1, \dots, N_z)$$

where "up(i,j,k)" indicates upwinding, $V_{i,k}$ is the volume of the prism, u_n is the outward normal velocity, $jsj=js(i,l)$ are 3 sides, and $q_l^{n+1} = \hat{P}_{jsj,k} (u_n)_{jsj,k}^{n+1}$ are 3 horizontal advective fluxes. The salinity equation is similarly discretized. Note that Eq. (36) reduces to Eq. (35) when $T=\text{const.}$ and $\dot{Q}=0$.

The stability condition for the upwind scheme, the Courant number restriction, is given by:

$$(37) \quad \Delta t \leq \frac{V_{i,k}}{\sum_{j \in S^+} |q_j|},$$

where S^+ indicates all outflow *horizontal* faces. Were the vertical advective fluxes on the left-hand side of Eq. (36) treated explicitly, the denominator in Eq. (37) would include the outflow faces for the top and bottom faces as well (Sweby 1984; Casulli and Zanolli 2005). But since the advective fluxes at the top and bottom faces are treated implicitly, S^+ excludes the top and bottom faces, and thus the more stringent stability constraints associated with the vertical advective fluxes are by-passed. The Courant number restriction (Eq. (37)) may still be too severe, and in this case the sub-division of a time step is necessary. Despite the fact that Eq. (36) does not conform to the depth integrated continuity Eq. (31), the FVUM guarantees mass conservation and the maximum principle (i.e., the solution is bounded by the maximum and minimum of the initial and boundary conditions; Casulli and Zanolli 2005), and thus is usually preferred over the ELM approach. To further reduce the numerical diffusion, we have recently implemented a higher-order finite-volume TVD scheme in SELFE (Sweby 1984).

SELFE solves the turbulence closure equations (Eqs. (6-7)) along each vertical column at each node with a finite-element method. The vertical mixing terms and the dissipation term in these equations are treated implicitly, but the production and buoyancy terms are treated either implicitly or explicitly, depending on the sign of their total contribution (Zhang et al. 2004). The advection terms in the turbulence closure equations are small compared to other terms, and are therefore neglected in SELFE.

APPENDIX B: The ICM Water Quality Model Formulation

This section summarizes water quality and eutrophication processes and their mathematical formulation in the ICM water quality-eutrophication model. The central issues in the water quality model are primary production of carbon by algae and concentration of dissolved oxygen. Primary production provides the energy required by the ecosystem to function. Dissolved oxygen is necessary to support the life functions of higher organisms and is considered an indicator of the health of estuarine systems. Different from earlier water quality model such as WASP (Ambrose et al. 1992), which use biochemical oxygen demand to represent oxygen demanding organic material, the ICM water quality model is carbon based. The four algae species are represented in carbon units and the three organic carbon variables play an equivalent role to BOD. Organic carbon, nitrogen and phosphorous were represented by up to three reactive sub-classes, refractory particulate, labile particulate and labile dissolve. Table B-1 lists the model's complete set of state variables and their interactions are illustrated in Figure 4.2 in the main text. The use of the sub-classes allows a more realistic distribution of organic material by reactive classes when data is to estimate distribution factors. The following sub-sections discuss the role of each variable and summarize there kinetic interaction processes. The kinetic sources and sinks, as well as the external loads for each state variable, are described in details in Chapter 2 and 4 in the main text. The kinetic processes include the horizontal transport fluxes described in Chapter 3 by hydrodynamic process as well as at the sediment-water interface, including sediment oxygen demand. The kinetic processes included in the ICM water quality model are mostly from the Chesapeake Bay three-dimensional water quality model, CE-QUAL-ICM (Cercio and Cole 1994). The description of the ICM water column water quality model in this section is from Park et al. (1995).

Table B-1. ICM model water quality state variables

(1) cyanobacteria	(12) labile particulate organic nitrogen
(2) diatom algae	(13) dissolved organic nitrogen
(3) green algae	(14) ammonia nitrogen
(4) refractory particulate organic carbon	(15) nitrate nitrogen
(5) labile particulate organic carbon	(16) particulate biogenic silica
(6) dissolved organic carbon	(17) dissolved available silica
(7) refractory particulate organic phosphorus	(18) chemical oxygen demand
(8) labile particulate organic phosphorus	(19) dissolved oxygen
(9) dissolved organic phosphorus	(20) salinity
(10) total phosphate	(21) temperature
(11) refractory particulate organic nitrogen	

B1 Model State Variables

B1.1 Algae

Algae are grouped into three model classes: cyanobacteria, diatoms, and green algae. The grouping is based upon the distinctive characteristics of each class and upon the significant role the characteristics play in the ecosystem. Cyanobacteria are characterized by their bloom-forming characteristics in fresh water. Cyanobacteria are unique in that some species fix atmospheric nitrogen, although nitrogen fixers are not believed to be predominant in many river systems. Diatoms are distinguished by their requirement of silica as a nutrient to form cell walls. Diatoms are large algae characterized by high settling velocities. Settling of spring diatom blooms to the sediments may be a significant source of carbon for sediment oxygen demand. Algae that do not fall into the preceding two groups are lumped into the heading of green algae. Green algae settle at a rate intermediate between cyanobacteria and diatoms and are subject to greater grazing pressure than cyanobacteria.

B1.2 Organic Carbon

Three organic carbon state variables are considered: dissolved, labile particulate, and refractory particulate. Labile and refractory distinctions are based upon the time scale of decomposition. Labile organic carbon decomposes on a time scale of days to weeks whereas refractory organic carbon requires more time. Labile organic carbon decomposes rapidly in the water column or the sediments. Refractory organic carbon decomposes slowly, primarily in the sediments, and may contribute to sediment oxygen demand years after deposition.

B1.3 Nitrogen

Nitrogen is first divided into organic and mineral fractions. Organic nitrogen state variables are dissolved organic nitrogen, labile particulate organic nitrogen, and refractory particulate organic nitrogen. Two mineral nitrogen forms are considered: ammonium and nitrite and nitrate combined. Both ammonium and nitrate are utilized to satisfy algal nutrient requirements, although ammonium is preferred. The primary reason for distinguishing the two is that ammonium is oxidized by nitrifying bacteria into nitrate. This oxidation can be a significant sink of oxygen in the water column and sediments. An intermediate in the complete oxidation of ammonium, nitrite, also exists. Nitrite concentrations are usually much less than nitrate, and for modeling purposes, nitrite is combined with nitrate. Hence the nitrate state variable actually represents the sum of nitrate plus nitrite.

B1.4 Phosphorus

As with carbon and nitrogen, organic phosphorus is considered in three states: dissolved, labile particulate, and refractory particulate. Only a single mineral form, total phosphate, is considered. Total phosphate exists as several states within the model ecosystem: dissolved phosphate, phosphate sorbed to inorganic solids, and phosphate incorporated in algal cells. Equilibrium partition coefficients are used to distribute the total among the three states.

B1.5 Silica

Silica is divided into two state variables: available silica and particulate biogenic silica. Available silica is primarily dissolved and can be utilized by diatoms. Particulate biogenic silica cannot be utilized. In the model, particulate biogenic silica is produced through diatom mortality. Particulate biogenic silica undergoes dissolution to available silica or else settles to the bottom sediments.

B1.6 Chemical Oxygen Demand

In the context of this study, chemical oxygen demand is the concentration of reduced substances that are oxidizable by inorganic means. The primary component of chemical oxygen demand is sulfide released from sediments. Oxidation of sulfide to sulfate may remove substantial quantities of dissolved oxygen from the water column.

B1.7 Dissolved Oxygen

Dissolved oxygen is one of the most important parameters of water quality. It is a basic requirement for a healthy aquatic ecosystem and is used to measure the amount of oxygen available for biochemical activity in water.

B1.8 Salinity

Salinity is a conservative tracer that provides verification of the transport component of the model and facilitates examination of conservation of mass. Salinity also influences the dissolved oxygen saturation concentration and is used in the determination of kinetics constants that differ in saline and fresh water. Salinity is simulated in the hydrodynamic component of the model.

B1.9 Temperature

Temperature is a primary determinant of the rate of biochemical reactions. Reaction rates increase as a function of temperature, although extreme temperatures result in the mortality of organisms. Temperature is simulated in the hydrodynamic component of the model.

B2 Conservation of Mass Equation

The governing mass-balance equation for each of the water quality state variables may be expressed as

$$\frac{\partial C}{\partial t} + \frac{\partial(uC)}{\partial x} + \frac{\partial(vC)}{\partial y} + \frac{\partial(wC)}{\partial z} = \frac{\partial}{\partial x} \left(K_x \frac{\partial C}{\partial x} \right) + \frac{\partial}{\partial y} \left(K_y \frac{\partial C}{\partial y} \right) + \frac{\partial}{\partial z} \left(K_z \frac{\partial C}{\partial z} \right) + S_C \quad (\text{B.1})$$

where

C = concentration of a water quality state variable.

u, v, w = velocity components in the x-, y- and z-directions, respectively.

K_x, K_y, K_z = turbulent diffusivities in the x-, y- and z-directions, respectively.

S_C = internal and external sources and sinks per unit volume.

The equation (B.1) incorporates transport due to flow advection and dispersion, external pollutant inputs and the kinetic interaction between the water quality variables. The last three terms on the left-hand side (LHS) of equation (B.1) account for the advective transport, and the first three terms on the right-hand side (RHS) of equation (B.1) account for the diffusive transport. These six terms for physical transport are analogous to, and thus the numerical method of solution is the same as, those in the mass-balance equation for salinity in the hydrodynamic model. The last term in equation (B.1) represents the kinetic processes and external loads for each of the state variables. The present model solves equation (B.1) after decoupling the kinetic terms from the physical transport terms.

The governing mass-balance equation for water quality state variables (equation B.1) consists of physical transport, advective and diffusive, and kinetic processes. When solving equation B.1, the kinetic terms are decoupled from the physical transport terms. The mass-balance equation for physical transport only, which takes the same form as the salt-balance equation, is:

$$\frac{\partial C}{\partial t} + \frac{\partial(uC)}{\partial x} + \frac{\partial(vC)}{\partial y} + \frac{\partial(wC)}{\partial z} = \frac{\partial}{\partial x} \left(K_x \frac{\partial C}{\partial x} \right) + \frac{\partial}{\partial y} \left(K_y \frac{\partial C}{\partial y} \right) + \frac{\partial}{\partial z} \left(K_z \frac{\partial C}{\partial z} \right) \quad (\text{B.2})$$

The equation for kinetic processes only, which will be referred to as the kinetic equation, is:

$$\frac{\partial C}{\partial t} = S_c \quad (\text{B.3})$$

which may be expressed as:

$$\frac{\partial C}{\partial t} = k \cdot C + R \quad (\text{B.4})$$

where K is kinetic rate (time⁻¹) and R is source/sink term (mass volume⁻¹ time⁻¹).

Equation (B.4) is obtained by linearizing some terms in the kinetic equations, mostly Monod type expressions. Hence, K and R are known values in equation (B.4).

The remainder of this section details the kinetics portion of the mass-conservation equation for each state variable. For consistency with reported rate coefficients, kinetics are detailed using a temporal dimension of days. Within the CE-QUAL-ICM computer code, kinetics sources and sinks are converted to a dimension of seconds before employment in the mass-conservation equation.

B2.1 Algae

Algae are primary producers which are able to utilize light, carbon dioxide, and nutrients to synthesize new organic material. Algae play a key role in the eutrophication process and are essential for water quality modeling. Algae affect the nitrogen cycle, the phosphorus cycle, the DO balance, and the food chain, primarily through nutrient uptake and algae death. As algae grow and die, they form part of the nutrient cycles.

Algae are grouped into three model state variables: cyanobacteria, diatoms and green algae. The algae kinetics is governed by the following processes:

1. Algal growth
2. Metabolism, including respiration and excretion
3. Predation
4. Settling
5. External sources

and a general equation that includes all of these processes can be expressed as:
Net algal production = algal growth – metabolism – predation – settling + external sources

The kinetic equation can now be written for algae as:

$$\frac{\partial B_x}{\partial t} = (P_x - BM_x - PR_x)B_x + \frac{\partial}{\partial z}(WS_x \cdot B_x) + \frac{WB_x}{V} \quad (\text{B.5})$$

where

B_x = algal biomass of algal group x (g C m^{-3})

t = time (day)

P_x = production rate of algal group x (day^{-1})

BM_x = basal metabolism rate of algal group x (day^{-1})

PR_x = predation rate of algal group x (day^{-1})

WS_x = settling velocity of algal group x (m day^{-1})

WB_x = external loads of algal group x (g C day^{-1})

V = volume (m^3)

subscript x = c, d, g are cyanobacteria, diatoms and green algae, respectively.

Algal growth (production)

Algal growth is the most important process for algae modeling. The algal growth rate is a complicated function of temperature, light, and nutrients and is often the determining factor for the net algal production. The effects of these processes are considered to be multiplicative:

$$P_x = PM_x \cdot f_1(N) \cdot f_2(I) \cdot f_3(T) \quad (\text{B.6})$$

where

PM_x = maximum growth rate for algal group x (day^{-1})

$f_1(N)$ = growth limiting function for nutrients ($0 \leq f_1 \leq 1$)

$f_2(I)$ = growth limiting function for light intensity ($0 \leq f_2 \leq 1$)

$f_3(T)$ = growth limiting function for temperature ($0 \leq f_3 \leq 1$)

The freshwater cyanobacteria coming from upstream rivers can undergo rapid mortality in salt water. Hence, the growth of freshwater blue-green algae in saline water can be limited by (Cerco and Cole, 1994):

$$P_x = PM_x \cdot f_1(N) \cdot f_2(I) \cdot f_3(T) \cdot f_4(S) \quad (\text{B.7})$$

where $f_4(S)$ = growth limiting function for salinity ($0 \leq f_4 \leq 1$) and

Effects of nutrients for algal growth

Using Liebig's Law of the Minimum, which states that growth is determined by the nutrient in least supply, the nutrient limitation for growth of blue-green algae and green algae is expressed as:

$$f_1(N) = \text{minimum} \left(\frac{NH_4 + NO_3}{KHN_x + NH_4 + NO_3}, \frac{PO_4d}{KHP_x + PO_4d} \right) \quad (\text{B.8})$$

where

KHN_x = nitrogen half saturation constant for algal group x, mass/volume

KHP_x = phosphorus half saturation constant for algal group x, mass/volume

subscript x = c for cyanobacteria and g for green algae, respectively, mass/volume

When diatoms are considered, silicon limitation should be included, and Eq. (B.8) is modified to:

$$f_1(N) = \text{minimum} \left(\frac{NH4 + NO3}{KHN_d + NH4 + NO3}, \frac{PO4d}{KHP_d + PO4d}, \frac{SAd}{KHS + SAd} \right) \quad (\text{B.9})$$

where KHN_d = nitrogen half saturation constant for diatoms, mass/volume
 KHP_d = phosphorus half saturation constant for diatoms, mass/volume

Effect of light on algal growth

The daily and vertically integrated form of Steel's equation is:

$$f_2(I) = \frac{2.718 \cdot FD}{Kess \cdot \Delta z} (e^{-\alpha_B} - e^{-\alpha_T}) \quad (\text{B.10})$$

with

$$\alpha_B = \frac{I_o}{FD \cdot (I_s)_x} \cdot \exp(-Kess[H_T + \Delta z]) \quad (\text{B.11})$$

$$\alpha_T = \frac{I_o}{FD \cdot (I_s)_x} \cdot \exp(-Kess \cdot H_T) \quad (\text{B.12})$$

where

FD = fractional daylength ($0 \leq FD \leq 1$)

Kess = K_e = total light extinction coefficient (m^{-1})

Δz = layer thickness (m)

I_o = daily total light intensity at water surface (langley days $^{-1}$)

$(I_s)_x$ = optimal light intensity for algal group x (langley days $^{-1}$)

H_T = depth from the free surface to the top of the layer (m).

The total light extinction coefficient, Kess, is given by

$$Kess = Ke_b + Ke_{TSS} \cdot TSS + Ke_{chl} \cdot \sum_{x=c,d,g} \left(\frac{B_x}{CChl_x} \right) \quad (\text{B.13})$$

where

Ke_b = background light extinction, m^{-1}

Ke_{TSS} = light extinction coefficient for total suspended solid, m^{-1} per $g\ m^{-3}$

TSS = total suspended solid concentration provided from the hydrodynamic model in unit of $g\ m^{-3}$

Ke_{chl} = light extinction coefficient for chlorophyll a, m^{-1} per $mg\ Chl\ m^{-3}$

$CChl_x$ = carbon-to-chlorophyll ratio in algal group x, g C per mg Chl.

The optimal light intensity (I_s) for photosynthesis is expressed as:

$$(I_s)_x = \text{minimum} \left[(I_o)_{avg} \cdot e^{-K_{ess} \cdot (D_{opt})_x}, (I_s)_{min} \right] \quad (\text{B.14})$$

where

$(D_{opt})_x$ = depth of maximum algal growth for algal group x (m)

$(I_o)_{avg}$ = adjusted surface light intensity (langleys day⁻¹).

A minimum, $(I_s)_{min}$, in Eq. (B.14) is specified so that algae do not thrive at extremely low-light levels. The adjusted surface light intensity, $(I_o)_{avg}$, is estimated as:

$$(I_o)_{avg} = CI_a \cdot I_o + CI_b \cdot I_1 + CI_c \cdot I_2 \quad (\text{B.15})$$

where

I_1 = daily light intensity one day preceding model day (langleys day⁻¹)

I_2 = daily light intensity two days preceding model day (langleys day⁻¹)

CI_a , CI_b , and CI_c = weighting factors for I_o , I_1 and I_2 , respectively: $CI_a + CI_b + CI_c = 1$.

Effects of temperature on algal growth

Most water quality processes are temperature dependent. Temperature significantly influences the kinetic rates of nutrient transformations; the rate of chemical reactions increases with temperature.

Algal growth rate is controlled by temperature, water movement, nutrients, and light. It increases with temperature until an optimum is reached, after which further temperature increase will inhibit growth. The value of this optimum temperature varies with the species concerned and with light and nutrients. This temperature effect can be expressed as:

$$f_3(T) = \begin{cases} e^{-KTG1_x(T-TM1_x)^2} & \text{if } T < TM1_x \\ 1.0 & \text{if } TM1_x \leq T \leq TM2_x \\ e^{-KTG2_x(T-TM2_x)^2} & \text{if } T > TM2_x \end{cases} \quad (\text{B.16})$$

where

$f_3(T)$ = algal growth function

$TM1_x$ = lower end of optimal temperature range for algal growth for algal group x

$TM2_x$ = upper end of optimal temperature range for algal growth for algal group x

$KTG1_x$ = effect of temperature below $TM1_x$ on growth for algal group x

$KTG2_x$ = effect of temperature above $TM2_x$ on growth for algal group x

subscript x = c for cyanobacteria, d for diatom, and g for green algae

Effects of salinity on growth of freshwater Cyanobacteria

The growth of freshwater cyanobacteria in salt water is limited by:

$$f_4(S) = \frac{STOX^2}{STOX^2 + S^2} \quad (B.17)$$

where $STOX$ = salinity at which algal growth is halved, ppt

S = salinity in water column, ppt

Algal basal metabolism

Basal metabolism is a general term for biochemical processes that occur in living organisms by which energy is provided for vital processes and activities. Basal metabolism in the present model is the sum of all internal processes that decrease algal biomass and consists of two parts: respiration and excretion. In basal metabolism, algal matter (carbon, nitrogen, phosphorus, and silica) is returned to organic and inorganic pools in the environment, mainly to dissolved organic and inorganic matter. Respiration, which may be viewed as a reversal of production, consumes dissolved oxygen. Basal metabolism is considered to be an exponentially increasing function of temperature

$$BM_x = BMR_x \exp(KTB_x [T - TR_x]) \quad (B.18)$$

where

BMR_x = basal metabolism rate at TR_x for algal group x , 1/time

KTB_x = temperature function for basal metabolism, dimensionless

TR_x = reference temperature for basal metabolism for algal group x , °C

Algal predation

Zooplankton is the plankton consisting of animal life that is moved by flows. It includes the larval forms of large adult organisms (e.g., crabs, fish) and small animals that never get larger than several millimeters. Zooplankton consumes algae, bacteria, detritus, and sometimes other zooplankton, and is in turn eaten by small fish. Algal predation is the consumption of algae by zooplankton or other aquatic organisms. Present model does not include zooplankton; instead a temperature dependent rate is specified for algal predation:

$$PR_x = PRR_x \exp(KTB_x [T - TR_x]) \quad (\text{B.19})$$

where

PR_x = predation rate of algal group x, day^{-1}

KTB_x = temperature function for predation, dimensionless

Algal settling

Algal settling in natural waters is a complex phenomenon and depends on many factors, such as:

1. The density, size, and shape of the algae
2. The density, velocity, turbulence strength, and viscosity of the water.

It is impractical to calculate the algal settling velocity in a water quality model. Settling velocities for three algal groups, WSc , WSd , WSg , are specified as an input. Seasonal variations in settling velocity of diatoms can be accounted for by specifying time-varying WSd .

B2.2 Organic Carbon

The production of organic carbon is a key process in eutrophication study. The organic carbon cycle consists of photosynthesis, respiration, and decomposition. Because some organic carbons decay at faster rates than others, organic carbon can be divided into those that decay at a fast rate (labile) and those that decay at a slower rate (refractory). In water quality models, organic carbon can be categorized as:

1. Refractory particulate organic carbon (RPOC)
2. Labile particulate organic carbon (LPOC)
3. Dissolved organic carbon (DOC)

Total organic carbon (TOC) is the sum of all organic carbon compounds and can be expressed as: $TOC = RPOC + LPOC + DOC$

Particulate organic carbon

Labile and refractory distinctions are based on the time scale of decomposition. LPOC has a decomposition time scale of days to weeks and decays rapidly either in the water column or sediment bed. RPOC has a decomposition time scale of months to seasons, after being settled to the sediment bed. Through the sediment diagenesis processes, the settled RPOC in the bed may affect the water quality in the water column for a long time (seasons and even years). Sources of organic carbon include excretion and death of living organisms (such as algae) and external loadings. The discharges of organic matter from point sources (such as wastewater treatment plants) can be a major source of organic carbon, leading to large DO deficits and violation of water quality standards.

The governing equation for RPOC and LPOC are:

$$\frac{\partial RPOC}{\partial t} = \sum_{x=c,d,g} FCRP \cdot PR_x \cdot B_x - K_{RPOC} \cdot RPOC + \frac{\partial}{\partial z} (WS_{RP} \cdot RPOC) + \frac{WRPOC}{V} \quad (B.20)$$

and

$$\frac{\partial LPOC}{\partial t} = \sum_{x=c,d,g} FCLP \cdot PR_x \cdot B_x - K_{LPOC} \cdot LPOC + \frac{\partial}{\partial z} (WS_{LP} \cdot LPOC) + \frac{WLPOC}{V} \quad (B.21)$$

where

RPOC = concentration of refractory particulate organic carbon (g C m⁻³)

LPOC = concentration of labile particulate organic carbon (g C m⁻³)

FCRP = fraction of predated carbon produced as refractory particulate organic carbon

FCLP = fraction of predated carbon produced as labile particulate organic carbon

K_{RPOC} = hydrolysis rate of refractory particulate organic carbon (day⁻¹)

K_{LPOC} = hydrolysis rate of labile particulate organic carbon (day⁻¹)

WS_{RP} = settling velocity of refractory particulate organic matter (m day⁻¹)

WS_{LP} = settling velocity of labile particulate organic matter (m day⁻¹)

WRPOC = external loads of refractory particulate organic carbon (g C day⁻¹)

WLPOC = external loads of labile particulate organic carbon (g C day⁻¹).

Dissolved organic carbon

Sources and sinks for dissolved organic carbon include:

1. Algal excretion
2. Algal predation
3. Hydrolysis from RPOC
4. Hydrolysis from LPOC
5. Heterotrophic respiration of DOC
6. Denitrification
7. External loads

This yields: Net change of DOC = algal excretion + algal predation
 + RPOC hydrolysis + LPOC hydrolysis
 – DOC heterotrophic respiration - denitrification
 + external loads

The governing equation for DOC is:

$$\frac{\partial DOC}{\partial t} = \sum_{x=c,d,g} \left[FCD_x + (1 - FCD_x) \frac{KHR_x}{KHR_x + DO} \right] BM_x \cdot B_x + \sum_{x=c,d,g} FC DP \cdot PR_x \cdot B_x + K_{RPOC} \cdot RPOC + K_{LPOC} \cdot LPOC - K_{HR} \cdot DOC - Denit \cdot DOC + \frac{WDOC}{V} \quad (B.22)$$

where

DOC = concentration of dissolved organic carbon (g C m⁻³)

FCD_x = a constant for algal group x (0 < FCD_x < 1)

KHR_x = half-saturation constant of dissolved oxygen for algal dissolved organic carbon excretion for group x (g O₂ m⁻³)

DO = dissolved oxygen concentration (g O₂ m⁻³)

FC DP = fraction of predated carbon produced as dissolved organic carbon

K_{HR} = heterotrophic respiration rate of dissolved organic carbon (day⁻¹)

Denit = denitrification rate (day⁻¹)

WDOC = external loads of dissolved organic carbon (g C day⁻¹).

The remainder of this section explains the processes expressed in equations (B.20) - (B.22). Two algal processes affect organic carbon concentrations: algal excretion and

algal predation by zooplankton are represented by the terms with summation ($\sum_{x=c,d,g}$) in Eqs. (B.20), (B.21), and (B.22).

Basal metabolism

Basal metabolism, consisting of respiration and excretion, returns algal matter (carbon, nitrogen, phosphorus, and silica) back to the environment. Loss of algal biomass through basal metabolism is expressed as first order reaction equation:

$$\frac{\partial B_x}{\partial t} = -BM_x \cdot B_x \quad (\text{B.23})$$

which indicates that the total loss of algal biomass due to basal metabolism is independent of ambient dissolved oxygen concentration.

In the governing equation for algae, Eq. (B.5), the basal metabolism term ($-BM_x \cdot B_x$) actually includes two separated processes: the algal excretion and respiration. In this model, it is assumed that the distribution of total loss between respiration and excretion is constant as long as there is sufficient dissolved oxygen for algae to respire. Under that condition, the losses by respiration and excretion may be written as:

$$(1 - FCD_x) \cdot BM_x \cdot B_x \quad \text{due to respiration} \quad (\text{B.24})$$

$$FCD_x \cdot BM_x \cdot B_x \quad \text{due to excretion} \quad (\text{B.25})$$

where FCD_x is a constant of value between 0 and 1. However, algae cannot respire in the absence of oxygen. Although the total loss of algal biomass due to basal metabolism is oxygen independent (equation B.23), the distribution of total loss between respiration and excretion is oxygen-dependent. When oxygen level is high, respiration is a large fraction of the total. As dissolved oxygen becomes scarce, excretion becomes dominant. Thus, equation (B.24) represents the loss by respiration only at high oxygen levels. In general, equation (B.24) can be decomposed into two fractions as a function of dissolved oxygen availability:

$$(1 - FCD_x) \cdot \frac{DO}{KHR_x + DO} \cdot BM_x \cdot B_x \quad \text{due to respiration} \quad (\text{B.26})$$

$$(1 - FCD_x) \cdot \frac{KHR_x}{DO + KHR_x} \cdot BM_x \cdot B_x \quad \text{due to excretion} \quad (\text{B.27})$$

Equation (B.26) represents the loss of algal biomass by respiration, and equation (B.27) represents additional excretion due to insufficient dissolved oxygen concentration. The parameter KHR_x , which is defined as the half-saturation constant of dissolved oxygen for algal dissolved organic carbon excretion in equation (B.22), can also be defined as the half-saturation constant of dissolved oxygen for algal respiration in equation (B.26).

Combining equations (B.25) and (B.27), the total loss due to excretion is:

$$\left\{ (1 - FCD_x) \square \frac{KHR_x}{DO + KHR} \right\} BM_x \square B_x \quad (B.28)$$

Equations (B.26) and (B.28) combine to give the total loss of algal biomass due to basal metabolism. The definition of FCD_x in equation (B.22) becomes apparent in equation (B.28) (i.e., fraction of basal metabolism exuded as dissolved organic carbon at infinite dissolved oxygen concentration). At zero oxygen level, 100 percent of total loss due to basal metabolism is by excretion regardless of FCD_x . The end carbon product of respiration is primarily carbon dioxide, an inorganic form not considered in the present model, while the end carbon product of excretion is primarily dissolved organic carbon. Therefore, equation (B.28), that appears in equation (B.22), represents the contribution of excretion to dissolved organic carbon, and there is no source term for particulate organic carbon from algal basal metabolism in equations (B.20) and (B.21).

Predation

Algae produce organic carbon through the effects of predation. Zooplankton take up and redistribute algal carbon through grazing, assimilation, respiration, and excretion. Since zooplankton are not included in the model, routing of algal carbon through zooplankton predation is simulated by empirical distribution coefficients in equations (B.20) to (B.22): FCRP, FCLP and FCDP. The sum of these three predation fractions should be unity.

Heterotrophic respiration and dissolution

The fifth term on the RHS of Eq. (B.22), $-K_{HR} \cdot DOC$, represents the heterotrophic respiration that converts DOC into CO_2 . Heterotrophic respiration needs oxygen. A Michaelis-Menten function can be used to represent the dependency of heterotrophic respiration rate, K_{HR} , on DO concentration. It has the form:

$$K_{HR} = \frac{DO}{KHOR_{DO} + DO} K_{DOC} \quad (B.29)$$

where

$KHOR_{DO}$ = oxic respiration half-saturation constant for dissolved oxygen ($g O_2 m^{-3}$)

K_{DOC} = heterotrophic respiration rate of dissolved organic carbon at infinite dissolved oxygen concentration (day^{-1}).

The dissolution (hydrolysis) rates of RPOC and LPOC and the heterotrophic respiration

rate of DOC, K_{RPOC} , K_{LPOC} , and K_{DOC} , can be specified by the following:

$$K_{RPOC} = (K_{RC} + K_{RCalg} \sum_{x=c,d,g} B_x) \cdot e^{KT_{HDR}(T-TR_{HDR})} \quad (B.30)$$

$$K_{LPOC} = (K_{LC} + K_{LCalg} \sum_{x=c,d,g} B_x) \cdot e^{KT_{HDR}(T-TR_{HDR})} \quad (B.31)$$

$$K_{DOC} = (K_{DC} + K_{DCalg} \sum_{x=c,d,g} B_x) \cdot e^{KT_{MNL}(T-TR_{MNL})} \quad (B.32)$$

where

K_{RC} = minimum dissolution rate of refractory particulate organic carbon (day^{-1})

K_{LC} = minimum dissolution rate of labile particulate organic carbon (day^{-1})

K_{DC} = minimum respiration rate of dissolved organic carbon (day^{-1})

K_{RCalg} & K_{LCalg} = constants that relate dissolution of refractory and labile particulate organic carbon, respectively, to algal biomass (day^{-1} per g C m^{-3})

K_{DCalg} = constant that relates respiration to algal biomass (day^{-1} per g C m^{-3})

KT_{HDR} = effect of temperature on hydrolysis of particulate organic matter ($^{\circ}\text{C}^{-1}$)

TR_{HDR} = reference temperature for hydrolysis of particulate organic matter ($^{\circ}\text{C}$)

KT_{MNL} = effect of temperature on mineralization of dissolved organic matter ($^{\circ}\text{C}^{-1}$)

TR_{MNL} = reference temperature for mineralization of dissolved organic matter ($^{\circ}\text{C}$).

Eqs. (B.30) - (B.32) indicate that RPOC and LPOC are converted to DOC via an hydrolysis process, while DOC is converted to CO_2 via a mineralization process. Hydrolysis and mineralization will also be used to describe the conversions of organic phosphorus and organic nitrogen later in this chapter.

Effects of denitrification on dissolved organic carbon

As oxygen is depleted from natural systems, organic matter is oxidized by the reduction of alternate electron acceptors. Thermodynamically, the first alternate acceptor reduced in the absence of oxygen is nitrate. The reduction of nitrate by a large number of heterotrophic anaerobes is referred to as denitrification, and the stoichiometry of this reaction is:



The 4th term in equation (B.22) accounts for the effect of denitrification on dissolved organic carbon. The kinetics of denitrification in the model are first-order:

$$Denit = \frac{KHOR_{DO}}{KHOR_{DO} + DO} \frac{NO3}{KHDN_N + NO3} AANOX \cdot K_{DOC} \quad (B.34)$$

where

KHDNN = denitrification half saturation constant for nitrate (g N m⁻³)

AANOX = ratio of denitrification rate to oxic dissolved organic carbon respiration rate.

In equation (B.34), the dissolved organic carbon respiration rate, K_{DOC} , is modified so that significant decomposition via denitrification occurs only when nitrate is freely available and dissolved oxygen is depleted. The ratio, AANOX, makes the anoxic respiration slower than oxic respiration. Note that K_{DOC} , defined in equation (B.32), includes the temperature effect on denitrification.

B2.3 Phosphorus

Phosphorus exists in organic and inorganic forms. Both forms include particulate and dissolved phases. Total phosphorus (TP) is a measure of all forms of phosphorus and is widely used for setting trophic state criteria. In the present model, TP was split into the following state variables in a water quality model:

1. Refractory particulate organic phosphorus (RPOP)
2. Labile particulate organic phosphorus (LPOP)
3. Dissolved organic phosphorus (DOP)
4. Total phosphate (PO₄t)

Phosphorus processes are closely linked to sediment processes, especially shallow waters. It is critical to have a good representation of sediment processes, before phosphorus processes can be described realistically.

Particulate organic phosphorus

For particulate organic phosphorus (POP), the source and sinks are:

1. Algal metabolism
2. Algal predation
3. Hydrolysis of POP to dissolved organic phosphorus
4. Settling
5. External loads

and can be described as:

The change of POP = Algal basal metabolism + algal predation – POP hydrolysis
– settling + external source

The kinetic equations for RPOP and LPOP are thus (Cerco and Cole, 1994; Park et al., 1995):

$$\begin{aligned} \frac{\partial RPOP}{\partial t} = & \sum_{x=c,d,g} (FPR_x \cdot BM_x + FPRP \cdot PR_x) APC \cdot B_x - K_{RPOP} \cdot RPOP \\ & + \frac{\partial}{\partial z} (WS_{RP} \cdot RPOP) + \frac{WRPOP}{V} \end{aligned} \quad (B.35)$$

and

$$\begin{aligned} \frac{\partial LPOP}{\partial t} = & \sum_{x=c,d,g} (FPL_x \cdot BM_x + FPLP \cdot PR_x) APC \cdot B_x - K_{LPOP} \cdot LPOP \\ & + \frac{\partial}{\partial z} (WS_{LP} \cdot LPOP) + \frac{WLPOP}{V} \end{aligned} \quad (B.36)$$

where

RPOP = concentration of refractory particulate organic phosphorus (g P m^{-3})

LPOP = concentration of labile particulate organic phosphorus (g P m^{-3})

FPR_x = fraction of metabolized phosphorus by algal group x produced as refractory particulate organic phosphorus

FPL_x = fraction of metabolized phosphorus by algal group x produced as labile particulate organic phosphorus

FPRP = fraction of predated phosphorus produced as refractory particulate organic phosphorus

FPLP = fraction of predated phosphorus produced as labile particulate organic phosphorus

APC = mean phosphorus-to-carbon ratio in all algal groups (g P per g C)
 K_{RPOP} = hydrolysis rate of refractory particulate organic phosphorus (day^{-1})
 K_{LPOP} = hydrolysis rate of labile particulate organic phosphorus (day^{-1})
 $WRPOP$ = external loads of refractory particulate organic phosphorus (g P day^{-1})
 $WLPOP$ = external loads of labile particulate organic phosphorus (g P day^{-1}).

Dissolved organic phosphorus

For dissolved organic phosphorus, the major source and sinks are:

1. Algal metabolism
2. Algal predation
3. Hydrolysis from RPOP and LPOP
4. Mineralization to phosphate phosphorus
5. External loads

These processes can be expressed as:

The change of DOP = Algal basal metabolism + algal predation + POP hydrolysis
 – mineralization + external source

The corresponding kinetic equation is:

$$\begin{aligned}
 \frac{\partial DOP}{\partial t} = & \sum_{x=c,d,g} (FPD_x \cdot BM_x + FPDP \cdot PR_x) APC \cdot B_x \\
 & + K_{RPOP} \cdot RPOP + K_{LPOP} \cdot LPOP - K_{DOP} \cdot DOP + \frac{WDOP}{V}
 \end{aligned}
 \tag{B.37}$$

where

DOP = concentration of dissolved organic phosphorus (g P m^{-3})

FPD_x = fraction of metabolized phosphorus by algal group x produced as dissolved organic phosphorus

FPDP = fraction of predated phosphorus produced as dissolved organic phosphorus

K_{DOP} = mineralization rate of dissolved organic phosphorus (day^{-1})

WDOP = external loads of dissolved organic phosphorus (g P day^{-1}).

Total phosphate

Total phosphate (PO4t) includes dissolved phosphate (PO4d) and sorbed phosphate (PO4p) or $PO4t = PO4d + PO4p$. The amount of total phosphate in a water body depends on:

1. Algal metabolism, predation, and uptake
2. Mineralization from dissolved organic phosphorus
3. Settling of sorbed phosphate
4. Exchange of dissolved phosphate at the sediment bed - water column interface
5. External loads

The corresponding kinetic equation is:

$$\frac{\partial PO4t}{\partial t} = \sum_{x=c,d,g} (FPI_x \cdot BM_x + FPIP \cdot PR_x - P_x) APC \cdot B_x + K_{DOP} \cdot DOP + \frac{\partial}{\partial z} (WS_{TSS} \cdot PO4p) + \frac{BFPO4d}{\Delta z} + \frac{WPO4t}{V} \quad (B.38)$$

where

PO4t = total phosphate (g P m⁻³)

PO4p = particulate (sorbed) phosphate (g P m⁻³)

FPI_x = fraction of metabolized phosphorus by algal group x produced as inorganic phosphorus

FPIP = fraction of predated phosphorus produced as inorganic phosphorus

WS_{TSS} = settling velocity of suspended sediment (m day⁻¹), provided by the sediment model

BFPO4d = sediment-water exchange flux of phosphate (g P m⁻² day⁻¹), applied to the bottom layer only

WPO4t = external loads of total phosphate (g P day⁻¹).

Sorption and desorption of phosphate

In the presence of oxygen, dissolved phosphates combine with suspended particles. These particles eventually settle to the sediment bed and are temporarily removed from the cycling process. The settling of suspended solids and sorbed phosphorus can provide a significant loss mechanism of phosphorus from the water column to the bed. The sorption-desorption processes of phosphate are much faster than those for biological kinetics. The former are on the order of minutes; the latter are on the order of days. This difference permits an instantaneous equilibrium assumption for the calculation of phosphate. The dissolved phosphate and the particulate (sorbed) phosphate is treated as a single state variable. The dissolved and particulate

phosphates may be expressed as:

$$PO4p = \frac{K_{PO4p} \cdot S}{1 + K_{PO4p} \cdot S} PO4t \quad (B.39)$$

$$PO4d = \frac{1}{1 + K_{PO4p} \cdot S} PO4t \quad (B.40)$$

where

K_{PO4p} = partition coefficient of phosphate (m^3/g)

S = sediment concentration (g/m^3)

Dividing Eq. (B.39) by Eq. (B.40) gives:

$$K_{PO4p} = \frac{PO4p}{PO4d} \frac{1}{S} \quad (B.41)$$

The meaning of K_{PO4p} becomes apparent in Eq. (B.41): the partition coefficient is the ratio of the particulate concentration to the dissolved concentration per unit concentration of suspended solid.

Algal phosphorus-to-carbon ratio (APC)

Algal biomass is often expressed in units of carbon per volume of water. In order to estimate the nutrients contained in algal biomass, the ratio of phosphorus-to-carbon, APC, should be known.

Algal composition varies as a function of nutrient availability and adapts to ambient phosphorus concentration. When the concentrations of available phosphorus and nitrogen are low, algae adjust their composition so that smaller quantities of these nutrients are needed to produce carbonaceous biomass. Algal phosphorus content is high when ambient phosphorus is high, and is low when ambient phosphorus is low. Based on measured data, Cerco and Cole (1994) reported large variations of the algal phosphorus-to-carbon ratio and used the following empirical formulation to estimate the algal phosphorus-to-carbon ratio:

$$APC = \frac{1}{CP_{prm1} + CP_{prm2} \cdot e^{-CP_{prm3} \cdot PO4d}} \quad (B.42)$$

where

CP_{prm1} = minimum carbon-to-phosphorus ratio (g C per g P)

CP_{prm2} = difference between minimum and maximum carbon-to-phosphorus ratio (g C per g P)

CP_{prm3} = effect of dissolved phosphate concentration on carbon-to-phosphorus ratio (per g P m^{-3}).

Effects of algae on phosphorus

As algae grow, dissolved inorganic phosphorus (PO₄d) is taken up, stored, and incorporated into algal biomass. Living algal cells are a major component of the total phosphorus pool in the water. Settling of algae to the bottom sediments is a major loss pathway of phosphorus from the water column. As algae respire and die, algal biomass (and the phosphorus) is recycled to nonliving organic and inorganic matters. The effects

of algae are represented by the summation terms ($\sum_{x=c,d,g}$) in Eqs. (B.35), (B.36), (B.37), and (B.38). The total algal loss by basal metabolism in Eq. (B.5), is split using distribution coefficients FPR_x, FPL_x, FPD_x and FPI_x. The algal predation is accounted for by the terms associated with PR_x, the predation rate of algal group x. The total loss by predation, the term of PR_x·B_x in Eq. (B.5), is split using distribution coefficients, FPRP, FPLP, FPDP, and FPIP, in which FPRP + FPLP + FPDP + FPIP = 1.

Mineralization and hydrolysis

Organic nutrients undergo hydrolysis and mineralization to become inorganic nutrients before being consumed by algae. The hydrolysis of particulate organic phosphorus is represented by the term of K_{RPOP} in Eq. (B.35) and the term of K_{LPOP} in Eq. (B.36). The mineralization of dissolved organic phosphorus is represented by the term of K_{DOP} in Eq. (B.37). The formulations for hydrolysis and mineralization rates are (Park et al., 1995):

$$K_{RPOP} = (K_{RP} + \frac{KHP}{KHP + PO4d} K_{RPalg} \sum_{x=c,d,g} B_x) \cdot e^{KT_{HDR}(T-TR_{HDR})} \quad (B.43)$$

$$K_{LPOP} = (K_{LP} + \frac{KHP}{KHP + PO4d} K_{LPalg} \sum_{x=c,d,g} B_x) \cdot e^{KT_{HDR}(T-TR_{HDR})} \quad (B.44)$$

$$K_{DOP} = (K_{DP} + \frac{KHP}{KHP + PO4d} K_{DPalg} \sum_{x=c,d,g} B_x) \cdot e^{KT_{MNL}(T-TR_{MNL})} \quad (B.45)$$

where

K_{RP} = minimum hydrolysis rate of refractory particulate organic phosphorus (day⁻¹)

K_{LP} = minimum hydrolysis rate of labile particulate organic phosphorus (day⁻¹)

K_{DP} = minimum mineralization rate of dissolved organic phosphorus (day⁻¹)

K_{RPalg} and K_{LPalg} = constants that relate the hydrolysis of refractory and labile particulate organic phosphorus, respectively, to algal biomass (day⁻¹ per g C m⁻³)

K_{DPalg} = constant that relates mineralization to algal biomass (day⁻¹ per g C m⁻³)

KHP = mean half saturation constant for algal phosphorus uptake (g P m⁻³)

The mean half saturation constant for algal phosphorus uptake, KHP , is calculated using:

$$KHP = \frac{1}{3} \sum_{x=c,d,g} KHP_x \quad (B.46)$$

Eqs. (B.43) – (B.45) reveal that these rates are functions of water temperature and dissolved phosphate, and their values increase exponentially with water temperature.

B2.4 Nitrogen

The forms of nitrogen modeled are grouped into 5 categories:

1. Refractory particulate organic nitrogen (RPON)
2. Labile particulate organic nitrogen (LPON)
3. Dissolved organic nitrogen (DON)
4. Ammonium (NH_4)
5. Nitrate and nitrite (NO_3)

Two of the nitrogen state variables are in inorganic forms: NH_4 and NO_3 . The other three are in organic forms: refractory, labile, and dissolved. The nitrate state variable in the model represents the sum of nitrate and nitrite.

Particulate organic nitrogen

Particulate organic nitrogen, including RPON and LPON, has the following sources and sinks:

1. Algal basal metabolism
2. Algal predation
3. Hydrolysis to DON
4. Settling
5. External loads

The kinetic equations for RPON and LPON are (Park et al., 1995):

$$\begin{aligned} \frac{\partial RPON}{\partial t} = & \sum_{x=c,d,g} (FNR_x \cdot BM_x + FNRP \cdot PR_x) ANC_x \cdot B_x - K_{RPON} \cdot RPON \\ & + \frac{\partial}{\partial z} (WS_{RP} \cdot RPON) + \frac{WRPON}{V} \end{aligned} \quad (B.47)$$

and

$$\begin{aligned} \frac{\partial LPON}{\partial t} = & \sum_{x=c,d,g} (FNL_x \cdot BM_x + FNLP \cdot PR_x) ANC_x \cdot B_x - K_{LPON} \cdot LPON \\ & + \frac{\partial}{\partial z} (WS_{LP} \cdot LPON) + \frac{WLPON}{V} \end{aligned} \quad (B.48)$$

where

RPON = concentration of refractory particulate organic nitrogen (g N m^{-3})

LPON = concentration of labile particulate organic nitrogen (g N m^{-3})

FNR_x = fraction of metabolized nitrogen by algal group x as refractory particulate organic nitrogen

FNL_x = fraction of metabolized nitrogen by algal group x produced as labile particulate organic nitrogen

FNRP = fraction of predated nitrogen produced as refractory particulate organic nitrogen

FNLP = fraction of predated nitrogen produced as labile particulate organic nitrogen

ANC_x = nitrogen-to-carbon ratio in algal group x (g N per g C)

K_{RPON} = hydrolysis rate of refractory particulate organic nitrogen (day^{-1})

K_{LPON} = hydrolysis rate of labile particulate organic nitrogen (day^{-1})

WRPON = external loads of refractory particulate organic nitrogen (g N day^{-1})

WLPON = external loads of labile particulate organic nitrogen (g N day^{-1}).

By examining the field data in the Chesapeake Bay, Cerco and Cole (1994) showed that the variation of nitrogen-to-carbon stoichiometry was small and thus used a constant algal nitrogen-to-carbon ratio, ANC_x .

Dissolved organic nitrogen

Sources and sinks for dissolved organic nitrogen include:

1. Algal basal metabolism
2. Algal predation
3. Hydrolysis from RPON and LPON
4. Mineralization to ammonium
5. External loads

The kinetic equation describing these processes is:

$$\frac{\partial DON}{\partial t} = \sum_{x=c,d,g} (FND_x \cdot BM_x + FNDP \cdot PR_x) ANC_x \cdot B_x + K_{RPON} \cdot RPON + K_{LPON} \cdot LPON - K_{DON} \cdot DON + \frac{WDON}{V} \quad (B.49)$$

where

DON = concentration of dissolved organic nitrogen (g N m^{-3})

FND_x = fraction of metabolized nitrogen by algal group x produced as dissolved organic nitrogen

FNDP = fraction of predated nitrogen produced as dissolved organic nitrogen

K_{DON} = mineralization rate of dissolved organic nitrogen (day^{-1})

WDON = external loads of dissolved organic nitrogen (g N day^{-1}).

Ammonium nitrogen

Major sources and sinks for ammonia nitrogen include:

1. Algal basal metabolism, predation, and uptake
2. Mineralization from dissolved organic nitrogen
3. Nitrification to nitrate
4. Exchange at the sediment bed -water column interface
5. External loads

The kinetic equation for NH_4 described the process is:

$$\frac{\partial \text{NH}_4}{\partial t} = \sum_{x=c,d,g} (FNI_x \cdot BM_x + FNIP \cdot PR_x - PN_x \cdot P_x) ANC_x \cdot B_x + K_{DON} \cdot DON - \text{Nit} \cdot \text{NH}_4 + \frac{BF\text{NH}_4}{\Delta z} + \frac{W\text{NH}_4}{V} \quad (B.50)$$

where

FNI_x = fraction of metabolized nitrogen by algal group x produced as inorganic nitrogen

FNIP = fraction of predated nitrogen produced as inorganic nitrogen

PN_x = preference for ammonium uptake by algal group x ($0 < PN_x < 1$), given by Eq. (B.52)

Nit = nitrification rate (day^{-1}) given in Eq. (B.58).

BFNH4 = sediment-water exchange flux of ammonium ($\text{g N m}^{-2} \text{day}^{-1}$), applied to the bottom layer only

WNH4 = external loads of ammonium (g N day^{-1}).

Algae can uptake both ammonia and nitrate; however, ammonia is the preferred form of nitrogen for algal growth and is characterized by the parameter PN_x . The NH_4 flux from the sediment bed, $BFNH_4$ is calculated by simulating the sediment diagenesis process.

Nitrate nitrogen

Major sources and sinks for nitrate nitrogen include:

1. Algal uptake
2. Nitrification from ammonium
3. Denitrification to nitrogen gas
4. NO_3 flux at the sediment bed -water column interface
5. External source

$$\frac{\partial NO_3}{\partial t} = - \sum_{x=c,d,g} (1 - PN_x) P_x \cdot ANC_x \cdot B_x + Nit \cdot NH_4 - ANDC \cdot Denit \cdot DOC + \frac{BFNO_3}{\Delta z} + \frac{WNO_3}{V} \quad (B.51)$$

where

ANDC = mass of nitrate nitrogen reduced per mass of dissolved organic carbon oxidized (0.933 g N per g C)

BFNO₃ = sediment-water exchange flux of nitrate (g N m⁻² day⁻¹), applied to the bottom layer only

WNO₃ = external loads of nitrate (g N day⁻¹).

The NO_3 flux from the sediment bed, $BFNO_3$ is calculated by simulating the sediment diagenesis process.

Effects of algae on nitrogen

The terms within summation ($\sum_{x=c,d,g}$) in Eqs. (B.47) – (B.51) represent the effects of algae on nitrogen. The nitrogen of algal biomass can be recycled to organic nitrogen and inorganic nitrogen, and is represented by the distribution coefficients. For algal basal metabolism, the distribution coefficients are: FNR_x , FNL_x , FND_x , FNI_x , in which $FNR_x + FNL_x + FND_x + FNI_x = 1$

and for algal predation, the distribution coefficients are: $FNRP$, FNL_P , FND_P , $FNIP$, in which

$$FNRP + FNL_P + FND_P + FNIP = 1$$

Two forms of nitrogen, ammonia (NH_4) and nitrate (NO_3), are used during algal uptake

and growth, and NH_4 is the preferred form of nitrogen over NO_3 for algal growth. The value of the ammonia preference factor, PN_x is a function of the ammonia and nitrate concentrations, and is expressed as:

$$\text{PN}_x = \text{NH}_4 \frac{\text{NO}_3}{(\text{KHN}_x + \text{NH}_4)(\text{KHN}_x + \text{NO}_3)} + \text{NH}_4 \frac{\text{KHN}_x}{(\text{NH}_4 + \text{NO}_3)(\text{KHN}_x + \text{NO}_3)} \quad (\text{B.52})$$

Eq. (B.52) is somewhat similar to the Michaelis-Menten formulation that has been used to describe limiting functions. The preference for ammonium is 1 when nitrate is absent and is 0 when ammonium is absent. At $\text{PN}_x = 1$, NO_3 is zero and algae uptake nitrogen only in the form of NH_4 . At $\text{PN}_x = 0$, NH_4 is zero and algae uptake nitrogen only in the form of NO_3 .

Mineralization and hydrolysis

The third term on the RHS of equation (B.47) and (B.48) represents hydrolysis of particulate organic nitrogen, and the 3rd term in the 2nd line of equation (B.49) represents mineralization of dissolved organic nitrogen. The three parameters, K_{RPON} , K_{LPON} , and K_{DON} , have the following formulations:

$$K_{\text{RPON}} = (K_{\text{RN}} + \frac{\text{KHN}}{\text{KHN} + \text{NH}_4 + \text{NO}_3} K_{\text{RNalg}} \sum_{x=c,d,g} B_x) \cdot e^{K_{\text{THDR}}(T - \text{TR}_{\text{HDR}})} \quad (\text{B.53})$$

$$K_{\text{LPON}} = (K_{\text{LN}} + \frac{\text{KHN}}{\text{KHN} + \text{NH}_4 + \text{NO}_3} K_{\text{LNalg}} \sum_{x=c,d,g} B_x) \cdot e^{K_{\text{THDR}}(T - \text{TR}_{\text{HDR}})} \quad (\text{B.54})$$

$$K_{\text{DON}} = (K_{\text{DN}} + \frac{\text{KHN}}{\text{KHN} + \text{NH}_4 + \text{NO}_3} K_{\text{DNalg}} \sum_{x=c,d,g} B_x) \cdot e^{K_{\text{TMNL}}(T - \text{TR}_{\text{MNL}})} \quad (\text{B.55})$$

where

K_{RN} = minimum hydrolysis rate of refractory particulate organic nitrogen (day^{-1})

K_{LN} = minimum hydrolysis rate of labile particulate organic nitrogen (day^{-1})

K_{DN} = minimum mineralization rate of dissolved organic nitrogen (day^{-1})

K_{RNalg} and K_{LNalg} = constants that relate hydrolysis of refractory and labile particulate organic nitrogen, respectively, to algal biomass (day^{-1} per g C m^{-3})

K_{DNalg} = constant that relates mineralization to algal biomass (day^{-1} per g C m^{-3})

KHN = mean half-saturation constant for algal nitrogen uptake (g N m^{-3}), which has the form:

$$\text{KHN} = \frac{1}{3} \sum_{x=c,d,g} \text{KHN}_x \quad (\text{B.56})$$

Equations (B.53) – (B. 55) have exponential functions relates rates to temperature.

Nitrification

Nitrification is the process in which an ammonium ion (NH_4^+) is oxidized to nitrite (NO_2^-) and then to nitrate (NO_3^-). The stoichiometry equation for nitrification can be expressed as:



This is related to the first term in the second line of equation (B.50) and its corresponding term in equation (B.51) representing the effect of nitrification on ammonium and nitrate, respectively. The kinetics of complete nitrification processes are formulated as a function of available ammonium, dissolved oxygen and temperature:

$$\text{Nit} = \frac{\text{DO}}{\text{KHNit}_{\text{DO}} + \text{DO}} \frac{\text{NH}_4}{\text{KHNit}_{\text{N}} + \text{NH}_4} \text{Nit}_m \cdot f_{\text{Nit}}(T) \quad (\text{B.58})$$

and

$$f_{\text{Nit}}(T) = \begin{cases} e^{-\text{KNit}1 \cdot (T - \text{TNit})^2} & \text{if } T \leq \text{TNit} \\ e^{-\text{KNit}2 \cdot (\text{TNit} - T)^2} & \text{if } T > \text{TNit} \end{cases} \quad (\text{B.59})$$

where

KHNit_{DO} = nitrification half saturation constant for dissolved oxygen ($\text{g O}_2 \text{ m}^{-3}$)

KHNit_{N} = nitrification half saturation constant for ammonium (g N m^{-3})

Nit_m = maximum nitrification rate at TNit (day^{-1})

TNit = optimum temperature for nitrification ($^\circ\text{C}$)

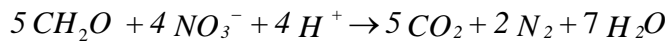
$\text{KNit}1$ = effect of temperature below TNit on nitrification rate ($^\circ\text{C}^{-2}$)

$\text{KNit}2$ = effect of temperature above TNit on nitrification rate ($^\circ\text{C}^{-2}$).

Eq. (B.58) shows that the nitrification process can be limited by low concentrations of DO and NH_4 .

Denitrification

Denitrification is the process in which nitrate is reduced to nitrite and then to nitrogen gas by bacteria. The stoichiometry relation for net denitrification reaction is described by the following equation:



In water columns, denitrification is usually not responsible for a significant nitrogen loss. However, under the anaerobic conditions found in the sediment bed or during extremely low oxygen conditions in the water column, denitrification can be important and may remove a substantial fraction of the nitrogen from a waterbody by converting nitrate and nitrite into nitrogen gas. Denitrification oxidizes dissolved organic carbon (DOC) and converts nitrate (NO₃) to nitrite (NO₂) and then to nitrogen gas (N₂).

B2.5. Silica

Silica is included in water quality modeling only when diatoms are considered. Silica is represented by two state variables: particulate biogenic silica (SU) and available silica (SA). SU represents the silica unavailable to diatom growth. The sources and sinks for particulate biogenic silica included in the model are:

1. Diatom basal metabolism (BM_d) and predation (PR_d)
2. Dissolution to available silica
3. Settling
4. External loads

The corresponding kinetic equation is:

$$\frac{\partial SU}{\partial t} = (FSP_d \cdot BM_d + FSPP \cdot PR_d) ASC_d \cdot B_d - K_{SUA} \cdot SU + \frac{\partial}{\partial z} (w_s \cdot SU) + \frac{WSU}{V} \quad (\text{B. 60})$$

where

SU = concentration of particulate biogenic silica (g Si m⁻³).

FSP_d = fraction of metabolized silica by diatoms produced as particulate biogenic silica

FSPP = fraction of predated diatom silica produced as particulate biogenic silica

ASC_d = silica-to-carbon ratio of diatoms (g Si per g C)

K_{SUA} = dissolution rate of particulate biogenic silica (day⁻¹)

w_s = settling velocity of cohesive sediment, m/s

WSU = external loads of particulate biogenic silica (g Si day⁻¹).

The available silica includes both the dissolved (SAd) and the particulate (SAp), where SA = SAd + SAp. SA includes the following sources and sinks:

1. Diatom basal metabolism (BM_d), predation (PR_d), and uptake (P_d)
2. Settling of sorbed (particulate) available silica
3. Dissolution from particulate biogenic silica
4. Sediment-water exchange of dissolved silica in the bottom layer
5. External loads

The kinetic equation describing these processes is:

$$\frac{\partial SA}{\partial t} = (FSI_d \cdot BM_d + FSIP \cdot PR_d - P_d) ASC_d \cdot B_d + K_{SUA} \cdot SU + \frac{\partial}{\partial z} (w_s \cdot SAP) + \frac{BFSAd}{\Delta z} + \frac{WSA}{V} \quad (B.61)$$

where

SA = concentration of available silica (g Si m⁻³)

SAd = dissolved available silica (g Si m⁻³)

SAp = particulate (sorbed) available silica (g Si m⁻³)

FSI_d = fraction of metabolized silica by diatoms produced as available silica

FSIP = fraction of predated diatom silica produced as available silica

BFSAd = sediment-water exchange flux of available silica (g Si m⁻² day⁻¹), applied to bottom layer only.

Δz = the thickness of the bottom layer in the numerical model

WSA = external loads of available silica (g Si day⁻¹)

Effects of diatoms on silica

In equations (B.60) and (B.61), those terms expressed as a function of diatom biomass (B_d) account for the effects of diatoms on silica. As in phosphorus and nitrogen, both basal metabolism (respiration and excretion) and predation are considered, and thus silica is formulated, to contribute to particulate biogenic and available silica. That is, diatom silica released by both basal metabolism and predation are represented by distribution coefficients (FSP_d, FSI_d) and (FSPP, FSIP). The sum of two distribution coefficients for basal metabolism should be unity and so is that for predation. Diatoms require silica as well as phosphorus and nitrogen, and diatom uptake of available silica is represented by (- P_d • ASC_d • B_d) in equation (B.61).

Dissolution

The term (- K_{SUA} • SU) in equation (B.60) and its corresponding term in equation (B.61) represent dissolution of particulate biogenic silica to available silica. The dissolution rate is expressed as an exponential function of temperature:

$$K_{SUA} = K_{SU} \cdot e^{KT_{SUA}(T-TR_{SUA})} \quad (B.64)$$

where

K_{SU} = dissolution rate of particulate biogenic silica at TR_{SUA} (day⁻¹)

KT_{SUA} = effect of temperature on dissolution of particulate biogenic silica (°C⁻¹)

TR_{SUA} = reference temperature for dissolution of particulate biogenic silica (°C).

B2.6. Chemical Oxygen Demand

In the present model, chemical oxygen demand is the concentration of reduced substances that are oxidizable through inorganic means. The COD source is from the sediment diagenesis process in the sediment bed. The kinetic equation is:

$$\frac{\partial COD}{\partial t} = -\frac{DO}{KH_{COD} + DO} KCOD \cdot COD + \frac{BFCOD}{\Delta z} + \frac{WCOD}{V} \quad (B.65)$$

where

COD = COD concentration (g O₂-equivalents m⁻³)

KH_{COD} = half-saturation constant of DO required for oxidation of COD (g O₂ m⁻³)

KCOD = oxidation rate of COD (day⁻¹)

BFCOD = COD sediment flux (g O₂-equivalents m⁻² day⁻¹), applied to the bottom layer only

WCOD = external loads of COD (g O₂-equivalents day⁻¹).

An exponential function is used to describe the temperature effect on the oxidation rate of COD:

$$KCOD = K_{CD} \cdot e^{KT_{COD}(T-TR_{COD})} \quad (B.66)$$

where

K_{CD} = oxidation rate of COD at TR_{COD} (day⁻¹)

KT_{COD} = effect of temperature on oxidation of COD (°C⁻¹)

TR_{COD} = reference temperature for oxidation of COD (°C)

B.2.7. Dissolved Oxygen

Water obtains oxygen directly from the atmosphere via reaeration and from plants via photosynthesis. Vertical mixing between surface and deep waters transfers DO to lower levels. With adequate sunlight, algae and aquatic plants consume nutrients and produce oxygen as a result of photosynthesis. In water layers where photosynthetic rates are very high, such as during an algal bloom, the water may become supersaturated, i.e., the oxygen content may exceed the DO saturation concentration. During periods of strong stratification, photosynthesis is the only potential source of DO in the deeper waters, and this occurs only if light penetrates to the deeper layers. External loads can be either a DO source increasing the DO concentration in the receiving water or a DO sink decreasing the DO concentration, depending on the inflow DO concentration.

The oxidation and decomposition of organic matter consume oxygen. The nitrification process uptakes oxygen and oxidize ammonium (NH₄⁺) to nitrite (NO₂⁻) and then to nitrate (NO₃⁻). Algal respiration needs oxygen to convert organic carbon to carbon dioxide and water. Chemical and biological processes in the sediment bed often uptake oxygen from the water column. Oxygen is consumed by the sediment organism respiration and the benthic decomposition of organic material, which can be a significant fraction of the total oxygen demand in a waterbody. Sediment oxygen demand (SOD) is

used to represent the oxygen depletion due to benthic reactions. It is the rate of oxygen consumption exerted by the bottom sediment on the overlying water. Sulfide and methane provide additional oxygen demands. Microbial activities tend to increase with increased temperature. The stratification may prevent DO in the surface layer from reaching the bottom. Therefore, the benthic effects can be particularly acute in summer under low-flow conditions or highly stratified conditions.

Processes and equations of dissolved oxygen

Based on the description above, the major sources of DO consisted of: (1) Reaeration (2) Photosynthesis (3) External loads and major sinks of DO consist of:

1. Oxidation of organic matter
2. Nitrification
3. Algal respiration
4. Sediment oxygen demand due to sediment diagenesis in the bed
5. Chemical oxygen demand due to reduced substances released from the sediment bed

If the contribution of DO sources is less than the summation of DO sinks, there is an oxygen deficit in the waterbody. The DO deficit is the difference between the saturated DO concentration and the existing DO concentration.

The corresponding DO kinetic equation is:

$$\begin{aligned} \frac{\partial DO}{\partial t} = & \sum_{x=c,d,g} \left((1.3 - 0.3 \cdot PN_x) P_x - (1 - FCD_x) \frac{DO}{KHR_x + DO} BM_x \right) AOCR \cdot B_x \\ & - AONT \cdot Nit \cdot NH_4 - AOCR \cdot K_{HR} \cdot DOC - \frac{DO}{KH_{COD} + DO} KCOD \cdot COD \\ & + K_r (DO_s - DO) + \frac{SOD}{\Delta z} + \frac{WDO}{V} \end{aligned} \quad (B.67)$$

where

PN_x = preference for ammonium uptake by algal group x ($0 \leq PN_x \leq 1$), given by Eq. (B.52)

AONT = mass of DO consumed per unit mass of ammonium nitrogen nitrified (4.33 g O₂ per g N)

AOCR = dissolved oxygen-to-carbon ratio in respiration (2.67 g O₂ per g C)

K_r = reaeration coefficient (day⁻¹), applied to the surface layer only

DO_s = saturation concentration of dissolved oxygen (g O₂ m⁻³)

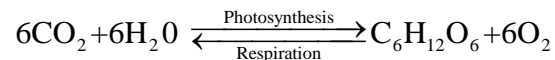
SOD = sediment oxygen demand (g O₂ m⁻² day⁻¹), applied to the bottom layer only; a direction of positive is towards the water column

WDO = external loads of dissolved oxygen (g O₂ day⁻¹)

The two sink terms in equation (B.67), heterotrophic respiration and chemical oxygen demand, are explained equation (B.29) and equation (B.66), respectively. The remainder of this section explains the effects of algae, nitrification, and surface reaeration on dissolved oxygen.

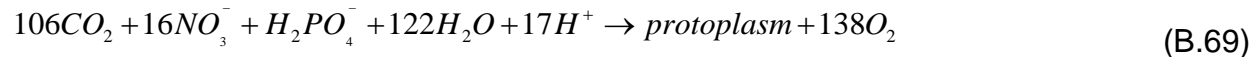
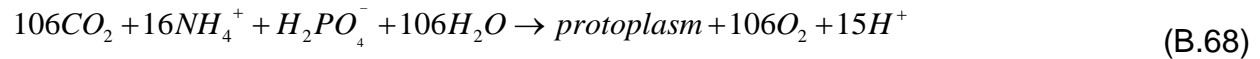
Effects of algae on dissolved oxygen

The first line on the RHS of (B.67) accounts for the effects for the effects of algae on dissolved oxygen. In water quality modeling, respiration and photosynthesis are considered as the same reaction but occur in opposite directions. However, photosynthesis only occurs during daylight hours, whereas respiration and decomposition proceed at all times and are not dependent on solar energy. These reactions can be represented by the following simplified stoichiometry reaction relationship:



where glucose, C₆H₁₂O₆, represents organic compounds in plants. In this reaction, photosynthesis converts carbon dioxide and water into glucose and oxygen and leads to a net gain of DO in the waterbody. Conversely, respiration converts glucose and oxygen into carbon dioxide and water resulting in a net loss of DO in the waterbody. Plants generally produce more organic matter and oxygen than they use.

The quantity of DO produced also depends on the form of nitrogen utilized for algal growth. Morel (1983) gave the following equations for DO production:



where protoplasm is the living substance of algae cells. It is a chemically active mixture of protein, fats, and many other complex substances suspended in water.

Eq. (B.68) indicates that, when ammonium is the nitrogen source, one mole of oxygen is produced per mole of carbon dioxide fixed. Eq. (B.69) shows that, when nitrate is the nitrogen source, 1.3 (= 138/106) moles of oxygen are produced per mole of carbon dioxide fixed. These two equations are reflected in the first term on the RHS of Eq. (B.67) by the quantity of $(1.3 - 0.3 \cdot PN_x)$, which is the photosynthesis ratio and represents the molar quantity of oxygen produced per mole of carbon dioxide fixed. When the entire nitrogen source is from ammonium (ammonium preference factor, PN_x , is equal to 1.0), the quantity is 1.0. When the entire nitrogen source is from nitrate ($PN_x = 0.0$), the quantity is 1.3.

The last term in the first line of equation (B.67) accounts for oxygen consumption due to algal respiration (equation B.26). Again, representation of respiration process is:



The rate of oxygen production (and nutrient uptake) is proportional to the algal growth rate for each gram of algae carbon produced by photosynthesis, 32/12 (or 2.67 approximately) grams of O_2 are produced. Conversely, for every gram of algae carbon consumed by respiration, 32/12 grams of oxygen are also consumed. Hence, the dissolved oxygen-to-carbon ratio, AOCR, in Eq. (B.67) should have: $AOCR = 2.67 \text{ g } O_2 \text{ per g C}$.

Effect of Nitrification on dissolved oxygen

The nitrification of ammonia has the potential for removing large amounts of oxygen from a waterbody. The stoichiometry of reactions indicates that two moles of oxygen are required to nitrify one mole of ammonium into nitrate: 3.43 (= $1.5 \times 32/14$) g O_2 per g N for transforming ammonia to nitrite and 1.14 (= $0.5 \times 32/14$) g O_2 per g N for transforming nitrite to nitrate. Thus, for every gram of ammonium nitrogen oxidized, 4.57 (= $2 \times 32/14$) grams of oxygen are consumed. However, Wezernak and Gannon (1968) reported that due to the effect of nitrifying bacteria, less than two moles of oxygen are actually consumed per mole of ammonium nitrified, and a total of 4.33 grams of oxygen

is required to oxidize 1.0 gram of ammonia nitrogen. This explains why AONT has the value of 4.33 (instead of 4.57) g O₂ per g N in the DO equation Eq.(B.67).

Effect of Reaeration on dissolved oxygen

The rate of reaeration is proportional to the DO deficit, which is the difference between the DO concentration and the oxygen saturation value. The DO deficit is a useful water quality parameter and is influenced by temperature, salinity, and atmospheric pressure. The saturated concentration of dissolved oxygen, which decrease as temperature and salinity increase, is specified using an empirical formula by Hyer et al. (1971):

$$DO_s = 14.6244 - 0.367134 \cdot T + 0.0044972 \cdot T^2 + S \cdot (-0.0966 + 0.00205 \cdot T + 0.0002739 \cdot S) \quad (\text{B.71})$$

Typically, oxygen is transferred from the atmosphere into the water, since DO levels in natural waters are generally below saturation. However, when photosynthesis produces supersaturated DO levels (e.g., in the afternoon of a eutrophic reservoir) the net transfer of oxygen can be from the water into the atmosphere.

Reaeration occurs by diffusion of oxygen from the atmosphere into the water (when DO is not saturated) and by the turbulent mixing of water and air. In general, the reaeration rate in natural waters depends on:

1. Water flow speed and wind speed
2. Water temperature and salinity
3. Water depth

The reaeration coefficient includes the effect of turbulence generated by bottom friction (O'Connor and Dobbins, 1958) and that by surface wind stress (Banks and Herrera, 1977):

$$K_r = \left(K_{ro} \sqrt{\frac{u_{eq}}{h_{eq}}} + W_{rea} \right) \frac{1}{\Delta z} \cdot K T_r^{T-20} \quad (\text{B.72})$$

where

K_{ro} = proportionality constant = 3.933 in MKS units

u_{eq} = weighted velocity over cross-section (m sec^{-1})

h_{eq} = weighted depth over cross-section (m)

B_η = width at the free surface (m)

W_{rea} = wind-induced reaeration (m day^{-1})

$K T_r$ = constant for temperature adjustment of DO reaeration rate

Δz = the thickness of the surface layer in numerical model

The wind-induced reaeration from (B.72) can be expressed as:

$$W_{rea} = 0.728 U_w^{1/2} - 0.317 U_w + 0.0372 U_w^2 \quad (\text{B.73})$$

with U_w = wind speed (m sec^{-1}) at the height of 10 m above surface

Other relationships also exist for estimating the reaeration rate and DO saturated concentration (refer to Ji, 2008).

Sediment flux

The sediment flux obtained in HEM3D model is primarily based on the Chesapeake Bay Sediment Flux Model developed by Di Toro and Fitzpatrick (1993), which is now commonly accepted and used in water quality modeling (e.g., Cerco and Cole, 1994; Park et al., 1995; HydroQual, 1995). Many discussions and equations in this chapter originate from the report by Park et al. (1995). Complete model documentation can be found in Di Toro and Fitzpatrick (1993) and Di Toro (2001).

APPENDIX C: Summary of Parameters Used for ICM Water Quality Model

Table C-1: Parameters related to algae in the water column.

Parameter	Description	Value	Unit
PM _c	maximum growth rate of algae group 1	2.5	day ⁻¹
PM _d	maximum growth rate of algae group 2	2.5	day ⁻¹
PM _g	maximum growth rate of algae group 3	2.5	day ⁻¹
KHN _x	half-saturation constant of N uptake by algae	0.01	g N m ⁻³
KHP _x	half-saturation constant of P uptake by algae	0.001	g P m ⁻³
KHS	half-saturation constant of Si uptake by diatoms	0.05	g Si m ⁻³
KHR _x	half-saturation constant of DO for algal excretion of DOC	0.5	g O ₂ m ⁻³
IH _c	half-saturation light intensity for algal group 1 growth	50	langley day ⁻¹
IH _d	half-saturation light intensity for algal group 2 growth	30	langley day ⁻¹
IH _g	half-saturation light intensity for algal group 3 growth	40	langley day ⁻¹
KE _B	background light attenuation coefficient	0.12 - 0.15	m ⁻¹
KE _{CHL}	light attenuation coefficient due to self-shading of algae	0.017	m ² per mg CHL
KE _{TSS}	light attenuation coefficient due to TSS	0.07	m ² per g TSS
CCHL _x	C-to-CHL ratio in algae	60.0	g C per g CHL
TM _c	optimum T for algal group 1 growth	25.0	°C
TM _d	optimum T for algal group 2 growth	20.0	°C
TM _g	optimum T for algal group 3 growth	22.5	°C
KTG1 _c	effect of T below optimum T on algal group 1 growth	0.006	°C ⁻²
KTG2 _c	effect of T above optimum T on algal group 1 growth	0.006	°C ⁻²
KTG1 _d	effect of T below optimum T on algal group 2 growth	0.004	°C ⁻²
KTG2 _d	effect of T above optimum T on algal group 2 growth	0.006	°C ⁻²

Table C-1: Parameters related to algae in the water column.

KTG1 _g	effect of T below optimum T on algal group 3 growth	0.012	°C ⁻²
KTG2 _g	effect of T above optimum T on algal group 3 growth	0.007	°C ⁻²
BMR _c	basal metabolism rate of algae group 1 at reference T	0.05	day ⁻¹
BMR _d	basal metabolism rate of algae group 2 at reference T	0.05	day ⁻¹
BMR _g	basal metabolism rate of algae group 3 at reference T	0.05	day ⁻¹
PRR _c	predation rate of algae group 1 at reference T	0.05	day ⁻¹
PRR _d	predation rate of algae group 2 at reference T	0.05	day ⁻¹
PRR _g	predation rate of algae group 3 at reference T	0.20	day ⁻¹
KTB _x	effect of T on basal metabolism of algae	0.069	v
TR _x	reference T for basal metabolism of algae	20.0	°C
WS _c	settling velocity for algal group 1	0.01	m day ⁻¹
WS _d	settling velocity for algal group 2	0.25	m day ⁻¹
WS _g	settling velocity for algal group 3	0.1	m day ⁻¹

Table C-2: Parameters related to organic carbon in the water column.

Parameters	description	value	unit
$\overline{\text{FCRP}}$	fraction of predated algal C produced as RPOC	0.35	none
FCLP	fraction of predated algal C produced as LPOC	0.55	none
FCDP	fraction of predated algal C produced as DOC	0.10	none
FCD _x	fraction of metabolized C by algae produced as DOC	0.0	none
KHR _x	half-saturation constant of DO for algal excretion of DOC	0.5	g O ₂ m ⁻³
KHO _{DOC}	half-saturation constant of DO for oxic respiration of DOC	0.5	g O ₂ m ⁻³
K _{RC}	minimum respiration rate of RPOC	0.005	day ⁻¹
K _{LC}	minimum respiration rate of LPOC	0.075	day ⁻¹
K _{DC}	minimum respiration rate of DOC	0.020	day ⁻¹
K _{Rcalg}	constant relating respiration of RPOC to algal biomass	0.0	day ⁻¹ per g C m ⁻³
K _{Lcalg}	constant relating respiration of LPOC to algal biomass	0.0	day ⁻¹ per g C m ⁻³
K _{Dcalg}	constant relating respiration of DOC to algal biomass	0.0	day ⁻¹ per g C m ⁻³
KT _{HDR}	effect of T on hydrolysis/mineralization of POM/DOM	0.069	°C ⁻¹
KT _{MNL}	effect of T on hydrolysis/mineralization of POM/DOM	0.069	°C ⁻¹
TR _{HDR}	reference T for hydrolysis of POM	20.0	°C
TR _{MNL}	reference T for mineralization of DOM	20.0	°C
KHNDN _N	half-saturation constant of NO ₂₃ for Denitrification	0.1	g N m ⁻³
AANOX	ratio of denitrification to oxic DOC respiration rate	0.5	none

Table C-3: Parameters related to nitrogen in the water column.

Parameters	description	Value	unit
FNRP	fraction of predated algal N produced as RPON	0.35	none
FNLP	fraction of predated algal N produced as LPON	0.55	none
FNDP	fraction of predated algal N produced as DON	0.10	none
FNIP	fraction of predated algal N produced as NH ₄	0.00	none
FNR	fraction of metabolized algal N produced as RPON	0.0	none
FNL	fraction of metabolized algal N produced as LPON	0.0	none
FND	fraction of metabolized algal N produced as DON	1.0	none
FNI	fraction of metabolized algal N produced as NH ₄	0.0	none
ANC _x	N-to-C ratio in algae	0.167	g N per g C
ANDC	mass of NO ₂₃ -N consumed per mass DOC oxidized	0.933	g N per g C
K _{RN}	minimum hydrolysis/mineralization rate of RPON	0.005	day ⁻¹
K _{LN}	minimum hydrolysis/mineralization rate of LPON	0.075	day ⁻¹
K _{DN}	minimum hydrolysis/mineralization rate of DON	0.015	day ⁻¹
K _{Rnalg}	constant relating hydrolysis/mineralization of RPON to algal biomass	0.0	day ⁻¹ per g N m ⁻³
K _{Lnalg}	constant relating hydrolysis/mineralization of LPON to algal biomass	0.0	day ⁻¹ per g N m ⁻³
K _{Dnalg}	constant relating hydrolysis/mineralization of DON to algal biomass	0.0	day ⁻¹ per g N m ⁻³
KHDO _{NIT}	half-saturation constant of DO for nitrification	1.0	g O ₂ m ⁻³
KHN _{NIT}	half-saturation constant of NH ₄ for nitrification	1.0	g N m ⁻³
NT _M	maximum nitrification at optimum T	0.007	day ⁻¹

Table C-3 (con't)

Parameters	description	Value	unit
$K_{T_{NT1}}$	effect of T below optimum T on nitrification rate	0.0045	$^{\circ}\text{C}^{-2}$
$K_{T_{NT1}}$	effect of T above optimum T on nitrification rate	0.0045	$^{\circ}\text{C}^{-2}$
$T_{M_{NT}}$	optimum T for nitrification rate	27.0	$^{\circ}\text{C}$

Table C-4: Parameters related to phosphorus in the water column.

Parameter	description	Value	unit
FPRP	fraction of predated algal P produced as RPOP	0.1	none
FPLP	fraction of predated algal P produced as LPOP	0.2	none
FPDP	fraction of predated algal P produced as DOP	0.5	none
FPR _x	fraction of metabolized P by algae produced as RPOP	0.0	none
FPL _x	fraction of metabolized P by algae produced as LPOP	0.0	none
FPD _x	fraction of metabolized P by algae produced DOP	0.5	none
APCMIN	minimum P-to-C ratio in algae	0.01	g P per g C
APCMAX	maximum P-to-C ratio in algae	0.024	g P per g C
PO4DMAX	maximum PO ₄ d beyond which APC = APCMAX	0.01	g P m ⁻³
K _{RP}	minimum hydrolysis/mineralization rate of RPOP		0.005 day ⁻¹
K _{LP}	minimum hydrolysis/mineralization rate of LPOP	0.075	day ⁻¹
K _{DP}	minimum hydrolysis/mineralization rate of DOP	0.1	day ⁻¹
K _{Rpalg}	constant relating hydrolysis/mineralization of RPOP to algal biomass	0.0	day ⁻¹ per g P m ⁻³
K _{Lpalg}	constant relating hydrolysis/mineralization of LPOP to algal biomass	0.0	day ⁻¹ per g P m ⁻³
K _{Dpalg}	constant relating hydrolysis/mineralization of DOP to algal biomass	0.0	day ⁻¹ per g P m ⁻³

Table C-5: Parameters related to silica in the water column.

Parameter	description	Value	unit
FSA	fraction of predated diatom Si produced as SA	0.0	none
ASC _d	Si-to-C ratio in diatoms	0.5	g Si per g C
K _{SU}	dissolution rate of SU at reference T	0.025	day ⁻¹
KT _{SUA}	effect of T on dissolution of SU	0.092	°C ⁻¹
TR _{SUA}	reference T for dissolution of SU	20.0	°C

Table C-6. Parameters related to chemical oxygen demand and dissolved oxygen in the water column.

Parameters	description	Value	unit
KHO _{COD}	half-saturation constant of DO for oxidation of COD	1.5	g O ₂ m ⁻³
K _{CD}	oxidation rate of COD at reference temperature	20.0	day ⁻¹
KT _{COD}	effect of T on oxidation of COD	0.041	°C ⁻¹
TR _{COD}	reference T for oxidation of COD	20.0	°C
K _{RDO}	reaeration coefficient	2.4	m day ⁻¹
AOCR	mass DO consumed per mass C respired by algae	2.67	g O ₂ per g C
ANOT	mass DO consumed per mass NH ₄ -N nitrified	4.33	g O ₂ per g N

Table C-7: Parameters used in the sediment flux model.

Parameter	description	value	unit
HSEDALL	depth of sediment	10	cm
DIFFT	heat diffusion coefficient between water column and sediment	0.0018	cm ² sec ⁻¹
SALTSW	salinity for dividing fresh and saltwater for SOD kinetics (sulfide in saltwater or methane in freshwater) and for PO ₄ sorption coefficients	1.0	ppt
SALTND	salinity for dividing fresh or saltwater for nitrification/denitrification rates (larger values for freshwater)	1.0	ppt
FRPPH1(1)	fraction of POP in algal group No 1 routed into G ₁ class	0.65	none
FRPPH1(2)	fraction of POP in algal group No 1 routed into G ₂ class	0.255	none
FRPPH1(3)	fraction of POP in algal group No 1 routed into G ₃ class	0.095	none
FRPPH2(1)	fraction of POP in algal group No 2 routed into G ₁ class	0.65	none
FRPPH2(2)	fraction of POP in algal group No 2 routed into G ₂ class	0.255	none
FRPPH2(3)	fraction of POP in algal group No 2 routed into G ₃ class	0.095	none
FRPPH3(1)	fraction of POP in algal group No 3 routed into G ₁ class	0.65	none
FRPPH3(2)	fraction of POP in algal group No 3 routed into G ₂ class	0.255	none
FRPPH3(3)	fraction of POP in algal group No 3 routed into G ₃ class	0.095	none
FRNPH1(1)	fraction of PON in algal group No 1 routed into G ₁ class	0.65	none
FRNPH1(2)	fraction of PON in algal group No 1 routed into G ₂ class	0.28	none
FRNPH1(3)	fraction of PON in algal group No 1 routed into G ₃ class	0.07	none
FRNPH2(1)	fraction of PON in algal group No 2 routed into G ₁ class	0.65	none
FRNPH2(2)	fraction of PON in algal group No 2 routed into G ₂ class	0.28	none

Table C-7 (con't)

Parameter	description	value	unit
FRNPH2(3)	fraction of PON in algal group No 2 routed into G ₃ class	0.07	none
FRNPH3(1)	fraction of PON in algal group No 3 routed into G ₁ class	0.65	none
FRNPH3(2)	fraction of PON in algal group No 3 routed into G ₂ class	0.28	none
FRNPH3(3)	fraction of PON in algal group No 3 routed into G ₃ class	0.07	none
FRCPH1(1)	fraction of POC in algal group No 1 routed into G ₁ class	0.65	none
FRCPH1(2)	fraction of POC in algal group No 1 routed into G ₂ class	0.255	none
FRCPH1(3)	fraction of POC in algal group No 1 routed into G ₃ class	0.095	none
FRCPH2(1)	fraction of POC in algal group No 2 routed into G ₁ class	0.65	none
FRCPH2(2)	fraction of POC in algal group No 2 routed into G ₂ class	0.255	none
FRCPH2(3)	fraction of POC in algal group No 2 routed into G ₃ class	0.095	none
FRCPH3(1)	fraction of POC in algal group No 3 routed into G ₁ class	0.65	none
FRCPH3(2)	fraction of POC in algal group No 3 routed into G ₂ class	0.255	none
FRCPH3(3)	fraction of POC in algal group No 3 routed into G ₃ class	0.095	none
KPDIAG(1)	reaction (decay) rates for G ₁ class POP at 20°C	0.035	day ⁻¹
KPDIAG(2)	reaction (decay) rates for G ₂ class POP at 20°C	0.0018	day ⁻¹
KPDIAG(3)	reaction (decay) rates for G ₃ class POP at 20°C	0.0	day ⁻¹
DPTHTA(1)	constant for T adjustment for G ₁ class POP decay	1.10	none
DPTHTA(2)	constant for T adjustment for G ₂ class POP decay	1.15	none
KNDIAG(1)	reaction (decay) rates for G ₁ class PON at 20°C	0.035	day ⁻¹
KNDIAG(2)	reaction (decay) rates for G ₂ class PON at 20°C	0.0018	day ⁻¹

Table C-7 (con't)

Parameter	description	value	unit
KNDIAG(3)	reaction (decay) rates for G ₃ class PON at 20°C	0.0	day ⁻¹
DNTHTA(1)	constant for T adjustment for G ₁ class PON decay	1.10	none
DNTHTA(2)	constant for T adjustment for G ₂ class PON decay	1.15	none
KCDIAG(1)	reaction (decay) rates for G ₁ class POC at 20°C	0.035	(day ⁻¹)
KCDIAG(2)	reaction (decay) rates for G ₂ class POC at 20°C	0.0018	(day ⁻¹)
KCDIAG(3)	reaction (decay) rates for G ₃ class POC at 20°C	0.0	(day ⁻¹)
DCTHTA(1)	constant for T adjustment for G ₁ class POC decay	1.10	none
DCTHTA(2)	constant for T adjustment for G ₂ class POC decay	1.15	none
KSI	1 st -order reaction (dissolution) rate of P _{Si} at 20°C	0.5	day ⁻¹
THTASI	constant for T adjustment for P _{Si} dissolution	1.1	none
M1	solid concentrations in Layer 1	0.5	kg l ⁻¹
M2	solid concentrations in Layer 2	0.5	kg l ⁻¹
THTADP	constant for T adjustment for diffusion coefficient for particle mixing	1.117	none
THTADD	constant for T adjustment for diffusion coefficient for dissolved phase	1.08	none
KAPPNH4F	optimum reaction velocity for nitrification in Layer 1 for freshwater	0.20	m day ⁻¹
KAPPNH4S	optimum reaction velocity for nitrification in Layer 1 for saltwater	0.14	m day ⁻¹
THTANH4	constant for T adjustment for nitrification	1.08	none
KMNH4	half-saturation constant of NH ₄ for nitrification	1500.0	mg N m ⁻³
KMNH4O2	half-saturation constant of DO for nitrification	1.0	g O ₂ m ⁻³

Table C-7 (con't)

Parameter	description	value	unit
PIENH4	partition coefficient for NH ₄ in both layers	1.0	per kg l ⁻¹
KAPPNO3F	reaction velocity for denitrification in Layer 1 at 20°C for freshwater	0.3	m day ⁻¹
KAPPNO3S	reaction velocity for denitrification in Layer 1 at 20°C for saltwater	0.125	m day ⁻¹
K2NO3	reaction velocity for denitrification in Layer 2 at 20°C	0.25	m day ⁻¹
THTANO3	constant for T adjustment for denitrification	1.08	none
KAPPD1	reaction velocity for dissolved H ₂ S oxidation in Layer 1 at 20°C	0.2	m day ⁻¹
KAPPP1	reaction velocity for particulate H ₂ S oxidation in Layer 1 at 20°C	0.4	m day ⁻¹
PIE1S	partition coefficient for H ₂ S in Layer 1	100.0	per kg l ⁻¹
PIE2S	partition coefficient for H ₂ S in Layer 2	100.0	per kg l ⁻¹
THTAPD1	constant for T adjustment for both dissolved & particulate H ₂ S oxidation	1.08	none
KMHSO2	constant to normalize H ₂ S oxidation rate for oxygen	4.0	g O ₂ m ⁻³
CSISAT	saturation concentration of Si in the pore water	40000.0	mg Si m ⁻³
DPIE1SI	incremental partition coefficient for Si in Layer 1	10.0	per kg l ⁻¹
PIE2SI 2	partition coefficient for Si in Layer 2	100.0	per kg l ⁻¹
O2CRITSI	critical DO concentration for Layer 1 incremental Si sorption	1.0	g O ₂ m ⁻³
KMPSI	half-saturation constant of P _{Si} for Si dissolution	5 × 10 ⁷	mg Si m ⁻³
JSIDETR	detrital flux of P _{Si} to account for P _{Si} settling to the sediment that is not associated with algal flux of P _{Si}	100.0	mg Si m ⁻² day ⁻¹
DPIE1PO4F	incremental partition coefficient for PO ₄ in Layer 1 for freshwater	3000.0	per kg l ⁻¹
DPIE1PO4S	incremental partition coefficient for PO ₄ in Layer 1 for saltwater	300.0	per kg l ⁻¹
PIE2PO4	partition coefficient for PO ₄ in Layer 2	100	per kg l ⁻¹
O2CRIT	critical DO concentration for Layer 1 incremental PO ₄ sorption	2.0	g O ₂ m ⁻³

Table C-7 (con't)

Parameter	description	value	unit
KMO2DP	half-saturation constant of DO for particle mixing	4.0	g O ₂ m ⁻³
TEMPBEN	temperature at which benthic stress accumulation is reset to zero	10.0	°C
KBENSTR	1 st -order decay rate for benthic stress	0.03	day ⁻¹
KLBNTH	ratio of bio-irrigation to bioturbation	0.0	none
DPMIN	minimum diffusion coefficient for particle mixing	3×10 ⁻⁶	m ² day ⁻¹
KAPPCH4	reaction velocity for dissolved CH ₄ oxidation in Layer 1 at 20°C	0.2	m day ⁻¹
THTACH4	constant for T adjustment for dissolved CH ₄ oxidation	1.08	none
VSED	net burial (sedimentation) rate	0.25	cm yr ⁻¹
VPMIX	diffusion coefficient for particle mixing	1.2×10 ⁻⁴	m ² day ⁻¹
VDMIX	diffusion coefficient in pore water	0.001	m ² day ⁻¹
WSCNET	net settling velocity for algal group 1	0.1	m day ⁻¹
WSDNET	net settling velocity for algal group 2	0.3	m day ⁻¹
WSGNET	net settling velocity for algal group 3	0.1	m day ⁻¹